



National Library
of Canada

Bibliothèque nationale
du Canada

Canadian Theses Service

Service des thèses canadiennes

Ottawa, Canada
K1A 0N4

NOTICE

The quality of this microform is heavily dependent upon the quality of the original thesis submitted for microfilming. Every effort has been made to ensure the highest quality of reproduction possible.

If pages are missing, contact the university which granted the degree.

Some pages may have indistinct print especially if the original pages were typed with a poor typewriter ribbon or if the university sent us an inferior photocopy.

Previously copyrighted materials (journal articles, published tests, etc.) are not filmed.

Reproduction in full or in part of this microform is governed by the Canadian Copyright Act, R.S.C. 1970, c. C-30.

AVIS

La qualité de cette microforme dépend grandement de la qualité de la thèse soumise au microfilmage. Nous avons tout fait pour assurer une qualité supérieure de reproduction.

S'il manque des pages, veuillez communiquer avec l'université qui a conféré le grade.

La qualité d'impression de certaines pages peut laisser à désirer, surtout si les pages originales ont été dactylographiées à l'aide d'un ruban usé ou si l'université nous a fait parvenir une photocopie de qualité inférieure.

Les documents qui font déjà l'objet d'un droit d'auteur (articles de revue, tests publiés, etc.) ne sont pas microfilmés.

La reproduction, même partielle, de cette microforme est soumise à la Loi canadienne sur le droit d'auteur, SRC 1970, c. C-30.

THE UNIVERSITY OF ALBERTA

PHOTOLYSIS OF, AND THE REACTIONS OF
H ATOMS WITH, ALKANE THIOLS

BY

WENDY W. LAM

A THESIS

SUBMITTED TO THE FACULTY OF GRADUATE STUDIES AND RESEARCH
IN PARTIAL FULFILMENT OF THE REQUIREMENTS FOR THE DEGREE OF
DOCTOR OF PHILOSOPHY

DEPARTMENT OF CHEMISTRY

EDMONTON, ALBERTA

SPRING, 1988

Permission has been granted to the National Library of Canada to microfilm this thesis and to lend or sell copies of the film.

The author (copyright owner) has reserved other publication rights, and neither the thesis nor extensive extracts from it may be printed or otherwise reproduced without his/her written permission.

L'autorisation a été accordée à la Bibliothèque nationale du Canada de microfilmer cette thèse et de prêter ou de vendre des exemplaires du film.

L'auteur (titulaire du droit d'auteur) se réserve les autres droits de publication; ni la thèse ni de longs extraits de celle-ci ne doivent être imprimés ou autrement reproduits sans son autorisation écrite.

ISBN 0-315-42871-6

THE UNIVERSITY OF ALBERTA

RELEASE FORM

NAME OF AUTHOR: Wendy W. Lam

TITLE OF THESIS: Photolysis of, and the Reactions
of H Atoms with, Alkane Thiols

DEGREE: Ph.D.

YEAR THIS DEGREE GRANTED: 1988

Permission is hereby granted to THE UNIVERSITY OF ALBERTA LIBRARY to reproduce single copies of this thesis and to lend or sell such copies for private, scholarly or scientific research purposes only.

The author reserves other publication rights, and neither the thesis nor extensive extracts from it may be printed or otherwise reproduced without the author's written permission.

Wendy W. Lam
.....
(Signature)

1003 Vanier House
.....
(Permanent Address)

Michener Park
.....

Edmonton, Alberta
.....

T6H 4N1
.....

Date: December 16, 1987

THE UNIVERSITY OF ALBERTA

FACULTY OF GRADUATE STUDIES AND RESEARCH

The undersigned certify that they have read, and recommend to the Faculty of Graduate Studies and Research for acceptance, a thesis entitled:

PHOTOLYSIS OF, AND THE REACTIONS OF
H ATOMS WITH, ALKANE THIOLS

submitted by :

WENDY W. LAM

in partial fulfilment of the requirements for the degree of
Doctor of Philosophy in Chemistry.

O. P. Strausz
.....
O. P. Strausz - Supervisor

Martin Cowie
.....
M. Cowie

G. R. Freeman
.....
G. R. Freeman

A. Kalantar
.....
A. Kalantar

I. G. Dalla Lana
.....
I. G. Dalla Lana - Chemical
Engineering

D. A. Armstrong
.....
D. A. Armstrong - External
Examiner

Date: December 16, 1987.

To my husband, and my parents

ABSTRACT

The 254 nm photolyses of C_2H_5SH , $i-C_3H_7SH$ and $t-C_4H_9SH$ have been investigated as a function of substrate and inert gas pressure, time and temperature up to $150^\circ C$. With increasing inert gas pressure the quantum yields of the primary products, H_2 and $RSSR$, increase very gradually and those of the minor products, RH , $R(-H)$ and H_2S , correspondingly decrease, until limiting values are attained at tenfold excess of thermalizer. The quantum yields for the three primary processes were deduced from steady-state treatment of a 16-step mechanism, featuring "hot" and thermal \bar{H} -atom reactions. For the sequence C_2H_5SH , $i-C_3H_7SH$, $t-C_4H_9SH$, ϕ_1 ($RSH + h\nu \rightarrow RS + H$) = 0.96, 0.93 and 0.90; ϕ_2 ($RSH + h\nu \rightarrow R + SH$) = 0.029, 0.057 and 0.070 and ϕ_3 ($RSH + h\nu \rightarrow H_2S + R(-H)$) = 0.010, 0.009 and 0.033, respectively, independent of temperature. The data also allowed the derivation of rate constants for the $H + RSH$ reactions. Although H-abstraction, $H + RSH \xrightarrow{k_7} H_2 + RS$, is a well documented reaction, the gas-phase displacement reaction, $H + RSH \xrightarrow{k_8} H_2S + R$, was believed to be important only for the case of "hot" H atoms. Direct evidence for the occurrence of this reaction was obtained from experiments on the $Hg(^3P_1)$ -photosensitized decomposition of H_2 in the presence of C_2H_5SH since there is no source, other than the displacement reaction (8), for the observed products H_2S and C_2H_6 . By incorporating this reaction in the overall mechanism for the photochemical decomposition of the above

thiols it was possible to derive k_7/k_8 values as a function of temperature for each thiol and, since values of k_7 could be derived from literature data, Arrhenius parameters for k_8 were calculated: $A_8 = 5.1, 2.8$ and $3.0 \times 10^{12} \text{ cm}^3 \text{ mol}^{-1} \text{ s}^{-1}$, and $E_8 = 2.38, 2.60$ and $1.49 \text{ kcal mol}^{-1}$, for $\text{C}_2\text{H}_5\text{SH}$, $i\text{-C}_3\text{H}_7\text{SH}$ and $t\text{-C}_4\text{H}_9\text{SH}$, respectively. These values of E_8 , along with that reported in the literature for $n\text{-C}_4\text{H}_9\text{SH}$, follow the linear relationship $E_8 = -5.08 - 0.37\Delta H$, from which E_8 values for higher molecular weight thiols may be predicted.

These studies also led to the measurement of combination/disproportionation rate constant ratios for $\text{C}_2\text{H}_5\text{S}$, $i\text{-C}_3\text{H}_7\text{S}$ and $t\text{-C}_4\text{H}_9\text{S}$ radicals as a function of temperature, from which $E_{\text{dispr.}} = 3.12, 2.65$ and $1.68 \text{ kcal mol}^{-1}$, respectively, and $A_{\text{dispr.}} = 7.3 \times 10^{13}, 4.8 \times 10^{13}$ and $7.1 \times 10^{12} \text{ cm}^3 \text{ mol}^{-1} \text{ s}^{-1}$.

ACKNOWLEDGEMENT

I wish to express my sincere appreciation and gratitude to Professor O. P. Strausz for his guidance throughout the course of this research.

The many interesting and illuminating discussions with Drs. I. Safarik, M. Torres and T Yokota are specially recognized.

I am also grateful to Dr. E. M. Lown for her helpful suggestions and cheerful assistance in the preparation of this thesis.

In addition, I am deeply indebted to Professors W. S. Fyfe and B. I. Kronberg who have inspired my interests in research through their candid and consistent encouragement.

Special thanks go to the many individuals for their genuine friendship and incessant humour during the past few years.

I am especially grateful to my husband, Lonnie G. Haine, not only for his continuing devotion and support, but also for his tremendous computer assistance during the writing of this manuscript.

Finally, the financial supports provided by the University of Alberta and by the Alberta Oil Sands Technology and Research Authority are acknowledged.

TABLE OF CONTENTS

	PAGE
ABSTRACT.....	v
ACKNOWLEDGEMENTS.....	vii
LIST OF TABLES.....	xii
LIST OF FIGURES.....	xvi
CHAPTER 1: INTRODUCTION.....	1
1.1 Physical and Chemical Properties of Thiols.....	3
1.1.1 Molecular Parameters.....	3
1.1.2 Spectral Parameters.....	6
1.1.3 Reactions of Thiols.....	7
1.2 Photolysis of Thiols.....	8
1.2.1 Photolysis.....	8
1.2.2 Hydrogen Atom Reactions.....	17
1.2.2.1 Generation of H Atoms.....	17
1.2.2.2 Abstraction / Displacement.....	18
1.3 Thermolysis of Thiols.....	25
1.4 Thiyl Radicals.....	32
1.4.1 Physical and Spectral Properties.....	32
1.4.2 Reactions of Thiyl Radicals.....	34
1.4.2.1 Displacement / Combination.....	34
1.4.2.2 Abstraction.....	35
1.4.2.3 Addition.....	37
1.4.2.4 Metathetical Reactions.....	40
1.5 Transition State Theory for Bimolecular Reactions.....	43
1.6 RRKM Theory for the Unimolecular Decomposition of Alkyl Radicals.....	47

1.7	Aim of the Present Investigation.....	49
CHAPTER 2: EXPERIMENTAL.....		52
2.1	The High Vacuum System.....	52
2.2	The Photolytic Assembly.....	55
2.3	Light Sources and Actinometry.....	56
2.4	The Analytical System.....	59
2.5	Materials and Purification.....	61
2.6	Operational Procedure.....	62
CHAPTER 3: THE REACTIONS OF HYDROGEN ATOMS WITH ETHANETHIOL.....		70
3.1	Results.....	70
3.1.1	Incident Light Absorption.....	70
3.1.2	Effects of Time and Ethanethiol Pressure on Product Quantum Yields.....	72
3.2	Discussion.....	76
CHAPTER 4: PHOTOLYSIS OF, AND THE REACTIONS OF HYDROGEN ATOMS WITH, ETHANETHIOL.....		82
4.1	Results.....	82
4.1.1	H ₂ S Actinometry.....	82
4.1.2	Photolysis of Pure Ethanethiol.....	83
4.1.3	Photolysis of Ethanethiol with Added Thermalizer, CO ₂	85
4.1.4	Effects of Temperature on Product Yields.....	89
4.2	Discussion.....	89
4.2.1	Reaction Mechanism.....	96
4.2.2	Quantum Efficiencies of the Primary Photochemical Steps: Quantum Yield of C ₂ H ₄	103
4.2.3	H-Atom Reactions with Ethanethiol: Quantum Yields of H ₂ and H ₂ S.....	115

4.2.4	Relative Rate Parameters for the H-Atom Reactions: Quantum Yields of H ₂ and C ₂ H ₆	119
4.2.5	Disproportionation-Combination Reactions of Thiyl Radicals: Quantum Yield of C ₂ H ₅ SSC ₂ H ₅	132
CHAPTER 5: PHOTOLYSIS OF AND THE REACTIONS OF HYDROGEN ATOMS WITH, ISOPROPANETHIOL.....		137
5.1	Results.....	137
5.1.1	H ₂ S Actinometry.....	137
5.1.2	Photolysis of Pure Isopropanethiol.....	139
5.1.3	Photolysis of Isopropanethiol with Added Thermalizer, n-C ₄ H ₁₀	139
5.1.4	Effect of Temperature on Product Yields.....	142
5.2	Discussion.....	149
5.2.1	Reaction Mechanism.....	149
5.2.2	Quantum Efficiencies of the Primary Photochemical Steps: Quantum Yield of C ₃ H ₆	154
5.2.3	H-Atom Reactions with Isopropanethiol: Quantum Yields of H ₂ and H ₂ S.....	164
5.2.4	Relative Rate Parameters for the H-Atom Reactions: Quantum Yields of H ₂ and C ₃ H ₈	167
5.2.5	Disproportionation-Combination Reactions of Thiyl Radicals: Quantum Yield of (i-C ₃ H ₇) ₂ S ₂	176
CHAPTER 6: PHOTOLYSIS OF, AND THE REACTIONS OF HYDROGEN ATOMS WITH, t-BUTANETHIOL.....		182
6.1	Results.....	182
6.1.1	H ₂ S Actinometry.....	182
6.1.2	Photolysis of Pure t-Butanethiol.....	184
6.1.3	Photolysis of t-Butanethiol with Added Thermalizer, C ₂ H ₆	187

6.1.4	Effect of Temperature on Product Yields.....	187
6.2	Discussion.....	190
6.2.1	Reaction Mechanism.....	190
6.2.2	Quantum Efficiencies of the Primary Photochemical Steps: Quantum Yield of $i\text{-C}_4\text{H}_8$	201
6.2.3	H-Atom Reactions with t -Butanethiol: Quantum Yields of H_2 and H_2S	209
6.2.4	Relative Rate Parameters for the H-Atom Reactions: Quantum Yields of H_2 and $i\text{-C}_4\text{H}_{10}$	212
6.2.5	Disproportionation-Combination Reactions of Thiyl Radicals: Quantum Yield of $(t\text{-C}_4\text{H}_9)_2\text{S}_2$	220
CHAPTER 7: SUMMARY AND CONCLUSIONS.....		226
BIBLIOGRAPHY.....		240
APPENDIX		
A.	Competitive Quenching Between H_2 and $\text{C}_2\text{H}_5\text{SH}$	255
B.	Determination of I_a from Chemical Actinometry....	257
C.	Competitive Quenching Between Thiol and Added Thermalizer.....	260
D.	Product Quantum Yield Expressions Derived in the Photolysis of Alkane Thiols.....	263

LIST OF TABLES

TABLE	PAGE
1.1 Bond strengths and bond angles for thiols and alcohols.....	4
1.2 Thermodynamic properties of some organosulfur compounds and radicals.....	9
1.3 Rate constants and Arrhenius parameters for the H-atom reactions with thiols.....	26
1.4 Rate parameters for the reaction: RSH + H ₂ S + alkene.....	33
1.5 Rate constants for metathetical reactions of thiy radical.....	44
2.1 GC retention data and operation conditions.....	60
2.2 Sources and purification of thiols.....	63
2.3 Sources and purity of materials used.....	64
3.1 The effect of exposure time on product quantum yields.....	73
3.2 The effect of C ₂ H ₅ SH pressure on product quantum yields.....	77
4.1 The results of chemical actinometry in the photolysis of C ₂ H ₅ SH.....	84
4.2 Product quantum yields in the photolysis of pure C ₂ H ₅ SH.....	86
4.3 Average product quantum yields in the photolysis of pure C ₂ H ₅ SH.....	88
4.4 Product quantum yields in the photolysis of C ₂ H ₅ SH with added thermalizer (CO ₂), T = 25°C....	90
4.5 Product quantum yields in the photolysis of C ₂ H ₅ SH with added thermalizer (CO ₂), T = 80°C....	92
4.6 Product quantum yields in the photolysis of C ₂ H ₅ SH with added thermalizer (CO ₂), T = 120°C...	93
4.7 Product quantum yields in the photolysis of C ₂ H ₅ SH with added thermalizer (CO ₂), T = 150°C...	94
4.8 Product quantum yields at high CO ₂ pressure limits.....	95

4.9	Variations of $[\phi(\text{C}_2\text{H}_4) - \phi_3]^{-1}$ with pressure and temperature.....	111
4.10	Intercepts of the plots in Figure 4.7.....	112
4.11	Quantum yields for the primary photochemical processes.....	113
4.12	Effects of CO_2 pressure and temperature on the values of $[\phi(\text{H}_2) - \delta]/[\phi(\text{H}_2\text{S}) - \phi_3]$	117
4.13	Intercepts of the plots in Figure 4.9 and 4.10..	124
4.14	Temperature dependence of k_7/k_8	125
4.15	Arrhenius parameters for the H-atom reactions...	129
4.16	Derived values of $\frac{k_7 \phi_2}{(k_7+k_8)(1+\alpha P_E)}$	131
4.17	Temperature dependence of k_{13}/k_{12}	134
5.1	The results of chemical actinometry in the photolysis of \underline{i} - $\text{C}_3\text{H}_7\text{SH}$	138
5.2	Product quantum yields in the photolysis of pure \underline{i} - $\text{C}_3\text{H}_7\text{SH}$	140
5.3	Product quantum yields in the photolysis of \underline{i} - $\text{C}_3\text{H}_7\text{SH}$ with added thermalizer (\underline{n} - C_4H_{10}), $T = 25^\circ\text{C}$	143
5.4	Product quantum yields in the photolysis of \underline{i} - $\text{C}_3\text{H}_7\text{SH}$ with added thermalizer (\underline{n} - C_4H_{10}), $T = 65^\circ\text{C}$	145
5.5	Product quantum yields in the photolysis of \underline{i} - $\text{C}_3\text{H}_7\text{SH}$ with added thermalizer (\underline{n} - C_4H_{10}), $T = 105^\circ\text{C}$	146
5.6	Product quantum yields in the photolysis of \underline{i} - $\text{C}_3\text{H}_7\text{SH}$ with added thermalizer (\underline{n} - C_4H_{10}), $T = 145^\circ\text{C}$	147
5.7	Effect of temperature on product quantum yields at high total pressure limits.....	148
5.8	Variations of $[\phi(\text{C}_3\text{H}_6) - \phi_3]^{-1}$ with pressure and temperature.....	160
5.9	Intercepts of the plots in Figure 5.7.....	162
5.10	Quantum yields for the primary photochemical	

processes.....	163
5.11 Effects of n -C ₄ H ₁₀ pressure and temperature on the values of $[\phi(H_2) - \delta]/[\phi(H_2S) - \phi_3]$	165
5.12 Intercepts of the plots in Figure 5.9 and 5.10..	171
5.13 Temperature dependence of k_7/k_8	173
5.14 Derived values of $\frac{k_7 \phi_2}{(k_7+k_8)(1+\alpha P_i)}$	177
5.15 Temperature dependence of k_{13}/k_{12}	179
6.1 The results of chemical actinometry in the photolysis of t -C ₄ H ₉ SH.....	183
6.2 Product quantum yields in the photolysis of pure t -C ₄ H ₉ SH.....	185
6.3 Product quantum yields in the photolysis of t -C ₄ H ₉ SH with added thermalizer (C ₂ H ₆), T = 25°C.....	188
6.4 Product quantum yields in the photolysis of t -C ₄ H ₉ SH with added thermalizer (C ₂ H ₆), T = 65°C.....	191
6.5 Product quantum yields in the photolysis of t -C ₄ H ₉ SH with added thermalizer (C ₂ H ₆), T = 95°C.....	192
6.6 Product quantum yields in the photolysis of t -C ₄ H ₉ SH with added thermalizer (C ₂ H ₆), T = 140°C.....	193
6.7 Effect of temperature on product quantum yields at high total pressure limits.....	194
6.8 Quantum yields for the primary photochemical processes.....	208
6.9 Effects of C ₂ H ₆ pressure and temperature on the values of $[\phi(H_2) - \delta]/[\phi(H_2S) - \phi_3]$	210
6.10 Intercepts of the plots in Figure 6.7 and 6.8...	216
6.11 Temperature dependence of k_7/k_8	217
6.12 Derived values of $\frac{k_7 \phi_2}{(k_7+k_8)(1+\alpha P_t)}$	221

6.13	Temperature dependence of k_{13}/k_{12}	223
7.1	Quantum yields for the primary photochemical processes.....	227
7.2	Variation of k_7/k_8 with temperature.....	229
7.3	Arrhenius parameters for abstraction/displacement reactions by H atoms.....	230
7.4	Rate constants and Arrhenius parameters for the displacement reactions by H atoms.....	232
7.5	Arrhenius parameters for disproportionation/combination reactions of thiyl radicals.....	236

LIST OF FIGURES

FIGURE	PAGE
2.1 The high vacuum system.....	53
2.2 The photolytic assembly.....	54
2.3 The actinometry assembly.....	58
3.1 Product quantum yields as a function of exposure time.....	74
4.1 Product quantum yields <u>versus</u> C ₂ H ₅ SH pressure....	87
4.2 Product quantum yields <u>versus</u> CO ₂ pressure at constant C ₂ H ₅ SH pressure of 10.0 Torr.....	91
4.3 Plots of quantum yield of C ₂ H ₄ as a function of P(CO ₂)/P(C ₂ H ₅ SH).....	104
4.4 Relation between ϕ_3 and the correlation coefficient in the LMS treatment of $[\phi(C_2H_4) - \phi_3]^{-1}$ against CO ₂ pressure.....	106
4.5 Quantum yield of C ₂ H ₄ <u>versus</u> C ₂ H ₅ SH pressure....	107
4.6 $[\phi(C_2H_4) - \phi_3]^{-1}$ <u>versus</u> C ₂ H ₅ SH pressure. The best fitted value of $\phi_3 = 0.010$ was used.....	109
4.7 Plots of $[\phi(C_2H_4) - \phi_3]^{-1}$ as a function of P(CO ₂)/P(C ₂ H ₅ SH). The best fitted value of $\phi_3 = 0.010$ was used.....	110
4.8 Plots of $[\phi(H_2) - \delta]/[\phi(H_2S) - \phi_3]$ as a function of the ratio P(CO ₂)/P(C ₂ H ₅ SH).....	118
4.9 Plots of $\phi(H_2)$ as a function of the reciprocal of CO ₂ concentration at [C ₂ H ₅ SH] = 5.38 x 10 ⁻⁴ M...	120
4.10 Plots of $\phi(C_2H_6)$ as a function of the reciprocal of CO ₂ concentration at [C ₂ H ₅ SH] = 5.38 x 10 ⁻⁴ M.....	121
4.11 Plot of ln k ₇ /k ₈ <u>versus</u> the reciprocal of temperature.....	126,
4.12 Plot of ln k ₁₃ /k ₁₂ <u>versus</u> the reciprocal of temperature.....	136
5.1 Product quantum yields <u>versus</u> i-C ₃ H ₇ SH pressure.....	141
5.2 Product quantum yields <u>versus</u> n-C ₄ H ₁₀ pressure	

	at constant i -C ₃ H ₇ SH pressure of 20.0 Torr.....	144
5.3	Plots of quantum yield of C ₃ H ₆ as a function of P(n -C ₄ H ₁₀)/P(i -C ₃ H ₇ SH).....	155
5.4	Relation between ϕ_3 and the correlation coefficient in the LMS treatment of $[\phi(C_3H_6) - \phi_3]^{-1}$ against n -C ₄ H ₁₀ pressure.....	156
5.5	Quantum yield of C ₃ H ₆ <u>versus</u> i -C ₃ H ₇ SH pressure..	158
5.6	$[\phi(C_3H_6) - \phi_3]^{-1}$ <u>versus</u> i -C ₃ H ₇ SH pressure. The best fitted value of $\phi_3 = 0.009$ was used.....	159
5.7	Plots of $[\phi(C_3H_6) - \phi_3]^{-1}$ as a function of P(n -C ₄ H ₁₀)/P(i -C ₃ H ₇ SH). The best fitted value of $\phi_3 = 0.009$ was used.....	161
5.8	Plots of $[\phi(H_2) - \delta]/[\phi(H_2S) - \phi_3]$ as a function of the ratio P(n -C ₄ H ₁₀)/P(i -C ₃ H ₇ SH).....	166
5.9	Plots of $\phi(H_2)$ as a function of the reciprocal of n -C ₄ H ₁₀ concentration at [i -C ₃ H ₇ SH] = 1.04×10^{-3} M.....	168
5.10	Plots of $\phi(C_3H_8)$ as a function of the reciprocal of n -C ₄ H ₁₀ concentration at [i -C ₃ H ₇ SH] = 1.04×10^{-3} M.....	169
5.11	Plot of $\ln k_7/k_8$ <u>versus</u> the reciprocal of temperature.....	174
5.12	Plot of $\ln k_{13}/k_{12}$ <u>versus</u> the reciprocal of temperature.....	180
6.1	Product quantum yields <u>versus</u> t -C ₄ H ₉ SH pressure.	186
6.2	Product quantum yields <u>versus</u> C ₂ H ₆ pressure at constant t -C ₄ H ₉ SH pressure of 20.0 Torr.....	189
6.3	Plots of quantum yield of i -C ₄ H ₈ as a function of P(C ₂ H ₆)/P(t -C ₄ H ₉ SH).....	202
6.4	Quantum yield of i -C ₄ H ₈ <u>versus</u> t -C ₄ H ₉ SH pressure.....	204
6.5	$[\phi(i-C_4H_8) - \phi_3]^{-1}$ <u>versus</u> t -C ₄ H ₉ SH pressure. The value of $\phi_3 = 0.021$ was used.....	206
6.6	Plots of $[\phi(H_2) - \delta]/[\phi(H_2S) - \phi_3]$ as a function of the ratio P(C ₂ H ₆)/P(t -C ₄ H ₉ SH).....	211
6.7	Plots of $\phi(H_2)$ as a function of the reciprocal of C ₂ H ₆ concentration at [t -C ₄ H ₉ SH]	

	= 1.04×10^{-3} M.....	213
6.8	Plots of $\phi(i-C_4H_{10})$ as a function of the reciprocal of C_2H_6 concentration at [$t-C_4H_9SH$] = 1.04×10^{-3} M.....	214
6.9	Plot of $\ln k_7/k_8$ <u>versus</u> the reciprocal of temperature.....	218
6.10	Plot of $\ln k_{13}/k_{12}$ <u>versus</u> the reciprocal of temperature.....	224
7.1	Empirical correlation between E_a and H for the displacement reactions by H atoms.....	233

CHAPTER ONE

INTRODUCTION

Amongst the many classes of organosulfur compounds, thiols and disulfides have generated considerable theoretical and experimental interest, due to their important roles in a wide range of practical systems. For example, the sulfhydryl and disulfide groups, present in biological systems as amino acids, peptides, proteins and enzymes, have been investigated extensively for their vital functions towards radiative damage, protection and repair.¹⁻³ The S-S and C-S linkage in protein and DNA molecules are highly susceptible to cleavages by free radical attack causing permanent cell damages.^{4,5} It has also been suggested that the process of aging may be due, at least in part, to free-radical reactions.⁶ In view of this, the unraveling of the mechanisms of free-radical production, stabilization and termination presents challenges ahead for investigators in the diverse fields of biology and biochemistry. Over the past two decades, the biological thiol most closely studied is cysteine,⁷⁻¹³ $\text{NH}_2\text{CH}(\text{CO}_2\text{H})\text{CH}_2\text{SH}$, along with the corresponding disulfide, cystine,^{7,14} $[\text{NH}_2\text{CH}(\text{CO}_2\text{H})\text{CH}_2\text{S}]_2$, a major product in the radiolysis of cysteine. Much of recent studies has been centered on the basic radiation chemistry of related thiols such as penicillamine,^{15,16} $\text{HSC}(\text{CH}_3)_2\text{CH}(\text{NH}_2)\text{COOH}$, and 2-mercaptoethanol,¹⁷ $\text{HOCH}_2\text{CH}_2\text{SH}$.

The presence of organically-bound sulfur in heavy oils, bitumen and coal is of increasing concern in the petroleum

industry. During upgrading of light and heavy oils nearly all of the sulfur is removed as H_2S , the remainder winding up in the coke. Combustion of low grade coals may give rise to the evolution of $RS\cdot$ radicals, though¹⁸. Consequently, the emission of sulfur as SO_2 into the environment contributes to the production of acid rain, which is detrimental to many fragile ecosystems. Thiols, sulfides and disulfides are only minor constituents of the total organosulfur content of oils.¹⁹ Most of the sulfur is incorporated into saturated and unsaturated (e.g. thiophenic) ring forms and, in the case of Athabasca bitumen, in the form of sulfide in the side chain substituents. Knowledge of the H-atom reactions with model organosulfur compounds serves to elucidate the reaction mechanism of hydrodesulfurization,²⁰⁻²² a major process in the upgrading of crude oils and coal liquids. The process of sulfur removal is particularly vital in Alberta, where the sulfur contents of the Athabasca and the Cold Lake bitumens are high, ~5%;^{23,24} this leads not only to serious catalytic problems but also to problems in the removal of volatile sulfur-containing components from the effluent gases. In general, H-abstraction reactions involving S-H bonds occur with low activation energies and S-H moieties are highly effective free-radical traps at moderate temperatures. Therefore in coal reactions, thiyl radicals will be particularly effective H-transfer agents.²⁵ Also in another practical area of importance, the polymer industry, relative chain transfer rates in styrene polymeri-

zation provide striking evidence for the effectiveness of thiyl radicals as H-transfer agents in alkylaromatic systems. At 60°C, $n\text{-C}_4\text{H}_9\text{S-H}$ transfers H atoms $10^{4.8}$ and $10^{4.2}$ times faster than $\phi_3\text{C-H}$ and $\phi\text{O-H}$, respectively, even though the S-H bond is stronger than the other two.²⁵

Before embarking on the discussions of the photolysis of thiols, it is appropriate at this point to review the physical and chemical properties of this particular class of organosulfur compounds.

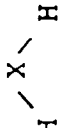

1.1 Physical and Chemical Properties of Thiols

1.1.1 Molecular Parameters of Thiols

As seen in Table 1.1, the S-H and C-S bonds are weaker than the corresponding O-H and C-O bonds and this accounts, in part, for the ease of H-abstraction from S-H, in comparison with that from O-H, and for the greater acidity of the thiols than the alcohols. Also, the bond angles around the sulfur atom are smaller than those around the oxygen atom, indicating greater p-character in the sulfur bond orbitals than in the oxygen bond orbitals. The covalent radius of the sulfur atom is larger than that of oxygen or carbon atoms; the bond lengths^{26,27} are, C-O, 1.45 Å; C-C, 1.53 Å and C-S, 1.82 Å. Similarly, the sulfhydryl bond length, S-H (1.33 Å) is greater than that of O-H (0.96 Å) or C-H (1.09 Å) bonds. In general, thiols have less ability for hydrogen-bonding than the corresponding alcohols. Consequently, they are lower-boiling compounds than their oxygen analogues.

Structural studies for CH_3SH , carried out by electron

Table 1.1. Bond Strengths and Bond Angles for Thiols and Alcohols

	Bond Strength ^a (kcal mol ⁻¹)		Bond Angles ^b (degree)	
	X = S	X = O	X = S	X = O
HX-H	91	119		104.5
Alk ^c X-H	87	104		108
Ph ^c X-H	75	85		
Alk-XH	69	91		
Ph-XH	86	110		

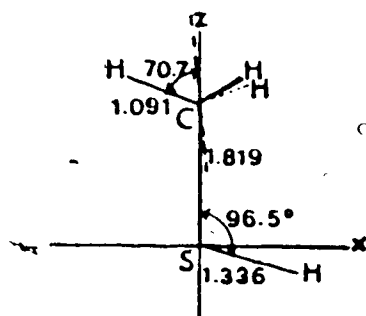
^afrom reference 28

^bfrom reference 29

^cAlk = alkyl group; Ph = benzyl group

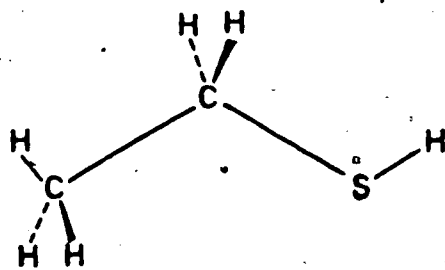
^dfrom reference 32

diffraction,³⁰ microwave spectroscopy,³¹ and ab initio SCF-MO calculations,³² have shown that CH_3SH has the following structure:

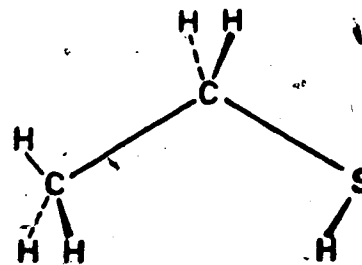


with an angle of $2^\circ 10'$ between the three-fold axis of the methyl group and the C-S bond. In addition, from the microwave work, dipole moments parallel and perpendicular to the molecular axis were determined to be 1.33 D and 0.73 D, respectively, and the height of the barrier to internal rotation about the C-S bond, $\approx 1.27 \text{ kcal mol}^{-1}$.

Microwave³³ and far-IR³⁴ spectroscopic methods have been used for structural studies of $\text{C}_2\text{H}_5\text{SH}$ which exhibits trans-gauche isomerism around the CC-SH bond. It has been found that the bond angle α (CCS) of $\text{C}_2\text{H}_5\text{SH}$ widens sharply on going from the trans form (T-form) to the gauche (G-form):



(T-form)



(G-form)

The experimental data are in good agreement with the predicted theoretical parameters,³⁵ for which α (CCS) = 108.6° (T-form) and α (CCS) = 113.6° (G-form), and the dihedral angle in the G-form, τ (CCSH) = 61.8° .

1.1.2 Spectral Parameters of Thiols

In general the UV spectra of aliphatic thiols show a peak maximum at ~ 195 nm with a shoulder at ~ 230 nm, which are associated with electronic transitions from the non-bonding n orbital (p type) to the antibonding σ^* and π^* orbitals, respectively.^{36,37} For 1-pentanethiol, the shoulder peak has been found to be displaced slightly toward shorter wavelengths, 224 nm.³⁷ The lowest-lying level for CH_3SH has been predicted from emission spectra to be predominantly $3d_s$, followed in order by essentially pure $4s_s$ and degenerate $3d_s$ levels,³⁸ with the observed transition energies, 5.39, 6.08 and 6.75 eV, respectively. These values concur with the theoretically calculated results³² which attribute the weak, broad absorption at 5.39 eV to a valence transition, $3p_y \rightarrow \sigma_{SC}^*$, the broad, structureless absorption at 6.08 eV to $3p_y \rightarrow 4s$, and the third absorption at 6.75 eV to the lowest energy component of the $3p \rightarrow 4p$ excitation manifold.

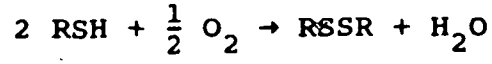
In the IR region,³⁶ thiols exhibit characteristic absorption bands at 2564 cm^{-1} due to an S-H stretching vibration. They also exhibit absorption bands between 820 and 909 cm^{-1} , probably due to C-S-H bending vibrations, and intense C-S stretching bands in the region $645 - 769 \text{ cm}^{-1}$.

The remaining bands in the IR spectra include: rocking vibrations due to CH₃, twisting and wagging vibrations of CH₂ in the usual regions, 735 - 1389 cm⁻¹, and a C-H stretching vibration at 2941 cm⁻¹.

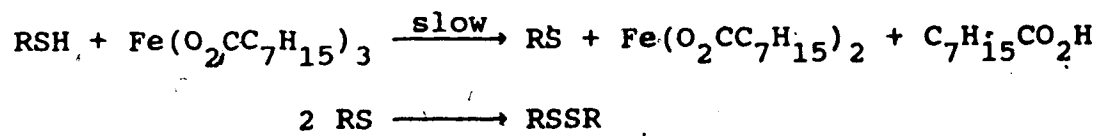
1.1.3 Reactions of Thiols

The chemistry of the thiol group has been subjected to broad and detailed investigations.²⁹ Amongst the possible reactions of thiols, focus has been mainly on the redox reactions, thiol-disulfide thermal exchange reactions, and photochemical reactions.

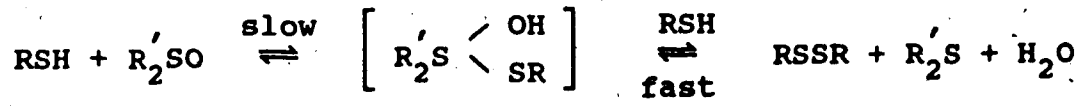
Oxidation of thiols proceeds stepwise to give initially the disulfide, then thiolsulfinic acid and finally sulfonic acid.³⁹ There are several means²⁹ by which thiols are readily oxidized. For example: by air,



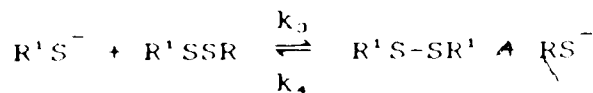
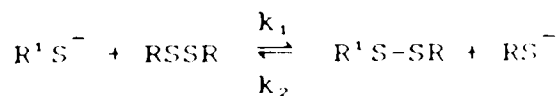
by metal alkoxides,



by organic oxides,



Thiol-disulfide exchange reactions are of greatest biological interest¹ since thiols and disulfides are present together in cells. The rate of the exchange reaction is pH-dependent because the thiol participates in the reaction as RS⁻,



The thermodynamic properties of some organosulfur compounds and radicals are given in Table 1.2, along with those of species relevant to the present investigation.

1.2 Photolysis of Thiols

1.2.1 Photolysis

Thiols have been photolyzed under a wide range of conditions, in rigid glasses at 77K as single crystals, in solution, and in the gas phase.^{40,41} In early investigations⁵⁵⁻⁵⁸ of the photolysis of CH₃SH and C₂H₅SH in the gas phase, hydrogen and disulfide were detected as major products. Their formation appeared to be accountable at the time by a simple reaction mechanism,



(R = CH₃, C₂H₅), suggesting that S-H bond scission is the only important primary photochemical process. Small amounts of hydrocarbons, CH₄ or C₂H₆, were also detected at higher conversions. Inaba and Darwent⁵⁸ also photolyzed CH₃SD and found that the noncondensable gases were D₂ and CH₃SD, thus showing that the reactions

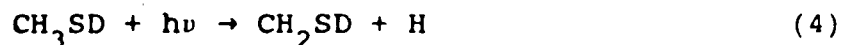


Table 1.2. Thermodynamic Properties of Some Organosulfur Compounds and Radicals

Species	ΔH_f (kcal, mol ⁻¹)	Reference	Bond Strength (kcal mol ⁻¹)	Reference
<u>Thiols</u>				
CH ₃ SH	5.5	45, 48	88.1	44
C ₂ H ₅ SH	-11.0	42, 43, 45, 46	88.6	44, 47
1-C ₃ H ₇ SH	-18.2	42, 43, 46	88.4	44
n-C ₄ H ₉ SH	-21.1	43	88.0	47
1-C ₄ H ₉ SH	-26.2	42, 43, 46	88.6	44
			<u>D (S-H)</u>	
GH ₃ SH			73	47
C ₂ H ₅ SH			71	47
1-C ₃ H ₇ SH			70	47
n-C ₄ H ₉ SH			74 (71)	47
1-C ₄ H ₉ SH			69 (66)	47
			<u>D (C-S)</u>	

.....continued

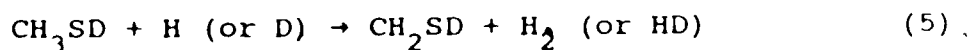
Table 1.2. (Continued)

Species	ΔH_f (kcal mol ⁻¹)	Reference	Species	ΔH_f (kcal mol ⁻¹)	Reference
<u>Disulfides</u>					
(CH ₃) ₂ S ₂	- 5.8	45	D (S-S)		
(C ₂ H ₅) ₂ S ₂	-17.4	46	67	47	47
(i-C ₃ H ₇) ₂ S ₂	-38 ^a		69	47	47
(n-C ₄ H ₉) ₂ S ₂	-44 ^a		Alk-S-S-Alk = 74	45	45
(t-C ₄ H ₉) ₂ S ₂	-52 ^a				
<u>Thiyl Radicals</u>					
HS	35	45, 47, 48	Alkanes		
CH ₃ S	30.5	47	CH ₄	-17.9	48
C ₂ H ₅ S	25.5	47, 48	C ₂ H ₆	-20.2	54
i-C ₃ H ₇ S	18	47	C ₃ H ₈	-25.0	43
n-C ₄ H ₉ S	15	47	n-C ₄ H ₁₀	-30.0	43
t-C ₄ H ₉ S	11	47	i-C ₄ H ₁₀	-32.1	43
				continued

Table 1.2. (Continued)

Species	ΔH_f (kcal mol ⁻¹)	Reference	Species	ΔH_f (kcal mol ⁻¹)	Reference
<u>Alkyl Radicals</u>					
CH ₃	35.1	48	<u>Alkenes</u>		
C ₂ H ₅	25.9 (28.4)	54, (49)	C ₂ H ₄	12.5	48
i-C ₃ H ₇	18 (21)	50, (51)	C ₃ H ₆	4.9	54
n-C ₄ H ₉	16	54	i-C ₄ H ₈	-4.1	53
t-C ₄ H ₉	9.1 (13)	52, (51)			
<u>Others</u>					
H	52.1	54			
H ₂ S	-4.8	45, 46, 48			

^a estimated from $2\Delta H_f(\text{RS}) - D(\text{S-S})$



do not occur to any appreciable extent.

Later, Steer *et al.*⁵⁹ and Dzantiev *et al.*⁶⁰ detected the presence of H_2S amongst the photolysis products of CH_3SH . Its formation was explained by the occurrence of a secondary primary photolysis step, C-S bond cleavage, estimated to occur with a quantum yield of 0.1,⁶⁰



followed by the secondary reactions



However, in subsequent more detailed studies of the photolysis of CH_3SH , Steer and Knight⁶¹ observed that the sum of $\phi(\text{H}_2)$ and $\phi(\text{CH}_4)$ was always greater than unity and therefore suggested that step (6) cannot be occurring in parallel with step (1). Although the authors had considered the displacement step in their study,

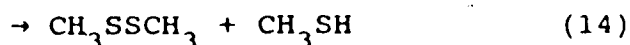


they concluded that (9) accounts for a maximum of 2% of H atoms at room temperature and is significant only at higher temperatures. This was based on the data from the analogous displacement reaction by CH_3 radicals reported by Greig and Thynne,⁶² who had determined relative rate constants for the reactions



and reported $k_{10}/k_{11} = 710$ at 25°C . In order to account for the observation that the CH_4 and H_2S yields decreased with

increasing pressure, Steer and Knight⁶¹ proposed a sequence of reactions involving excited disulfide molecules formed by the recombination of CH_3S^* radicals,



However, it was later shown that (13) and (14) do not occur,⁶³ since neither CH_4 nor H_2S was detected in the photolysis of CH_3SSCH_3 , which produces excited $\text{CH}_3\text{SSCH}_3^*$ molecules via (12), in the presence of CH_3SH .

The formation of hot H atoms was considered by both the Steer and Knight⁶⁴ and Sturm and White⁶⁵ groups, based on their observations that the H_2 yields were reduced significantly in the presence of high thermalizer (CO_2 , He and Ne) pressures. Consequently, White and coworkers^{63,66} included hot H atoms in their proposed reaction mechanism,



The second primary step (6) was suggested by the authors to be wavelength-dependent, from the observation that the CH_4

and H_2S yields obtained at high thermalizer pressures increased when the wavelength was changed from 254 to 214 nm. Although the metathetical displacement reaction step (16) by hot H atoms was considered as another H_2S -producing step in the mechanism, that by thermal H atoms, step (9), was not considered to take place at a measurable rate.

The gas-phase photolysis of C_2H_5SH at 254 nm was also investigated in detail by Steer and Knight⁶⁷ (SK) and by Bridges, Hemphill and White⁶³ (BHW). Both groups, SK and BHW, obtained H_2 and $C_2H_5SSC_2H_5$ as the major photolysis products and smaller amounts of H_2S , C_2H_6 and C_2H_4 , but the product yields and their pressure dependence, and also the kinetic interpretations differed in several areas. SK proposed only one primary step,



from the observation that the H_2 yield is close to unity.

The ensuing processes deemed important were:

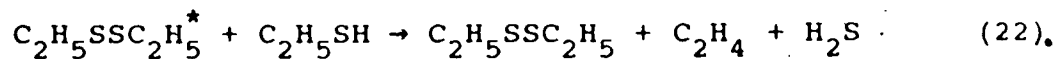


It was concluded that the reaction



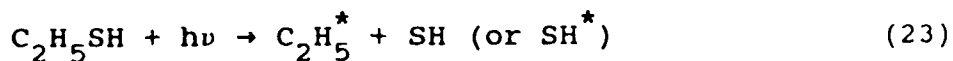
did not occur since products from (21) were not detected even at long exposure times. The minor products, H_2S and C_2H_6 , were accounted for by a molecular sensitization scheme analogous to that for the photolysis of CH_3SH , *i.e.* reaction steps (12) - (14), (7) - (8). The alkene product, C_2H_4 , was

also believed to be formed from the sensitized decomposition reaction,



However, as mentioned above, this scheme was later questioned by White and coworkers.^{63,66}

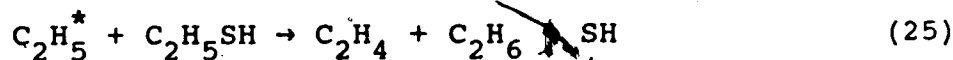
In turn, BHW proposed a reaction mechanism slightly different than SK's, for the photolysis of $\text{C}_2\text{H}_5\text{SH}$. Along with the scission of the S-H bond in the primary step (18), BHW included two additional ones, one involving cleavage of the C-S bond to form hot radicals,



while the other is a molecular process,



introduced to account for the H_2S and C_2H_4 yields at high thermalizer pressures. In contrast to the step (22) proposed by SK, BHW introduced one involving hot ethyl radicals,



to account for the formation of C_2H_4 . The remaining steps in the reaction mechanism proposed by BHW for the photolysis of $\text{C}_2\text{H}_5\text{SH}$ are analogous to those proposed for CH_3SH .

In all the gas-phase photochemical studies of thiols, the isoenergetic reaction,



was suggested for the decay of SH radicals and also as another H_2S -producing step. Yet, the metathetical displacement reaction by thermal H atoms,



analogous to other radical reactions with organosulfur compounds,⁶⁸ was not included in the overall mechanism. White and coworkers⁶⁶ have suggested that the H atom must possess excess translational energy in order for (27) to occur. If this is correct, then photolysis in the liquid phase, where H atoms generated from (1) are rapidly thermalized, should result in smaller H₂S and alkane yields relative to that in the gas phase, provided that the other primary step,



is occurring, otherwise, neither products (H₂S and alkane) would be observed if (1) is the sole primary step.

In the liquid-phase photolysis of C₂H₅SH at 254 nm, Carlson and Knight⁶⁹ detected only H₂ and C₂H₅SSC₂H₅ as products and this is in apparent agreement with White and coworkers' suggestion above. However, in later developments, Pryor and Olsen⁷⁰ studied the photolyses of *t*-butanethiol, cyclohexanethiol and thiophenol in the liquid phase and found that H₂S is a product, along with H₂, alkanes and disulfides. The H₂/H₂S ratios at 25°C were: 1.45 (*t*-butanethiol), 4.35 (cyclohexanethiol) and 5.88 (thiophenol). Since the yield of H₂ increased and that of H₂S decreased with increasing concentration of inert hydrogen donors, QH, and the H₂/H₂S ratios were a linear function of [QH]/[RSH], the authors concluded that the displacement reaction (27), and not the C-S cleavage in the primary step

(28), is the important H₂S-producing step in the mechanism. Direct evidence for the occurrence of (27) was also established in the photolysis of *t*-butylperoxyformate at 350 nm in the presence of *t*-C₄H₉SH (which does not absorb at this wavelength), from which H₂ and H₂S were both products, formed in the ratio 1.41 at 25°C. Thus, a general mechanism for the liquid-phase photolysis of thiols at λ = 254 nm would feature the following reaction steps:



On the other hand, for the gas-phase photolysis of thiols, where hot H atoms are formed, two additional reactions analogous to (2) and (27), i.e.



would also be included in the overall reaction mechanism.

1.2.2 Hydrogen Atom Reactions

1.2.2.1 Generation of H atoms

Chemical reactions of H atoms in the gas phase has been reviewed recently.⁷¹ In particular, those with organosulfur compounds have recently been compiled and evaluated.⁷² The many methods developed for the generation of thermal H atoms for kinetic studies include: radio-frequency and high-frequency microwave discharge, Hg(³P₁) photosensitized

decomposition of H_2 , radiolysis and shock-tube methods. On the other hand, photolysis of HBr , HI , H_2S , and, to a lesser extent, alkanethiols, is a good source of H atom with excess kinetic energy and consequently requires large amounts of moderating gases in the thermalization. The importance of the chemistry of hot H atoms has only been widely recognized since the mid-1960s.⁷³ The subject of energy transfer in hot H atoms during non-reactive and reactive collisions remains elusive, especially when more dissociative channels become available as potential surfaces of higher energies are reached.⁷⁴

1.2.2.2 Abstraction / Displacement

Much of the early kinetic data on the $H + CH_3SH$ reaction was derived from the mechanistic investigations of photolysis studies. Inaba and Darwent⁵⁸ photolyzed CH_3SH at 254 nm in the presence of C_2H_4 to study the relative rates of H -scavenging by CH_3SH



and by C_2H_4



From these competing experiments, the values derived for k_2/k_{30} were: 1.7 ($50^\circ C$), 2.0 ($120^\circ C$), and 2.22 ($220^\circ C$), from which the average value $(E_2 - E_{30}) = 0.54 \text{ kcal mol}^{-1}$ was obtained.

Kuntz⁷⁵ also photolyzed a series of alkanethiols in the gas phase at 254 nm in the presence of scavenger C_2H_4 to determine the effect of substituents on the rate of H atom

removal from the thiol group. The presence of hot H atoms was suggested, based on the observation that the ratios remain constant over the low pressure range, then decrease rapidly after a few cm of pressure. The values of k_2/k_{30} determined in the pressure-independent region are: CH_3SH , 1.7, $\text{C}_2\text{H}_5\text{SH}$, 1.9, $n\text{-C}_3\text{H}_7\text{SH}$, 3.2, and $n\text{-C}_4\text{H}_9\text{SH}$, 3.7, showing the increase in lability of the sulfhydryl H with increasing alkyl substitution on the S atom.

Additional evidence for the occurrence of hot H-atom reactions was provided by the results of Steer and Knight,^{59,61,64} who at first reported a different k_2/k_{30} value of 2.32, but later found that it decreases to 1.15 at very high pressures of added CO_2 , reflecting thermal H-atom reactions. The displacement step



was not considered in the overall mechanism.⁶¹ Since step (9) has been established by Pryor and Olsen⁷⁰, as noted earlier, to be important, the ratio k_2/k_{30} is actually

$$\frac{k_2}{k_{30} + k_9} \quad \text{Thus,}$$

$$\frac{1}{1.15} = \frac{k_{30}}{k_2} + \frac{k_9}{k_2}$$

The displacement/abstraction ratio, k_9/k_2 , can be estimated from the $\text{C}_2\text{H}_6/\text{H}_2$ ratio of 0.13,⁶⁷ obtained for the photolysis of $\text{C}_2\text{H}_5\text{SH}$ at 25°C and high CO_2 pressure, giving the corrected k_2/k_{30} value of 1.35. Using the absolute rate constant for (30) reported by Lee *et al.*,⁷⁶ $k_{30} = 6.61 \times$

$10^{11} \text{ cm}^3 \text{ mol}^{-1} \text{ s}^{-1}$ at 25°C , it follows therefore that $k_2 = 8.92 \times 10^{11}$, and $k_9 = 1.16 \times 10^{11} \text{ cm}^3 \text{ mol}^{-1} \text{ s}^{-1}$.

Direct determination of the rate constant for the $\text{H} + \text{CH}_3\text{SH}$ reaction was made by Amano *et al.*⁷⁷ in a discharge flow system. They found H_2S , C_2H_6 and C_2H_4 as major products, with smaller amounts of CH_3SCH_3 and CH_3SSCH_3 . The rate constants for (2) and (9) were derived by an optimization procedure to be $k_2 = 2.9 \times 10^{13} \exp(-2600/RT)$ and $k_9 = 0.69 \times 10^{13} \exp(-1670/RT) \text{ cm}^3 \text{ mol}^{-1} \text{ s}^{-1}$. At 25°C , $k_2/k_9 = 0.9$, which is at variance with the earlier results of Steer and Knight⁶⁷ and Pryor and Olsen.⁷⁰

Recently, other values for k_2 were reported: $2.5 \times 10^{11} \text{ cm}^3 \text{ mol}^{-1} \text{ s}^{-1}$, by Balla and Heicklen,⁷⁸ based on the photolysis of CH_3SH at 254 nm in the presence of NO; and $2.08 \times 10^{13} \exp(-1679/RT) \text{ cm}^3 \text{ mol}^{-1} \text{ s}^{-1}$, by Wine *et al.*,⁷⁹ based on the 248 nm pulsed-laser photolysis of CH_3SH . Unfortunately, neither group had included the displacement reaction (9) in the overall mechanism and therefore these values refer only to the total rate of reaction.

Much of the information on the $\text{H} + \text{C}_2\text{H}_5\text{SH}$ reaction was also derived from photolysis studies. Steer and Knight⁶⁷ reported that k_{19}/k_{30} , where k_{19} refers to



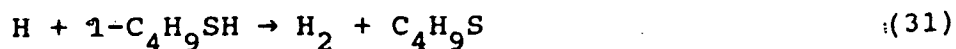
decreased from 2.03 to 1.05 under high CO_2 pressure. In a manner similar to the photolysis of CH_3SH , k_{19}/k_{30} should be corrected for the displacement reaction,



hence $\frac{k_{19}}{k_{30} + k_{27}} = 1.05$. Since $k_{27}/k_{19} = 0.13$, it follows

that $k_{19}/k_{30} = 1.20$. Since $k_{30} = 6.61 \times 10^{11} \text{ cm}^3 \text{ mol}^{-1} \text{ s}^{-1}$, k_{19} is therefore 7.93×10^{11} , and $k_{27} = 1.03 \times 10^{10} \text{ cm}^3 \text{ mol}^{-1} \text{ s}^{-1}$.

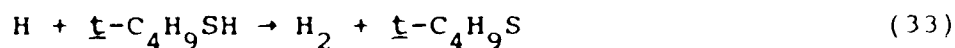
The $\text{H} + 1\text{-C}_4\text{H}_9\text{SH}$ reactions were investigated by Horie *et al.*⁸⁰ at 295 and 576K using the discharge method. The major products were *n*-butane, 1-butene and H_2S , while the minor products were propylene, propane, ethylene, ethane and methane. At 576K, however, the relative yield of *n*-butene was much greater, and that of *n*-butane was much smaller, than the corresponding yields at 295K, and the 1-butene yield decreased much more drastically with increasing conversion. Using numerical integration in the kinetic analysis, the rate constants were derived for the following initial H-atom reaction steps,



$k_{31} = 1.3 \times 10^{13} \exp(-3180/RT)$ and $k_{32} = 1.6 \times 10^{12} \exp(-2223/RT) \text{ cm}^3 \text{ mol}^{-1} \text{ s}^{-1}$. At 25°C, $k_{31}/k_{32} = 1.6$, indicating that the displacement reaction is slower than the abstraction, as expected. The activation energy value, 3.18 kcal mol⁻¹, for the $\text{H} + 1\text{-C}_4\text{H}_9\text{SH}$ abstraction reaction is higher than that for the $\text{H} + \text{CH}_3\text{SH}$ reaction, 1.68 - 2.60 kcal mol⁻¹. In view of the fact that the S-H bond energies in the alkanethiols are the same, this is somewhat

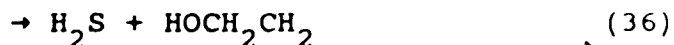
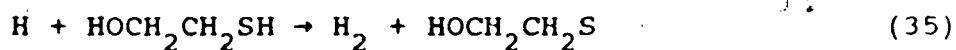
surprising.

The effect of molecular structure on the rate of H-atom scavenging by thiols was investigated by Severs *et al.*,⁸¹ who irradiated aqueous solutions of primary, secondary and tertiary butanethiols. The following rate constant ratios for the abstraction/displacement reactions were obtained: 4.2 (primary), 1.8 (secondary), and 0.8 (tertiary), reflecting a trend corresponding to the C-S bond strength. In contrast, different rate constant ratios were reported by Pryor and Olsen:⁷⁰ 4.4 (cyclohexanethiol) and 1.5 (t-butanethiol). From the measurements of the H₂/H₂S ratio at 298K and 314K which correspond to the following H + t-C₄H₉SH reactions:



the parameters, $k_{33} = 3.2 \times 10^{11} \text{ cm}^3 \text{ mol}^{-1} \text{ s}^{-1}$ and $(E_{34} - E_{33}) = 3.8 \pm 0.3 \text{ kcal mol}^{-1}$ were derived.

The liquid-phase reaction of H atoms with 2-mercaptoethanol was studied by Jayson *et al.*⁸³. H atoms, generated by the pulse radiolysis of H₂O, react with 2-mercaptoethanol in the primary reactions:



At 25°C, $k_{35} = (1.7 \pm 0.2) \times 10^{12}$ and $k_{36} = (3.3 \pm 0.4) \times 10^{11} \text{ cm}^3 \text{ mol}^{-1} \text{ s}^{-1}$ were reported, thus $k_{35}/k_{36} = 5.2$. This is in agreement with the later results of Lal and Armstrong¹⁷ who obtained the value of 5 at pH = 0.5.

In the realm of H atom reactions with biological thiols, cysteine has received the most attention. Littman *et al.*⁸³ generated H atoms by electrical discharge and attributed the formation of the disulfide, cystine, and the H₂S products to the following initial reactions:



where Cy = HOOCCH(NH₂)CH₂. Apparently, attack on the amino group does not occur. In acidic or neutral solutions, disulfide was the major and H₂S, the minor product. However, the relative product yields are reversed in alkaline solutions, due to the ionization of the thiol group:



and the replacement of reactions (68) to (70) by:



From the measurement of product yields from the γ -irradiation of aqueous solution of cysteine and cystine, under various experimental conditions, Markakis and Tappel⁷ suggested that (68) was the major primary step and that (69) and (70), with (69) occurring faster than (70), also took place to a lesser extent.

Navon and Stein⁸⁴ studied the H + cysteine reaction in aqueous solutions at pH = 6, by generating the H atoms from electrical discharge in H₂. From the rate of disappearance of cystine, they derived the rate constant, $k_{68} = 1.0 \times 10^{12} \text{ cm}^3 \text{ mol}^{-1} \text{ s}^{-1}$, and from the rate of H₂S formation,

they estimated that the rate of the displacement reaction (69), was one-fifth that of the abstraction reaction (68).

Support for the mechanism postulated earlier, steps (68) to (70), was provided by the experimental results obtained in the γ -radiolysis of aqueous cysteine solutions. At pH = 0 and 1°C, Armstrong and coworkers^{11,12} estimated that the rate constant ratio k_{68}/k_{69} was 8.6, from the H₂ and H₂S yields and from the material balance. A smaller k_{68}/k_{69} value of 3.5 was reported at 23°C, indicating that the activation energy for (69) is much higher than that for (68). Similar results obtained by Al-Thannon *et al.*⁸ at pH = 0.5 and 1.0 also lent support to the occurrence of reactions (68) - (70).

The rate constant for (68) was also obtained by Neta and Schuler,⁸⁵ who monitored the H-atom concentrations by ESR during the radiolysis of aqueous solution of cysteine and cystine at pH = 1.0. Thus, $k_{68} = 4.0 \times 10^{12} \text{ cm}^3 \text{ mol}^{-1} \text{ s}^{-1}$, but does not include the displacement reaction (69). On the other hand, Tung and Kuntz¹⁰ determined the rate constant for both (68) and (69) by utilizing allyl alcohol as an H-atom scavenger in the γ -irradiated aqueous cysteine solutions at pH = 1.0. The values for the rate constants are: $k_{68} = (1.3 \pm 0.1) \times 10^{12}$ and $k_{69} = (2.5 \pm 0.4) \times 10^{11} \text{ cm}^3 \text{ mol}^{-1} \text{ s}^{-1}$, from which $k_{68}/k_{69} = 5.2$ at 24°C, in good agreement with the value reported by Armstrong and coworkers.^{11,12} In the liquid-phase photolysis of cysteine, Wu and Kuntz⁹ observed that the total rate constants, $k_{68} +$

k_{69} , increased slightly on going from pH = 1.0 to 6.0, from 1.69×10^{12} to $2.25 \times 10^{12} \text{ cm}^3 \text{ mol}^{-1} \text{ s}^{-1}$.

The liquid-phase reactions of H atoms with cysteine are the same as those postulated for another biological thiol, penicillamine, $\text{HS-C}(\text{CH}_3)_2\text{CH}(\text{NH}_2)\text{CO}_2\text{H}$. In the γ -radiolysis of penicillamine, Goyal and Armstrong^{15,16} observed from the $\text{H}_2/\text{H}_2\text{S}$ yields that the rate constant ratio, k_{68}/k_{69} , was much smaller, 0.5 at pH = 0 and 1.3 at pH = 5, than that obtained for cysteine, which is ~5. This difference is probably due to the lower C-S bond energy in the tertiary ~~sulphydryl~~ compound, which aids the displacement reaction (69).

The rate constants and Arrhenius parameters for the H-atom reactions with thiols available in the literature to date are summarized in Table 1.3.

1.3 Thermolysis of Thiols

Contrary to the photolysis of thiols, only meager data are available on the thermal decomposition of thiols. Until recently, the thermal chemistry of thiols has been investigated solely with regard to the kinetics of the disappearance of the initial thiol, with limited characterization of the ensuing reaction products. Even then, the mechanisms of thermal decomposition of thiols has yet to be reconciled. Early investigations⁸⁶⁻⁸⁸ reported H_2S and alkenes as predominant products. However, the reaction mixture was frequently complicated by the presence of elemental sulfur, sulfides, disulfides and lower molecular weight hydro-

Table 1.3. Rate Constants and Arrhenius Parameters
for the H Atom Reactions with Thiols

Reaction	k_{298} ($\text{cm}^3 \text{ mol}^{-1} \text{ s}^{-1}$)	A	E (kcal mol^{-1})	Method	Reference
H + CH ₃ SH → H ₂ + CH ₃ S	8.9 × 10 ¹¹			relative	64
	3.7 × 10 ¹¹	2.9 × 10 ¹³	2.60	discharge	77
	2.5 × 10 ¹¹ a			photolysis	78
	1.2 × 10 ¹² a	2.1 × 10 ¹³	1.68	photolysis	79
H + CH ₃ SH → H ₂ S + CH ₃	1.2 × 10 ¹¹			relative	64
	4.1 × 10 ¹¹	6.9 × 10 ¹²	1.67	discharge	77
H + C ₂ H ₅ SH → H ₂ + C ₂ H ₅ S	7.9 × 10 ¹¹			relative	67
H + C ₂ H ₅ SH → H ₂ S + C ₂ H ₅	1.0 × 10 ¹¹			relative	67
H + 1-C ₄ H ₉ SH → H ₂ + C ₄ H ₉ S	6.0 × 10 ¹⁰	1.3 × 10 ¹³	3.18	discharge	80
H + 1-C ₄ H ₉ SH → H ₂ S + C ₄ H ₉	3.7 × 10 ¹⁰	1.6 × 10 ¹²	2.22	discharge	80
H + <u>1</u> -C ₄ H ₉ SH → H ₂ + <u>1</u> -C ₄ H ₉ S	3.2 × 10 ¹¹			photolysis	70

....continued

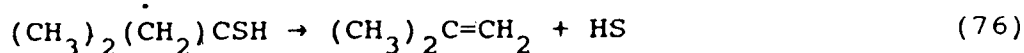
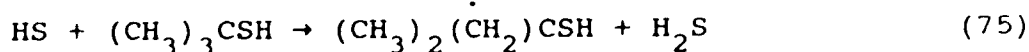
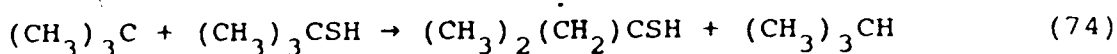
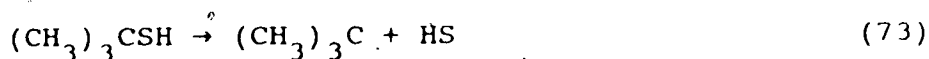
Table 1.3. (Continued)

Reaction	k_{298} ($\text{cm}^3 \text{mol}^{-1} \text{s}^{-1}$)	A	E (kcal mol^{-1})	Method	Reference
$\text{H} + \text{HOCH}_2\text{CH}_2\text{SH} \rightarrow \text{H}_2 + \text{HOCH}_2\text{CH}_2\text{S}$	1.7×10^{12}			radiolysis	82
$\text{H} + \text{HOCH}_2\text{CH}_2\text{SH} \rightarrow \text{H}_2\text{S} + \text{HOCH}_2\text{CH}_2$	3.3×10^{11}			radiolysis	82
$\text{H} + \text{CYS}^{\text{b}} \rightarrow \text{H}_2 + \text{CYS}$	1.0×10^{12} a			discharge	84
	4.0×10^{12} a			radiolysis	85
	1.3×10^{12}			radiolysis	10
$\text{H} + \text{CYS} \rightarrow \text{H}_2\text{S} + \text{CY}$	2.5×10^{11}			radiolysis	10

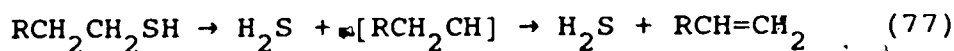
^athe displacement reaction is not included

^bCY = $\text{HOOCCH}(\text{NH}_2)\text{CH}_2$

carbons. As well, an understanding of the reaction mechanism has been hindered by the dependence of the product mixture on reaction conditions and structure of the thiol.^{86,89,90} For example, Thompson *et al.*⁸⁶ thermally decomposed *t*-C₄H₉SH from 300 to 500°C using a flow system in the presence of large amounts of toluene as a carrier gas and a free radical trap. They found H₂S, *i*-C₄H₁₀ and *i*-C₄H₈ as major decomposition products and subsequently proposed a free-radical chain-type mechanism to account for their formation:



On the other hand, a 1,1-elimination of H₂S from 1-pentanethiol⁸⁷



was proposed to account for the difference in reactivities between the primary and tertiary alkanethiols. Alternatively, a concerted 1,2-elimination of H₂S from the thiol to form the alkene product was suggested by Sehon and Darwent⁸⁸ for the thermal decomposition of C₂H₅SH



The authors also found that methanethiol, ethanethiol and phenylmethanethiol decomposed by a homogeneous first-order free-radical process analogous to step (73). Since the

activation energy for (78) was estimated to be 55 kcal mol⁻¹, which is lower than the C-S bond energy of 63.5 kcal mol⁻¹ determined for C₂H₅SH, the elimination reaction was the favoured process in the thermal decomposition of thiols. However, this is in disagreement with the theoretical results of Baldrige *et al.*,²⁷ who carried out *ab initio* SCF-MO calculations for the initial steps in the decompositions of CH₃SH and C₂H₅SH and in both cases, obtained higher activation energies for the H₂S-elimination reaction, namely, 108.3 and 76.9 kcal mol⁻¹, respectively.

The kinetics of the thermal decomposition of butanethiols were recently investigated by Tsang,⁸⁹ Bamkole⁹⁰ and Amano and coworkers^{92,93} under different reaction conditions. Tsang⁸⁹ used a single-pulse shock tube technique to study the thermal decomposition of *t*-C₄H₉SH over the temperature range 670 - 960°C. The radical process, (73), was completely inhibited by adding excess amounts of propylene to the system and thus, under these conditions, the decomposition proceeded solely *via* a four-centered unimolecular elimination reaction,



The rate expression for (79) was then determined to be:

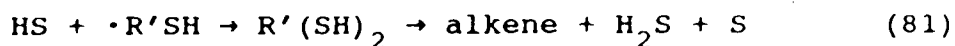
$$k_{79} = 2 \times 10^{13} \exp(-55000/RT) \text{ s}^{-1}.$$

In contrast, Bamkole⁹⁰ used a static system to study the pyrolyses of primary, secondary and tertiary butanethiols in the presence of cyclohexene. The products were shown to be essentially H₂S and the corresponding alkenes. They were

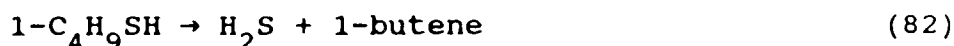
accounted for by a homogeneous free-radical mechanism which is consistent with the one proposed by Thompson *et al.*,⁸⁶ steps (73) to (76). However, the mechanism is complicated by the introduction of an additional terminating step for the case \underline{t} -C₄H₉SH,



and, for 1-C₄H₉SH and 2-C₄H₉SH,



By applying the initial rates method to the reaction immediately following the end of the induction period, Bamkole claimed that the orders of reactions were 3/2 for \underline{t} -C₄H₉SH,⁸ and one for both 1-C₄H₉SH and 2-C₄H₉SH. The following Arrhenius parameters were determined for the overall decomposition of butanethiols in the temperature range 425 - 490°C:



$$k_{82} = 6.9 \times 10^9 \exp(-42570/RT) \text{ s}^{-1};$$



$$k_{83} = 4.9 \times 10^8 \exp(-41730/RT) \text{ s}^{-1}; \text{ (the butene mixture from (83) consisted of: 1-butene, -17\%; cis-2-butene, -38\% and trans-2-butene, -45\%); and } (k_{79})^{1.5} = 1.2 \times 10^{12} \exp(-40580/RT) \text{ cm}^{1.5} \text{ mol}^{-0.5} \text{ s}^{-1}.$$

The difference in the results of Tsang⁸⁹ and Bamkole⁹⁰ on the decomposition of \underline{t} -C₄H₉SH was postulated to be due to temperature effects. Indeed, this is in apparent agreement with the results of Martin and Barroeta⁹¹ who observed that in the gas-phase thermolysis of ditertiary butylsulfide,

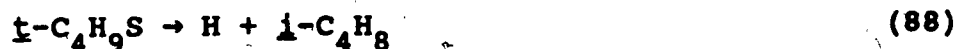
$t\text{-C}_4\text{H}_9\text{SH}$ is a major initial product but decomposes rapidly above 380°C to $i\text{-C}_4\text{H}_8$ and H_2S unless the inhibitor cyclohexene was present.

The thermal decomposition of butanethiols was investigated by Amano and coworkers^{92,93} using a low-pressure pyrolysis method at temperatures above 625°C . The distinctive feature of this method, as compared with the high-pressure pyrolysis method, is the formation of lower molecular weight alkenes as additional major products. For $1\text{-C}_4\text{H}_9\text{SH}$,⁹² the following mechanism was proposed to account for the formation of C_2H_4 , 1-butene and H_2S :



The activation energy for (84) at 0 K was obtained from RRKM calculation to be $67 - 69 \text{ kcal mol}^{-1}$, which corresponds to the C-S bond energy.

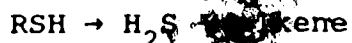
An analogous mechanism was proposed for the decomposition of $2\text{-C}_4\text{H}_9\text{SH}$ ⁹³ above 625°C , where the products included propylene, methane, H_2S and butenes. For $t\text{-C}_4\text{H}_9\text{SH}$,⁹³ no differentiation was made experimentally for the formation of $i\text{-C}_4\text{H}_8$ from both the H_2S -elimination step (79) and the unimolecular decomposition of the t -butyl radical:



Amano and coworkers^{92,93} concluded that butanethiols

decomposed through two pathways, namely, C-S bond cleavage, a radical process, and H₂S-elimination, a molecular process. The ratio of the two reactions appears to be dependent on molecular structure, with the proportion of H₂S-elimination increasing in the order primary < secondary < tertiary butanethiols. This is in the same order as H₂O-elimination in the pyrolysis of alcohols and HX-elimination in the pyrolysis of alkyl halides.

The rate parameters for the reaction,



are listed in Table 1.4 for some of the alkanethiols.

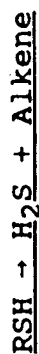
1.4 Thiyl Radicals

1.4.1 Physical and Spectral Properties

Thiyl radicals are stable and easy to generate, either from the direct and the Hg(³P₁) sensitized photolysis of thiols, sulfides and disulfides, or from the thermolysis of sulfides and disulfides. Information on the nature of the thiyl radicals has been obtained from ESR and optical spectroscopies, kinetic techniques and product analysis.

The spectral characteristics of several thiyl radicals have already been tabulated by Ekwenchi.⁹⁴ The UV spectra are commonly obtained upon irradiation of thiols, sulfides and disulfides in either rigid glass or neat matrices at 77K. Yet, there is considerable uncertainty in the precise assignment of absorption bands in these low-temperature spectra. Recently, the characteristic absorption band at

Table 1.4. Rate Parameters for the Reaction:



Reaction	Process	k_{298} (s^{-1})	A	E (kcal mol^{-1})	Method	Ref.
$\text{CH}_3\text{SH} \rightarrow \text{H}_2\text{S} + \text{CH}_2$	molecular ^a			108.3	theoretical	27
$\text{C}_2\text{H}_5\text{SH} \rightarrow \text{H}_2\text{S} + \text{C}_2\text{H}_4$	molecular			55.0	flow	88
$\text{1-C}_4\text{H}_9\text{SH} \rightarrow \text{H}_2\text{S} + \text{C}_4\text{H}_8$	radical ^b	3.9×10^{-22}	6.9×10^9	42.6	static	90
$\text{2-C}_4\text{H}_9\text{SH} \rightarrow \text{H}_2\text{S} + \text{butenes}$	radical	1.3×10^{-22}	4.9×10^8	41.7	static	90
$\text{1-C}_4\text{H}_9\text{SH} \rightarrow \text{H}_2\text{S} + \text{1-C}_4\text{H}_8$	molecular	9.1×10^{-28}	2.0×10^{13}	55.0	shock-tube	89
	radical	1.2×10^9 c	1.2×10^{12} c	40.1	static	90

^aH₂S-elimination

^bC-S bond cleavage

Overall order of reaction is 3/2, k in units of $\text{cm}^{1.5} \text{mol}^{-0.5} \text{s}^{-1}$

300 nm has been assigned to simple alkylthiyl (RS) radicals,^{95,96} and that at 400 - 420 nm to the formation of the thiol adduct, RSS(H)R, in glassy matrices at 77K.⁹⁷ In contrast, the lowest gas-phase UV absorption band for CH₃S radicals has been reported to be located at 218.5 nm.^{98,99}

The asymmetric ESR spectra of irradiated thiols¹⁰⁰⁻¹⁰³ give three characteristic g-values, $g_{XX} \approx 2.06$, $g_{YY} \approx 2.025$ and $g_{ZZ} \approx 2.000$, which were attributed to alkylthiyl radicals. Recently, however, it has been suggested that the ESR spectra of thiyl radicals cannot be observed due to the degeneracy of p-orbital of the S-atom¹⁰⁴ and that the g-values assigned to the RS radicals before are actually due to the perthiyl radicals, RS₂¹⁰⁵ or the adduct RSS(H)R.^{97,106}

1.4.2 Reactions of Thiyl Radicals

Thiyl radicals undergo reactions which are similar to alkyl radicals, namely, disproportionation, combination, abstraction, addition and metathetical reactions. More kinetic data have become available since knowledge of the reactivities of alkylthiyl radicals is necessary in order to develop accurate models for both atmospheric and combustion chemistry. For example, the gas-phase reactions of CH₃S with O₂, NO and NO₂ have been thoroughly reviewed recently by Heicklen.¹⁰⁷

1.4.2.1 Disproportionation / Combination

Thiyl radicals, generated from the photolysis or

thermolysis of thiols, alkylsulfides and disulfides, will disproportionate or combine:

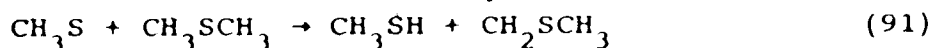


The disproportionation/combination ratio, k_{89}/k_{90} , can be calculated from the relative yields of thiols and disulfides. For CH_3S , the value $k_{89}/k_{90} = 0.05 - 0.11$, has been derived from the Hg-photosensitized decomposition of CH_3SCH_3 ,^{108,109} and from the reaction of H atoms, generated by the Hg(³P₁) sensitization of H₂, with CH_3SSCH_3 .¹¹⁰ From UV spectra,⁹⁹ the absorption band at 211.7 nm has been assigned to the disproportionation product, thioformaldehyde, based largely on chemical evidence. For C_2H_5S , $k_{89}/k_{90} = 0.13$ was also derived from the Hg-photosensitized decomposition of $C_2H_5SC_2H_5$.¹¹¹ The small k_{89}/k_{90} values for thiyl radicals are in contrast to those for the alkoxy analogs, e.g. $k_{89}/k_{90} = 9.3$ for CH_3O and 12.0 for C_2H_5O radicals.¹¹² This can be explained by the fact that organosulfur compounds do not readily undergo transformations in which the C-S single bonds are converted to double bonds, whereas their oxygen analogs do, due to the greater enthalpy change of the conversion $C-O \rightarrow C=O$ compared to that of $C-S \rightarrow C=S$.

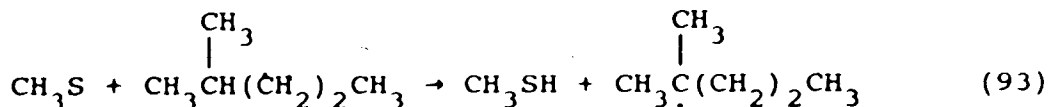
The rate constant for the combination of CH_3S radicals is $2.4 \times 10^{13} \text{ cm}^3 \text{ mol}^{-1} \text{ s}^{-1}$,¹⁰⁹ which is close to the value of $2.5 \times 10^{13} \text{ cm}^3 \text{ mol}^{-1} \text{ s}^{-1}$,¹¹³ reported for CH_3 radicals.

1.4.2.2 Abstraction

The occurrence of H-abstraction by thiyl radicals from sulfides and disulfides is evident from gas-phase thermolysis¹¹⁶ and photolysis^{108,111,114,115} experiments, where thiols are the major products. For CH_3S radicals, the following H-abstraction reactions both lead to the formation of CH_3SH :

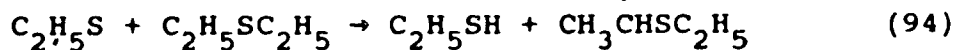


The apparent activation energies measured for (91)¹⁰⁸ and (92)¹¹⁴ are 5.4 and 1.5 kcal mol⁻¹, respectively. Also, from competitive experiments with 2-methylpentane,

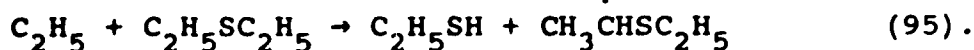


the activation energy for (93)¹⁰⁸ was approximated to be 7.5 kcal mol⁻¹.

In the overall mechanism of the gas-phase $\text{Hg}(^3\text{P}_1)$ photosensitized decomposition of $\text{C}_2\text{H}_5\text{SC}_2\text{H}_5$, the H-abstraction reaction

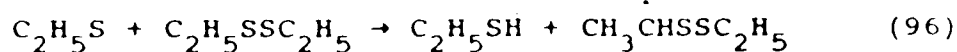


was considered by Smith and Knight¹¹¹ not to be important, relative to the corresponding H-abstraction reaction by ethyl radicals,



However, in the Hg-photosensitized decomposition of H_2 in

the presence of $C_2H_5SSC_2H_5$, Ekwenchi *et al.*¹¹⁵ have shown that the H-abstraction reaction,

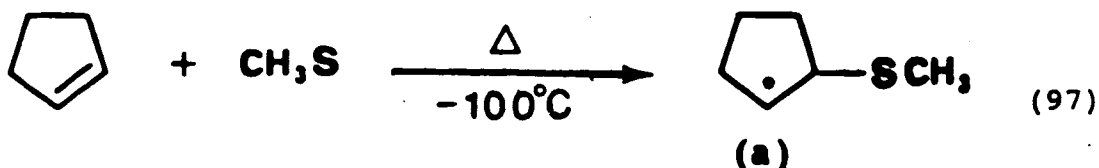


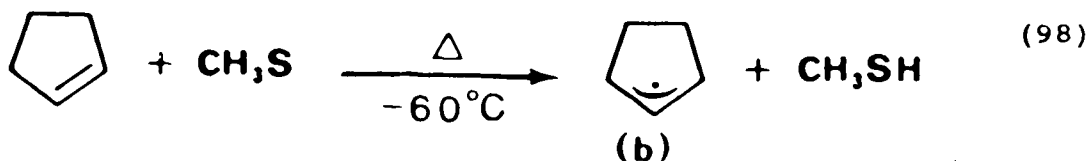
occurs with the rate constant, $k_{96} = \underline{2.1} \times 10^{12} \exp(-3600/RT) \text{ cm}^3 \text{ mol}^{-1} \text{ s}^{-1}$.

It is seen from reactions, (91) - (93), and (96), that alkylthiyl (RS) radicals require lower activation energies in abstraction reactions than alkyl radicals, for which abstraction from alkanes usually requires higher activation energies in the range 9 to 12 kcal mol⁻¹. Also, the fact that the RS radicals abstract more efficiently from sulfides and disulfides than from alkanes indicates a weaker adjacent C-H bond in the former than a typical tertiary C-H bond in the latter, $\approx 90 \text{ kcal mol}^{-1}$.

1.4.2.3 Addition

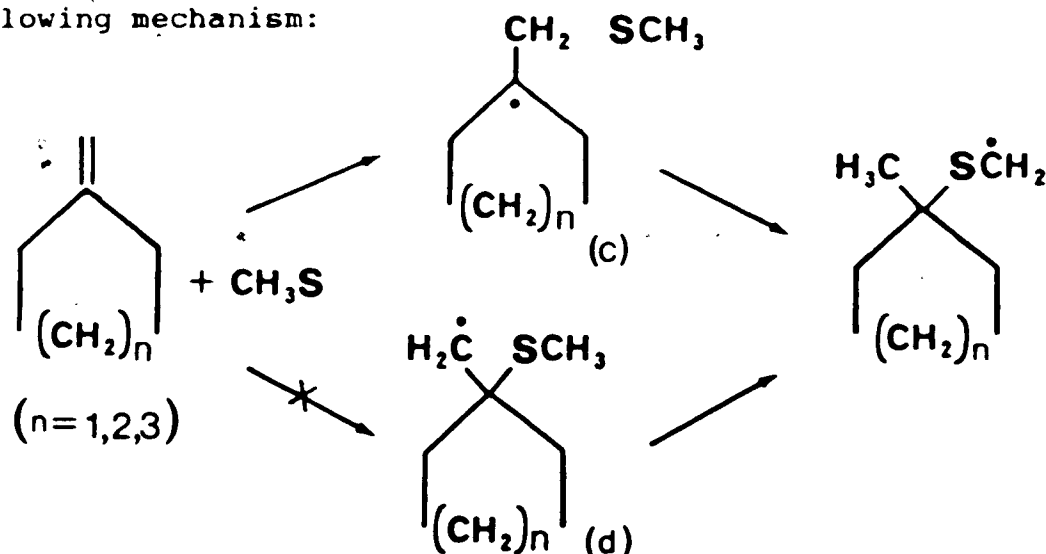
Unlike alkoxy radicals which, in most cases, abstract hydrogen from rather than add to unsaturated alkanes,¹¹⁷ thiyl radicals can add to as well as abstract from alkenes. The addition of CH_3S radicals to acyclic alkenes is well documented.^{118,119} For cycloalkenes, Lunazzi *et al.*¹²⁰ have found that the relative rates of addition to and abstraction from cyclopentene by CH_3S radicals are temperature dependent. In the photolysis of CH_3SSCH_3 with added cyclopentene in cyclopentane solution at -100°C ,





adduct (a) from the addition step (97) was observed by ESR spectroscopy. As the temperature increased from -100 to -60°C , (a) disappeared and radical (b) from the abstraction step (98) began to form. It was concluded from product analysis as a function of temperature that the addition reaction (97) has a lower activation energy than abstraction (98) and that the adduct (a) formed decomposes readily.

In the photolysis of CH_3SSCH_3 in the presence of a series of methylene-cycloalkanes using cyclopropane as solvent,¹²¹ the addition products were formed via the following mechanism:



Rearrangement through a 1,4-hydrogen-shift between CH_3S and the radical center, intermediate (c), was postulated since intermediate (d) was not detected by ESR spectroscopy.

Other addition reactions, such as the addition of CH_3S to 1,3-butadiene¹²² have also been studied recently.

An increasing number of photooxidation studies of simple alkyl thiols, sulfides and disulfides are being carried out in view of the escalating concerns about the role of the complex reaction sequences involved in the pollution of the atmosphere. The CH_3S radicals, produced from the initial step in the photolysis of CH_3SH , react with O_2 to give the adduct CH_3SOO and subsequently CH_3SCH_3 and SO_2 as major products.¹²³ This is in contrast to the CH_3O radicals which transfer an H-atom to O_2 :¹²⁴



From analysis of the SO_2 product formed via:

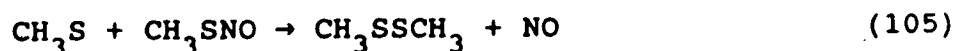


the rate constant ratio, k_{102}/k_{101} is estimated to be ~ 4 .¹²³

Balla and Heiklen¹²⁵ photolyzed CH_3SH in the presence of NO and found CH_3SNO as the primary addition product, formed from,



where $[\text{M}] = [\text{NO}] + [\text{Ar}] + [\text{CH}_3\text{SH}]$. At 23°C , $k_{103}/k_{104} \approx 83 \pm 52$ Torr. The CH_3SSCH_3 product was formed from the secondary process,



with the rate constant ratio, $k_{105}/k_{103} \approx 0.84 \pm 0.27$.

The photooxidations of CH_3SH , CH_3SCH_3 and CH_3SSCH_3 were carried out in the presence of trace amounts of NO, i.e.

atmospheric conditions, by Hatakeyama and Akimoto.¹²⁶ They measured the relative rate coefficient for the reactions of CH_3S with NO ,



and O_2 to be $k_{106}/k_{100} \approx 2 \times 10^3$. From the value of $k_{100} = 3.0 \times 10^6 \text{ cm}^3 \text{ mol}^{-1} \text{ s}^{-1}$ at 23°C , reported by Balla and Heiklen¹²⁷ in the 254 nm photooxidation of CH_3SSCH_3 in the presence and absence of N_2 , it follows that $k_{106} \approx 6.0 \times 10^9 \text{ cm}^3 \text{ mol}^{-1} \text{ s}^{-1}$.

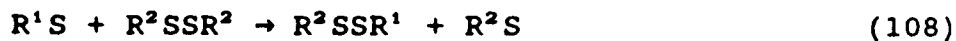
At present, the reactions of CH_3S with NO_2 are not well understood. Grosjean¹²⁸ studied the photolysis of R_2S and RSH ($\text{R} = \text{CH}_3, \text{C}_2\text{H}_5$) in air and in the presence of nitrogen oxides and deduced that NO reacts with CH_3S and $\text{C}_2\text{H}_5\text{S}$ about 2.3 and 6 times, respectively, faster than did NO_2 . He also deduced that NO_2 removes CH_3S about 2×10^6 times more efficiently than O_2 to form the stable adduct, CH_3SNO_2 ,



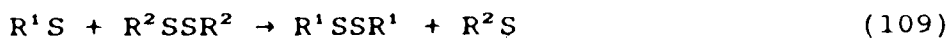
This is in apparent conflict with the results of Balla and Heiklen,¹²⁹ who found no evidence for reaction (107) in their studies of thermal reactions of NO_2 with organic sulfur compounds.

1.4.2.4 Metathetical Reactions

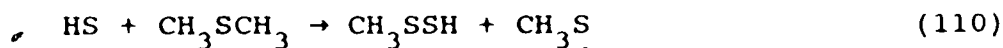
Asymmetrical disulfides are usually formed with high quantum yields from the metathetical reactions of thiyl radicals in the co-photolysis or thermolysis of symmetrical disulfides,¹³⁰



Conversely, photolysis of asymmetrical disulfides leads to symmetrical disulfide products,¹¹⁵

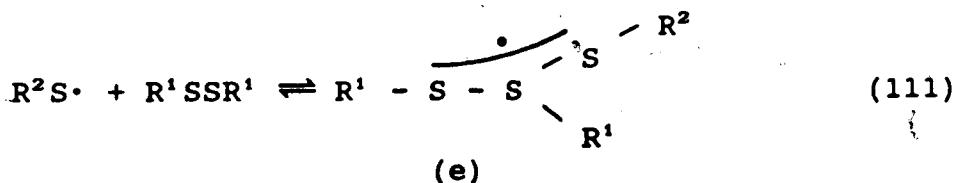


The analogous metathetical reaction of HS radicals with CH_3SCH_3 ,



has also been shown to occur,¹³¹ with the rate parameters estimated to be $A_{110} \approx 10^9 - 10^{10} \text{ cm}^3 \text{ mol}^{-1} \text{ s}^{-1}$ and $E_{110} \approx 2.7 \text{ kcal mol}^{-1}$; thus, at 25°C , $k_{110} \approx 10^7 - 10^8 \text{ cm}^3 \text{ mol}^{-1} \text{ s}^{-1}$.

Although Pryor and Smith¹³² have suggested an addition-elimination sequence in the mechanism of the metathetical reactions (108) and (109), they did not provide positive experimental evidence for a transient intermediate. Recently, Bonifacic and Asmus¹³³ used the time-resolved pulse radiolysis technique to show that the metathetical reaction of thiyl radicals with disulfides proceeds via the adduct, $(RSS(R)SR)$, a sulfuranyl radical with an unpaired electron delocalized in an antibonding σ^* orbital within a trisulfide bridge,

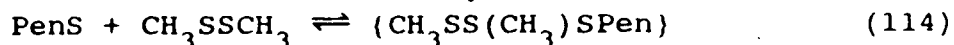


The transient intermediate, (e), was stable with a half-life estimated to be $> 100 \mu\text{s}$ and exhibited optical absorption in

the UV at $\lambda_{\max} = 375 \pm 10$ nm and $\epsilon_{\max} = (3.4 \pm 0.4) \times 10^3$ $M^{-1} \text{cm}^{-1}$. For the first time, absolute rate constants were measured for the forward and backward reactions,



in the pulsed radiolysis of aqueous and methanolic solutions of CH_3SSCH_3 and cystine, $[\text{NH}_2\text{CH}(\text{CO}_2\text{H})\text{CH}_2\text{S}]_2$. For $R = \text{CH}_3$ and neutral solution, $k_{113} = 3.8 \times 10^9 \text{ cm}^3 \text{ mol}^{-1} \text{ s}^{-1}$ and $k_{-113} = 2.3 \times 10^7 \text{ s}^{-1}$. For $R =$ cysteine residue, $\text{NH}_2\text{CH}(\text{CO}_2\text{H})\text{CH}_2\cdot$, and $\text{pH} = 10$, $k_{113} = 7.7 \times 10^8 \text{ cm}^3 \text{ mol}^{-1} \text{ s}^{-1}$ and $k_{-113} = 1.5 \times 10^7 \text{ s}^{-1}$. The equilibrium constant values for $R = \text{CH}_3$ and $\text{NH}_2\text{CH}(\text{CO}_2\text{H})\text{CH}_2$ were averaged from the kinetic data to be 180 ± 30 and $60 \pm 20 \text{ M}^{-1}$, respectively. No adduct was observed for $R = \text{C}_2\text{H}_5\text{S}$ and $i\text{-C}_3\text{H}_7$ and this was attributed to slower kinetics in these two systems. The mixed disulfide system,



where Pen = penicillamine residue, $\text{NH}_2\text{CH}(\text{CO}_2\text{H})\text{C}(\text{CH}_3)_2\cdot$, was also studied in a 2-propanol solution at $\text{pH} = 4.6$. The rate constant for the forward reaction, k_{114} , was found to be $2.7 \times 10^{10} \text{ cm}^3 \text{ mol}^{-1} \text{ s}^{-1}$.

Knight and coworkers^{134,135} have found that the disproportionation of disulfides



was predominant in the liquid-phase photolysis at 250 - 300 nm of a number of $\text{C}_2 - \text{C}_{10}$ symmetrical and asymmetrical dialkyldisulfides. The equilibrium constant, K_{115} , is ~ 4

for simple disulfides and smaller for higher molecular weight disulfides.¹³⁵ This was attributed to steric effects which would militate against radical diffusion, increase the probability of cage recombination and thus render the RS-disulfide exchange less facile.

The rate constants for the metathetical reactions of some thiyl radicals are listed in Table 1.5.

1.5 Transition State Theory for Bimolecular Reactions

Transition state theory is a major kinetic model for the interpretation of elementary, chemical rate processes. The theory, which was first proposed by Pelzer and Wigner¹³⁶ and extensively developed later by Eyring¹³⁷ and coworkers,¹³⁸ remains the method of choice in the calculation of absolute reaction rates from potential energy surfaces.¹³⁹ The transition state, or the activated complex, situated at a potential energy maximum along the reaction path, is considered to be a complex aggregate having the proper configuration in its passage through phase space and at a minimum energy for the reaction to occur.

Transition state theory is based on a quasi-equilibrium hypothesis in which the reactants, A and B, are assumed to be in thermodynamic equilibrium with the transition state, AB^\ddagger . The equilibrium constant for the elementary reaction,



is given by:

Table 1.5. Rate Constants for Metathetical Reactions of Thiyl Radicals

Reaction	k ₂₉₈		Method	Reference
	(cm ³ mol ⁻¹ s ⁻¹)			
CH ₃ S + CH ₃ SSC ₂ H ₅ → CH ₃ SSCH ₃ + C ₂ H ₅ S	1.4 × 10 ¹⁰		photolysis	115
C ₂ H ₅ S + CH ₃ SSC ₂ H ₅ → C ₂ H ₅ SSC ₂ H ₅ + CH ₃ S	7.8 × 10 ⁹		photolysis	115
C ₂ H ₅ S + CH ₃ SSCH ₃ → CH ₃ SSC ₂ H ₅ + CH ₃ S	3.1 × 10 ¹⁰		photolysis	115
CH ₃ S + C ₂ H ₅ SSC ₂ H ₅ → CH ₃ SSC ₂ H ₅ + C ₂ H ₅ S	1.9 × 10 ¹⁰		photolysis	115
HS + CH ₃ SCH ₃ → CH ₃ SSH + CH ₃	(0.1 - 1.0) × 10 ⁸		photolysis	131
CH ₃ S + CH ₃ SSCH ₃ = (CH ₃ SS(CH ₃)SCH ₃)	3.8 × 10 ⁹ a 2.3 × 10 ⁷ b		radiolysis, neutral solution	133
CY ^C S + CYSSCY = (CYSS(CY)SCY)	7.7 × 10 ⁸ a 1.5 × 10 ⁷ b		radiolysis, pH = 10	133
Pen ^C S + CH ₃ SSCH ₃ = (CH ₃ SS(CH ₃)SPen)	2.7 × 10 ¹⁰ a		radiolysis, pH = 4.6	133

a rate constant for the forward reaction

b rate constant for the backward reaction, in units of s⁻¹

cCY = NH₂CH(CO₂H)CH₂; Pen = NH₂CH(CO₂H)C(CH₃)₂

$$K_{AB}^\ddagger = \frac{[AB]^\ddagger}{[A][B]} \quad [1]$$

The overall bimolecular rate constant, k^\ddagger , is then described by:

$$k^\ddagger = \left[\frac{kT}{h} \right] K_{AB}^\ddagger \quad [2]$$

where k is the Boltzman constant, T the temperature and h the Planck's constant. From the thermodynamic relation,

$$-RT \ln K_{AB}^\ddagger = \Delta G^\ddagger = \Delta H^\ddagger - T\Delta S^\ddagger \quad [3]$$

equation [1] can then be expressed in terms of ΔH^\ddagger and ΔS^\ddagger ,

$$k^\ddagger = \left[\frac{kT}{h} \right] \exp \left[\frac{\Delta S^\ddagger}{R} \right] \exp \left[\frac{-\Delta H^\ddagger}{RT} \right] \quad [4]$$

Relating [4] to the Arrhenius form of the rate constant,

$$k = A \exp \left[\frac{-E}{RT} \right] \quad [5]$$

and assuming that ΔH^\ddagger and ΔS^\ddagger are independent of temperature over the range $T = T_m \pm \Delta T$, where T_m is the center of the temperature range chosen, it is seen that

$$A = \frac{ekT_m}{h} \exp \left[\frac{\Delta S_m^\ddagger}{R} \right] \quad [6]$$

and

$$E = \Delta H_m^\ddagger + RT_m \quad [7]$$

where ΔS_m^\ddagger and ΔH_m^\ddagger are the entropy and the enthalpy of activation between the reactants and the activated complex calculated at T_m .

Thus, the entropy of activation, ΔS^\ddagger , can be calculated

directly from the pre-exponential factor in [6]. Conversely, the latter can be estimated from ΔS^\ddagger , if experimental data for the reactions are not readily available.

From the definition,

$$\Delta S^\ddagger = S^\ddagger - S_{\text{reactant}} \quad [8].$$

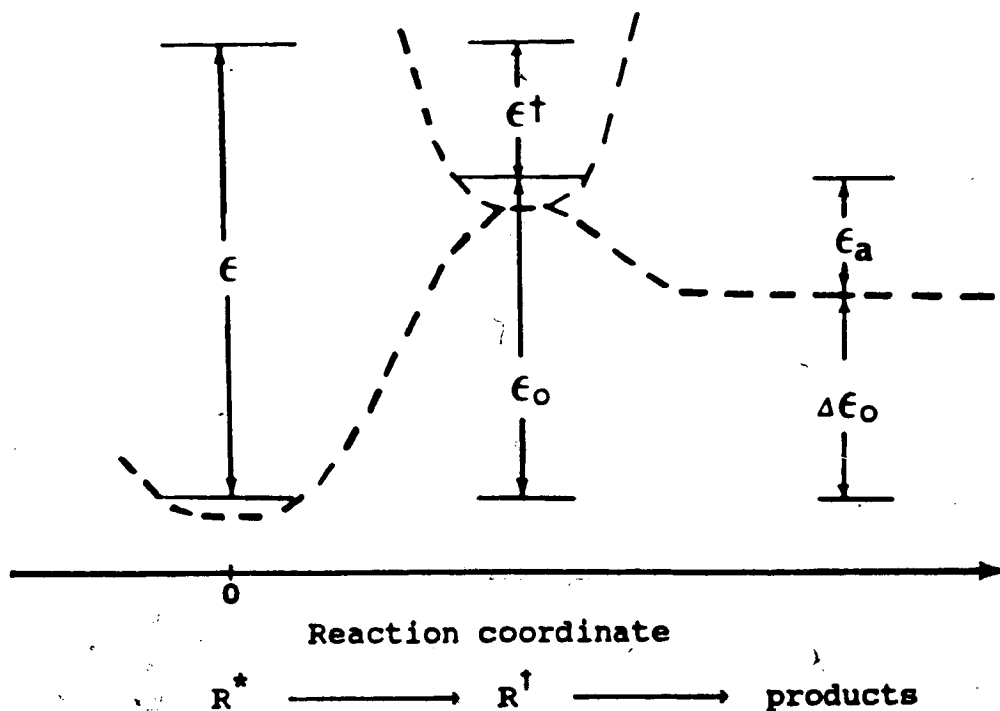
The standard entropies for ground state molecules are either known or can be calculated from statistical mechanics with good precision. Another method is an empirical one developed by Benson^{140,141} and is based on additivities of molecular properties with the assumption that the activated complex is a rigid, or "tight" molecule, *i.e.* one in which the bond lengths and bond angles are within 0.3 Å and 20°, respectively, of the values which describe a stable structure. The latter method provides a very useful means, with good accuracy, of calculating the entropy of the activated complex, S^\ddagger , by evaluating the translational, rotational, vibrational, symmetry and spin contributions to the entropy. For example, in the metathesis reactions involving a light atom, such as H or D, with a large polyatomic molecule, the transition state complex has the same intrinsic entropy as the molecule, and hence

$$\begin{aligned} \Delta S^\ddagger &\approx S^\circ(\text{substrate}) + R \ln 2 - [S^\circ(\text{substrate}) + S^\circ(\text{H})] \\ &\approx 1.4 - S^\circ(\text{H}) \end{aligned}$$

where $R \ln 2 = 1.4$ is the spin correction. Symmetry corrections may also be necessary.

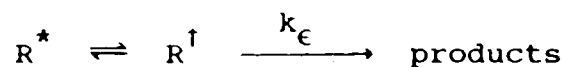
1.6 RRKM Theory for the Unimolecular Decomposition of Alkyl Radicals

The unimolecular decomposition of alkyl radicals has often been initiated by photolysis. On the other hand, secondary unimolecular reactions usually result either ~~from~~ the production of hot species by chemical activation or from conventional thermal activation. The profile of potential energy surfaces¹⁴² which are representative of any decomposition reactions is schematically shown as follows,



where $\Delta\epsilon_0$ and ϵ_0 are the heat and critical energy of the decomposition reaction at 0 K, respectively, ϵ_a the activation energy for the reverse reaction, ϵ the energy possessed by the vibrationally excited species R^* , and ϵ^\ddagger the excess energy above ϵ_0 , contained in the activated complex R^\ddagger by some distribution function.

The RRKM theory is formulated from a quantum statistical concept of reaction with transition state theory. The reaction of energized molecules is considered to occur via the quasi-equilibrium concentration of activated complexes,



The rate constant, k_ϵ , is given by,

$$k_\epsilon = \frac{1}{h} \frac{Z_1^\ddagger}{Z_1^*} \frac{\sum P(\epsilon^\ddagger)}{N^*(\epsilon)} \quad [9]$$

where Z_1^\ddagger and Z_1^* are the products of the partition functions for adiabatic degrees of freedom of the activated complex and of the molecule, respectively, $\sum P(\epsilon^\ddagger)$ the total sum of the degeneracies of all possible energy eigenstates at the total active energy ϵ^\ddagger , $N^*(\epsilon)$ the number of eigenstates per unit energy of the active modes of the molecule at energy ϵ , h Planck's constant, $\epsilon^\ddagger = \epsilon - \epsilon_0$, and the transmission coefficient is unity. The basic assumption in the RRKM theory is that all vibrational and internal rotational degrees of freedom are active both in the molecule and in the transition state complex, and that the overall rotations are adiabatic.

It is seen from Equation [9] that k_ϵ is dependent on the following parameters: the activated complex structure, ϵ^\ddagger , ϵ_0 and internal rotation. At $\epsilon^\ddagger \neq 0$, the energy-dependence of k_ϵ rests on the relative variation between the sum of states in the activated complex with energy ϵ^\ddagger , $\sum P(\epsilon^\ddagger)$, and

the density of states in the molecule with energy ϵ , $N^*(\epsilon)$. At low values of ϵ^\ddagger , k_ϵ increases much more rapidly for loose complexes than for tight complexes because the former have a larger number of low-lying energy states than the latter. A change in ϵ_0 effects a change in the absolute magnitude of k_ϵ , due to the term $\sum P(\epsilon^\ddagger)$, where $\epsilon^\ddagger = \epsilon - \epsilon_0$. Finally, a free rotational degree of freedom will change the value of k_ϵ greatly by increasing the number of energy states and thereby converting the $\sum P(\epsilon^\ddagger)$ into a more continuous function.

1.7 Aim of the Present Investigation

As seen from the foregoing discussion, kinetic data for atom and radical reactions with thiols are meager. In particular, for the case of H atoms, there is apparent disagreement over the occurrence of the metathetical reactions by thermal H atoms in the gas-phase photolysis of thiols. Yet, these reactions have been established for other classes of organosulfur compounds, alkylsulfides and disulfides, for which the atom and radical attack takes place, in some cases exclusively, at the nonbonding 3p orbital of sulfur, and recent kinetic data have been cited in the literature for some of the $H + RSR'$ and $H + RSSR'$ systems. As well, the source reactions for the formation of alkenes and H_2S , which are essentially the products of thermolysis of thiols from either the radical or the molecular initiation step, have not been determined unequivocally in the photolysis studies due to concurrent hot and thermal reactions.

It was therefore decided to undertake a kinetic-mechanistic study of the gas-phase photolysis of alkane thiols with the aim of elucidating the following facts of these reactions:

- the nature of the primary photochemical processes and their quantum yields;
- the mode of alkene and H_2S formation;
- the importance of the displacement reaction by H atoms; and
- the effect of inert gas pressure on the formation and distribution of the reaction products, and on the reactions of hot H atoms and hot alkyl radicals.

The above can be realized by means of product analysis, together with the effects of concentrations of substrate, thermalizer, and temperature on the product quantum yields. The clarification of the mechanism for the photolysis of thiols would ultimately lead to the extraction of reliable values for rate constant ratios for abstraction/displacement reactions, and the determination of Arrhenius parameters for some of the elementary reactions occurring in the H \neq thiol systems, which can be considered as a model for biologically and industrially important reactions. It is anticipated that the measured activation energies and pre-exponential factors would not only shed light on the thermochemistry of the reactions but also, to a greater extent, on the nature of the activated complex; knowledge of the latter would expand our understanding of the chemical reactivity of both

the H atoms and the C-S-H linkages.

Three alkanethiols were selected for this study:

1. Ethanethiol, the simplest in the series, to observe the aspects of alkene formation. Since detailed studies carried out by previous investigators gave rise to different kinetic interpretations, it is appropriate to begin the present work by repeating the photolysis experiments under a broader range of conditions and comparing the results;
2. 2-Propanethiol (Isopropanethiol), in order to observe whether increasing alkyl substitution would have any effect on the nature of the primary processes and consequently, the quantum yields of products;
3. 2-Methyl-2-Propanethiol (t-Butanethiol), to study the effects of bulky substituents and weaker C-S bond energy on the rate of the primary reactions and the nature of the disproportionation reaction of thiyl radicals since in this case there is no H atom on the carbon α to the sulfur atom.

Finally, some preliminary experiments on the Hg-photosensitization of H_2 in the presence of ethanethiol were planned in order to obtain independent and unambiguous evidence for the occurrence of the displacement reaction by thermal H atoms in the gas phase.

CHAPTER TWO

EXPERIMENTAL

2.1 The High Vacuum System

Experiments were carried out in a grease-free conventional high vacuum system (Figure 2.1). It consists of a photolytic assembly (Figure 2.2), distillation train, gas storage bulbs, Toepler pump-gas buret and metering units. Delmar mercury float, Springham and Helium tested Hoke valves, along with Rotaflo Teflon plug stopcocks, were used throughout the system to minimize sulfur product loss through stopcock grease and metal surfaces. Evacuation of the system down to 10^{-6} Torr was achieved using a two-stage mercury diffusion pump backed by a Welch Duoseal mechanical pump. Absolute pressures up to 100 Torr were measured by the MKS Baratron gauge, Type 315BHS-100, serial 21049, connected to a MKS Baratron range multiplier, Type 170M-6B and a 8000A digital multimeter, Fluke 530223. Absolute pressures greater than 100 Torr were measured by the Bourdon gauge (Matheson) and SpeediVac gauge, Type C.G.3. Pirani tubes (Consolidated Vacuum Corporation Catalogue No. Gp-001) were placed in strategic locations in the system to monitor gas transfers. The Pirani gauges (Type G-140) were calibrated using the McLeod gauge. The distillation unit has two U-traps, a coil trap and a solid nitrogen trap interconnected by Springham valves. Condensable products were introduced from the distillation train either directly or from the Toepler pump and gas buret to the attached gas

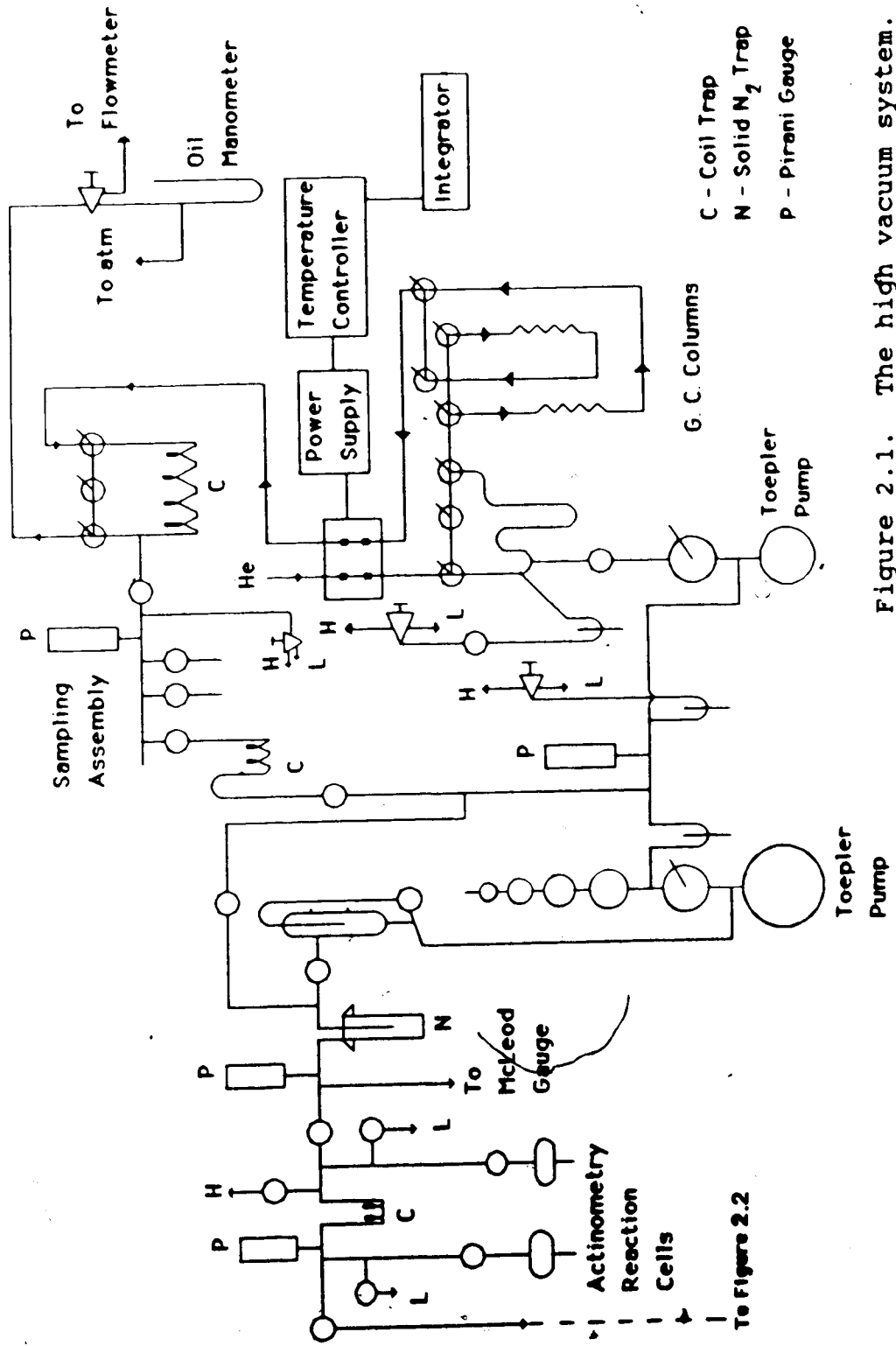


Figure 2.1. The high vacuum system.

To Figure 2.2

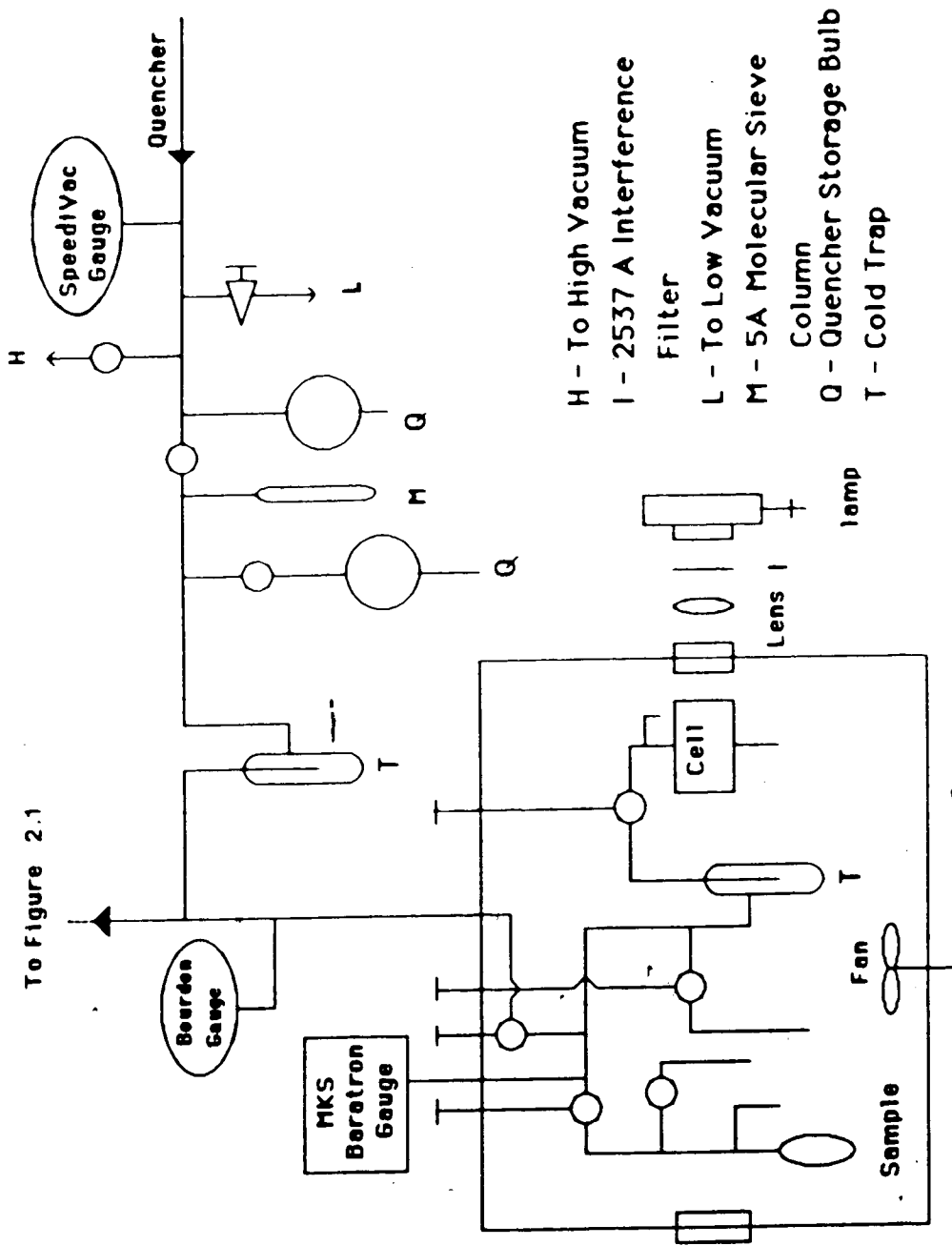


Figure 2.2. The photolytic assembly.

chromatograph inlet system.

2.2 The Photolytic Assembly

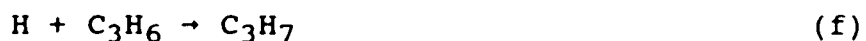
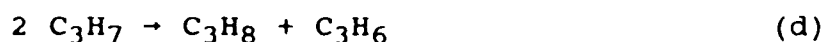
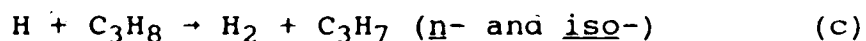
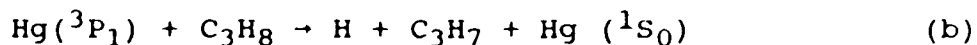
A cylindrical quartz photolytic cell equipped with a cold finger (10 x 5 cm), of volume 278 cm³, was employed in this study. It was enclosed in an aluminum block furnace insulated by a one inch thickness of fibreglass wool. Two 2-mm thick quartz plates in aluminum casings were placed at the open ends of the furnace to prevent cooling of cell faces by air currents and thereby to maintain uniform temperature throughout the reaction vessel. The furnace was heated by two 10-cm, 150-watt pencil heaters, inserted axially in the two halves of the block furnace. Temperatures of study (25 - 150°C) were maintained by an API 2-mode temperature controller, model 915B, and were monitored by standard Fe-constantan thermocouples and a thermometer placed in an axial hole located at the face of the block furnace. The sample storage bulb (3 x 5 cm) was surrounded by a small temperature-controlled metallic jacket and cooled by tap water when sample was not in use.

The entire photolytic assembly, consisting of the photolytic cell in a block furnace, the sample storage bulb, a calibrated volume, a cold trap and Hoke valves, was fitted inside a thermostatted box (100 x 70 x 50 cm), constructed of asbestos, 15 mm thick. The box was heated electrically to constant temperatures (25 - 50°C) by two spiral heaters located at the bottom of the box to facilitate gas transfers from the reaction vessel to the analytical system.

Uniform temperature ($\pm 1^\circ\text{C}$) inside the box was achieved by a fan, driven by an induction motor, to circulate the air.

2.3 Light Sources and Actinometry

For Hg-photosensitization experiments, the radiation source was a Hanovia low-pressure Hg resonance lamp, Type 687A45, serial 500600, equipped with a 254 nm Baird Atomic interference filter. The UV spectrum of the filter on the Unicam SP 800 UV spectrophotometer showed the range of transmittance to be 237 - 273 nm, with maximum transmittance of 20% at 252 nm. The light intensity of the lamp was determined by propane actinometry.^{143,144} Under low lamp intensity conditions, the important processes are the following:



Back¹⁴⁵ has shown that the quantum yield of H_2 production decreases with irradiation time until the concentration of C_3H_6 reaches a steady state, after which $\phi(\text{H}_2) = 0.581$ at 27°C and remains constant. In the present experiments, irradiation of 600 ± 10 Torr C_3H_8 was carried out repeatedly until the rate of H_2 production became constant. The lamp intensity was then calculated to be $0.068 \mu\text{Einstein min}^{-1}$. This value was kept low in order to minimize radical-radical

reactions and to maintain a low concentration of H atoms.

For direct photolysis experiments, the radiation source was a Hanovia medium-pressure mercury lamp, Type SH, model 45078, equipped with a 254 nm Baird Atomic interference filter. A four-inch focal length plane convex quartz lens was placed between the lamp and the reaction vessel to collimate the light.

The light intensity was determined also by chemical actinometry on a separate set-up along an optical bench (Figure 2.3). Here, the chemical actinometer used was hydrogen sulfide which has hydrogen as the only product of photolysis at 254 nm from the following processes:



The quantum yield of hydrogen has been well established by previous authors¹⁴⁶⁻¹⁴⁹ to be unity within experimental error. The optical train on the bench consisted of the same light source as the one used in the vacuum system, a 1-cm aperture, a 254 nm Baird Atomic interference filter, a double convex quartz lens, a cylindrical quartz reaction vessel (10 x 5 cm), a cylindrical quartz actinometer vessel (10 x 5 cm), a monochromator (Bausch & Lomb Catalog No. 33-8601, serial 9637MB) and a photo-cell connected to an output signal electronic meter (Photovolt Corporation model 501, serial 6942) in this order.

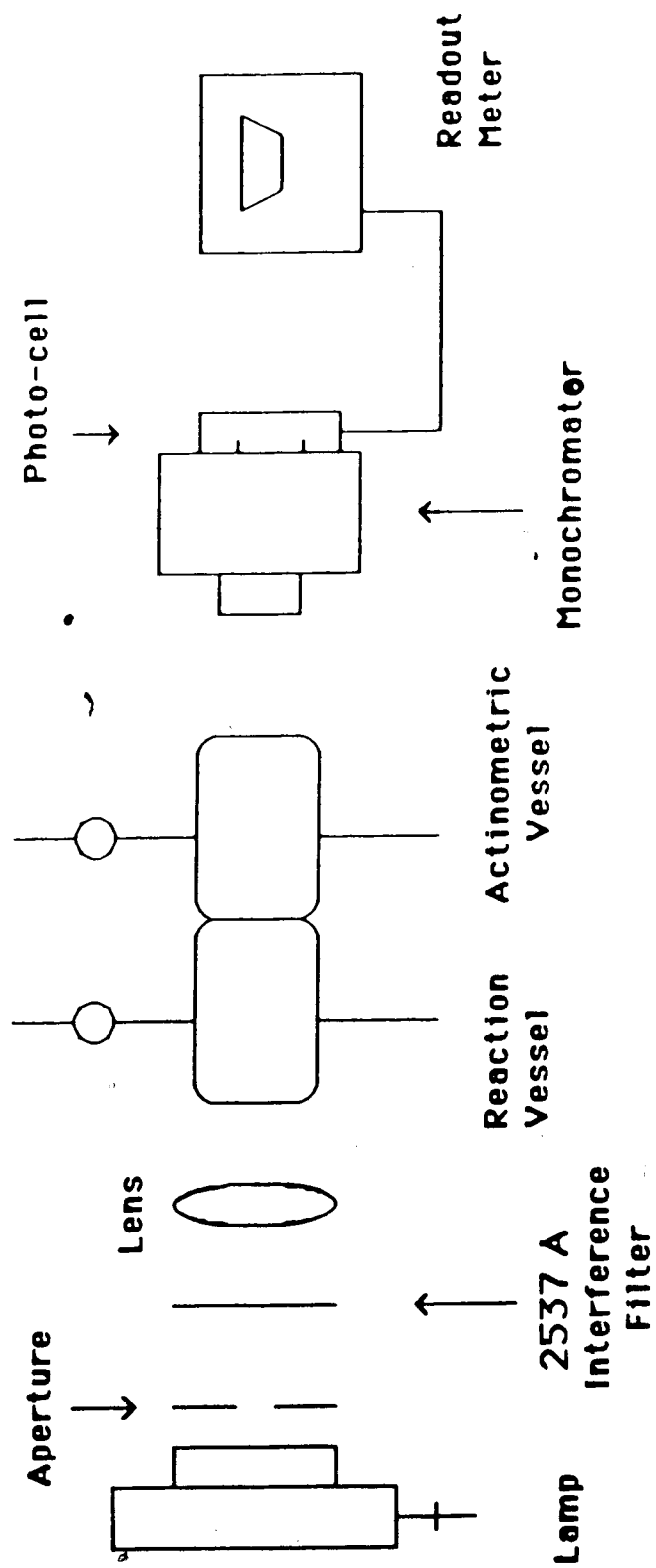


Figure 2.3. The actinometry assembly.

2.4 The Analytical System

Quantitative analyses of products and purity checks were carried out by gas chromatography. The GC unit consisted of a power supply (Gow-Mac model 24-500, serial 18312P) and a custom-made micro volume cell detector fitted with a pair of 8K thermistors (Gow-Mac 13-502) operated at 80°C with a bridge current of 8 mA. The temperature of the detector was kept constant inside a temperature-regulated cell assembly (Gow-Mac model 24-170, serial 18212P). GC signals were read out on a Hewlett-Packard model 3380A integrator.

Helium (Linde) was used as the carrier gas. It was dried and purified by passage through a 5 Å molecular sieve column. Flow rates were measured on a bubble flowmeter.

Pyrex or quartz glass GC columns were connected to the vacuum apparatus by means of either rubber septa or Beckman teflon tube fittings No. 404. The GC columns were placed in 212-watt heating columns constructed of aluminum and Nichrome wires and insulated by fibreglass wool in order to maintain constant temperatures. The GC columns used, the operating conditions and the retention times for all the analyses in this study are summarized in Table 2.1.

Effluents from the GC may be condensed at -196°C either in a waste trap and discarded in the fumehood or in a coil trap and sealed in vacuo in a sample tube for GC/MS analysis. Initial identification of products was made on the basis of comparison of GC retention times with those of authentic samples. Subsequent product identification was

Table 2.1. GC Retention Data and Operation Conditions

Column	Length (ft)	Injection Temperature (°C)	Column Temperature (°C)	Flow Rate (cm ³ min ⁻¹)	Compounds Analysed	Retention Time (min)
Porapak QS, 80/100 mesh	4	40	41	80	C ₂ H ₄	1.4
					C ₂ H ₆	2.8
					H ₂ S	4.2
					CO ₂	0.6
					C ₂ H ₅ SH	14.7
					C ₂ H ₅ OH	1.0
					(C ₂ H ₅) ₂ S ₂	33.0
Porapak Q:QS(1:1), 80/100 mesh	6	30	59	50	H ₂ S	7.2
					C ₃ H ₆	17.2
					C ₃ H ₈	19.8
12% Tricresyl- phosphate, WAW-DMCS 80/100 mesh	6	60	80	60	<u>1</u> -C ₃ H ₇ SH	1.9
					<u>1</u> -C ₃ H ₇ OH	2.8
					(<u>1</u> -C ₃ H ₇) ₂ S ₂	28.0
Porasil B 80/100 mesh	10	30	42	40	<u>1</u> -C ₄ H ₁₀	14.3
					H ₂ S	18.5
					<u>1</u> -C ₄ H ₈	42.5
10% Tricresyl- phosphate, WAW-DMCS 80/100 mesh	4.5	70	80	60	<u>1</u> -C ₄ H ₉ SH	2.5
					<u>1</u> -C ₄ H ₉ OH	1.0
					(<u>1</u> -C ₄ H ₉) ₂ S ₂	28.8

achieved by mass spectrometric analysis. Mass spectra were obtained on an AEI MS-12 instrument with the ion source operating at 70 eV and the ionization chamber temperature being kept at about 50°C. All the gas phase samples were analysed on an appropriate GC column adapted to the MS-12 chromatograph (Varian Aerograph series 1400). The detector response was calibrated from authentic samples and checked periodically for good reproducibility. Standard alkane, alkene and hydrogen sulfide samples were introduced into the system and measured by the gas buret. For the low vapour pressure disulfides, standard solutions of the disulfide in alcohol were prepared in order to minimize injection errors associated with small sample volume. Syringe injections of constant 4- μ l volume solution samples were made through a rubber septum into the system. The sample was then transferred through the distillation train and condensed in the GC injection port. Peak areas were integrated directly by the Hewlett-Packard recording instrument. Due to tailing of some of the disulfide peaks, the peak areas of the disulfides were also measured with an Otto planimeter for correlation purposes. Linear responses were obtained over the range of product yields obtained from experiments and the calibrations were reproducible to within $\pm 5\%$.

2.5 Materials and Purification

All the three thiols studied in this work were routinely purified by distillation in vacuo. Purity tests by GC were

carried out at each stage of the distillation. The final purity test was performed by GC/MS, after which the sample was stored and covered from light in the sample reservoir in the photolytic assembly. Table 2.2 lists the sources and distillation procedures used for ethanethiol, *i*-propanethiol and *t*-butanethiol. UV spectra of the thiol substrates were taken using a cylindrical quartz UV cell (10 x 2 cm) and a Hewlett-Packard 8480A Diode Array spectrophotometer prior to the start of photolysis study of each thiol.

The solvents used in the preparation of disulfide solutions for calibration purposes were of reagent grade. The remaining compounds used in this work were of research grade and used without further purification. These compounds and their sources are tabulated in Table 2.3.

2.6 Operational Procedure

All experiments were carried out in the gas phase. Warm-up time for the lamp prior to irradiation was at least 30 minutes. Control experiments were carried out at the lowest and the highest temperatures studied in order to check for occurrences of dark reactions, if any. After each experiment, reaction cell windows were flamed to remove sulfur deposits there.

For the Hg-photosensitization reactions, a small pool of mercury had been introduced into the side finger of the reaction vessel. It was subsequently removed prior to the start of direct photolysis studies. The thiol substrate was expanded from the sample reservoir to the photolytic region.

Table 2.2. Sources and Purification of Thiols

Material	Source	Grade and Purity	Purification
Ethanethiol	Aldrich	Research Grade, 97%	distilled in two stages at -130°C, -95°C, -88°C and -63.5°C
IsoPropanethiol	Aldrich	Research Grade, 98%	distilled in three stages at -95°C and once at -86°C
t-Butanethiol	Aldrich	Research Grade, 99%	distilled in two stages at -130°C, in three stages at -95°C and once at -63.5°C

Table 2.3. Sources and Purity of Materials Used

<u>Material</u>	<u>Source</u>	<u>Grade and Purity</u>
Ethylene	Matheson	Research Grade, 99.98%
Ethane	Phillips	Research Grade, 99.99%
Hydrogen Sulfide	Matheson	C. P. Grade, 99.6%
Diethylsulfide	Eastman	Research Grade
Ethanol		Reagent Grade, 95%
Carbon Dioxide	Matheson	Research Grade, 99.995%
Propylene	Matheson	Research Grade, 99.7%
Propane	Matheson	Research Grade, 99.98%
Diisopropylsulfide	Aldrich	Research Grade, 96%
Propan-2-ol	British Drug House	Reagent Grade, 95%
n-Butane	Phillips	Research Grade, 99.97%
Isobutylene	Matheson	Research Grade, 99.8%
Isobutane	Matheson	Research Grade, 99.96%
Ditertbutylsulfide	Aldrich	Research Grade, 97%
t-Butanol	A & C American Chemicals	Reagent Grade

Its pressure (≤ 60 Torr) was read off the digital multimeter. The reaction vessel was then isolated from the rest of the photolytic assembly and the substrate was condensed into the cold finger of the reaction vessel. Excess substrate was condensed back into the storage bulb. Afterwards, with the substrate condensed at -196°C in the cold finger, the reaction vessel was evacuated thoroughly using high vacuum. Hydrogen (Linde), which had been expanded from the cylinder into a storage bulb, was then admitted into the reaction vessel. The H_2 pressure from the cylinder to the storage bulb was measured by the Speedi-Vac pressure gauge while that from the storage bulb to the reaction vessel was measured by the Bourdon gauge. Approximately 600 Torr of H_2 was used in each experiment. Excess H_2 was condensed in a 5Å molecular sieve column kept at -196°C and was transferred back into the storage bulb. The reaction mixture was allowed to equilibrate for at least 30 minutes before irradiation. After photolysis, the cold finger of the reaction vessel was kept at -196°C . The H_2 was removed by pumping it very slowly through three cold traps at -196°C and one at -210°C , while maintaining the pressure reading on the digital multimeter at < 2 Torr. From the condensable fraction, the alkane and hydrogen sulfide products were separated from the disulfide product by distillation over two traps at -95°C . They were subsequently further separated and measured chromatographically. The remaining thiol and disulfide fraction was analysed by

the GC.

For propane actinometry, the C_3H_8 had been expanded from the lecture bottle into another storage bulb. In the same manner as that for H_2 , C_3H_8 was admitted into the reaction vessel. After a 60 or 120 minute photolysis, the only non-condensable product, H_2 , was passed over four cold traps at $-196^\circ C$ and was measured in a gas buret with the aid of a cathetometer (Guffin & George Ltd.) while all the rest of the condensable products were kept at $-196^\circ C$ in the cold finger of the reaction vessel. Afterwards, the unreacted C_3H_8 was transferred back into the storage bulb.

In the photolyses of pure thiols, the substrate (≤ 50 Torr) was expanded from the sample reservoir into the reaction vessel as previously described. The substrate was allowed to equilibrate at the temperature of study for at least 30 minutes before irradiation. After a 60 minute photolysis, the only non-condensable product, hydrogen, was passed over three cold traps at $-196^\circ C$ and one at $-210^\circ C$ and was measured in a gas buret as before. The condensable products were alternately thawed and refrozen to ensure complete removal of hydrogen from the product mixture to the gas buret for quantitative measurement. The minor products of photolysis, which were alkane, alkene and hydrogen sulfide were separated from the disulfide product by distillation over two traps at $-95^\circ C$ and condensed in a trap at $-210^\circ C$. They were subsequently further separated and measured chromatographically. In the final stage of

analysis, the thiols and disulfides were transferred into the GC sampler and were also separated chromatographically.

For experiments carried out in the presence of quencher gas, the substrate was condensed in the reaction vessel as before. It was then transferred to another cold finger in the photolytic assembly and isolated. The quencher gas of choice, which had been expanded from the lecture bottle into a storage bulb, was admitted into the reaction vessel.

Excess quencher gas was condensed back into the storage bulb. Finally, with the quencher gas substrate (28 - 400 Torr) kept condensed at -196°C in the cold finger of the reaction vessel, the thiol substrate (10 - 20 Torr) was transferred back into it.

The reaction mixture was equilibrated in the closed thermostatted box overnight prior to irradiation. It was found that equilibration time up to 24 hours did not result in any decomposition of the substrate. After a photolysis time of 60 minutes, hydrogen was measured in a gas buret in the same manner as before. The quencher gas and minor products were separated by distillation at appropriate temperatures, as described below for the photolyses of ethanethiol, isopropanethiol and t-butanethiol:

1. $\text{C}_2\text{H}_5\text{SH}$: CO_2 , C_2H_4 , C_2H_6 and H_2S , distilled in two stages at -160°C ; remaining CO_2 and $\text{C}_2\text{H}_5\text{SH}$, distilled at -95°C .

2. $i\text{-C}_3\text{H}_7\text{SH}$: H_2S , C_3H_8 and C_3H_6 , distilled in two stages at -117°C ; $n\text{-C}_4\text{H}_{10}$, distilled at -95°C .
3. $i\text{-C}_4\text{H}_9\text{SH}$: C_2H_6 , distilled in three stages at -160°C ; $i\text{-C}_4\text{H}_{10}$, H_2S and $i\text{-C}_4\text{H}_8$, distilled at -95°C .

The fractions evolved from each distillation step were measured chromatographically. The remaining condensables, consisting of the thiol substrate and disulfides, were analysed by GC.

For chemical actinometric experiments along the optical bench, warm-up time for the electronic readout meter was at least two hours. The instrumental correlation factor between light intensity and output signal at the photo-cell along the optical train set-up was determined using 760 Torr H_2S in both the reaction and the actinometry vessels. The two vessels were attached to the vacuum system and evacuated overnight. The chemical actinometer, H_2S , was expanded from the lecture bottle to the vessels. Excess H_2S was condensed into a storage bulb. The vessels were evacuated under high vacuum, while H_2S was kept condensed in the cold fingers at -196°C . Both vessels were then placed in appropriate positions along the optical train for irradiation. After photolysis of 60 minutes, both vessels were reattached to the vacuum system. The hydrogen produced from each vessel was collected and measured separately in the gas buret while unreacted H_2S was kept condensed at -196°C .

For the actinometry experiments carried out to determine

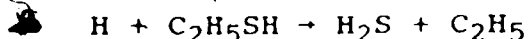
the light intensity absorbed in the photolytic cell, the reaction vessel was first evacuated of H_2S and then filled with the thiol, while the actinometry vessel remained unchanged with 760 Torr H_2S . The thiol substrate was expanded from the sample reservoir in the photolytic assembly to the photolytic cell in the same manner as before. It was then condensed into the cold finger of the reaction vessel and the vessel was evacuated thoroughly once again. After irradiation of 60 minutes, the reaction and actinometry vessels were reconnected to the vacuum system. The products from the reaction vessel were analysed in the same manner as that in the main experiments with pure thiols. Hydrogen produced in the actinometry vessel was collected and measured in a gas buret while unreacted H_2S was kept condensed at $-196^\circ C$.

CHAPTER THREE

THE REACTIONS OF HYDROGEN ATOMS WITH ETHANETHIOL

3.1 Results

The experiments to be described in this Chapter were carried out with the sole aim of obtaining independent, unambiguous evidence for the occurrence of the displacement reaction:



This was necessary in order to elucidate the mechanistic details of the photolysis of thiols (Chapters 4, 5 and 6).

The Hg-photosensitization of H_2 in the presence of $\text{C}_2\text{H}_5\text{SH}$ gave C_2H_6 , H_2S and $\text{C}_2\text{H}_5\text{SSC}_2\text{H}_5$ as retrievable products. Due to polymer deposits on the cell windows, actinometric measurements were carried out before and after each experiment to determine the average absorbed light intensity. Quenching of the excited Hg atoms by H_2 was estimated to be at least 95%, even at the highest concentration of $\text{C}_2\text{H}_5\text{SH}$ used; see Appendix A for the calculations.

3.1.1 Incident Light Absorption

Because $\text{C}_2\text{H}_5\text{SH}$ absorbs at 254 nm it was important to ensure that all the incident radiation was absorbed by Hg. It has been reported^{150,151} that the absorption of the incident radiation varies with gas pressure, owing to Lorentz broadening of the Hg resonance line. De Maré et al.¹⁵⁰ used a 2 x 5 cm reaction cell in the Hg-photosensitized decomposition of cyclohexene vapor and found that absorption of incident light is complete at > 100 Torr for cyclohexene

and > 150 Torr for propane. Strausz *et al.*¹⁵¹ carried out the Hg-photosensitization of mono- and difluoroethylenes using a 10x5 cm cylindrical quartz cell and obtained correction functions for the Lorentz broadening of the Hg resonance line. The correction functions for C₃H₈, C₂H₃F, C₂H₂F₂ and C₂HF₃ had the form $1/f = A + B/P$, where f is the fraction of incident intensity radiation absorbed and P the pressure in Torr. The values of A and B for all four gases studied were 1.000 ± 0.004 and 2.9 ± 0.1 respectively. In the present actinometric measurements, 600 Torr C₃H₈ was Hg-sensitized in a 10 x 5 cm reaction vessel. The correction function predicts that over 99.5% of the incident radiation was absorbed by Hg.

In a separate experiment, the extent of light intensity absorbed by Hg and a Hg-H₂ mixture was investigated. A 5 x 5 cm cell was saturated with Hg vapor by placing a mercury droplet inside the cell. This was placed in the incident light path between the lamp and the reaction vessel containing C₃H₈. The reduction in H₂ yields indicated that over 60% of the incident light was absorbed by the 5 x 5 cm Hg-saturated cell. The same experiment was performed with the Hg-saturated cell filled with 760 Torr H₂. The actinometric measurements indicated that over 95% of the incident light had been absorbed by the Hg-H₂ cell. Thus, complete absorption of the incident light would be obtained in the 10 x 5 cm reaction vessel used in Hg-photosensitization experiments with C₂H₅SH.

The gas-phase UV absorption spectrum of C_2H_5SH obtained is in agreement with that reported in the literature.^{36,37,63} The maximum absorbance is located at about 230 nm. The extinction coefficient at 298K for C_2H_5SH at 254 nm is $(3.1 \pm 0.1) \times 10^{-3} \text{ Torr}^{-1} \text{ cm}^{-1}$, in good agreement with the value $(3.32 \pm 0.04) \times 10^{-3} \text{ Torr}^{-1} \text{ cm}^{-1}$ reported by Bridges et al.,⁶³ when background correction for reflection by quartz cell is taken into account. Using the Hg vapor pressure value of $2 \times 10^{-3} \text{ Torr}$ ¹⁵² at 25°C and complete absorbance by Hg in a 10-cm cell, the extinction coefficient for Hg is calculated to be $50 \text{ Torr}^{-1} \text{ cm}^{-1}$ at 254 nm. This value is four orders of magnitude greater than that for C_2H_5SH , thus concurrent absorption by C_2H_5SH is negligible in this system.

3.1.2 Effects of Time and Ethanethiol Pressure on Product Quantum Yields

The quantum yields of C_2H_6 , H_2S and $C_2H_5SSC_2H_5$ were determined at 25°C as a function of exposure time at a constant C_2H_5SH pressure of 6.0 Torr. The results, listed in Table 3.1 and plotted in Figure 3.1, show that the quantum yields of C_2H_6 and H_2S are 0.17 ± 0.04 and 0.15 ± 0.05 , respectively, and invariant with exposure time up to 120 minutes; thus C_2H_6 and H_2S are primary products. The small decrease in the values of C_2H_6 and H_2S in runs longer than 30 minutes was likely due to the build-up of polymer deposit on the cell windows, thereby reducing the amount of light transmitted into the reaction vessel. On the other

Table 3.1. The Effect of Exposure Time on Product Quantum Yields^a

Time (minutes)	$\phi(\text{C}_2\text{H}_6)$	$\phi(\text{H}_2\text{S})$	$\phi(\text{C}_2\text{H}_5\text{SSC}_2\text{H}_5)$	I_a (ave) ($10^{-2} \mu\text{Einstein min}^{-1}$)
30	0.19 ± 0.04^b (1) ^c	0.19 ± 0.05 (1)	0.56 ± 0.02 (1)	7.00 ± 0.13 (2)
60	0.17 ± 0.02 (5)	0.14 ± 0.02 (5)	0.47 ± 0.04 (7)	6.78 ± 0.14 (5)
90	0.17 ± 0.02 (4)	0.12 ± 0.02 (4)	0.44 ± 0.01 (3)	7.01 ± 0.24 (5)
120	0.16 ± 0.04 (2)	0.14 ± 0.05 (2)	0.37 ± 0.04 (2)	6.97 ± 0.09 (3)
Average:	0.17 ± 0.04	0.15 ± 0.05	$0.59^d \pm 0.04$	6.92 ± 0.16

^a $T=25^\circ\text{C}$; $P(\text{H}_2)=600$ Torr; $P(\text{C}_2\text{H}_5\text{SH})=6.0$ Torr^bstandard error^cnumber of experiments^dcorrected to zero exposure time.

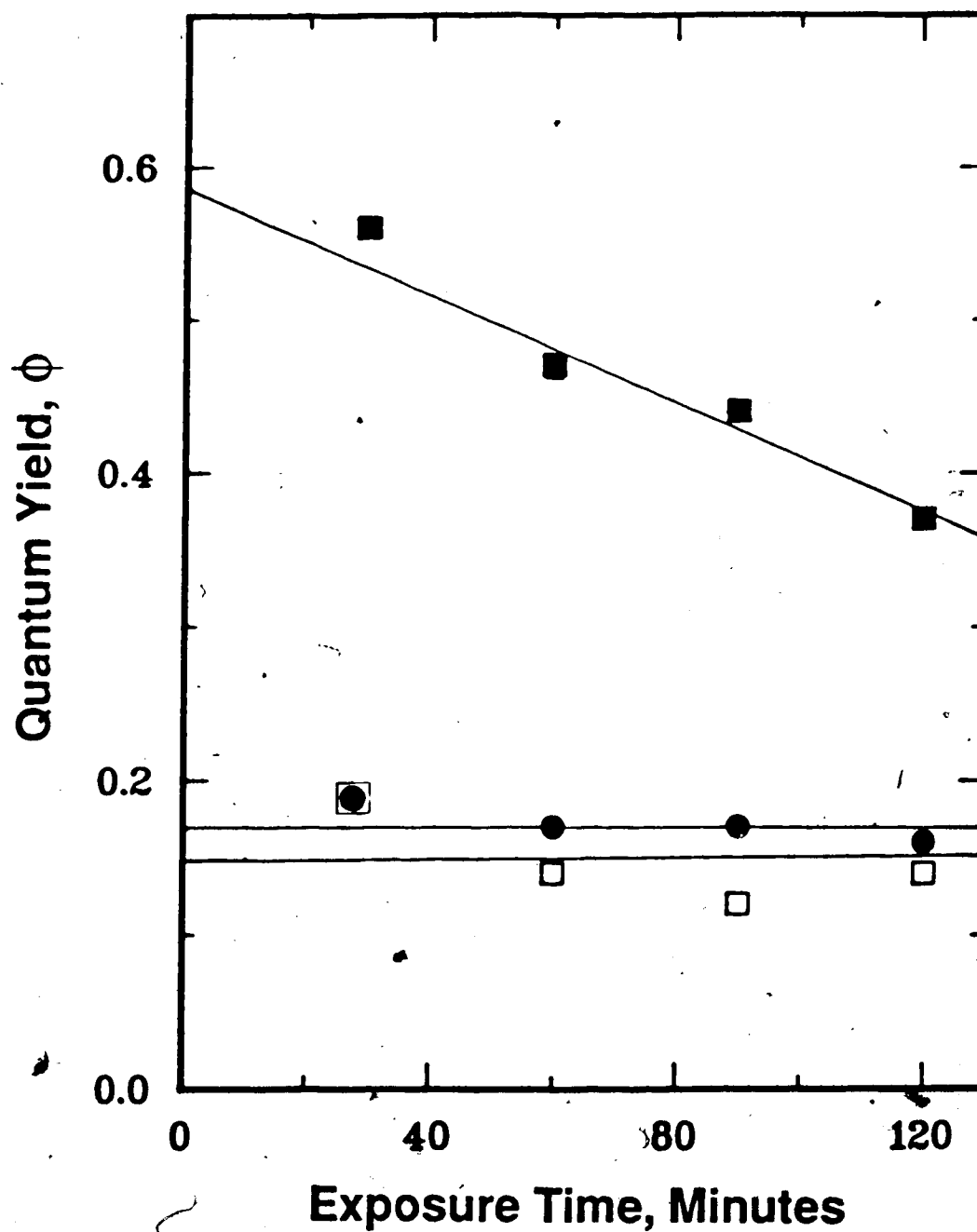
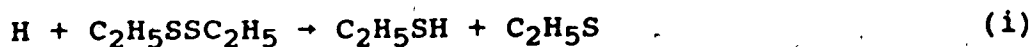


Figure 3.1. Product quantum yields as a function of exposure time. ●, C_2H_6 ; □, H_2S ; ■, $\text{C}_2\text{H}_5\text{SSC}_2\text{H}_5$.

hand, the largest decrease in the quantum yields with exposure time is observed to be in the $C_2H_5SSC_2H_5$ product (Figure 3.1). This loss can be attributed to increased absorption by $C_2H_5SSC_2H_5$ and also to the reaction of H atoms with $C_2H_5SSC_2H_5$, at higher conversion.

The liquid-phase UV absorption spectrum^{153, 154} of $C_2H_5S-SC_2H_5$ indicates that the maximum absorbance is located at 250 nm, with $\epsilon(C_2H_5SSC_2H_5) \approx 300 M^{-1} cm^{-1}$ at 25°C and 254 nm. At low C_2H_5SH pressure and short exposure time, conversion is low and therefore, absorption by $C_2H_5SSC_2H_5$ is minimized. At longer exposure time, however, conversion becomes higher, leading to an increase in the steady-state concentration of $C_2H_5SSC_2H_5$ molecules and therefore, increased absorption. Also at higher $C_2H_5SSC_2H_5$ concentration, the H-atom reaction with $C_2H_5SSC_2H_5$ might occur,



for which k_1 has been determined to be $(4.7 \pm 0.6) \times 10^{13} \exp [-(1710 \pm 70)/RT] cm^3 mol^{-1} s^{-1}$ relative to the rate constant of the $H + C_2H_4 \rightarrow C_2H_5$ reaction.¹¹⁵ Overall, due to absorption and reaction with H atoms, it is necessary to correct for the loss in the yield of $C_2H_5SSC_2H_5$ by extrapolating $\phi(C_2H_5SSC_2H_5)$ to zero exposure time. Thus, the rate of decrease of $\phi(C_2H_5SSC_2H_5)$ with respect to exposure time, t , has been determined by the least-square method to be:

$$\phi(C_2H_5SSC_2H_5) = (0.59 \pm 0.04) - (1.8 \pm 0.1) \times 10^{-3} t$$

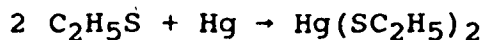
from which $\phi(C_2H_5SSC_2H_5, t \rightarrow 0) \approx 0.59 \pm 0.04$.

In the next set of experiments, the quantum yields of

C_2H_6 , H_2S and $C_2H_5SSC_2H_5$ were determined at $25^\circ C$ as a function of C_2H_5SH pressure. The results, tabulated in Table 3.2, show that $\phi(C_2H_6)$ and $\phi(H_2S)$ are almost constant at low C_2H_5SH pressures (6 - 25 Torr) but increase when the C_2H_5SH pressure is higher than 25 Torr. On the other hand, $\phi(C_2H_5SSC_2H_5)$ increases with increasing C_2H_5SH pressure in the range 6 - 60 Torr.

3.2 Discussion

The scatter in the results (Table 3.1) is probably caused by an unstable concentration of Hg vapor in the system. The appearances of a black film on the wall of the reaction vessel and of a red tinge on the surface of the mercury pool inside the vessel were observed to intensify with time. These are due to the formation of the known compounds, mercury ethyl mercaptide, $Hg(SC_2H_5)_2$, and mercuric sulfide, HgS , in both α (red) and β (black) forms. The reactions of Hg atoms with thiyl radicals may occur in the following manner:



Diethylsulfide was not observed in the products, indicating that its formation from each experimental run was relatively minor. At high pressures, the rate of production of C_2H_5S radicals will increase and the radical-radical combination reaction will occur more readily than the radical-Hg atom reaction. This is shown by the increase in $\phi(C_2H_5SSC_2H_5)$

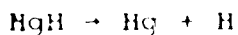
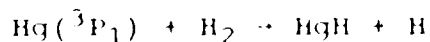
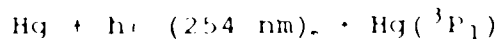
Table 3.2. The Effect of C_2H_5SH Pressure on Product Quantum Yields^a

$P(C_2H_5SH)$ (Torr)	$\phi(C_2H_6)$	$\phi(H_2S)$	$\phi(C_2H_5SSC_2H_5)$
6.0 ^b	0.17±0.01 ^c (11) ^d	0.15±0.03 (11)	0.59±0.01 (13)
10.0	0.20±0.04 (1)	0.14±0.02 (1)	0.57±0.02 (1)
15.0	0.19±0.03 (2)	0.14±0.01 (2)	0.61±0.02 (2)
20.0	0.21±0.04 (1)	0.14±0.02 (1)	0.66±0.03 (1)
25.0	0.21±0.04 (1)	0.17±0.02 (1)	0.67±0.03 (1)
30.0	0.31±0.03 (2)	0.24±0.03 (2)	0.72±0.02 (2)
40.1	0.30±0.04 (2)	0.23±0.02 (2)	0.77±0.03 (2)
60.0	0.28±0.04 (1)	0.26±0.05 (1)	0.70±0.02 (1)

^a $T=25^\circ C$; $P(H_2)=600$ Torr; photolysis time=60 minutes^bsee Table 3.1^cstandard error^dnumber of experiments

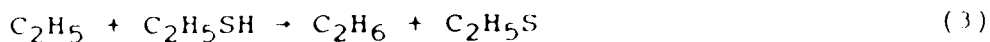
towards high C_2H_5SH pressures.

From the relative H_2/C_2H_5SH concentrations used in this study, it is estimated that > 95% of the excited Hg atoms are quenched by H_2 :



Due to the short lifetime of HgH, the overall kinetics of HgH, for which $\phi(HgH) = 0.67$,¹⁵⁵⁻¹⁵⁸ are indistinguishable from those of H atoms, for which $\phi(H) = 2.0$.¹⁵⁹

From the products observed and their invariance with exposure time, which indicates that they are primary products, the following reaction mechanism would seem to apply:



Although H_2 , produced in step (1), could not be measured in our system, the abstraction of sulfhydryl hydrogen by thermalized H atoms in the photochemical decomposition of gas-phase alkylthiols has been well documented in the literature.^{55,56,58-61,63-67,75,160} However, the molecular displacement by thermalized H atoms, reaction step (2), was not considered by earlier workers. In contrast, Pryor and Olsen⁷⁰ studied the photolyses of *t*-butanethiol, cyclo-

hexanethiol and thiophenol in the liquid phase where H atoms are rapidly thermalized, and from the strong effect of the presence of hydrogen donors on the H_2S yield, they concluded that the displacement reaction is an important step in the mechanism. Although this conclusion was in apparent disagreement with the earlier results of Carlson and Knight⁶⁹ who did not detect H_2S from the liquid phase photolysis of C_2H_5SH , it was supported by the photolysis results of Wu and Kuntz⁹ obtained for cysteine and penicillamine. The importance of the molecular displacement reaction to yield H_2S was further substantiated by the results of Severs *et al.*,⁸¹ Tung and Kuntz¹⁰ and Armstrong and coworkers^{11-13, 15-17} obtained in the radiolysis of butanethiols and different thiols of biological significance. Recently, both reactions (1) and (2) were included in the mechanism proposed by Amano and coworkers^{77, 80} for the H-atom reactions with CH_3SH and $1-C_4H_9SH$. The detection of C_2H_6 as a major product in the present work is clear evidence for the occurrence of the displacement step (2), since no other reaction can lead to the formation of C_2H_6 .

Ethylthiyl radicals can recombine in reaction step (4) to form $C_2H_5SSC_2H_5$, for which $\phi(C_2H_5SSC_2H_5)$ would be unity if this were the only pathway for the loss of C_2H_5S radicals. However, the fact that $\phi(C_2H_5SSC_2H_5)$ is less than unity (Table 3.2) indicates that there are one or more additional pathways for the loss of C_2H_5S radicals. One is through reaction step (5) which is the disproportionation

of C_2H_5S radicals to give the thiol substrate and thioacetaldehyde. Thioacetaldehyde was not detected amongst the products. It is inherently unstable and disappears most likely by a polymerization reaction similar to that for thioformaldehyde which trimerizes readily in the gas phase.^{108,134} The disproportionation/combination ratio for CH_3S radicals, k_5/k_4 , is believed to be 0.05 - 0.11,^{108,110,134} although a value of 0.4 has also been reported.¹⁶¹ For C_2H_5S radicals, Smith and Knight¹¹¹ obtained an upper limit of 0.13 for k_5/k_4 from the study of the Hg-photosensitized decomposition of $C_2H_5SC_2H_5$ vapor at 25°C. Unfortunately, a numerical value for k_5/k_4 cannot be computed from the present results, in part due to the loss of C_2H_5S radicals through other reactions involving Hg atoms as discussed earlier.

The quantum yield expressions obtained from the reaction mechanism for product formation are given by the following:

$$\phi(H_2) = 2k_1/(k_1+k_2)$$

$$\phi(C_2H_6) = \phi(H_2S) = 2k_2/(k_1+k_2)$$

$$\phi(C_2H_5SSC_2H_5) = k_4/(k_4+k_5)$$

These expressions predict that the ϕ 's of the three major products should be pressure-independent, yet the results (Table 3.2) suggest otherwise. The increase in the ϕ 's at higher C_2H_5SH pressures may be due to several causes:

- direct absorption by C_2H_5SH , which would lead to S-H cleavage;

- a small amount of quenching by C_2H_5SH , which also produces $H + C_2H_5S$;¹⁶²
 - for the case of $\phi(C_2H_5SSC_2H_5)$, more quantitative recovery.
- Taken individually, these factors are very small, yet collectively may help to explain the observed trends.

In any case, the observation that C_2H_6 is a major product at low C_2H_5SH pressures, where direct absorption and competitive quenching by C_2H_5SH can be neglected, constitutes additional unequivocal proof of the occurrence of the displacement reaction (2) because in this system, there are no other reactions which could lead to the formation of C_2H_6 . It was necessary to establish this, in order to fully account for the kinetic behaviour of the photolysis of thiols.

CHAPTER FOUR

PHOTOLYSIS OF, AND THE REACTIONS OF HYDROGEN ATOMS WITH, ETHANETHIOL

4.1 Results

The products of photolysis are H_2 , C_2H_4 , C_2H_6 , H_2S and $C_2H_5SSC_2H_5$. Total product conversion was kept low, 4-8%, throughout the pressure and temperature studies in order to avoid secondary absorption by H_2S and $C_2H_5SSC_2H_5$. Thus, over 95% of the incident light was absorbed by the thiol substrate.

4.1.1. H_2S Actinometry

H_2S was employed as the chemical actinometer in this study. The absorbed light intensity in the actinometer vessel, I_2 , is equal to the rate of H_2 production since $\phi(H_2) = 1.00$ in the photolysis of H_2S .¹⁴⁶⁻¹⁴⁹ The absorbed light intensity in the reaction vessel, I_a , is calculated from its relationship to I_2 in the actinometric set-up by the equation,

$$I_a(\text{Einstein min}^{-1}) = [w_1S_0 - (S_6/w_2w_3w_4)]\sigma - I_b/w_2w_3$$

where the w_i 's are the transmittances of vessel windows, determined directly using the empty vessels. S_0 and S_6 are the output signals of the photocell when there is no vessel and when the vessels in the train are filled with C_2H_5SH and H_2S , respectively. σ is the instrumental correlation factor between light intensity and output signal of the photo-cell; see Appendix B for the derivation.

The values of the extinction coefficients for H_2S and

C_2H_5SH were determined from the experimental measurements of S_0 , S_6 and w_i 's, and were found to be 1.09×10^{-4} and $3.39 \times 10^{-3} \text{ Torr}^{-1}\text{cm}^{-1}$ respectively. These extinction coefficients agreed well with the literature values.⁶³

The results of actinometric runs are summarized in Table 4.1. $R(H_2)$ and $R(C_2H_6)$ are the rates of H_2 and C_2H_6 , respectively, obtained from the reaction vessel. The average value for $[R(H_2) + R(C_2H_6)]/I_a$ was found to be 0.99 ± 0.09 . Therefore, the absorbed light intensity in the reaction vessel is equal to $1.01[R(H_2) + R(C_2H_6)]$. A slight increase in the values of $[R(H_2) + R(C_2H_6)]/I_a$ towards higher pressures of C_2H_5SH was observed. This may be caused by the non-axial light due to the compromise taken between perfect collimation and experimentally practical light intensity.

All the quantum yields were calculated by the relation $\phi_i = R_i/I_a$, where R_i ($i = H_2, C_2H_4, C_2H_6, H_2S$ and $C_2H_5SSC_2H_5$) is the rate of product formation and $I_a = 1.01[R(H_2) + R(C_2H_6)]$ as determined from actinometric experiments.

4.1.2 Photolysis of Pure Ethanethiol

The major products were found to be H_2 and $C_2H_5SSC_2H_5$ while the minor products were C_2H_6 , H_2S and C_2H_4 , in agreement with the results reported by Steer and Knight⁶⁷ (SK) and Bridges, Hemphill and White⁶³ (BHW). The dark reaction runs at 25° and 150°C did not produce any measurable products, indicating that C_2H_5SH is thermally stable

Table 4.1. The Results of Chemical Actinometry in C₂H₅SH Photolysis^a

P(C ₂ H ₅ SH) (Torr)	I _a (10 ⁻² μmoles min ⁻¹)	R(H ₂)+R(C ₂ H ₆) (10 ⁻² μmoles min ⁻¹)	I _a	
			R(H ₂)+R(C ₂ H ₆)	R(H ₂)+R(C ₂ H ₆)
5	5.05	4.49	0.889	0.810
5	5.41	4.38	1.006	0.997
10	7.22	7.23	1.027	1.056
10	7.25	9.46	1.052	1.064
15	9.21	10.98		
20	10.40	12.96		
35	12.32	14.53		
48	13.66			
			Average = 0.99±0.09	

^aT=25°C; photolysis time=60 min

within this temperature range. The quantum yields of these products are tabulated in Table 4.2 and are plotted against the pressure of C_2H_5SH in Figure 4.1. Reaction times up to two hours did not alter the quantum yields. The quantum yields of H_2 , C_2H_6 and C_2H_4 are nearly independent of C_2H_5SH pressure in the pressure range 5 - 48 Torr. The quantum yields of $C_2H_5SSC_2H_5$ and H_2S are more scattered at low C_2H_5SH pressures but are less so at pressures over 20 Torr. This scatter is probably caused by fluctuations in the concentration of residual Hg vapour in the system and also by the difficulty in measuring quantitatively small amounts of these products. The points for $\phi(H_2)$, $\phi(C_2H_6)$, $\phi(H_2S)$, $\phi(C_2H_4)$ and $\phi(C_2H_5SSC_2H_5)$ were averaged separately over the entire pressure range studied and found to be 0.77 ± 0.03 , 0.22 ± 0.03 , 0.24 ± 0.06 , 0.030 ± 0.008 and 0.92 ± 0.14 , respectively, at $25^\circ C$. These product quantum yield values are consistent with those of SK and BHW, as shown in Table 4.3.

4.1.3 Photolysis of Ethanethiol with Added Thermalizer, CO_2

Photolyses of C_2H_5SH with added thermalizer, CO_2 , were performed in order to observe the effect of thermalizer pressure on the product quantum yields. The pressure of C_2H_5SH was kept constant at 10 Torr throughout this series of experiments and the pressure of CO_2 was varied between 20 - 400 Torr. While the rates of product formation decreased with respect to increasing thermalizer pressure, the sum of $R(H_2)$ and $R(C_2H_6)$ remained invariant at $(7.4 \pm 0.5) \times 10^{-2}$

Table 4.2. Product Quantum Yields in the Photolysis of Pure C₂H₅SH^a

P(C ₂ H ₅ SH) (Torr)	[R(H ₂)+R(C ₂ H ₆)] (10 ⁻² μmoles min ⁻¹)	φ(H ₂) (±0.02)	φ(C ₂ H ₆) (±0.02)	φ(H ₂ S) (±0.04)	φ(C ₂ H ₄) (±0.005)	φ(C ₂ H ₅ SSC ₂ H ₅) (±0.05)
5	4.4 ± 0.2 ^b (3) ^c	0.765	0.225	0.265	0.0376	0.900
10	7.5 ± 0.1 (8)	0.770	0.220	0.277	0.0299	0.894
15	9.5 ± 0.2 (3)	0.770	0.220	0.232	0.0303	0.892
20	11.2 ± 0.2 (4)	0.769	0.221	0.209	0.0288	0.923
25	12.0 ± 0.3 (1)	0.772	0.218	0.242	0.0213	0.951
30	13.8 ± 0.2 (2)	0.768	0.222	0.242	0.0317	0.890
35	13.1 ± 0.3 (1)	0.782	0.208	0.230	0.0315	0.916
40	14.9 ± 0.2 (3)	0.766	0.223	0.226	0.0273	0.933
48	14.5 ± 0.2 (2)	0.768	0.222	0.221	0.0277	0.938
Average		0.77 ±0.03	0.22 ±0.03	0.24 ±0.06	0.030 ±0.008	0.92 ±0.14

^aT=25°C; photolysis time=60 min; I_a=1.01[R(H₂)+R(C₂H₆)]

^bstandard error

^cnumber of experiments

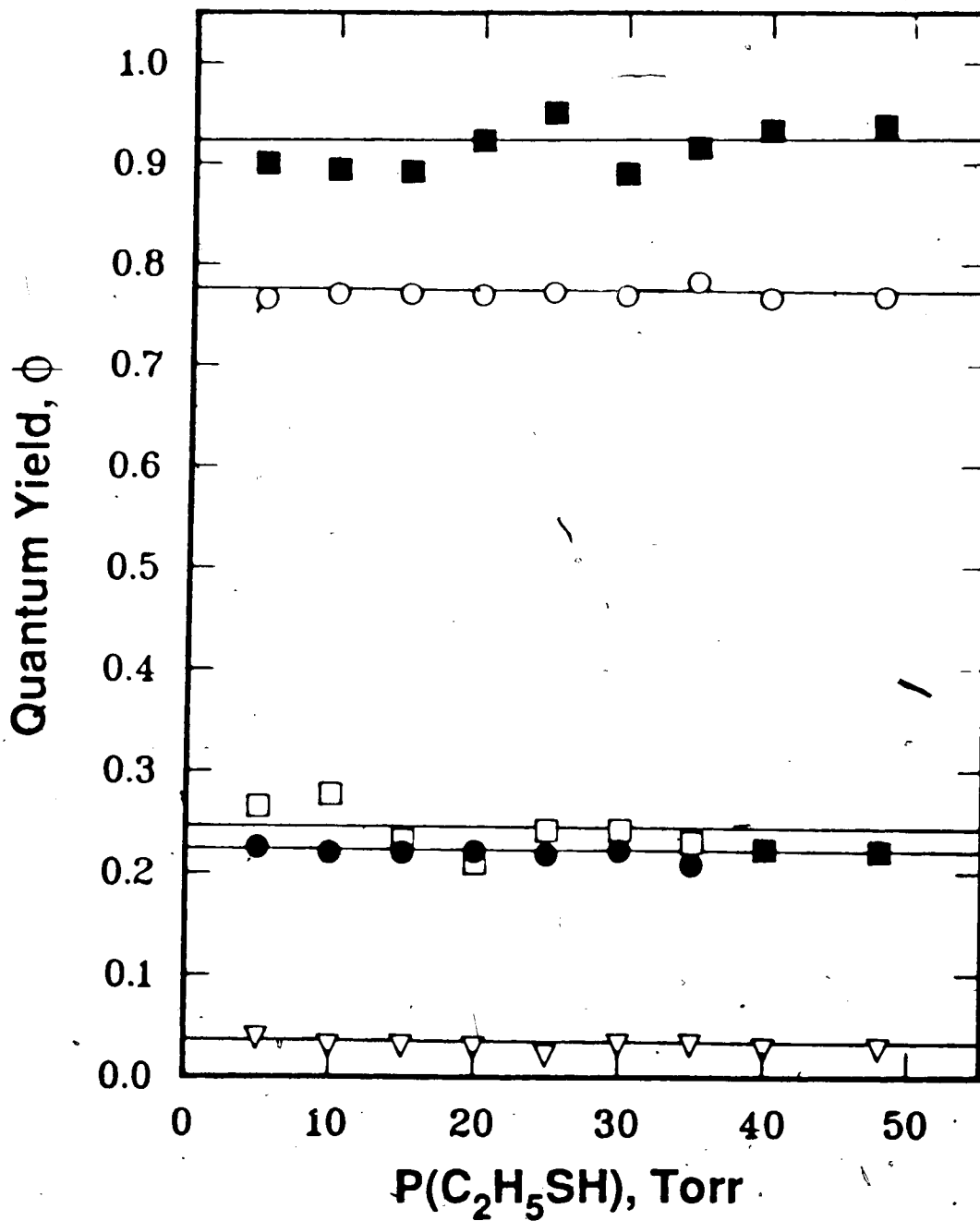


Figure 4.1. Product quantum yields versus C₂H₅SH pressure.

■, (C₂H₅SSC₂H₅); ○, (H₂); □, (H₂S); ●, (C₂H₆);
▽, (C₂H₄).

Table 4.3. Average Product Quantum Yields in the Photolysis of Pure C₂H₅SH^a

$\phi(\text{H}_2)$	$\phi(\text{C}_2\text{H}_6)$	$\phi(\text{H}_2\text{S})$	$\phi(\text{C}_2\text{H}_4)$	$\phi(\text{C}_2\text{H}_5\text{SSC}_2\text{H}_5)$	Reference
0.77 ±0.03	0.22 ±0.03	0.24 ±0.06	0.030 ±0.008	0.92 ±0.14	This work
0.82 ±0.02	0.16 ±0.02	0.19 ±0.03	0.025 ±0.006	--	BHW ^b
0.97 ±0.03	0.22	0.23	0.037	1.26	SK ^c

^a $\phi(\text{C}_2\text{H}_5\text{SH})=5-48$ Torr (This work), 5-22 Torr (BHW), 90-252 Torr (SK); T=25°C; t=60 min
^bvalues reported by BHW were based on HI actinometry
^cvalues reported by SK were calculated from their yields relative to that of H₂

$\mu\text{moles min}^{-1}$. This is shown in Table 4.4, where the experimental product quantum yield results are also listed. The product quantum yields are plotted against CO_2 pressure in the range 0-400 Torr in Figure 4.2. With increasing CO_2 pressure, $\phi(\text{H}_2)$ and $\phi(\text{C}_2\text{H}_5\text{SSC}_2\text{H}_5)$ increased gradually while there was a parallel decrease in $\phi(\text{C}_2\text{H}_6)$, $\phi(\text{H}_2\text{S})$ and $\phi(\text{C}_2\text{H}_4)$. All the quantum yields reach limiting values at a CO_2 pressure of ≥ 200 Torr, which is approximately a tenfold increase of the total pressures. These trends in the ϕ 's with respect to the pressure of inert gas are almost identical to those reported by SK and BHW, who found that the increase in $\phi(\text{H}_2)$ compensated for the decrease in $\phi(\text{C}_2\text{H}_6)$, and that $\phi(\text{H}_2\text{S})$ seemed to be the same as or slightly higher than, $\phi(\text{C}_2\text{H}_6)$.

4.1.4 Effects of Temperature on Product Yields

The photolysis of $\text{C}_2\text{H}_5\text{SH}$ with added thermalizer CO_2 was investigated at elevated temperatures, 80° , 120° and 150°C . The variation of product quantum yields with increasing CO_2 pressure at each temperature was the same as that observed at 25°C . On the other hand, different values of product quantum yields in the absence of CO_2 and at the high CO_2 pressure limit were observed with increasing temperature. As shown in Tables 4.5 to 4.8, $\phi(\text{H}_2)$ and $\phi(\text{C}_2\text{H}_5\text{SSC}_2\text{H}_5)$ decreased while $\phi(\text{C}_2\text{H}_6)$, $\phi(\text{H}_2\text{S})$ and $\phi(\text{C}_2\text{H}_4)$ increased, and the sum of $R(\text{H}_2)$ and $R(\text{C}_2\text{H}_6)$ remained invariant with respect to temperature increases.

Table 4.4. Product Quantum Yields in the Photolysis of C₂H₅SH

with Added Thermalizer, CO₂,^a T = 25°C

P(CO ₂) (Torr)	[R(H ₂)+R(C ₂ H ₆)] ^b (10 ⁻² μmoles min ⁻¹)	φ(H ₂) (±0.02)	φ(C ₂ H ₆) (±0.02)	φ(H ₂ S) (±0.04)	φ(C ₂ H ₄) (±0.005)	φ(C ₂ H ₅ SSC ₂ H ₅) (±0.05)
0 ^c	7.5 (8) ^e	0.77	0.22	0.24	0.030	0.92
20.0	7.6 (2)	0.796	0.194	0.207	0.0216	0.881
35.0	7.5 (2)	0.805	0.185	0.186	0.0176	0.896
50.0	7.3 (2)	0.811	0.179	0.179	0.0163	0.934
70.0	7.6 (2)	0.831	0.159	0.163	0.0146	0.945
100	7.6 (2)	0.835	0.155	0.179	0.0132	0.936
120	7.6 (2)	0.828	0.162	0.159	0.0134	0.925
150	7.4 (1)	0.842	0.148	0.166	0.0116	0.905
200	7.3 (2)	0.835	0.153	0.158	0.0121	0.934
300	7.0 (2)	0.842	0.149	0.156	0.0113	0.921
400	7.0 (3)	0.841	0.149	0.156	0.0101	0.944

^ap(C₂H₅SH)=10.0 Torr or [C₂H₅SH]=5.38 x 10⁻⁴ M; photolysis time=60 min
^baverage [R(H₂)+R(C₂H₆)]=(7.4±0.5) x 10⁻² μmoles min⁻¹; I_a=1.01[R(H₂)+R(C₂H₆)]
^csee results from Table 4.3
^dstandard error
^enumber of experiments

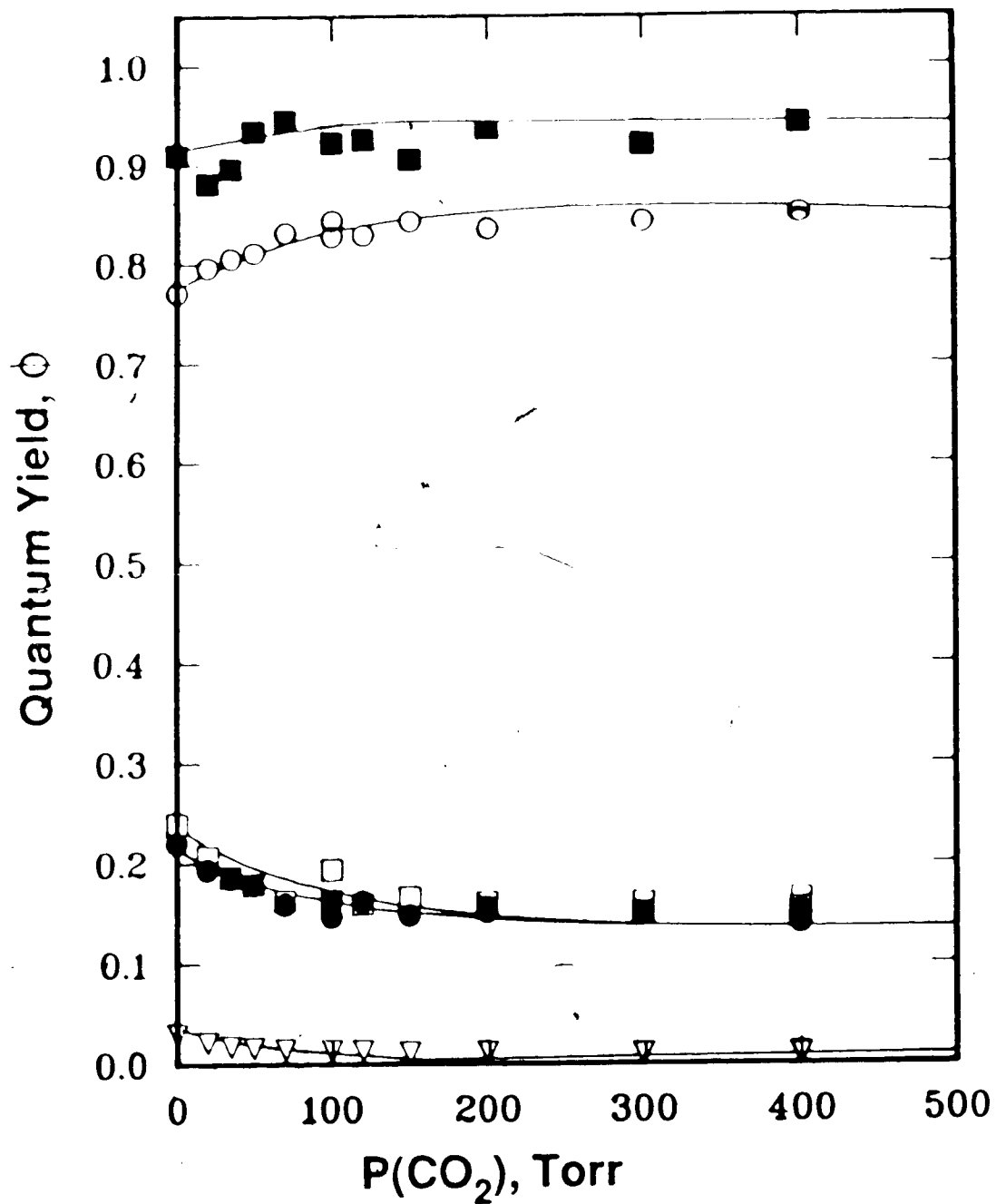


Figure 4.2. Product quantum yields versus CO₂ pressure at constant C₂H₅SH pressure of 10.0 Torr. ■, (C₂H₅SSC₂H₅);

○, (H₂); □, (H₂S); ●, (C₂H₆); ▽, (C₂H₄).

Table 4.5. Product Quantum Yields in the Photolysis of C_2H_5SH

with Added Thermalizer, CO_2 , a $T = 80^\circ C$

P(CO_2) (Torr)	$[R(H_2) + R(C_2H_6)]^b$ (10^{-2} $\mu moles\ min^{-1}$)	$\phi(H_2)$ (± 0.02) ^d	$\phi(C_2H_6)$ (± 0.02)	$\phi(H_2S)$ (± 0.04)	$\phi(C_2H_4)$ (± 0.005)	$\phi(C_2H_5SSC_2H_5)$ (± 0.05)
0	7.4 (5) ^d	0.740	0.250	0.265	0.0336	0.807
33.3	6.9 (1)	0.773	0.217	0.191	0.0226	0.834
41.7	7.5 (3)	0.779	0.211	0.139	0.0213	0.851
59.2	7.6 (2)	0.775	0.215	0.225	0.0181	0.851
83.3	7.3 (2)	0.788	0.202	0.188	0.0162	0.823
119	7.8 (2)	0.790	0.200	0.177	0.0146	0.859
240	7.1 (2)	0.799	0.191	0.195	0.0128	0.852
355	7.2 (2)	0.798	0.192	0.173	0.0114	0.838
475	7.4 (2)	0.804	0.186	0.153	0.0103	0.829

^ap(C_2H_5SH) = 11.9 Torr or [C_2H_5SH] = 5.38×10^{-4} M; photolysis time = 60 min
^baverage [$R(H_2) + R(C_2H_6)$] = $(7.4 \pm 0.5) \times 10^{-2}$ $\mu moles\ min^{-1}$; $I_a = 1.01 [R(H_2) + R(C_2H_6)]$
^cstandard error
^dnumber of experiments

Table 4.6. Product Quantum Yields in the Photolysis of C_2H_5SH

with Added Thermalizer, CO_2 , $I_a = 120 \text{ } ^\circ C$

P(CO_2) (Torr)	$[R(H_2) + R(C_2H_6)]^b$ (10^{-2} $\mu\text{moles min}^{-1}$)	$\phi(H_2)$ (± 0.02)	$\phi(C_2H_5)$ (± 0.02)	$\phi(H_2S)$ (± 0.04)	$\phi(C_2H_4)$ (± 0.005)	$\phi(C_2H_5SSC_2H_5)$ (± 0.05)
0	7.8 (2) ^d	0.728	0.262	0.294	0.0370	0.791
37.0	7.3 (2)	0.756	0.234	0.237	0.0232	0.788
46.2	7.2 (2)	0.752	0.238	0.242	0.0224	0.845
66.0	7.5 (2)	0.751	0.239	0.227	0.0195	0.819
92.4	7.1 (2)	0.758	0.232	0.230	0.0177	0.817
130	7.5 (2)	0.762	0.228	0.210	0.0155	0.846
265	7.5 (2)	0.767	0.223	0.216	0.0133	0.851
395	7.2 (2)	0.772	0.218	0.211	0.0112	0.840
530	7.0 (2)	0.776	0.214	0.209	0.0114	0.851

^a $P(C_2H_5SH) = 13.2$ Torr or $[C_2H_5SH] = 5.38 \times 10^{-4}$ M; photolysis time = 60 min
^baverage $[R(H_2) + R(C_2H_6)] = (7.3 \pm 0.4) \times 10^{-2}$ $\mu\text{moles min}^{-1}$; $I_a = 1.01 [R(H_2) + R(C_2H_6)]$;
^cstandard error
^dnumber of experiments

Table 4.7. Product Quantum Yields in the Photolysis of C_2H_5SH

with Added Thermalizer, CO_2 , $T = 150^\circ C$

P(CO ₂) (Torr)	[R(H ₂) + R(C ₂ H ₆)] ^b (10 ⁻² μmoles min ⁻¹)	φ(H ₂) (±0.02)	φ(C ₂ H ₆) (±0.02)	φ(H ₂ S) (±0.004)	φ(C ₂ H ₄) (±0.005)	φ(C ₂ H ₅ SSC ₂ H ₅) (±0.05)
0	7.4 (3) ^d	0.730	(0.260	0.209	0.0388	0.753
39.8	7.1 (2)	0.737	0.253	0.239	0.0282	0.766
49.7	7.0 (2)	0.739	0.251,	0.227	0.0248	0.789
71.0	7.2 (2)	0.740	0.250	0.267	0.0235	0.800
99.4	7.0 (2)	0.746	0.244	0.239	0.0229	0.772
140	7.3 (2)	0.744	0.246	0.241	0.0185	0.798
285	7.1 (2)	0.753	0.237	0.223	0.0141	0.854
425	7.2 (2)	0.755	0.235	0.217	0.0149	0.793
570	6.9 (2)	0.758	0.232	0.237	0.0134	0.831

^ap(C₂H₅SH)=14.2 Torr or [C₂H₅SH]=5.38 x 10⁻⁴ M; photolysis time=60 min
^baverage [R(H₂) + R(C₂H₆)]=(7.1±0.4) x 10⁻² μmoles min⁻¹; I_a=1.01[R(H₂)+R(C₂H₆)]
^cstandard error
^dnumber of experiments

Table 4.8. Product Quantum Yields^a at High Total Pressure Limits^b

Temperature (°C)	$[R(H_2)+R(C_2H_6)]^c$ (10^{-2} $\mu\text{moles min}^{-1}$)	$\phi(H_2)$	$\phi(C_2H_6)$	$\phi(H_2S)$	$\phi(C_2H_4)$	$\phi(C_2H_5SSC_2H_5)$
25	7.4 $\pm 0.5^d$	0.84 ± 0.02	0.15 ± 0.02	0.16 ± 0.02	0.011 ± 0.004	0.93 ± 0.04
80	7.4 ± 0.5	0.80 ± 0.02	0.19 ± 0.02	0.17 ± 0.02	0.012 ± 0.005	0.86 ± 0.03
120	7.3 ± 0.4	0.77 ± 0.03	0.22 ± 0.03	0.21 ± 0.02	0.012 ± 0.005	0.85 ± 0.02
150	7.1 ± 0.3	0.75 ± 0.03	0.24 ± 0.02	0.23 ± 0.03	0.014 ± 0.004	0.83 ± 0.03

^aeach quantum yield value is the average of 6-10 experimental points

^b $P(C_2H_5SH) = 10.0-14.2$ Torr or $[C_2H_5SH] = 5.38 \times 10^{-4}$ M

$P(CO_2) = 200-570$ Torr or $[CO_2] = (1.08-2.15) \times 10^{-2}$ M

^caverage of 18-20 experimental values; $I_a = 1.01 [R(H_2)+R(C_2H_6)]$

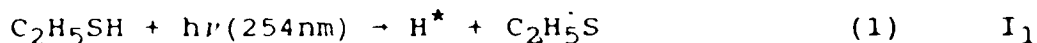
^dstandard error

4.2. Discussion

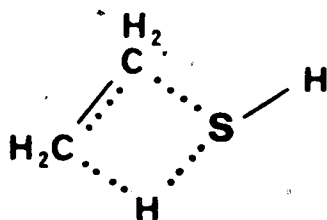
4.2.1 Reaction Mechanism

The following reaction mechanism is used to account for the products observed and to adequately explain our experimental results in quantitative terms. It consists of three sets of elementary reactions, namely, a set of primary photochemical steps, a set of hot reactions, and a set of thermal reactions.

The primary photochemical reactions are identical to those proposed by BHW. They are as follows:



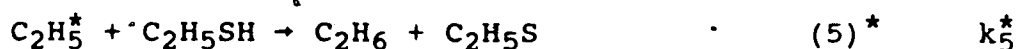
The first and second primary photochemical steps are simply the cleavage of S-H and C-S bonds respectively, while the third primary photochemical step is the concerted 1,2-elimination of H₂S reaction, involving a four-membered transition state,

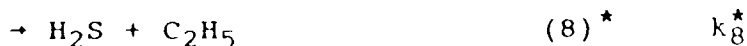


The enthalpies of reaction for 1, 2 and 3 are 88, 71 and 18 kcal mol⁻¹, respectively, using thermochemical data from Table 1.2. While the elimination step (3) is favoured thermodynamically, the activation barrier has been calculated, using ab initio SCF-MO calculations,⁵⁰ to be much

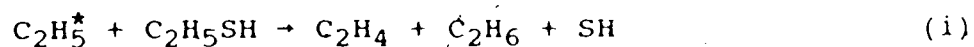
higher at $-77 \text{ kcal mol}^{-1}$. From the available photon energy at 254 nm, $E_0 = 113 \text{ kcal Einstein}^{-1}$, the excess energies for (1) and (2) are calculated from $E_0 - [D(\text{S-H}) \text{ or } D(\text{C-S})]$, to be 24 and 41 kcal mol^{-1} , respectively. White and coworkers^{65,167,168} have examined the energy distribution in the first primary step at several wavelengths (185 - 254 nm) and have shown that the excess energy resides chiefly in the translational motion of the H atom produced rather than in the internal modes of the $\text{C}_2\text{H}_5\text{S}$ radical. The energy distribution for the second primary step has not been studied. However, photolyses of alkyl halides^{169,170} are generally considered to be suitable sources for hot alkyl radicals, presumably formed from the primary dissociation. The question of excess energy distribution in steps (1) and (2) can only be explained when more information concerning the nature and the energy hypersurface(s) of the electronically excited state(s) become known. It may be that two different states are populated, one of which dissociates immediately to $\text{C}_2\text{H}_5\text{S} + \text{H}$, with the energy being carried away by the H atom, while the other has a longer lifetime and undergoes redistribution of excess energy before decomposing; alternatively, perhaps only one state is available and the dissociation (2) takes place from vibrationally and rotationally relaxed levels of the excited state.

The hot reactions are as follows;





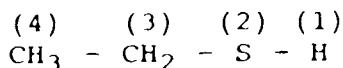
The unimolecular decomposition of C_2H_5^* to give the C_2H_4 product from (4)* is different from the step proposed by BHW,



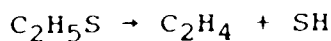
The average excess energy in the ethyl radicals is the sum of 42 kcal mol⁻¹, step (2), and 5 - 8 kcal mol⁻¹, the internal energy in C_2H_5 , which is calculated from $0.5(sRT)$,¹⁶³ where s is the number of oscillators estimated from $3N - 6$ degrees of freedom. Thus, the total excess energy of 47 - 50 kcal mol⁻¹ is greater than the critical energy for (4)*, estimated to be 38 kcal mol⁻¹, from the results of Trenwith,¹⁷¹ obtained in the pyrolysis of ethane at the limiting high-pressure. The difference of about 9 - 12 kcal mol⁻¹ is the active energy available to the C_2H_5 radicals. Rabinovitch and Setser¹⁴² have determined the variation of the rate constant for (4)* with the amount of active energy residing in the C_2H_5 radicals. They estimated that for an active energy content of 9 - 12 kcal mol⁻¹, $k_4^* \approx 10^9 \text{ s}^{-1}$, which is about four orders of magnitude greater than the k_4^* value of $6.3 \times 10^5 \text{ s}^{-1}$, obtained with no active energy. Therefore, it is reasonable to assume that some of the C_2H_5 radicals dissociate readily into $\text{H} + \text{C}_2\text{H}_4$ before losing the excess energy by collisional quenching processes. This source reaction for C_2H_4 formation is more attractive

than the esoteric reaction step (i) proposed by BHW which requires the rearrangement of many bonds. Reaction (i) is unlikely to occur when we consider the four possible

attacking sites in C_2H_5SH by $C_2H_5^*$

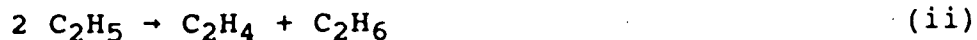


The abstraction of H from SH produces C_2H_6 and $C_2H_5S^*$ radicals which do not have sufficient energy in order to further dissociate into C_2H_4 and SH,



This reaction is endothermic with an enthalpy of reaction, 61 kcal mol⁻¹. Another possible attack at S in C_2H_5SH by $C_2H_5^*$ could cause cleavage of the S-H bond or the C-S bond. The former leads to the formation of H and $C_2H_5SC_2H_5$ which was not found in the reaction products. The latter exchanges C_2H_5 and is equivalent to the quenching step. Neither mode of reaction leads to the formation of C_2H_4 . The last two possible cases, where $C_2H_5^*$ attacks an H in the C_2H_5 group, both cause the cleavage of a C-H bond which leads to the formation of C_2H_6 and H_2CCH_2SH or H_3CCHSH . Again, these radicals cannot decompose subsequently into C_2H_4 and HS, since there is no energy transfer. Finally, the equivalent reaction by H^* must occur if this mode of reaction by $C_2H_5^*$ is taking place. This, however, is not considered by earlier investigators^{58,63,67} to be important.

The possibility of C_2H_4 and C_2H_6 being formed from the disproportionation reaction of C_2H_5 radicals



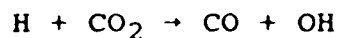
was also considered, for which the constant for the disproportionation to the combination reaction,



$k_{\text{iii}}/k_{\text{iiii}}$, has been determined to be 0.14 ± 0.02 .^{164,171}

However, since no n-C₄H₁₀ was observed in the photolysis products, disproportionation is not considered to be an alternative pathway for the formation C₂H₄ and C₂H₆.

Quenching of hot H and C₂H₅ radicals by collisional deactivation is indicated by reactions steps (6)* and (9)*. The collisional deactivating molecule may be either the substrate C₂H₅SH or the thermalizer CO₂ molecules. The possibility of H-atom reacting with CO₂ was rejected on the basis of the endothermicity of the reaction,

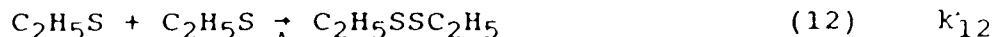
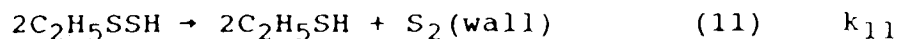
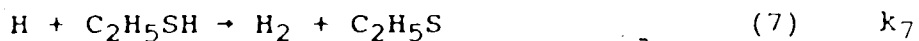


which requires a threshold energy of 24.4 kcal mol⁻¹.¹⁷²

At low total pressures, quenching by C₂H₅SH predominates over that by CO₂. However, quenching by CO₂ becomes more efficient at about a twentyfold increase in the CO₂ pressure, with the percentage quenching by CO₂ increasing from 63% at P(CO₂) = 20 Torr to 97% at P(CO₂) = 400 Torr; see Appendix C for the calculation. Complete quenching occurs at P(CO₂) ≥ 200 Torr, as shown by the flat portion of the plot in Figure 4.2.

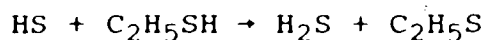
The corresponding thermal reactions for H and C₂H₅ radicals, and the fates of thiyl radicals are as follows:



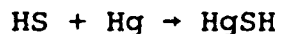


The occurrence of all of these thermal reaction steps, with the exception of (10) and (11), have been confirmed in the Hg-photosensitization study of the $\text{H} + \text{C}_2\text{H}_5\text{SH}$ system (Chapter 3).

Both SK and BHW postulated the isoenergetic reaction of HS radicals with $\text{C}_2\text{H}_5\text{SH}$ for the formation of H_2S in the gas phase,



The rate constant for this reaction is not known. If it is slow, then HS radicals will be consumed faster by $\text{C}_2\text{H}_5\text{S}$ radicals in Reaction (10), leading to the formation of the unstable alkyl-hydrodisulfide,¹⁷³ $\text{C}_2\text{H}_5\text{SSH}$, which decomposes subsequently via Reaction (11) and contributes to the deposit of solid material on the walls of the reaction vessel. The scatter in the quantum yield of H_2S and $\text{C}_2\text{H}_5\text{SSC}_2\text{H}_5$ at low total pressures, as seen in Figure 4.1, is caused by the presence of Hg atoms in our system. The reactions of $\text{C}_2\text{H}_5\text{S}$ radicals with Hg atoms have already been discussed in Chapter 3. The reactions of HS radicals with Hg atoms occur in a similar manner:





These second-order reactions may occur at low total pressures since a relatively heavy deposit of solid material was observed on the walls of the reaction vessel. However, almost no deposit could be seen at high total pressures. This is likely due to the faster diffusion of Hg vapour to the walls at low pressures than at high pressures. Also, at high substrate pressures, the production of HS and C₂H₅S radicals will increase, and thus radical-radical reactions (10) - (13) will occur more readily than radical-Hg atom reactions.

A steady-state treatment of the proposed mechanism yields the following expressions for the quantum yields of products; see Appendix D for the complete derivation.

$$\phi(\text{C}_2\text{H}_4) = \phi_3 + \frac{k_4^* \phi_2}{k_4^* + k_5^*[\text{E}] + k_6^*[\text{M}]} \quad [1]$$

$$\begin{aligned} \phi(\text{H}_2) = & \frac{k_7 \phi_1}{k_7 + k_8} - \frac{(k_7 k_8^* - k_7^* k_8) \phi_1 [\text{E}]}{(k_7 + k_8) \{ (k_7^* + k_8^*) [\text{E}] + k_9^* [\text{M}] \}} \\ & + \frac{k_4^* k_7 \phi_2}{(k_7 + k_8) (k_4^* + k_5^* [\text{E}] + k_6^* [\text{M}])} \quad [2] \end{aligned}$$

$$\begin{aligned} \phi(\text{C}_2\text{H}_6) = & \frac{k_8 \phi_1}{k_7 + k_8} + \phi_2 + \frac{(k_7 k_8^* - k_7^* k_8) \phi_1 [\text{E}]}{(k_7 + k_8) \{ (k_7^* + k_8^*) [\text{E}] + k_9^* [\text{M}] \}} \\ & - \frac{k_4^* k_7 \phi_2}{(k_7 + k_8) (k_4^* + k_5^* [\text{E}] + k_6^* [\text{M}])} \quad [3] \end{aligned}$$

$$\phi(\text{H}_2\text{S}) = \frac{k_8 \phi_1}{k_7 + k_8} + \phi_3 + \frac{(k_7 k_8^* - k_7^* k_8) \phi_1 [E]}{(k_7 + k_8) ((k_7^* + k_8^*) [E] + k_9^* [M])} + \frac{k_4^* k_8 \phi_2}{(k_7 + k_8) (k_4^* + k_5^* [E] + k_6^* [M])} \quad [4]$$

$$\phi(\text{C}_2\text{H}_5\text{SSC}_2\text{H}_5) = \frac{k_{12} \phi_1}{k_{12} + k_{13}} \quad [5]$$

ϕ_1 , ϕ_2 and ϕ_3 are the quantum yields associated with the three primary photochemical reactions, (1) - (3). M is a collisional deactivating molecule and may be either the substrate $\text{C}_2\text{H}_5\text{SH}$ or the thermalizer CO_2 molecules. The expressions for $k_6^* \text{M}$ and $k_9^* \text{M}$ are $k_{6\text{E}}^* [\text{E}] + k_{6\text{C}}^* [\text{C}]$ and $k_{9\text{E}}^* [\text{E}] + k_{9\text{C}}^* [\text{C}]$, respectively. [E] is the concentration or pressure of $\text{C}_2\text{H}_5\text{SH}$ and [C] is that of added CO_2 .

4.2.2 Quantum Efficiencies of Primary Photochemical Steps: Quantum Yield of C_2H_4

The quantum yield of C_2H_4 was plotted against the ratio $P(\text{CO}_2)/P(\text{C}_2\text{H}_5\text{SH})$ in Figure 4.3 in order to show detailed changes of $\phi(\text{C}_2\text{H}_4)$ as a function of CO_2 pressure at 25, 80, 120 and 150°C, Tables 4.4 - 4.7. At each temperature, $\phi(\text{C}_2\text{H}_4)$ decreases very rapidly with increasing CO_2 pressure and becomes approximately constant at high pressures of CO_2 . This indicates that there are two different sources of C_2H_4 . One pathway does not depend on CO_2 pressure, while the other is completely suppressed at high pressures of CO_2 . The first corresponds to the primary photochemical step (3) and the second, to Reaction (4)*, where the hot ethyl radicals decompose to H and C_2H_4 . This is clearly shown in Equation [1]

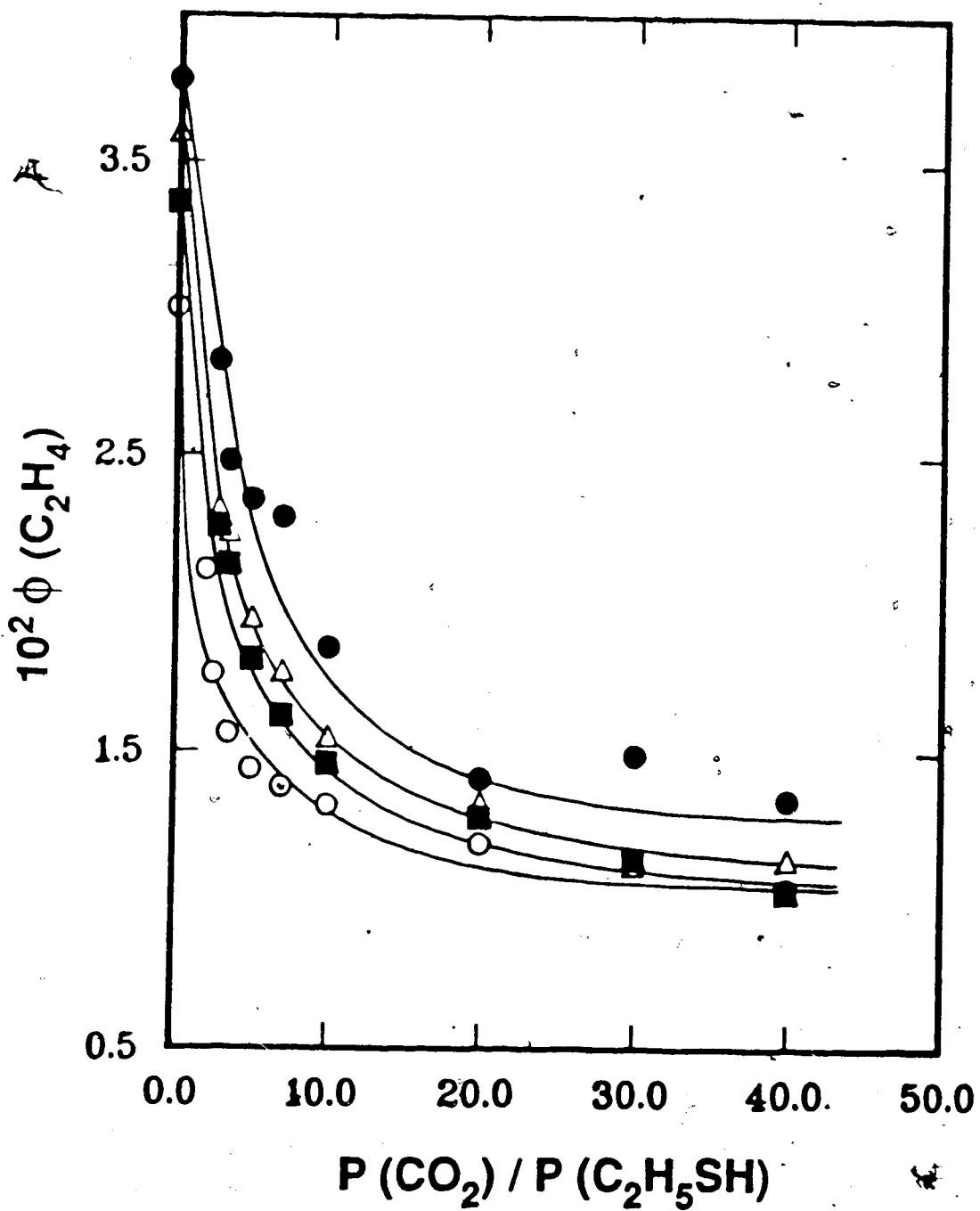


Figure 4.3. Plots of quantum yield of C_2H_4 as a function of $P(CO_2)/P(C_2H_5SH)$. ○, 25°C; ■, 80°C; △, 120°C; ●, 150°C.

which consists of a constant term and a pressure-dependent term. In order to find the value of ϕ_3 , Equation [1] is modified as follows;

$$[\phi(\text{C}_2\text{H}_4) - \phi_3]^{-1} = (1 + \alpha P_E)/\phi_2 + \beta P_C/\phi_2 \quad [6]$$

where $\alpha = (k_5^* + k_{6E}^*)/k_4^*$, $\beta = k_{6C}^*/k_4^*$ and $[\phi(\text{C}_2\text{H}_4) - \phi_3]^{-1}$ is a linear function of P_C at constant P_E .

In the first approximation, the linear correlation coefficient for Equation [6] was calculated for ten values of ϕ_3 , ranging from 0.0095 to 0.0105. The result, Figure 4.4, shows that the highest coefficient is obtained with $\phi_3 = 0.010$, which corresponds closely to the average experimental value $\phi(\text{C}_2\text{H}_4) = 0.011$ in the high (200 - 400 Torr) CO_2 pressure region at 25°C (see Figure 4.3).

Equation [6] predicts that for $P_C = 0$, $\phi(\text{C}_2\text{H}_4)$ becomes a linear function of P_E :

$$[\phi(\text{C}_2\text{H}_4) - \phi_3]^{-1} = 1/\phi_2 + \alpha P_E/\phi_2 \quad [7]$$

Although the plot of $\phi(\text{C}_2\text{H}_4)$ versus $P(\text{C}_2\text{H}_5\text{SH})$, Figure 4.1, does not appear to exhibit any pressure dependence, the results in Table 4.2 indicate that $\phi(\text{C}_2\text{H}_4)$ does in fact very marginally decrease with increasing $\text{C}_2\text{H}_5\text{SH}$ pressure. This is clearly shown in Figure 4.5, where the ordinate scale is much expanded. As does Figure 4.3, Figure 4.5 clearly indicates that there are two sources of C_2H_4 formation as postulated in the mechanism.

The values for $[\phi(\text{C}_2\text{H}_4) - \phi_3]^{-1}$ at $P_C = 0$ were calculated using $\phi_3 = 0.010$ and were plotted against $\text{C}_2\text{H}_5\text{SH}$ pressure in Figure 4.6. The following linear relation was

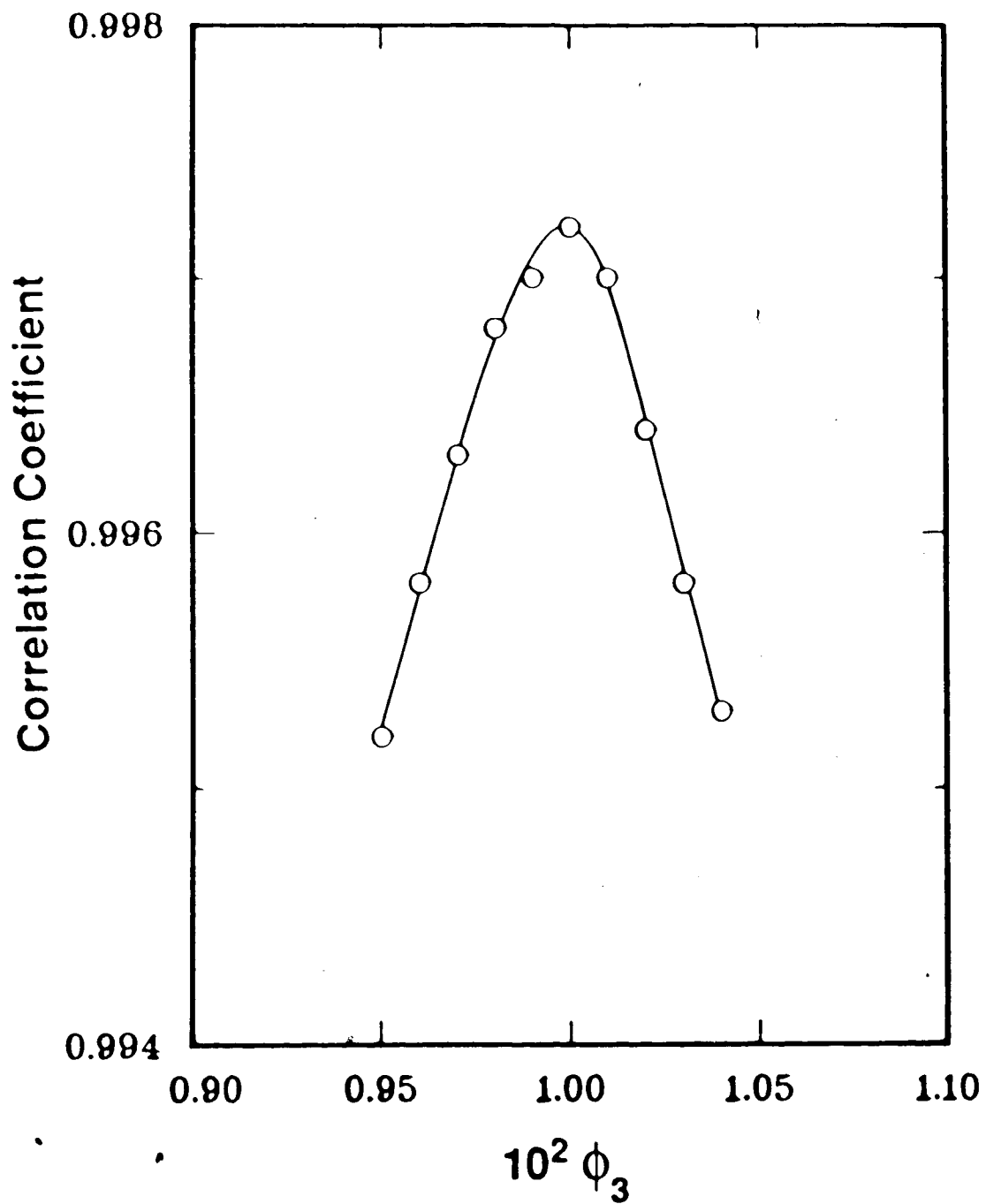


Figure 4.4. Relation between ϕ_3 and the correlation coefficient in the LMS treatment of $[\phi(\text{C}_2\text{H}_4) - \phi_3]^{-1}$ against CO_2 pressure.

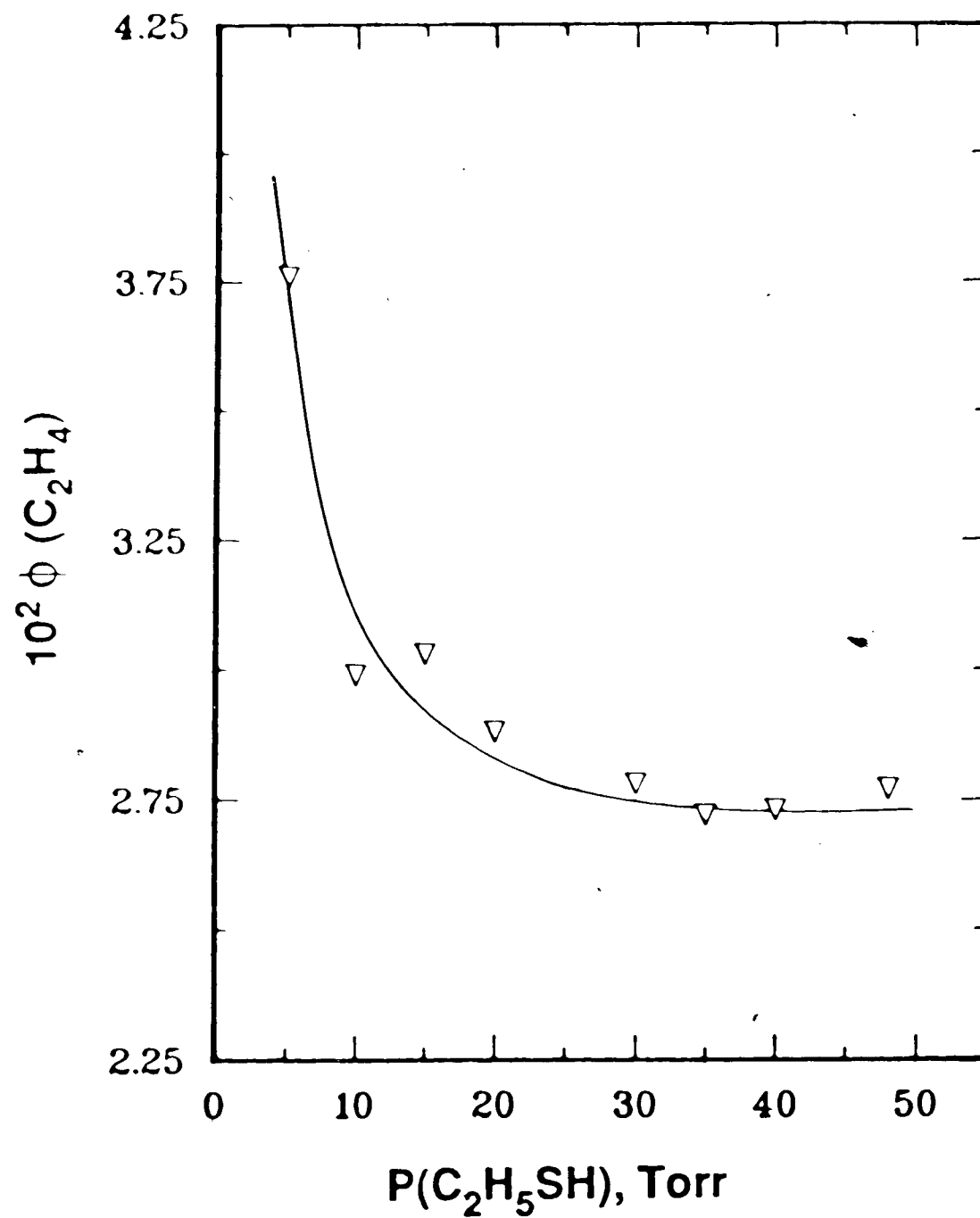


Figure 4.5. Quantum yield of C_2H_4 versus C_2H_5SH pressure.

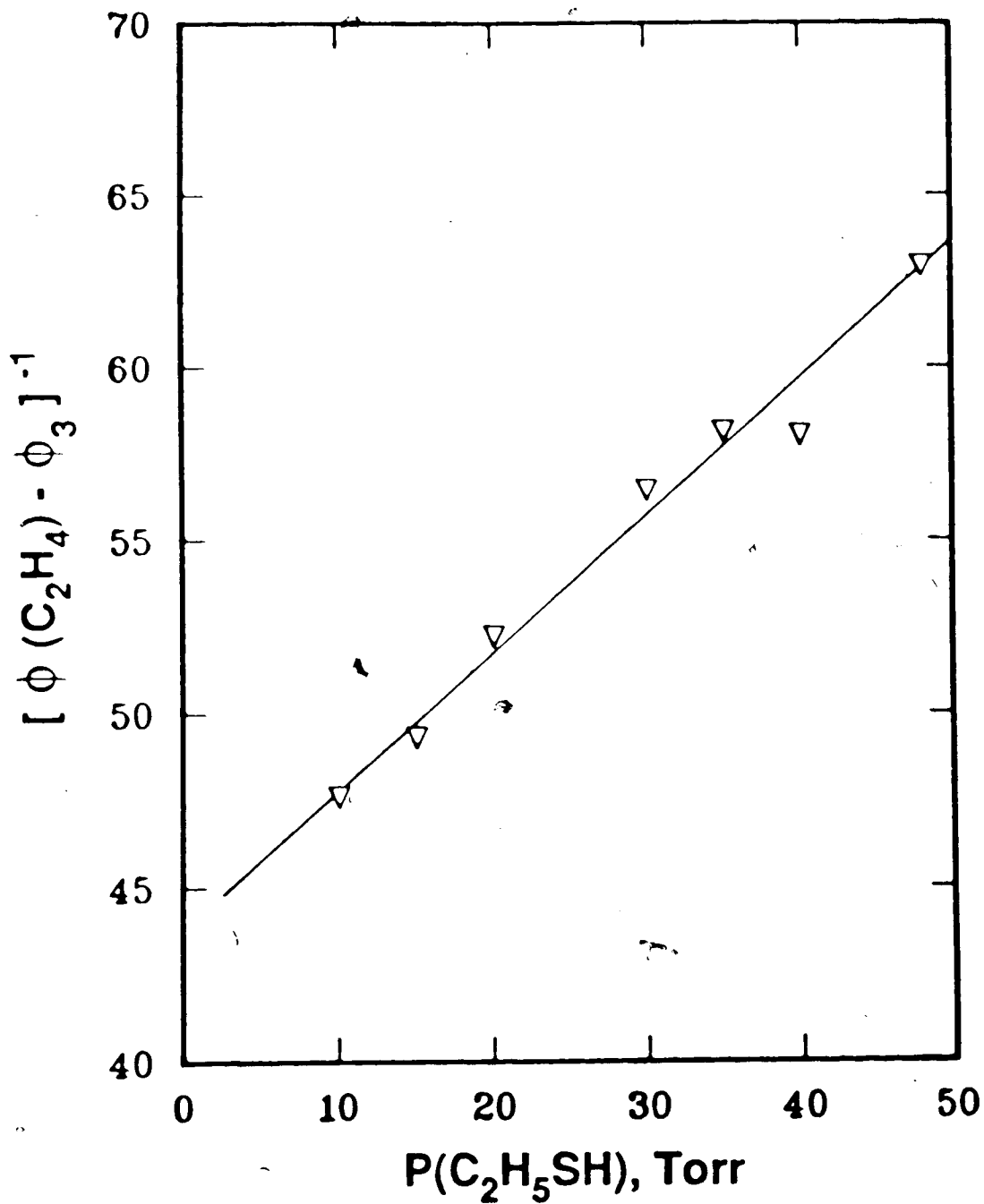


Figure 4.6. $[\phi(\text{C}_2\text{H}_4) - \phi_3]^{-1}$ versus $\text{C}_2\text{H}_5\text{SH}$ pressure. The best fitted value of $\phi_3 = 0.010$ was used.

derived by the LMS method, for the condition $P_C = 0$;

$$[\phi(\text{C}_2\text{H}_4) - \phi_3]^{-1} = (44.0 \pm 0.9) + (0.38 \pm 0.03)P_E \quad [8]$$

Combining this equation with Equation [7], ϕ_2 and α were determined to be 0.023 ± 0.002 and $(8.7 \pm 0.8) \times 10^{-3} \text{ Torr}^{-1}$, respectively, at room temperature.

The values of ϕ_2 may now be obtained from the intercepts of Equation [6]. Figure 4.7 shows the plots of $[\phi(\text{C}_2\text{H}_4) - \phi_3]^{-1}$ versus $P(\text{CO}_2)/P(\text{C}_2\text{H}_5\text{SH})$ (Table 4.9), from which the derived intercepts are listed in Table 4.10. It is assumed that any temperature variations in α and ϕ_3 are minor and can be neglected. This assumption possibly may not be strictly valid for the case of ϕ_3 , nevertheless the experimental results (Table 4.8) indicate that the changes in ϕ_3 up to 150°C are almost within experimental error. The derived values of ϕ_2 are listed in Table 4.11, along with those of ϕ_1 ($\phi_1 + \phi_2 + \phi_3 = 1.0$). The results of BHW and SK are also included for the sake of comparison. A slight increase in ϕ_2 ($0.023 - 0.036$) and consequently a decrease in ϕ_1 ($0.97 - 0.95$) is observed with increasing temperature. However, this variation is small when compared with the experimental limitations. As a result, the quantum efficiencies of the primary photochemical reactions can be considered to be independent of temperature up to 150°C , within an experimental error of $\pm 3\%$. The average values for ϕ_1 , ϕ_2 and ϕ_3 from this work are then 0.96 ± 0.01 , 0.029 ± 0.006 and 0.010 ± 0.001 , respectively. The differences between these values and those of SK and BHW (Table

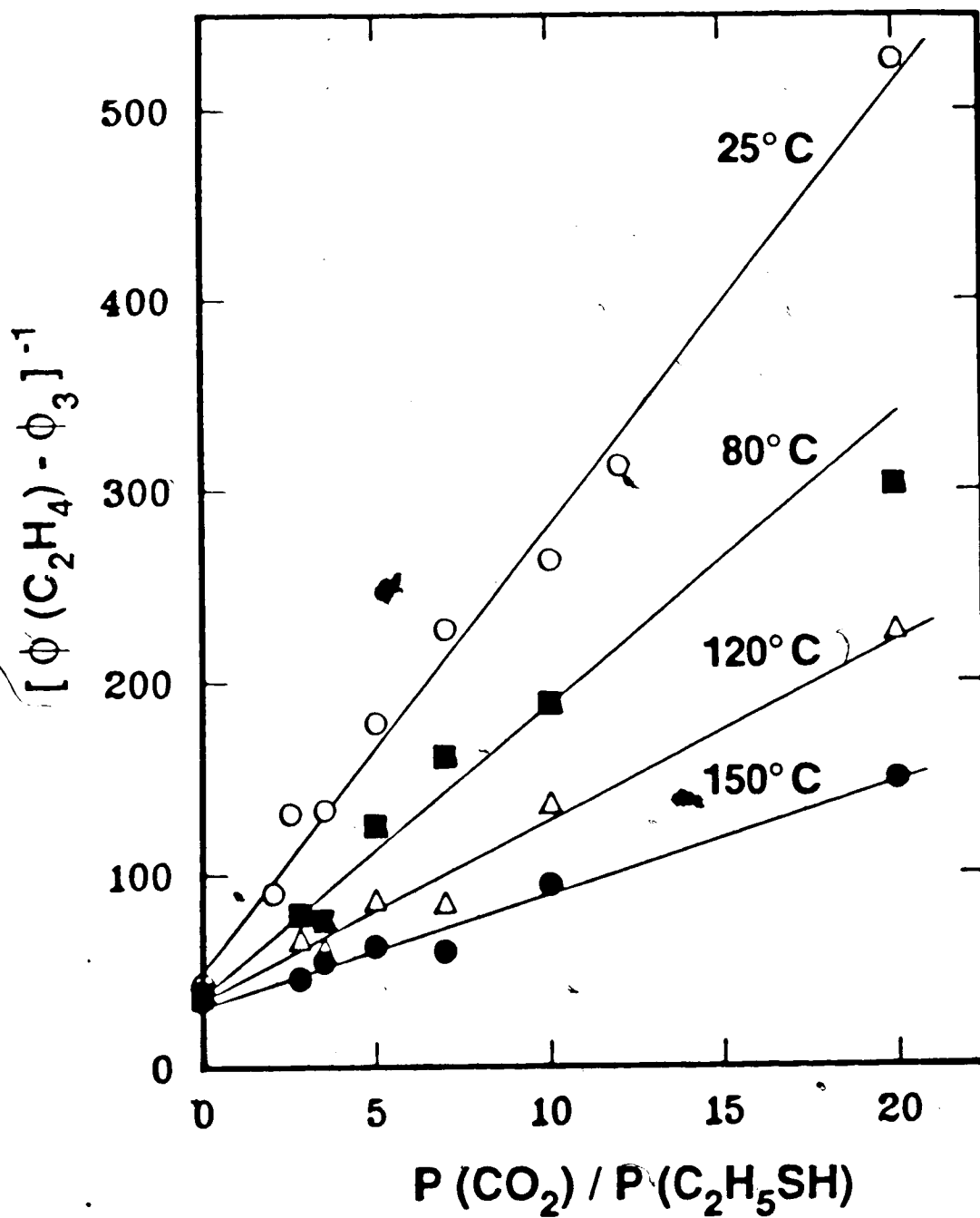


Figure 4.7. Plot of $[\phi(\text{C}_2\text{H}_4) - \phi_3]^{-1}$ as a function of $P(\text{CO}_2) / P(\text{C}_2\text{H}_5\text{SH})$. The best fitted value of $\phi_3 = 0.010$ was used.

Table 4.9. Variations of $[\phi(C_2H_4) - \phi_3]^{-1}$ a with Pressure^b and Temperature

[P(CO ₂)/P(C ₂ H ₅ SH)]	$[\phi(C_2H_4) - \phi_3]^{-1}$			
	25°C	80°C	120°C	150°C
0	43.3	38.3	36.4	34.7
2.0	90.1	-	-	-
2.5	131.6	-	-	-
2.8	-	79.4	66.7	45.9
3.5	133.3	76.3	61.7	54.5
5.0	178.6	125.5	87.0	62.5
7.0	227.3	161.3	85.5	59.9
10.0	263.2	188.7	137.0	94.3
12.0	312.5	-	-	-
20.0	526.3	303.0	227.3	149.3

^a $\phi_3 = 0.010$

^bP(CO₂) = 0-284 Torr or [CO₂] ≤ 1.08 × 10⁻² M

P(C₂H₅SH) = 10.0-14.2 Torr or [C₂H₅SH] = 5.38 × 10⁻⁴ M

Table 4.10. Intercepts of the Plots in Figure 4.7

Temperature (°C)	P(C ₂ H ₅ SH) (Torr)	Intercept ^a	Correlation Coefficient
25	10.0	53 ± 8 ^b	0.995
80	11.9	41 ± 5	0.997
120	13.2	39 ± 3	0.999
150	14.2	31 ± 4	0.989

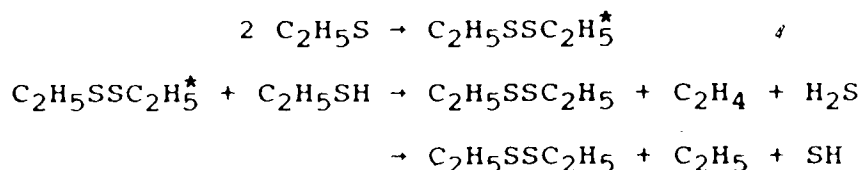
^aintercept = (1+αP_E)/φ₂; α = (k₅^{*}+k₆E^{*})/k₄, in units of Torr⁻¹ ;
^bstandard error

Table 4.11. Quantum Yields for the Primary Photochemical Processes

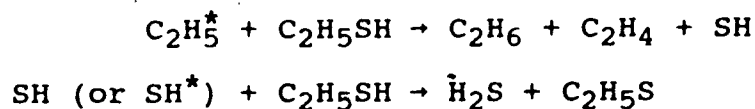
Temperature (°C)	ϕ_1	ϕ_2	ϕ_3^a	
25	0.967±0.002 ^b	0.023±0.002	0.010±0.001	This work
	0.900	0.090	0.010	BHW
	0.97	0.0	0.0	SK
80	0.963±0.003	0.027±0.003	0.010±0.001	This work
120	0.961±0.002	0.029±0.002	0.010±0.001	This work
150	0.954±0.004	0.036±0.004	0.010±0.001	This work
Average ^c :				0.96±0.01 0.029±0.006 0.010±0.001

^aassumed to be constant
^bstandard error
^cfrom This work

4.11) are due to mechanistic considerations. SK postulated only one primary step (1), from the observation that $\phi(\text{H}_2)$ is near unity. The formation of C_2H_4 , C_2H_6 and H_2S and their pressure dependence were accounted for by a sequence of sensitized reactions involving excited disulfide molecules formed from the recombination of $\text{C}_2\text{H}_5\text{S}$ radicals;



However, the hypothetical $\text{C}_2\text{H}_5\text{SSC}_2\text{H}_5^* + \text{C}_2\text{H}_5\text{SH}$ reaction was later rejected by BHW, who observed that no H_2S , C_2H_4 or C_2H_6 was formed when $\text{C}_2\text{H}_5\text{SSC}_2\text{H}_5$ was photolysed in the presence of $\text{C}_2\text{H}_5\text{SH}$ in the gas phase.⁶³ In turn, BHW proposed the three primary steps, (1) - (3). The values for ϕ_1 and ϕ_2 were estimated from $\phi(\text{H}_2)$ and $\phi(\text{C}_2\text{H}_6)$ respectively, obtained at the high $n\text{-C}_4\text{H}_{10}$ thermalizer pressure of about 250 Torr. ϕ_3 was determined by difference and is the same as that obtained from this work. The difference in the values of ϕ_1 and ϕ_2 between BHW's and the present work arises from kinetic interpretations. BHW postulated the reactions

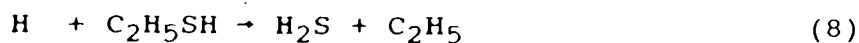
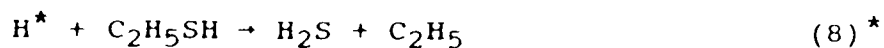
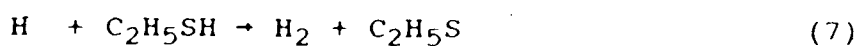
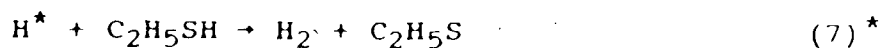


to partially account for the formation of C_2H_4 , C_2H_6 and H_2S . The uncertainties surrounding these reaction steps were discussed earlier. At the same time, BHW neglected the thermalized molecular displacement reaction (8) which,

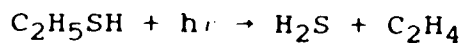
from Chapter 3, has been shown to be significant. Thus, ϕ_2 was overestimated, and ϕ_1 underestimated, by BHW.

4.2.3 H-Atom Reactions with Ethanethiol: Quantum Yields of H_2 and H_2S

Information about the hot and thermalized H-atom reactions with C_2H_5SH :



can be obtained from the variations of the H_2 and H_2S yields with pressure and temperature. The total $\phi(H_2S)$ is provided by both (8)* and (8), the cleavage of the C-S bond, and by the molecular primary step (3),



Since the H_2S yield contributed by (3) is ϕ_3 , which was determined above, the H_2S yield contributed by both (8)* and (8) is $[\phi(H_2S) - \phi_3]$. The total $\phi(H_2)$ is the sum of the two abstraction steps (7)* and (7). However, it is necessary to correct for the H-atom contribution from the unimolecular decomposition step,



This contribution is determined from the difference between the total C_2H_4 yield and that from the molecular primary step (3). Thus, the H_2 yield from steps (7)* and (7) is given by $[\phi(H_2) - \delta]$, where δ is the correction factor, $[\phi(C_2H_4) - \phi_3]$.

The variations of the ratio $[\phi(\text{H}_2) - \delta]/[\phi(\text{H}_2\text{S}) - \phi_3]$ with respect to CO_2 pressure and temperature, tabulated in Table 4.12, provide insight into the relative difference of the reaction rates with hot and thermalized H atoms. At low pressures, reactions with hot H^* atoms are important, while increasing the thermalizer pressure decreases the population of the energized H^* atoms and consequently increases that of the thermalized H atoms. At high CO_2 pressure, most of the H_2 and H_2S is produced with thermalized H atoms from reaction steps (7) and (8), respectively. If the rates of H_2 and H_2S production change similarly with the thermalization of the H atoms, then the ratio $[\phi(\text{H}_2) - \delta]/[\phi(\text{H}_2\text{S}) - \phi_3]$ would remain invariant with changes in the thermalizer pressure. However, it is observed from Table 4.12 and also illustrated in Figure 4.8, that in the temperature range of study, $[\phi(\text{H}_2) - \delta]/[\phi(\text{H}_2\text{S}) - \phi_3]$ increases with increasing thermalizer pressure, indicating that thermalization of the H atoms favours the H-abstraction reaction. The decrease of $[\phi(\text{H}_2) - \delta]/[\phi(\text{H}_2\text{S}) - \phi_3]$ for hot H^* atom reactions indicates that the displacement reaction (8) has a higher activation energy than the H-abstraction reaction (7).

Increasing the temperature results in a higher Boltzmann distribution of the energized H^* atoms, thereby altering the relative ratio of hot and thermalized H atoms. It is seen from Figure 4.8 that at higher temperatures, $[\phi(\text{H}_2) - \delta]/[\phi(\text{H}_2\text{S}) - \phi_3]$ decreases, that is, the rate of the displacement reaction increases faster than the H-abstraction

Table 4.12. Effects of CO₂ Pressure and Temperature on the Values^a

of $[\phi(\text{H}_2) - \delta]/[\phi(\text{H}_2\text{S}) - \phi_3]$ ^b

[P(CO ₂)/P(C ₂ H ₅ SH)] ^c	25°C	80°C	120°C	150°C
0	3.13±0.59 ^d	2.81±0.51	2.47±0.45	2.50±0.36
5	4.6 ± 1.2	3.57±0.90	3.4 ± 1.1	2.83±0.95
7	5.4 ± 1.4	4.4 ± 1.0	3.22±0.95	3.20±0.97
10	5.4 ± 1.5	4.2 ± 1.2	3.4 ± 1.0	3.2 ± 1.3
20	5.7 ± 1.5	4.3 ± 1.3	3.8 ± 1.4	3.5 ± 1.1
30	5.8 ± 1.6	4.9 ± 1.5	3.7 ± 1.2	3.6 ± 1.1
40	5.8 ± 1.6	5.6 ± 1.4	3.9 ± 1.3	3.3 ± 1.2

^aeach value is the average of 2-8 experimental points

^b $\delta = [\phi(\text{C}_2\text{H}_4) - \phi_3]$; $\phi_3 = 0.010$

^cP(CO₂) = 0-570 Torr or [CO₂] ≤ 2.15 × 10⁻² M

^dP(C₂H₅SH) = 10.0-14.2 Torr or [C₂H₅SH] = 5.38 × 10⁻⁴ M

standard error

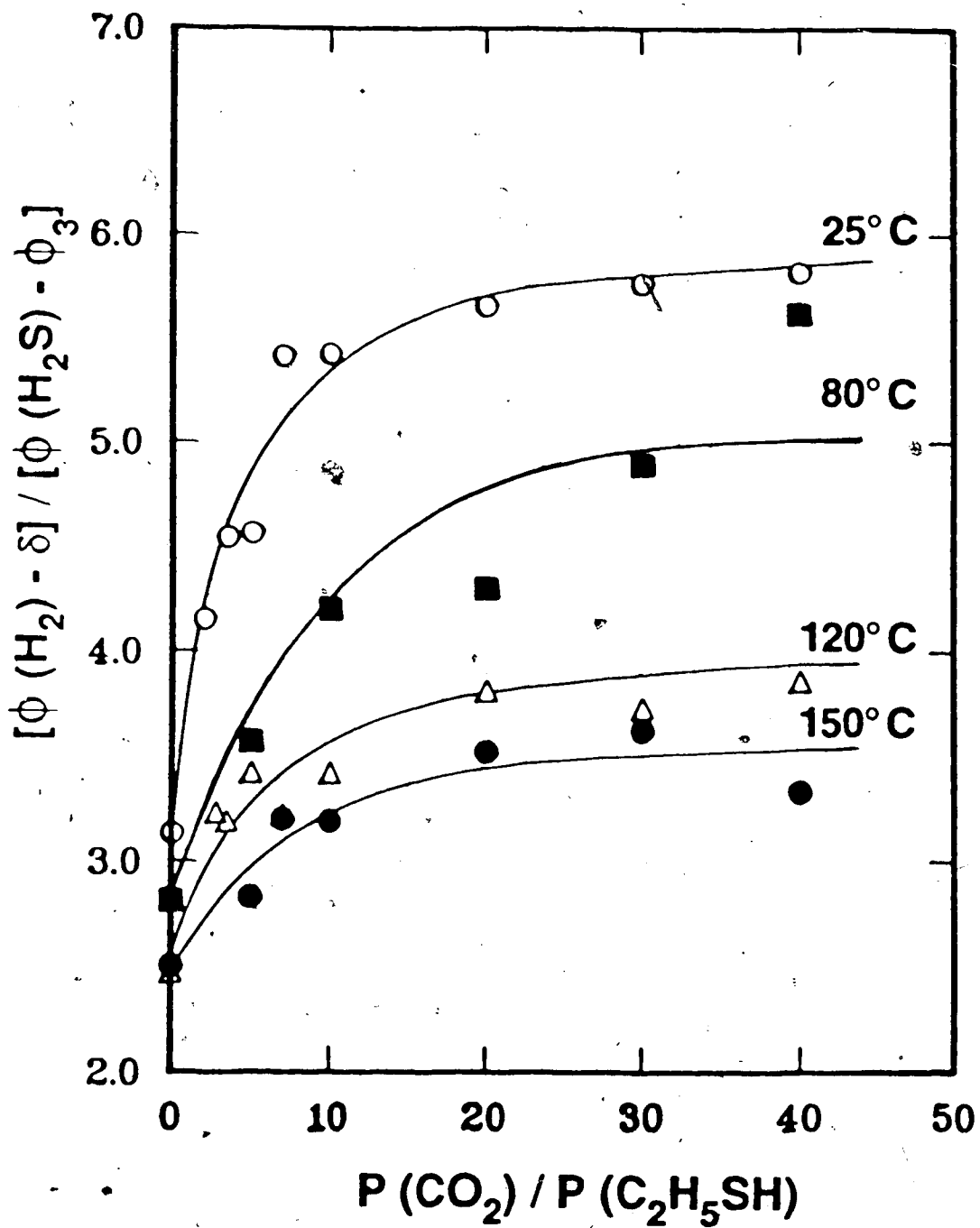


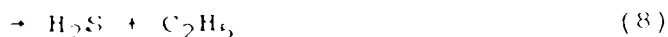
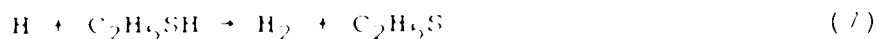
Figure 4.8. Plots of $[\phi(H_2) - \delta] / [\phi(H_2S) - \phi_3]$ as a function of the ratio $P(CO_2) / P(C_2H_5SH)$.

reaction, indicating a higher activation energy for the former.

4.2.4 Relative Rate Parameters for the H-atom Reactions:

Quantum Yields of H_2 and C_2H_6

The relative rate parameters for the thermalized H-atom reactions



are obtained from the H_2 and C_2H_6 yields. One important simple relation emerges from the quantum yield expressions for H_2 and C_2H_6 , Equations [2] and [3], i.e. their sum is independent of pressure:

$$\phi(H_2) + \phi(C_2H_6) = \phi_1 + \phi_2$$

Equations [2] and [3] contain the same pressure dependent terms,

$$\frac{(k_7 k_8^* - k_7^* k_8) \phi_1 [E]}{(k_7 + k_8) ((k_7^* + k_8^*) [E] + k_9^* [M])} \quad \text{and}$$

$$\frac{k_4^* k_7 \phi_2}{(k_7 + k_8) (k_4^* + k_5^* [E] + k_6^* [M])}$$

but with opposite signs. Thus, they are mirror image functions of each other with respect to $[\phi(H_2) + \phi(C_2H_6)]/2$. The symmetries of the $\phi(H_2)$ and $\phi(C_2H_6)$ functions are demonstrated in Figures 4.9 and 4.10 where they are plotted against inverse CO_2 concentration at each temperature, from the data in Tables 4.4 - 4.7. When $[CO_2]$ is relatively large, deactivation of hot radicals by C_2H_5SH can be neglected. After substituting for $k_9^*[M]$ and $k_6^*[M]$ by

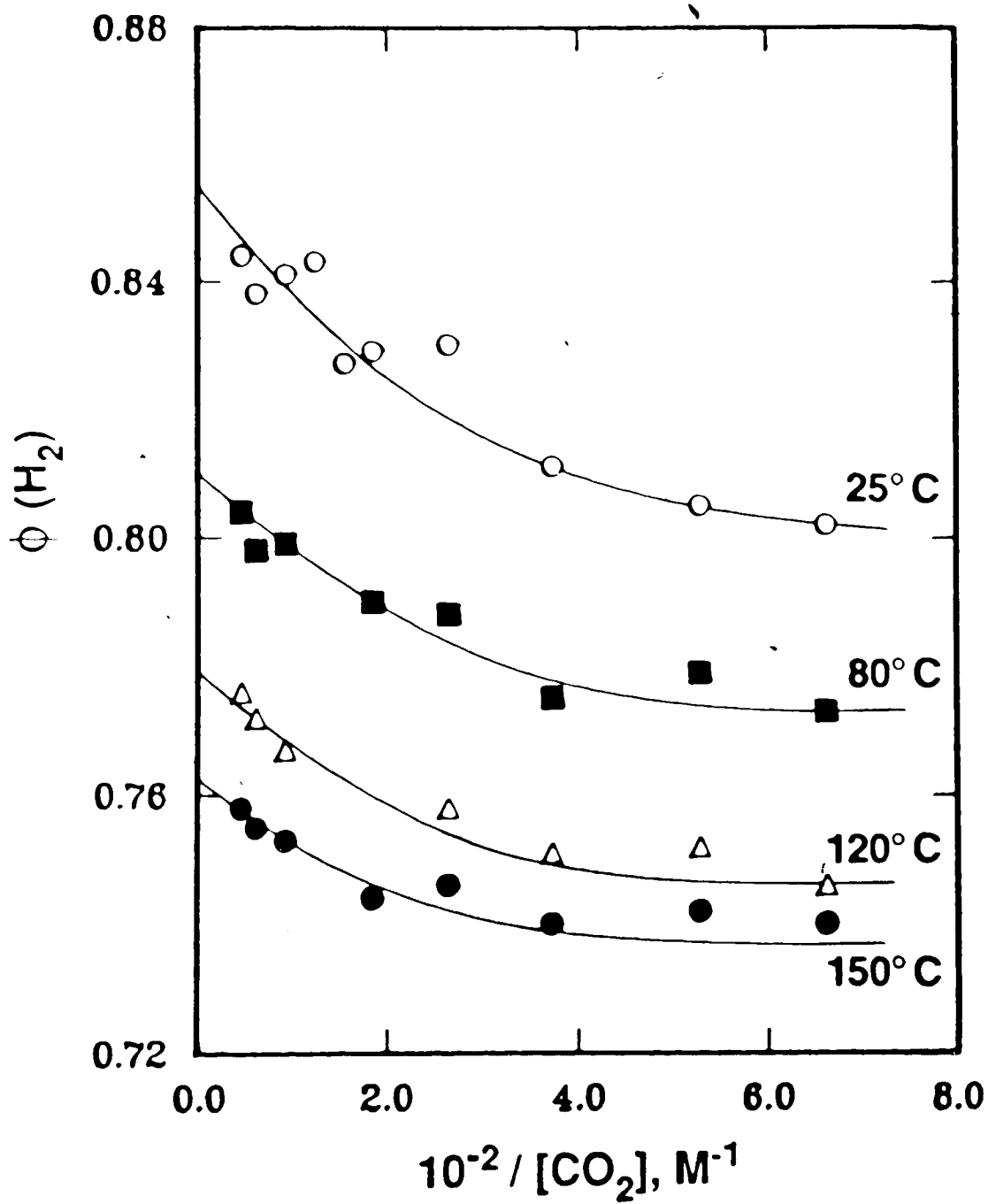


Figure 4.9. Plots of $\phi(\text{H}_2)$ as a function of the reciprocal of CO_2 concentration at $[\text{C}_2\text{H}_5\text{SH}] = 5.38 \times 10^{-4} \text{ M}$.

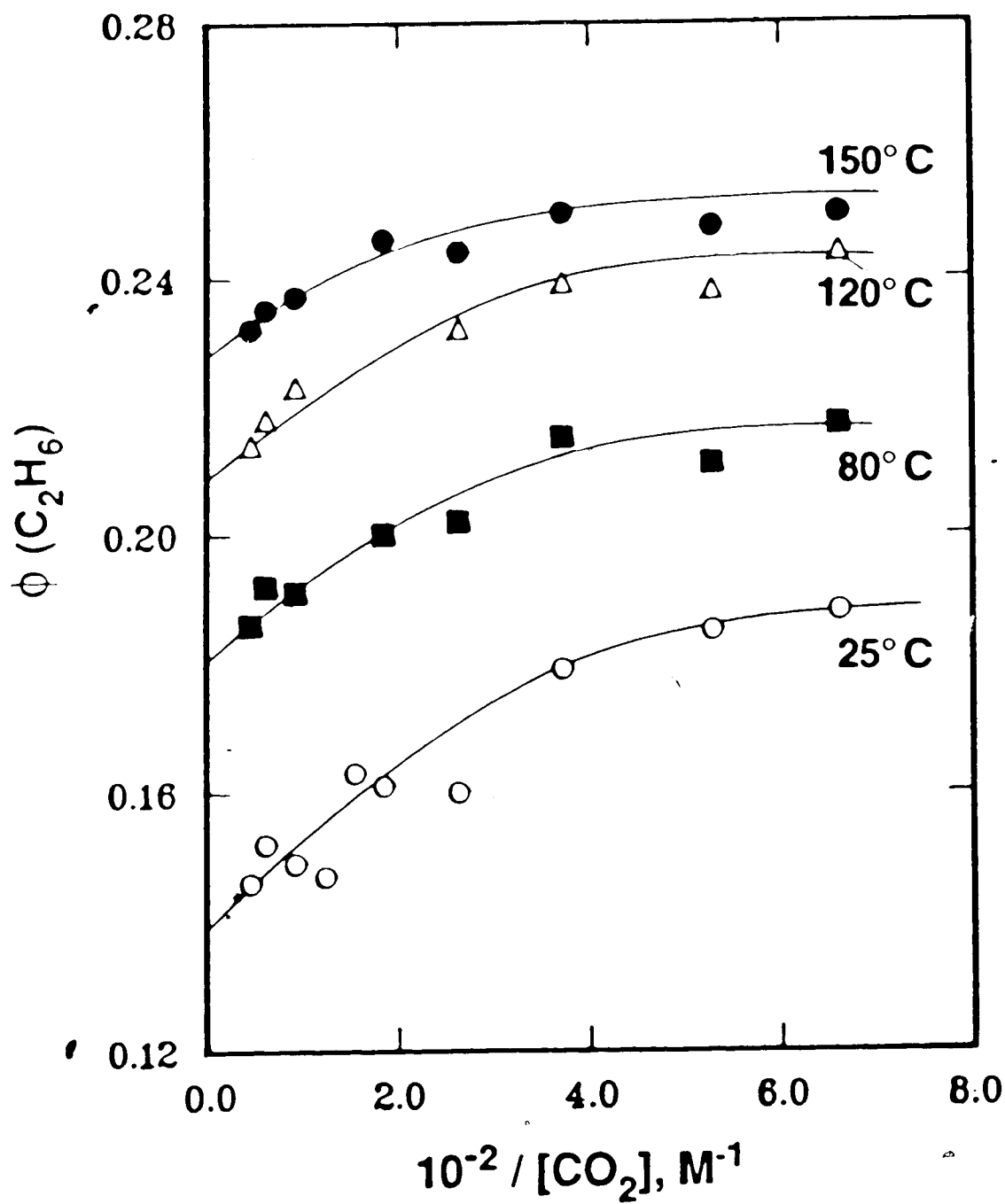


Figure 4.10. Plots of $\phi(C_2H_6)$ as a function of the reciprocal of CO_2 concentration at $[C_2H_5SH] = 5.38 \times 10^{-4} M$.

$k_{9C}^*[C]$ and $k_{6C}^*[C]$, respectively, Equations [2] and [3] thus become:

$$\begin{aligned} \phi(H_2) = & \frac{k_7 \phi_1}{(k_7 + k_8)} - \frac{(k_7 k_8^* - k_7^* k_8) \phi_1 [E]}{(k_7 + k_8) ((k_7^* + k_8^*) [E] + k_{9C}^*[C])} \\ & + \frac{k_4^* k_7 \phi_2}{(k_7 + k_8) (k_4^* + k_5^*[E] + k_{6C}^*[C])} \end{aligned} \quad [9]$$

$$\begin{aligned} \phi(C_2H_6) = & \frac{k_8 \phi_1}{(k_7 + k_8)} + \phi_2 + \frac{(k_7 k_8^* - k_7^* k_8) \phi_1 [E]}{(k_7 + k_8) ((k_7^* + k_8^*) [E] + k_{9C}^*[C])} \\ & + \frac{k_4^* k_7 \phi_2}{(k_7 + k_8) (k_4^* + k_5^*[E] + k_{6C}^*[C])} \end{aligned} \quad [10]$$

When $P_C \gg P_E$, the terms $((k_7^* + k_8^*) [E])$ and $(k_4^* + k_5^*[E])$ in Equations [9] and [10] may be neglected. The resulting linear relations are obtained;

$$\phi(H_2) = \frac{k_7 \phi_1}{(k_7 + k_8)} - \frac{(k_7 k_8^* - k_7^* k_8) k_{6C}^* \phi_1 [E] - k_4^* k_7 k_{9C}^* \phi_2}{(k_7 + k_8) k_{6C}^* k_{9C}^*[C]} \quad [11]$$

$$\begin{aligned} \phi(C_2H_6) = & \frac{k_8 \phi_1}{(k_7 + k_8)} + \phi_2 \\ & + \frac{(k_7 k_8^* - k_7^* k_8) k_{6C}^* \phi_1 [E] - k_4^* k_7 k_{9C}^* \phi_2}{(k_7 + k_8) k_{6C}^* k_{9C}^*[C]} \end{aligned} \quad [12]$$

The linear behaviour of $\phi(H_2)$ and $\phi(C_2H_6)$ at high CO_2 pressures is illustrated in Figures 4.9 and 4.10 for $P_C > 50$ Torr, or $[CO_2]^{-1} < 0.04 M^{-1}$. The intercepts of the linear portions of these plots are defined by [11] and [12] to be,

$$\phi(H_2, P_C \rightarrow \infty) = \frac{k_7 \phi_1}{k_7 + k_8} \quad [13]$$

$$\phi(\text{C}_2\text{H}_6, P_C \rightarrow \infty) = \frac{k_8 \phi_1}{k_7 + k_8} + \phi_2 \quad [14]$$

Their values are listed in Table 4.13. The rate constant ratio for H-atom reactions, steps (7) and (8), may then be calculated from the intercept values and the derived values of ϕ_1 and ϕ_2 (Table 4.11). The results are listed in Table 4.14.

Values of k_7/k_8 can also be obtained directly from the experimental data at high total pressure. Under this condition, quenching of hot H^* and C_2H_5^* is complete and therefore the hot reaction steps (4)* - (9)* do not occur in the reaction mechanism. Steady-state treatment of this simplified mechanism gives directly Equations [13] and [14]. Substituting the values of $\phi(\text{H}_2)$ and $\phi(\text{C}_2\text{H}_6)$ at 200 - 400 Torr (Table 4.8) into Equations [13] and [14] we obtain another set of values for k_7/k_8 , also listed in Table 4.14. The results from both methods of determining k_7/k_8 agree within $\pm 3\%$.

The Arrhenius plot for the H-atom reactions (7) and (8), shown in Figure 4.11, is constructed from the average values of k_7/k_8 (Table 4.14). The Arrhenius expression, obtained by the LMS method, is as follows;

$$\ln k_7/k_8 = (-0.25 \pm 0.04) + (660 \pm 10)/T \quad [15]$$

From Equation [15], the activation energy difference, ($E_7 - E_8$), of $-1.31 \pm 0.03 \text{ kcal mol}^{-1}$ and the ratio of pre-exponential factors, A_7/A_8 , of 0.78 ± 0.01 have been determined. Thus, the prediction that $E_8 > E_7$, obtained

Table 4.13. Intercepts of the Plots in Figures 4.9 and 4.10^a

Temperature (°C)	P(C ₂ H ₅ SH) (Torr)	Intercepts		
		H ₂	C ₂ H ₆	
25	10.0	0.848 ±0.003	0.142 ±0.003	
80	11.9	0.806 ±0.002	0.184 ±0.002	
120	13.2	0.776 ±0.002	0.214 ±0.002	
150	14.2	0.758 ±0.002	0.202 ±0.002	

^alinear region from [CO₂]⁻¹ < 0.04 M⁻¹ or P(CO₂) > 50 Torr

Table 4.14. Temperature Dependence of k_7/k_8

Temperature (°C)	(k_7/k_8) ^a	(k_7/k_8) ^b	Average
25	7.1 ±0.3 ^c	7.0 ±0.4	7.1 ±0.5
80	5.2 ±0.2	5.0 ±0.2	5.1 ±0.3
120	4.2 ±0.1	4.1 ±0.1	4.1 ±0.2
150	3.7 ±0.1	3.6 ±0.2	3.7 ±0.2

^acalculated from the intercept values in Table 4.13

^bcalculated from the experimental high pressure limits for $\phi(\text{H}_2)$ and $\phi(\text{C}_2\text{H}_6)$

^cstandard error

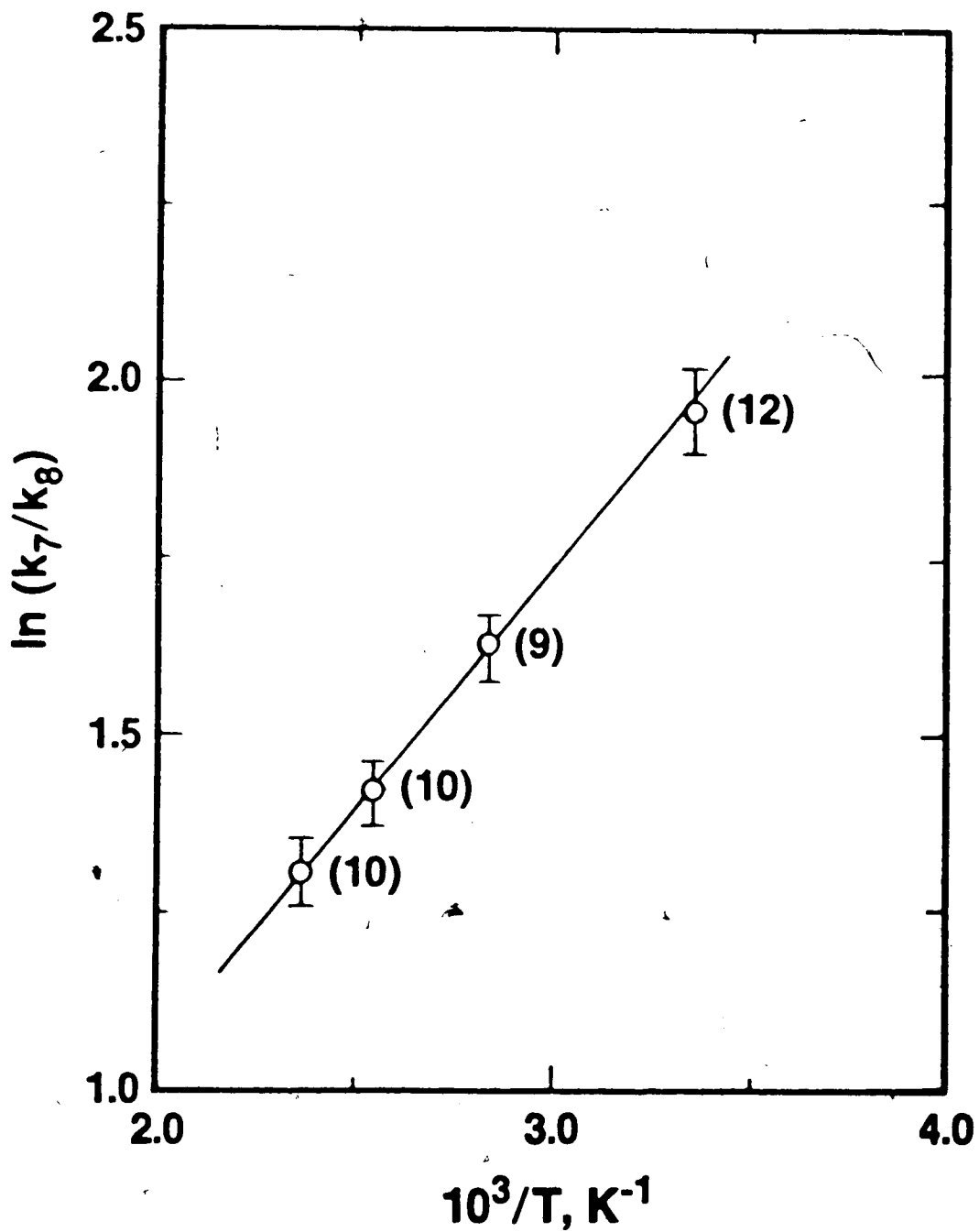


Figure 4.11. Plot of $\ln k_7/k_8$ versus the reciprocal of temperature. Figure in bracket indicates number of experiments.

from H_2/H_2S yields as functions of pressure and temperature, is verified by Equation [15].

An attempt is made here to determine the absolute rate parameters for reactions (7) and (8) by utilizing the data available in the literature. The $C_2H_5SH-C_2H_4$ system has been investigated by SK⁶⁷ to determine Arrhenius parameters for the H-atom reaction steps (7) and (iv);



from the photolysis of equimolar mixtures (25 Torr) of C_2H_5SH and C_2H_4 , in the presence of 760 Torr added CO_2 . Although the data were scattered, values of -1.0 ± 0.3 kcal mol^{-1} and 0.18 ± 0.06 were reported for $E_7 - E_{iv}$ and A_7/A_{iv} , respectively. Lee et al.⁷⁶ measured k_{iv} as a function of temperature from 198 to 320 K using the flash photolysis-resonance fluorescence technique and obtained, under a high pressure limit of 760 Torr Ar, the following Arrhenius expression for the $H + C_2H_4$ reaction,

$$k_{iv} \text{ (cm}^3 \text{ mol}^{-1} \text{ s}^{-1}\text{)} \\ \approx (2.2 \pm 0.4) \times 10^{13} \exp [(-2070 \pm 80)/RT] \quad [16]$$

Combining the results of SK and of Lee et al., the absolute rate constant for the H-abstraction step (7) is

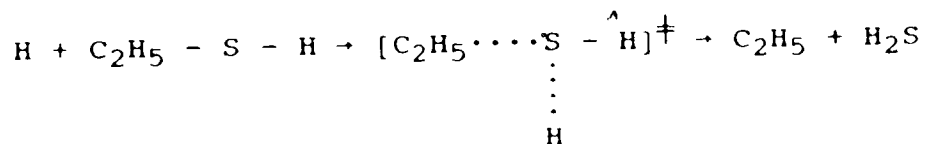
$$k_7 \text{ (cm}^3 \text{ mol}^{-1} \text{ s}^{-1}\text{)} \\ = (4.0 \pm 0.7) \times 10^{12} \exp [(-1070 \pm 40)/RT] \quad [17]$$

Substituting Equation [17] into [15], the absolute rate constant for the SH displacement step (8) is then given by,

$$k_8 \text{ (cm}^3 \text{ mol}^{-1} \text{ s}^{-1}\text{)} \\ = (5.1 \pm 0.9) \times 10^{12} \exp [(-2380 \pm 70)/RT] \quad [18]$$

The Arrhenius parameters for the H-atom reaction steps (7), (8) and (iv) are summarized in Table 4.15.

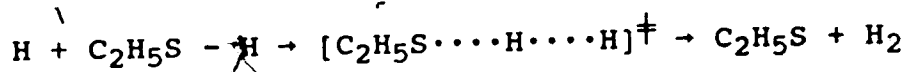
The experimental entropy of activation calculated from the A factor of (8) is -26.5 eu., for the standard state of 1 atm. This value is similar to those obtained for other displacement reactions by H atoms: $H + CH_3SCH_3$,¹³¹ -24.1 eu., and $H + C_2H_5SC_2H_5$,¹⁶⁵ -22.1 eu., suggesting transition states with similar structures. Using Benson's method¹⁴¹ for a transition state which involves an initial interaction between the H atom and the non-bonding 3p orbital of the sulfur atom:



we will obtain:

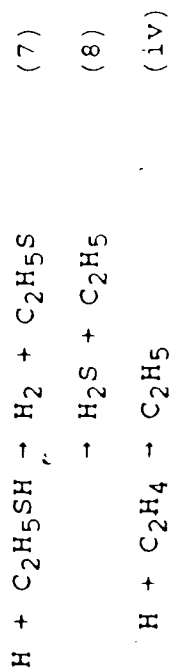
$$\begin{aligned} \Delta S^\ddagger &= S_0^\ddagger - S_0(C_2H_5SH) - S_0(H) \\ &= S_0(C_2H_5SH) + R \ln 2 + x - S_0(C_2H_5SH) - S_0(H) \\ &= 1.4 + x - 27.4 = -26.0 \\ x &= -0.5 \text{ eu.} \end{aligned}$$

This low value for the vibrational contribution to ΔS^\ddagger indicates a very tight structure for the activated complex. The experimental entropy of activation calculated from the A factor of (7) is -26.9 eu. for the standard state of 1 atm. The transition state involves the initial interaction between the two H atoms:



The low value of -0.9 eu. for the vibrational contribution to ΔS^\ddagger indicates also a tight structure for the activated

Table 4.15. Arrhenius Parameters for the H-atom Reactions



A ($\text{cm}^3 \text{ mol}^{-1} \text{ s}^{-1}$)	E (kcal mol^{-1})	Reference
$A_7/A_{\text{iv}} = 0.18 \pm 0.06$	$E_7 - E_{\text{iv}} = -1.0 \pm 0.3$	SK
$A_{\text{iv}} = (2.2 \pm 0.4) \times 10^{13}$	$E_{\text{iv}} = 2.07 \pm 0.08$	Lee <u>et al.</u>
$A_7/A_8 = 0.78 \pm 0.01$	$E_7 - E_8 = -1.31 \pm 0.03$	This work
$A_7 = (4.0 \pm 0.7) \times 10^{12}$	$E_7 = 1.07 \pm 0.04$	(a)
$A_8 = (5.1 \pm 0.9) \times 10^{12}$	$E_8 = 2.38 \pm 0.07$	(b)

^acalculated from the results of SK and Lee et al.

^bcalculated from the results of SK, Lee et al. and This work

complex.

Equations [2] and [3] can be simplified for the case of the photolysis of pure C_2H_5SH as follows;

$$\phi(H_2) = \frac{k_7 \phi_1}{(k_7 + k_8)} - \frac{(k_7 k_8^* - k_7^* k_8) \phi_1}{(k_7 + k_8)(k_7^* + k_8^* + k_9^* E)} + \frac{k_7 \phi_2}{(k_7 + k_8)(1 + \alpha P_E)} \quad [19]$$

$$\phi(C_2H_6) = \frac{k_8 \phi_1}{(k_7 + k_8)} + \phi_2 + \frac{(k_7 k_8^* - k_7^* k_8) \phi_1}{(k_7 + k_8)(k_7^* + k_8^* + k_9^* E)} - \frac{k_7 \phi_2}{(k_7 + k_8)(1 + \alpha P_E)} \quad [20]$$

where α has been previously defined as $(k_5^* + k_6^* E)/k_4^*$.

According to [19] and [20], $\phi(H_2, P_C=0)$ and $\phi(C_2H_6, P_C=0)$ are inverse functions of P_E . However, the predicted pressure dependence (Figure 4.1) is not apparent and $\phi(H_2)$ and $\phi(C_2H_6)$ are approximately constant at 0.77 ± 0.03 and 0.22 ± 0.03 , at $25^\circ C$, in the C_2H_5SH pressure range 5 - 48 Torr. This result suggests that the dependence of $\phi(H_2)$ and $\phi(C_2H_6)$ on C_2H_5SH pressure is relatively small in this pressure range, which can be verified by evaluating the magnitude of the pressure-dependent term in Equations [19] and [20], using the already derived values of ϕ_2 , α and k_7/k_8 . As seen in Table 4.16, this pressure term decreases with increasing C_2H_5SH pressure, the net change being only 0.006 on going from 5 to 48 Torr, which is much smaller than the magnitude of the experimental error. Therefore, C_2H_5SH pressure has negligible effects on $\phi(H_2)$ and $\phi(C_2H_6)$.

Table 4.16. Values of $\frac{k_7 \phi_2}{(k_7 + k_8)(1 + \alpha P_E)}$ ^a

$P(C_2H_5SH)$ (Torr)	$\frac{k_7 \phi_2}{(k_7 + k_8)(1 + \alpha P_E)}$
5	0.024
10	0.023
20	0.022
30	0.020
40	0.019
48	0.018

^a $T = 25^\circ C$, $(k_7/k_8)_{av} = 7.1$, $(\phi_2)_{av} = 0.029$, $\alpha = 8.7 \times 10^{-3} \text{ Torr}^{-1}$

4.2.5 Disproportionation-Combination of Thiyl Radicals:

Quantum Yield of $C_2H_5SSC_2H_5$

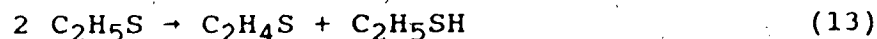
The quantum yield of $C_2H_5SSC_2H_5$, a major product, is given by Equation [5],

$$\phi(C_2H_5SSC_2H_5) = \frac{k_{12} \phi_1}{k_{12} + k_{13}} \quad [5]$$

If the recombination reaction (12) were the only mode for the loss of C_2H_5S radicals,



then $\phi(C_2H_5SSC_2H_5)$ would have the same value as ϕ_1 , as predicted by Equation [5]. Although this may be true at 25°C, where $\phi(C_2H_5SSC_2H_5)$ is found to be equal to ϕ_1 , within experimental error, $\phi(C_2H_5SSC_2H_5)$ is observed to be less than 0.96 at higher temperatures (Tables 4.5 to 4.7). Therefore, it is evident that the disproportionation reaction,



is another pathway for the loss of C_2H_5S radicals at higher temperatures. The observed high quantum yield for $C_2H_5SSC_2H_5$ and the fact that thioacetaldehyde was not observed in the products indicate that reaction (12) is the major pathway for the fate of C_2H_5S radical, while reaction (13) is a relatively minor one. Although thioaldehydes are considered to be unstable species¹⁷⁴, they have been generated by the thermolysis of alkyl thiosulphinates and trapped with aromatic and aliphatic 1,3-dienes.¹⁶⁶ In the present study, it is likely that thioacetaldehyde is lost.

on the wall through a polymerization reaction similar to that for thioformaldehyde which trimerizes readily in the gas phase.^{108,134}

Equation [5] does not predict any pressure dependence for $\phi(\text{C}_2\text{H}_5\text{SSC}_2\text{H}_5)$, in agreement with the results obtained (see Tables 4.4 to 4.8). The disproportionation to combination ratio, k_{13}/k_{12} , can be determined from Equation [5] to be,

$$\frac{k_{13}}{k_{12}} = \frac{\phi_1}{\phi(\text{C}_2\text{H}_5\text{SSC}_2\text{H}_5)} - 1 \quad [21]$$

and the results are listed in Table 4.17. At 25°C, k_{13}/k_{12} is estimated to be in the range 0.03 - 0.05. This value is smaller than the limiting value of 0.13 reported by Smith and Knight¹¹¹, obtained from the Hg-photosensitized decomposition of $\text{C}_2\text{H}_5\text{SC}_2\text{H}_5$ vapor at 25°C. The higher literature value may be due to the further loss of $\text{C}_2\text{H}_5\text{S}$ radicals through reactions with Hg atoms in the Hg-photosensitized system. The values of k_{13}/k_{12} increase with temperature, but even at 150°C, the disproportionation reaction is indeed a minor one, compared to combination. At elevated temperatures, the values of $\phi(\text{C}_2\text{H}_5\text{SSC}_2\text{H}_5)$ obtained in the photolysis of pure $\text{C}_2\text{H}_5\text{SH}$ are slightly lower than those measured at high CO_2 pressure (Tables 4.4 to 4.7), although the experimental errors are such that this apparent pressure dependence must be viewed with caution. The formation of $\text{C}_2\text{H}_5\text{SSC}_2\text{H}_5$ molecules from reaction (12) yields an excess energy of 69 - 74 kcal mol⁻¹, which is the energy for the

Table 4.17. Temperature Dependence of k_{13}/k_{12}

Temperature (°C)	$(k_{13}/k_{12})^a$	$(k_{13}/k_{12})^b$
25	0.05 ±0.05	0.03 ±0.06
80	0.20 ±0.06	0.12 ±0.06
120	0.22 ±0.07	0.13 ±0.04
150	0.28 ±0.07	0.16 ±0.06

^acalculated from the photolysis of pure C_2H_5SH

^bcalculated from the photolysis of C_2H_5SH with added CO_2 at the high pressure limit

S-S bond. This causes the $C_2H_5SSC_2H_5$ molecules to be slightly energized. At low total pressures, the probability of $C_2H_5SSC_2H_5$ being stabilized by collisional deactivation is lower and therefore some loss will occur through the decomposition of the energized $C_2H_5SSC_2H_5^*$ molecules and this loss progressively increases with increasing temperature. This loss is minimized at high total pressures where collisional deactivation of $C_2H_5SSC_2H_5^*$ molecules is faster. The form of Equation [21] is such that very large errors are associated with the calculated values of k_{13}/k_{12} , Table 4.17. Although the values obtained at high CO_2 pressure probably are more representative of the pressure-independent rate ratio, the rates of increase of k_{13}/k_{12} with temperature, *i.e.* $E_{13} - E_{12}$, are the same for both cases.

From the high pressure values of the disproportionation-combination steps (13) and (12), respectively, the Arrhenius plot is shown in Figure 4.12, from which the following rate expression is derived:

$$\ln (k_{13}/k_{12}) = (2.0 \pm 1.0) - (1.6 \pm 0.4) \times 10^3/T \quad [22]$$

from which $(E_{13} - E_{12}) = 3.1 \pm 0.7 \text{ kcal mol}^{-1}$ and $A_{13}/A_{12} = 7.3 \pm 3.1$. Since the recombination of radicals requires negligible activation energy, *i.e.* $E_{12} \approx 0$, the activation energy for the disproportionation reaction, E_{13} , is estimated to be $3.1 \pm 0.7 \text{ kcal mol}^{-1}$.

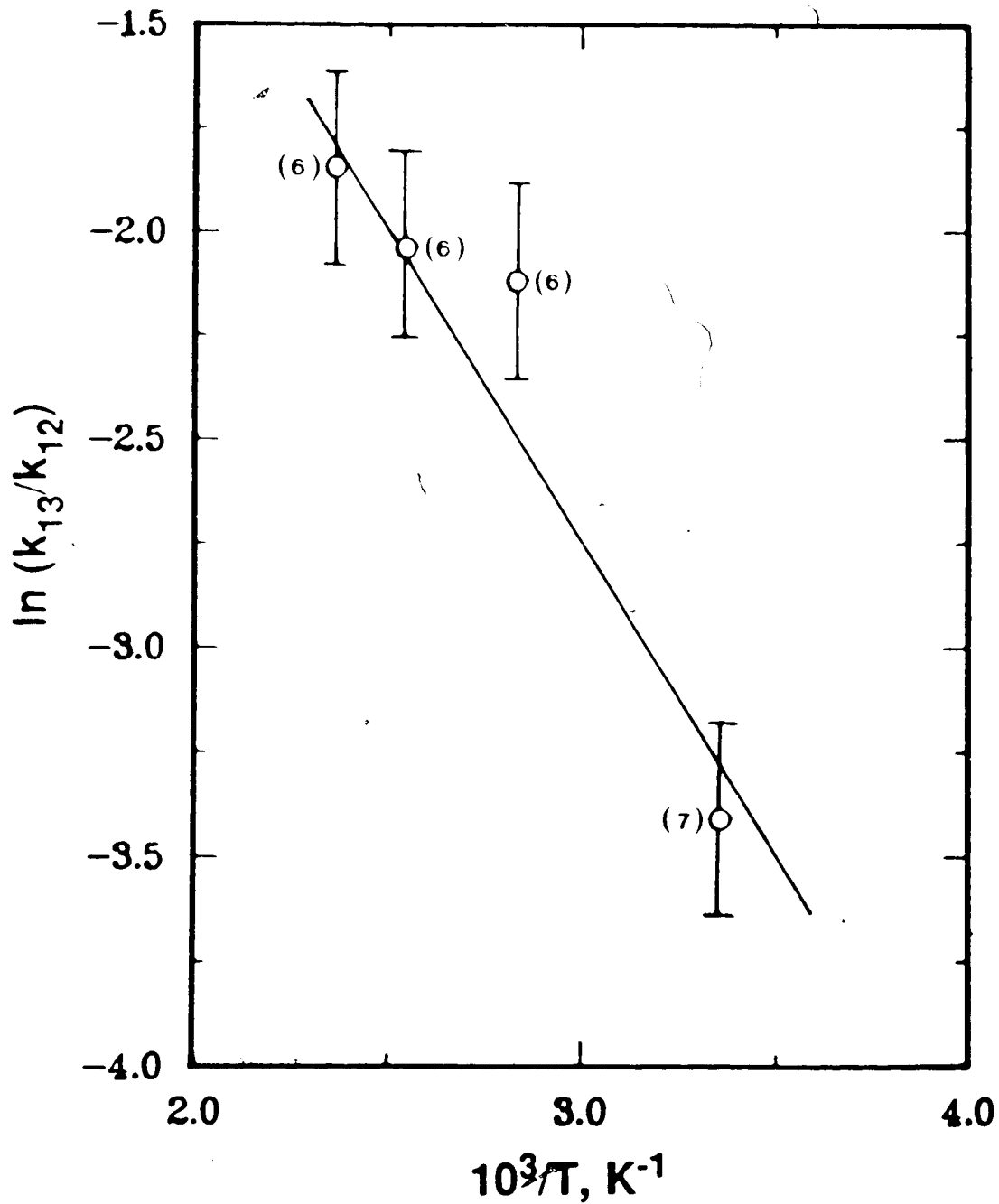


Figure 4.12. Plot of $\ln k_{13}/k_{12}$ versus the reciprocal of temperature. Figure in bracket indicates number of experiments.

CHAPTER FIVE

PHOTOLYSIS OF, AND THE REACTIONS OF HYDROGEN ATOMS WITH, ISOPROPANETHIOL

5.1 Results

The gas-phase UV absorption spectrum of $i\text{-C}_3\text{H}_7\text{SH}$ is similar to that for $\text{C}_2\text{H}_5\text{SH}$. The maximum absorbance in the 220 - 260 nm range is located near 225 nm. The extinction coefficient at 298K for $i\text{-C}_3\text{H}_7\text{SH}$ at 254 nm is about $4.17 \times 10^{-3} \text{ Torr}^{-1} \text{ cm}^{-1}$, after background for absorption by quartz cell is taken into account.

The products of photolysis are H_2 , C_3H_8 , H_2S , C_3H_6 and $(i\text{-C}_3\text{H}_7)_2\text{S}_2$. Total product conversion was maintained low at 2 - 6% in order to minimize secondary absorption by H_2S and $(i\text{-C}_3\text{H}_7)_2\text{S}_2$. As a result, over 95% of the incident light was absorbed by $i\text{-C}_3\text{H}_7\text{SH}$.

5.1.1 H_2S Actinometry

The absorbed light intensity in the reaction vessel, I_a , is calculated in the actinometric set-up as described in Chapter 4. The values of the extinction coefficients for H_2S and $i\text{-C}_3\text{H}_7\text{SH}$ were determined from the experimental measurements of S_0 , S_6 and w_i 's. At 254 nm, $\epsilon(\text{H}_2\text{S})$ was found to be $1.05 \times 10^{-4} \text{ Torr}^{-1} \text{ cm}^{-1}$, in good agreement with the literature values.^{63,142} $\epsilon(i\text{-C}_3\text{H}_7\text{SH})$ was found to be $3.98 \times 10^{-3} \text{ Torr}^{-1} \text{ cm}^{-1}$, in accordance with that obtained by spectral means.

The results of actinometric runs are summarized in Table 5.1. The average value for $[\text{R}(\text{H}_2) + \text{R}(\text{C}_3\text{H}_8)]/I_a$ was

Table 5.1. The Results of Chemical Actinometry in the Photolysis of *i*-C₃H₇SH^a

P(<i>i</i> -C ₃ H ₇ SH) (Torr)	I _a (10 ⁻² μmoles min ⁻¹)	R(H ₂)+R(C ₃ H ₈)	I _a	
			R(H ₂)+R(C ₃ H ₈)	R(H ₂)+R(C ₃ H ₈)
5	7.34	7.18	0.978	
10	12.5	12.0	0.960	
15	16.6	15.7	0.946	
20	17.9	18.5	1.03	
25	20.3	20.7	1.02	
30	21.3	20.8	0.977	
35	21.9	22.1	1.01	
45	23.1	23.7	1.03	
45	24.6	26.2	1.06	
50	24.2	26.1	1.08	
			Average = 1.01±0.04	

^aT=25°C; photolysis time=60 min

found to be 1.01 ± 0.04 . Therefore, the absorbed light intensity in the reaction vessel, I_a , is equal to $0.99[R(H_2) + R(C_3H_8)]$. All the quantum yields obtained from the photolysis of $i-C_3H_7SH$ were calculated by the relation $\phi_i = R_i/I_a$, where R_i [$i = H_2, C_3H_8, H_2S, C_3H_6$ and $(i-C_3H_7)_2S_2$] is the rate of product formation and $I_a = 0.99[R(H_2) + R(C_3H_8)]$ as determined from actinometric experiments.

5.1.2 Photolysis of Pure Isopropanethiol

The major photolysis products were H_2 and $(i-C_3H_7)_2S_2$, with small amounts of C_3H_8, H_2S and C_3H_6 . The dark reaction runs at $25^\circ C$ and $145^\circ C$ did not produce any measurable products, thus, $i-C_3H_7SH$ is thermally stable within this temperature range. The product quantum yields are tabulated in Table 5.2 and are plotted against $i-C_3H_7SH$ pressure in Figure 5.1. It was observed that reaction times up to 120 minutes did not affect the quantum yields and that these quantum yields seem to be independent of $i-C_3H_7SH$ pressure in the range 5 - 50 Torr. The points for $\phi(H_2), \phi(C_3H_8), \phi(H_2S), \phi(C_3H_6)$ and $\phi[(i-C_3H_7)_2S_2]$ were averaged separately over the entire pressure range studied and found to be $0.81 \pm 0.03, 0.21 \pm 0.02, 0.24 \pm 0.02, 0.042 \pm 0.004$ and 0.87 ± 0.07 , respectively, at $25^\circ C$.

5.1.3 Photolysis of Isopropanethiol with Added Thermalizer, $n-C_4H_{10}$

The effects of added $n-C_4H_{10}$ thermalizer pressure on the product quantum yields were investigated in this series of experiments. The pressure of $i-C_3H_7SH$ was kept constant

Table 5.2. Product Quantum Yields in the Photolysis of Pure $i\text{-C}_3\text{H}_7\text{SH}^a$

$P(i\text{-C}_3\text{H}_7\text{SH})$ (Torr)	$[R(\text{H}_2)+R(\text{C}_3\text{H}_8)]$ (10^{-2} $\mu\text{moles min}^{-1}$)	$\phi(\text{H}_2)$ (± 0.02)	$\phi(\text{C}_3\text{H}_8)$ (± 0.02)	$\phi(\text{H}_2\text{S})$ (± 0.02)	$\phi(\text{C}_3\text{H}_6)$ (± 0.003)	$\phi[(i\text{-C}_3\text{H}_7)_2\text{S}_2]$ (± 0.07)
5	3.4 ± 0.2^b (1) ^c	0.816	0.194	0.236	0.0523	0.890
10	5.7 ± 0.6 (2)	0.788	0.222	0.190	0.0483	0.739
15	7.6 ± 0.1 (2)	0.799	0.211	0.245	0.0431	0.817
20	9.0 ± 0.8 (3)	0.787	0.223	0.229	0.0444	0.794
25	9.8 ± 0.6 (2)	0.798	0.212	0.249	0.0429	0.803
30	10.3 ± 0.3 (2)	0.800	0.210	0.260	0.0405	0.802
35	11.2 ± 0.2 (3)	0.798	0.212	0.246	0.0425	0.743
40	11.8 ± 0.1 (2)	0.803	0.207	0.244	0.0392	0.844
45	11.8 ± 0.1 (2)	0.805	0.206	0.246	0.0393	0.817
50	12.5 ± 0.2 (2)	0.800	0.210	0.240	0.0369	0.823
Average		0.80 ± 0.03	0.21 ± 0.03	0.24 ± 0.04	0.042 ± 0.004	0.81 ± 0.11

^a $T=25^\circ\text{C}$; photolysis time=60 min; $I_a=0.99[R(\text{H}_2)+R(\text{C}_3\text{H}_8)]$

^bstandard error

^cNumber of experiments

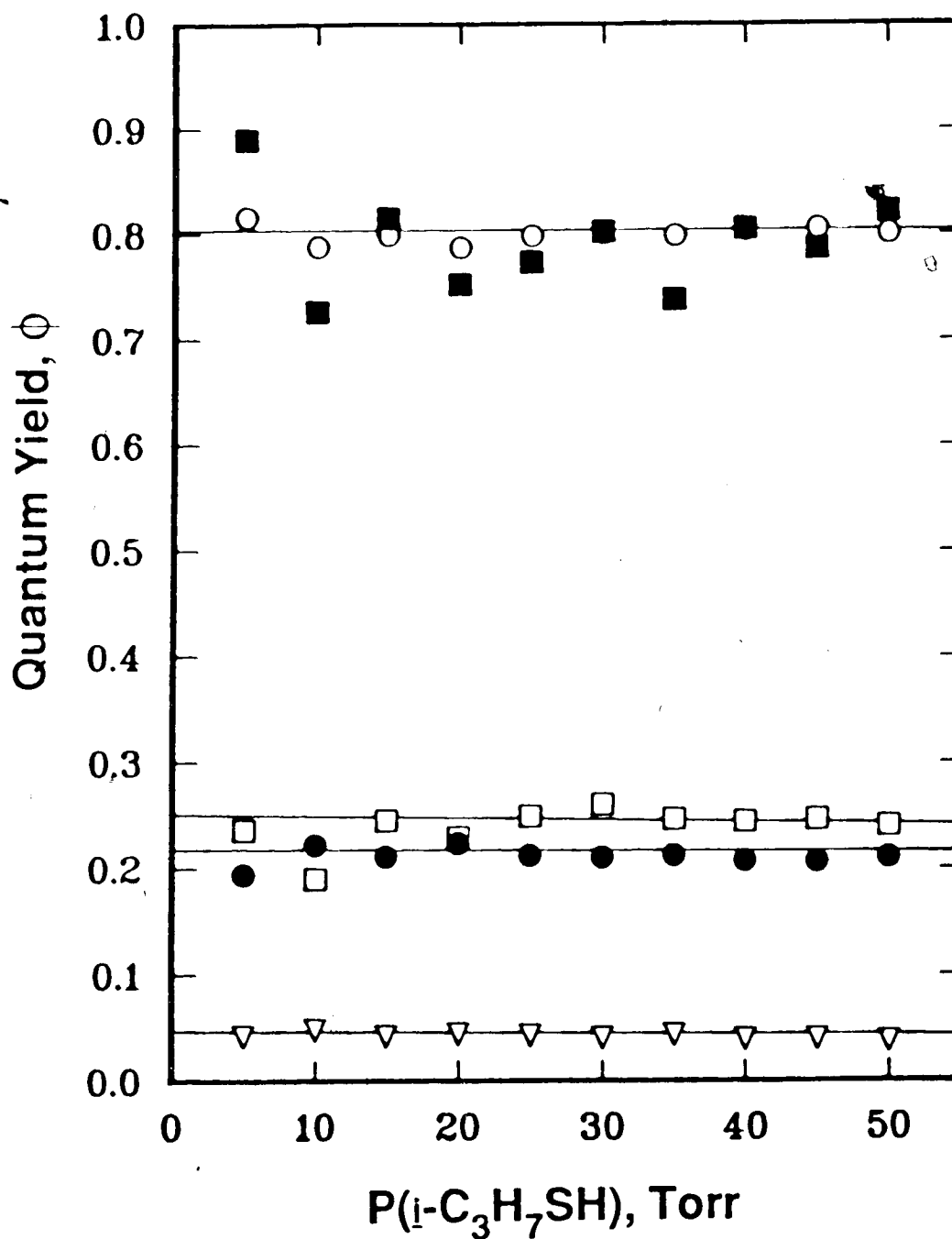


Figure 5.1. Product quantum yields versus $i\text{-C}_3\text{H}_7\text{SH}$ pressure. \blacksquare , $(i\text{-C}_3\text{H}_7)_2\text{S}_2$; \circ , H_2 ; \square , H_2S ; \bullet , C_3H_8 ; ∇ , C_3H_6 .

at 20 Torr while the pressure of $n\text{-C}_4\text{H}_{10}$ was varied between 28 and 400 Torr. It was observed that the rates of product formation decrease with increasing thermalizer pressure, but the sum of $R(\text{H}_2)$ and $R(\text{C}_3\text{H}_8)$ remained invariant at $(8.6 \pm 0.5) \times 10^{-8}$ moles min^{-1} . This is illustrated in Table 5.3, along with the experimental product quantum yield results. The product quantum yields are plotted against $n\text{-C}_4\text{H}_{10}$ pressure in the range 0 - 400 Torr in Figure 5.2. With increasing $n\text{-C}_4\text{H}_{10}$ pressure, $\phi(\text{H}_2)$ and $\phi[(i\text{-C}_3\text{H}_7)_2\text{S}_2]$ increased gradually while there was a parallel decrease in $\phi(\text{C}_3\text{H}_8)$, $\phi(\text{H}_2\text{S})$ and $\phi(\text{C}_3\text{H}_6)$. Also, it was observed that the increase in $\phi(\text{H}_2)$ compensated for the decrease in $\phi(\text{C}_3\text{H}_8)$, and that $\phi(\text{H}_2\text{S})$ seemed to be slightly higher than $\phi(\text{C}_3\text{H}_8)$. All the quantum yields reach limiting values at approximately a fifteenfold increase of $n\text{-C}_4\text{H}_{10}$ pressures over $i\text{-C}_3\text{H}_7\text{SH}$, which is at a $n\text{-C}_4\text{H}_{10}$ pressure of ≥ 300 Torr.

5.1.4 Effect of Temperature on Product Yields

The photolysis of $i\text{-C}_3\text{H}_7\text{SH}$ with added thermalizer, $n\text{-C}_4\text{H}_{10}$, was carried out at higher temperatures, 65°C , 105°C and 145°C . Although different product quantum yields were observed with increasing temperature, the variation of these yields with increasing $n\text{-C}_4\text{H}_{10}$ pressure at each temperature was the same as that observed at 25°C . The product quantum yields obtained as a function of $n\text{-C}_4\text{H}_{10}$ pressures and at the high $n\text{-C}_4\text{H}_{10}$ pressure limit, 300 - 400 Torr, are summarized in Tables 5.4 to 5.7, respectively. With temperature increases, $\phi(\text{H}_2)$ and $\phi[(i\text{-C}_3\text{H}_7)_2\text{S}_2]$ decrease while

Table 5.3. Product Quantum Yields in the Photolysis of *i*-C₃H₇SHwith Added Thermalizer, *n*-C₄H₁₀,^a T = 25°C

P(<i>n</i> -C ₄ H ₁₀) (Torr)	[R(H ₂)+R(C ₃ H ₈)] ^b (10 ⁻² μmoles min ⁻¹) (±0.2) ^c	φ(H ₂) (±0.02)	φ(C ₃ H ₈) (±0.02)	φ(H ₂ S) (±0.02)	φ(C ₃ H ₆) (±0.003)	φ[(<i>i</i> -C ₃ H ₇) ₂ S ₂] (±0.07)
0	9.0 ^d	0.80	0.21	0.24	0.042	0.81
28	8.48 (2) ^e	0.838	0.172	0.193	0.0211	0.887
35	8.92 (2)	0.840	0.171	0.183	0.0206	0.860
50	8.57 (2)	0.838	0.172	0.173	0.0182	0.793
70	8.71 (2)	0.851	0.159	0.168	0.0145	0.870
100	8.91 (3)	0.850	0.160	0.157	0.0126	0.840
150	8.76 (2)	0.859	0.151	0.153	0.0102	0.889
200	8.27 (2)	0.872	0.138	0.138	0.0097	0.855
250	8.38 (2)	0.878	0.133	0.129	0.0100	0.870
300	8.29 (2)	0.875	0.135	0.135	0.0097	0.890
350	8.41 (2)	0.887	0.123	0.129	0.0094	0.876
400	8.56 (3)	0.877	0.133	0.131	0.0087	0.896

^ap(*i*-C₃H₇SH)=20.0 Torr; T=25°C; photolysis time=60 min; I_a=0.99[R(H₂)+R(C₃H₈)]^baverage [R(H₂)+R(C₃H₈)]=(8.6±0.5) × 10⁻² μmoles min⁻¹^cstandard error^dsee results from Table 5.2^enumber of experiments

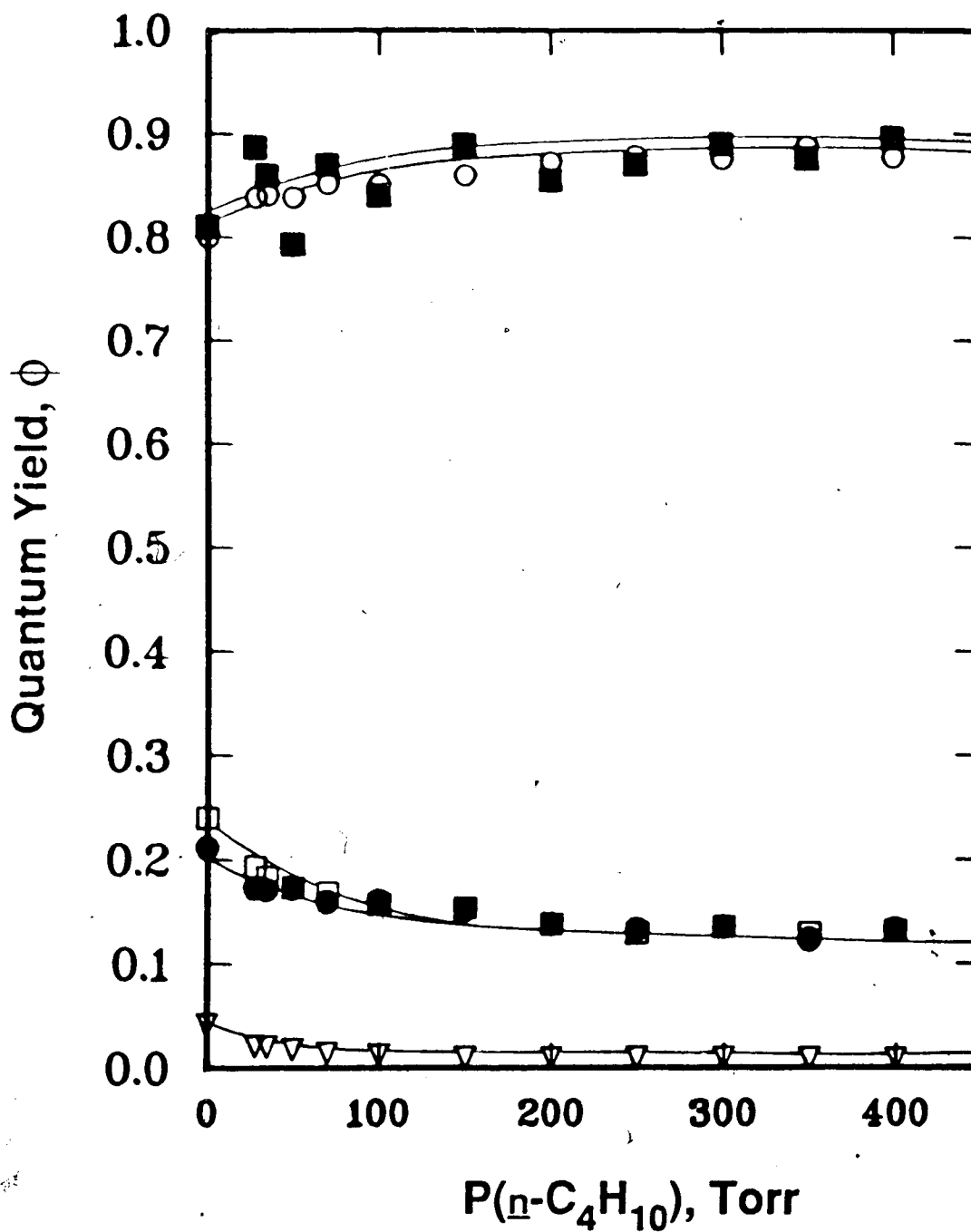


Figure 5.2. Product quantum yields versus $n\text{-C}_4\text{H}_{10}$ pressure at constant $i\text{-C}_3\text{H}_7\text{SH}$ pressure of 20.0 Torr. \blacksquare , $(i\text{-C}_3\text{H}_7)_2\text{S}_2$; \circ , (H_2) ; \square , (H_2S) ; \bullet , (C_3H_8) ; ∇ , (C_3H_6) .

Table 5.4. Product Quantum Yields in the Photolysis of $i\text{-C}_3\text{H}_7\text{SH}$

with Added Thermalizer, $n\text{-C}_4\text{H}_{10}$,^a $T = 65^\circ\text{C}$

P($n\text{-C}_4\text{H}_{10}$) (Torr)	$[\text{R}(\text{H}_2) + \text{R}(\text{C}_3\text{H}_8)]^b$ (10^{-2} $\mu\text{moles min}^{-1}$) (± 0.2) ^c	$\phi(\text{H}_2)$ (± 0.02)	$\phi(\text{C}_3\text{H}_8)$ (± 0.02)	$\phi(\text{H}_2\text{S})$ (± 0.02)	$\phi(\text{C}_3\text{H}_6)$ (± 0.003)	$\phi[(i\text{-C}_3\text{H}_7)_2\text{S}_2]$ (± 0.07)
0	9.5 (2) ^d	0.750	0.260	0.295	0.0523	0.890
31.8	9.3 (2)	0.777	0.233	0.245	0.0295	0.865
39.7	9.4 (2)	0.788	0.222	0.238	0.0230	0.880
56.7	9.1 (2)	0.796	0.214	0.229	0.0199	0.876
79.4	9.4 (2)	0.800	0.200	0.221	0.0178	0.840
113	9.0 (2)	0.823	0.187	0.204	0.0150	0.873
170	9.2 (1)	0.815	0.195	0.260	0.0141	0.894
230	9.0 (2)	0.821	0.189	0.192	0.0104	0.888
285	9.1 (2)	0.825	0.185	0.191	0.0094	0.872
340	9.3 (2)	0.829	0.181	0.180	0.0103	0.876
397	8.9 (1)	0.831	0.179	0.175	0.0091	0.872
455	9.0 (2)	0.843	0.167	0.169	0.0094	0.885

^a $\phi(i\text{-C}_3\text{H}_7\text{SH}) = 22.7$ Torr or $[i\text{-C}_3\text{H}_7\text{SH}] = 1.04 \times 10^{-3}$ M; photolysis time = 60 min
^baverage $[\text{R}(\text{H}_2) + \text{R}(\text{C}_3\text{H}_8)] = (9.2 \pm 0.2) \times 10^{-2}$ $\mu\text{moles min}^{-1}$; $I_a = 0.99[\text{R}(\text{H}_2) + \text{R}(\text{C}_3\text{H}_8)]$
^cstandard error
^dnumber of experiments

Table 5.5. Product Quantum Yields in the Photolysis of *i*-C₃H₇SHwith Added Thermalizer, n-C₄H₁₀.^a T = 105°C

P(n-C ₄ H ₁₀) (Torr)	[R(H ₂)+R(C ₃ H ₈)] ^b (10 ⁻² μmoles min ⁻¹) (±0.2) ^c	φ(H ₂) (±0.02)	φ(C ₃ H ₈) (±0.02)	φ(H ₂ S) (±0.02)	φ(C ₃ H ₆) (±0.003)	φ[(<i>i</i> -C ₃ H ₇) ₂ S ₂] (±0.07)
0	9.4 (2) ^d	0.739	0.271	0.324	0.0540	0.841
35.5	9.5 (2)	0.772	0.238	0.260	0.0312	0.875
44.4	9.3 (2)	0.768	0.242	0.262	0.0274	0.850
63.4	9.4 (2)	0.780	0.230	0.249	0.0238	0.893
88.8	9.1 (2)	0.794	0.216	0.231	0.0184	0.821
130	9.3 (2)	0.798	0.212	0.221	0.0173	0.842
190	9.0 (2)	0.802	0.208	0.211	0.0135	0.820
255	9.2 (2)	0.811	0.199	0.202	0.0114	0.860
320	8.9 (2)	0.810	0.200	0.203	0.0107	0.822
380	9.0 (2)	0.826	0.184	0.200	0.0098	0.834
445	8.8 (1)	0.828	0.182	0.208	0.0096	0.805
510	9.0 (2)	0.834	0.176	0.193	0.0095	0.842

^ap(*i*-C₃H₇SH)=25.4 Torr or [*i*-C₃H₇SH]=1.04 x 10⁻³ M; photolysis time=60 min
^baverage [R(H₂)+R(C₃H₈)]=(9.2±0.2) x 10⁻² μmoles min⁻¹; I_a=0.99[R(H₂)+R(C₃H₈)]
^cstandard error
^dnumber of experiments

Table 5.6. Product Quantum Yields in the Photolysis of $i\text{-C}_3\text{H}_7\text{SH}$

with Added Thermalizer, $n\text{-C}_4\text{H}_{10}$,^a $T = 145^\circ\text{C}$

P($n\text{-C}_4\text{H}_{10}$) (Torr)	$[\text{R}(\text{H}_2) + \text{R}(\text{C}_3\text{H}_8)]^b$ (10^{-2} $\mu\text{moles min}^{-1}$) (± 0.2) ^c	$\phi(\text{H}_2)$ (± 0.02)	$\phi(\text{C}_3\text{H}_8)$ (± 0.02)	$\phi(\text{H}_2\text{S})$ (± 0.02)	$\phi(\text{C}_3\text{H}_6)$ (± 0.003)	$\phi(i\text{-C}_3\text{H}_7\text{S}_2)$ (± 0.07)
0	9.4 (2) ^d	0.719	0.291	0.356	0.0680	0.803
39.3	9.7 (2)	0.753	0.257	0.296	0.0355	0.847
49.1	9.4 (2)	0.759	0.251	0.278	0.0311	0.827
70.1	9.4 (2)	0.765	0.245	0.268	0.0264	0.862
98.2	9.3 (2)	0.776	0.234	0.254	0.0228	0.794
140	9.0 (2)	0.784	0.226	0.258	0.0189	0.829
210	8.9 (2)	0.791	0.219	0.226	0.0165	0.813
280	9.0 (2)	0.797	0.213	0.228	0.0124	0.869
350	8.8 (2)	0.809	0.201	0.226	0.0126	0.838
420	9.1 (2)	0.812	0.198	0.215	0.0113	0.800
490	8.9 (2)	0.814	0.196	0.195	0.0102	0.833
560	8.8 (3)	0.824	0.186	0.197	0.0096	0.804

^a $p(i\text{-C}_3\text{H}_7\text{SH}) = 28.1$ Torr or $[i\text{-C}_3\text{H}_7\text{SH}] = 1.04 \times 10^{-3}$ M; photolysis time = 60 min
^baverage $[\text{R}(\text{H}_2) + \text{R}(\text{C}_3\text{H}_8)] = (9.1 \pm 0.3) \times 10^{-2}$ $\mu\text{moles min}^{-1}$; $I_a = 0.99[\text{R}(\text{H}_2) + \text{R}(\text{C}_3\text{H}_8)]$
^cstandard error
^dnumber of experiments

Table 5.7. Effect of Temperature on Product Quantum Yields^a

at High n -C₄H₁₀ Pressure Limits^b

Temperature, (°C)	$[R(H_2)+R(C_3H_8)]^c$ (10^{-2} μ moles min^{-1})	$\phi(H_2)$	$\phi(C_3H_8)$	$\phi(H_2S)$	$\phi(C_3H_6)$	$\phi(i-C_3H_7)_2S_2$
25	8.6 $\pm 0.3^d$	0.88 ± 0.01	0.13 ± 0.01	0.13 ± 0.01	0.009 ± 0.001	0.89 ± 0.02
65	9.1 ± 0.2	0.84 ± 0.01	0.17 ± 0.01	0.18 ± 0.01	0.010 ± 0.001	0.88 ± 0.04
105	9.0 ± 0.2	0.83 ± 0.01	0.18 ± 0.01	0.19 ± 0.01	0.010 ± 0.001	0.83 ± 0.03
145	8.9 ± 0.1	0.82 ± 0.01	0.19 ± 0.01	0.21 ± 0.02	0.011 ± 0.001	0.81 ± 0.04

^aeach quantum yield value is the average of 5-8 experimental points

photolysis time = 60 min; $I_a = 0.99[R(H_2) + R(C_3H_8)]$

^b $P(i-C_3H_7SH) = 20.0-28.1$ Torr or $[i-C_3H_7SH] = 1.04 \times 10^{-3}$ M

$P(n-C_4H_{10}) = 300-560$ Torr or $[n-C_4H_{10}] = (1.61-2.15) \times 10^{-2}$ M

^ccoverage of a minimum of 20 experimental values

^dstandard error

$\phi(\text{C}_3\text{H}_8)$, $\phi(\text{H}_2\text{S})$ and $\phi(\text{C}_3\text{H}_6)$ increase, and the sum of $R(\text{H}_2)$ and $R(\text{C}_3\text{H}_8)$ remains invariant.

5.2 Discussion

5.2.1 Reaction Mechanism

Because the photolysis results for \underline{i} - $\text{C}_3\text{H}_7\text{SH}$ are quite similar to those obtained for $\text{C}_2\text{H}_5\text{SH}$ (Chapter 4), a reaction mechanism analogous to that proposed for $\text{C}_2\text{H}_5\text{SH}$ can also be employed for \underline{i} - $\text{C}_3\text{H}_7\text{SH}$ to account for the products observed and to adequately explain our experimental results in a quantitative manner.

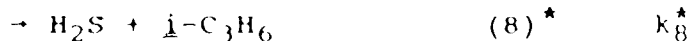
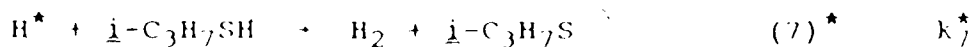
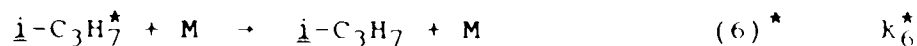
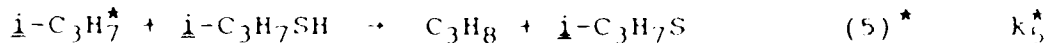
The set of primary photochemical reactions is:



The enthalpies of reaction for 1, 2 and 3 are the same as those for $\text{C}_2\text{H}_5\text{SH}$; namely, 88, 70 and 18 kcal mol⁻¹, respectively, from Table 1.2. Thus, from the available photon energy at 254 nm, 113 kcal Einstein⁻¹, the excess energies residing in the H and \underline{i} - C_3H_7 radicals are 25 and 43 kcal mol⁻¹, respectively. The thermal energy for the latter radicals is estimated from $0.5(\text{sRT})$,¹⁶³ to be 8 - 11 kcal mol⁻¹, in the temperature range 25-145°C, thus the total excess energy carried over to the \underline{i} - C_3H_7 radicals is 51 - 54 kcal mol⁻¹.

The set of hot reactions for H and \underline{i} - $\text{C}_3\text{H}_7\text{S}$ radicals is as follows:



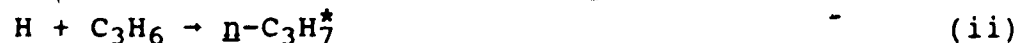


The unimolecular decomposition of $\underline{i}\text{-C}_3\text{H}_7^*$ to give the C_3H_6 product from (4)* has an enthalpy of reaction of $36 - 39$ kcal mol⁻¹, estimated from available thermochemical data in the literature.^{50,51} The critical energy for (4)* is given by Benson and O'Neal¹⁷⁵ to be about 41 kcal mol⁻¹. This is about 10 - 13 kcal mol⁻¹ less than the amount of the excess energy which was carried over to the $\underline{i}\text{-C}_3\text{H}_7$ radicals from the primary step (2) and the thermal energy. Unfortunately, no computations of the experimental rate constants and their energy dependence were carried out for $\underline{i}\text{-C}_3\text{H}_7$ radicals. However, Rabinovitch and Setser¹⁴² have found that for n-propyl radicals carrying an active energy content of -10 kcal mol⁻¹, $k_4^* \approx 10^8$ s⁻¹. Thus, it is postulated that the rate constant for Reaction (4)* will also be $\leq 10^8$ s⁻¹ for isopropyl radicals.

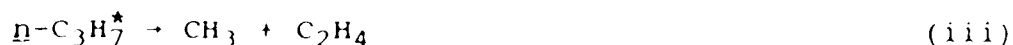
The addition reaction, which is the reverse of Reaction (4)*,



is known to have an activation energy of -1.6 kcal mol⁻¹.^{176,177} The alternative competitive reaction, which is the addition of H at the non-terminal carbon,



is relatively minor at 5%¹⁷⁸⁻¹⁸¹ and also requires a higher activation energy of about 4 kcal mol⁻¹.¹⁷⁷ Cvetanovic and coworkers¹⁷⁸⁻¹⁸⁰ have reported that over 95% of the $\dot{i}\text{-C}_3\text{H}_7^*$ radicals formed from (i) invariably dissociate back to the reactants. This is in contrast to hot $\dot{n}\text{-C}_3\text{H}_7$ radicals, which dissociate predominantly into a methyl radical and ethylene,¹⁴²



Overall, Reaction (4)* is the major source reaction for C₃H₆ formation. Also, no C₃H₆ is lost by steps (ii) and (iii), since the rate of step (ii) is very small under condition of low conversion, and C₂H₄ was not observed in the products. The other source reaction for C₃H₆ and C₃H₈ is the disproportionation reaction of $\dot{i}\text{-C}_3\text{H}_7$ radicals,



for which the rate constant ratio for the disproportionation to combination reaction,

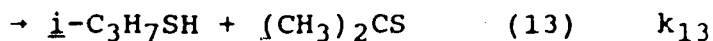
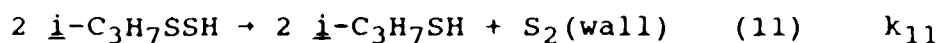
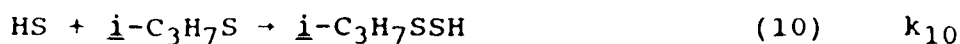
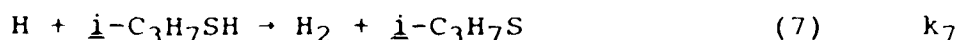
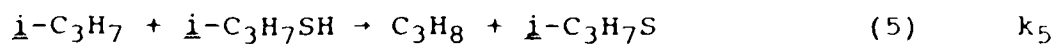


$k_{\text{iv}}/k_{\text{v}}$, has been determined to be 0.60 ± 0.01 .¹⁸² However, (iv) is viewed to be unimportant, since no 2,3-dimethylbutane was observed in the products.

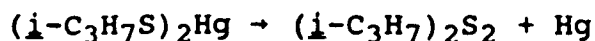
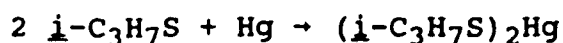
The collisional deactivating molecules for the quenching of hot H and $\dot{i}\text{-C}_3\text{H}_7$ radicals in Reactions (6)* and (9)*, may be either $\dot{i}\text{-C}_3\text{H}_7\text{SH}$ or $\dot{n}\text{-C}_4\text{H}_{10}$. The possibility of extra H₂ being produced by the hot H-atom reactions with $\dot{n}\text{-C}_4\text{H}_{10}$ was ruled out by Bridges *et al.*,⁶³ based on the results that a blank photolysis run at 254 nm using 200 Torr $\dot{n}\text{-C}_4\text{H}_{10}$ gave

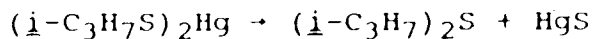
no products, and that $\phi(\text{H}_2)$ obtained in the photolysis of a 5:1 mixture of $n\text{-C}_4\text{H}_{10}$ and HI was not different from the $\phi(\text{H}_2)$ obtained for the photolysis of pure HI. However, these results are predictable since it was already known at the time that alkanes absorb in the vacuum UV region, below 200 nm.¹⁵⁴ In a similar manner as for $\text{C}_2\text{H}_5\text{SH}$ and CO_2 , quenching by $i\text{-C}_3\text{H}_7\text{SH}$ is more significant at low total pressures. However, quenching by $n\text{-C}_4\text{H}_{10}$ becomes more efficient as its pressure is increased from 28 to 400 Torr. Quenching is complete at $P(n\text{-C}_4\text{H}_{10}) \geq 300$ Torr, as indicated by the flat portion of the plot in Figure 5.2.

The set of thermal reactions is as follows, in parallel with that proposed for $\text{C}_2\text{H}_5\text{SH}$:



The scatter in $\phi[(i\text{-C}_3\text{H}_7)_2\text{S}_2]$ is observed to be more than that in $\phi(\text{H}_2\text{S})$. This may be due to the increased difficulty in measuring the heavier isopropyldisulfide product quantitatively, and also to the reactions of thiyl radicals with Hg,¹⁸³ as described in the previous Chapters,





The following quantum yield expressions have been derived from the steady-state treatment of the proposed mechanism.

$$\phi(\text{C}_3\text{H}_6) = \phi_3 + \frac{k_4^* \phi_2}{k_4^* + k_5^*[i] + k_6^*[M]} \quad [1]$$

$$\begin{aligned} \phi(\text{H}_2) = & \frac{k_7 \phi_1}{k_7 + k_8} - \frac{(k_7 k_8^* - k_7^* k_8) \phi_1 [i]}{(k_7 + k_8) \{ (k_7^* + k_8^*) [i] + k_9^*[M] \}} \\ & + \frac{k_4^* k_7 \phi_2}{(k_7 + k_8) (k_4^* + k_5^*[i] + k_6^*[M])} \end{aligned} \quad [2]$$

$$\begin{aligned} \phi(\text{C}_3\text{H}_8) = & \frac{k_8 \phi_1}{k_7 + k_8} + \phi_2 + \frac{(k_7 k_8^* - k_7^* k_8) \phi_1 [i]}{(k_7 + k_8) \{ (k_7^* + k_8^*) [i] + k_9^*[M] \}} \\ & - \frac{k_4^* k_7 \phi_2}{(k_7 + k_8) (k_4^* + k_5^*[i] + k_6^*[M])} \end{aligned} \quad [3]$$

$$\begin{aligned} \phi(\text{H}_2\text{S}) = & \frac{k_8 \phi_1}{k_7 + k_8} + \phi_3 + \frac{(k_7 k_8^* - k_7^* k_8) \phi_1 [i]}{(k_7 + k_8) \{ (k_7^* + k_8^*) [i] + k_9^*[M] \}} \\ & + \frac{k_4^* k_8 \phi_2}{(k_7 + k_8) (k_4^* + k_5^*[i] + k_6^*[M])} \end{aligned} \quad [4]$$

$$\phi[(\underline{i}\text{-C}_3\text{H}_7)_2\text{S}_2] = \frac{k_{12} \phi_1}{k_{12} + k_{13}} \quad [5]$$

ϕ_1 , ϕ_2 and ϕ_3 are the quantum yields associated with the three primary photochemical reactions, (1) - (3). M is the collisional deactivating molecule for hot H^* and $\underline{i}\text{-C}_3\text{H}_7^*$ radicals and may be either $\underline{i}\text{-C}_3\text{H}_7\text{SH}$ or $\underline{n}\text{-C}_4\text{H}_{10}$ molecules. The expressions for $k_6^*[M]$ and $k_9^*[M]$ are $k_{6i}^*[i] + k_{6n}^*[n]$ and

$k_{9i}^*[i] + k_{9n}^*[n]$, respectively. $[i]$ is the concentration or pressure of i -C₃H₇SH and $[n]$ is that of added n -C₄H₁₀.

5.2.2 Quantum Efficiencies of Primary Photochemical Steps: Quantum Yield of C₃H₆

Detailed changes of $\phi(C_3H_6)$ as a function of n -C₄H₁₀ pressure at 25, 65, 105 and 145°C are illustrated in Figure 5.3. Two different sources of C₃H₆ are evident in this plot, since $\phi(C_3H_6)$ decreases very rapidly with increasing n -C₄H₁₀ pressure and approaches a constant value at high pressures of n -C₄H₁₀. The former corresponds to the unimolecular decomposition step where hot isopropyl radicals decompose to H and C₃H₆, while the latter corresponds to the molecular primary photochemical step (3), which does not depend on n -C₄H₁₀ pressure.

In a kinetic treatment similar to that derived for the case of C₂H₄ from the photolysis of C₂H₅SH (Chapter 4), ϕ_3 is determined from the modified form of Equation [1];

$$[\phi(C_3H_6) - \phi_3]^{-1} = (1 + \alpha P_i) / \phi_2 + \beta P_n / \phi_2 \quad [6]$$

where $\alpha = (k_5^* + k_{6i}^*) / k_4^*$, $\beta = k_{6n}^* / k_4^*$ and $[\phi(C_3H_6) - \phi_3]^{-1}$ is a linear function of P_n at constant P_i .

The linear correlation coefficient for Equation [6] was calculated, in the first approximation, for ten values of ϕ_3 , ranging from 0.0081 to 0.0090. The results, shown in Figure 5.4, show that the coefficients are close to each other, with the highest value located at $\phi_3 = 0.0083$, which corresponds closely to the average experimental value $\phi(C_3H_6) \approx 0.009$ in the high (300 - 400 Torr) n -C₄H₁₀ pressure region

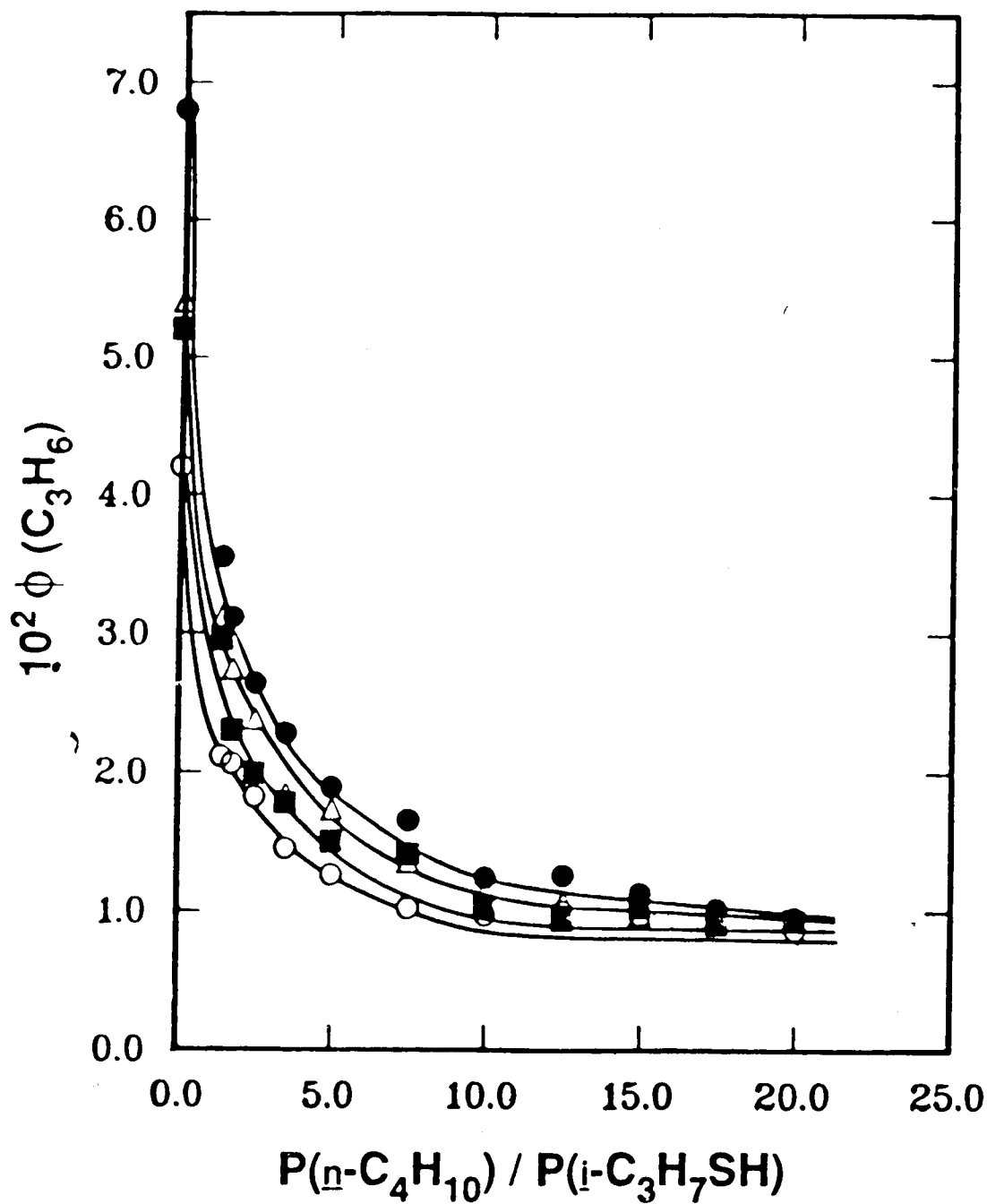


Figure 5.3. Plots of quantum yield of C₃H₆ as a function of P(n-C₄H₁₀)/P(i-C₃H₇SH). ○, 25°C; ■, 65°C; △, 105°C; ●, 145°C.

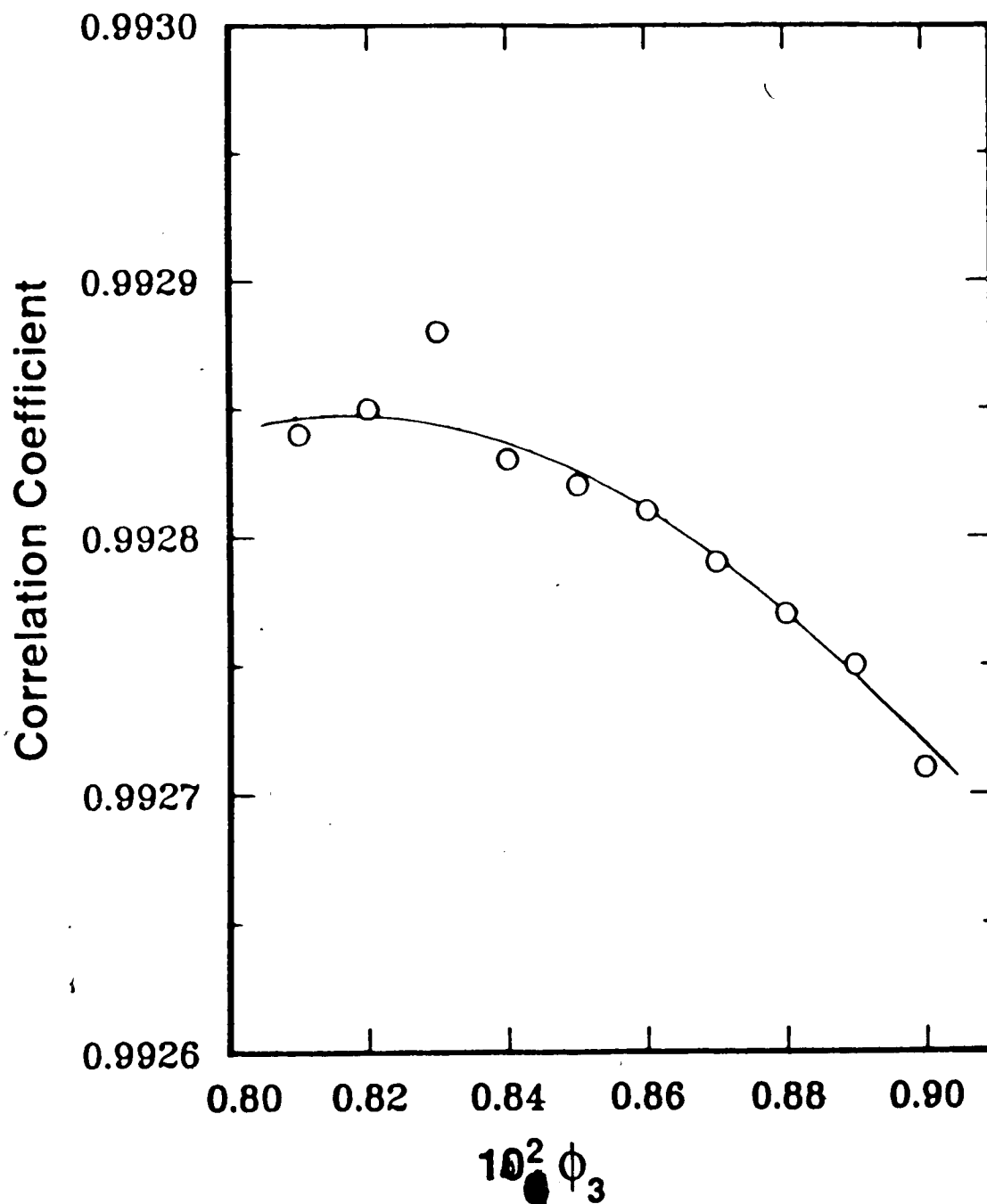


Figure 5.4. Relation between ϕ_3 and the correlation coefficient in the LMS treatment of $[\phi(\text{C}_3\text{H}_6) - \phi_3]^{-1}$ against $n\text{-C}_4\text{H}_{10}$ pressure.

at 25°C (see Figure 5.3).

Equation [6] becomes a linear function of P_i in the absence of thermalizer, *i.e.* $P_n = 0$,

$$[\phi(\text{C}_3\text{H}_6) - \phi_3]^{-1} = 1/\phi_2 + \alpha P_i/\phi_2 \quad [7]$$

The plot of $\phi(\text{C}_3\text{H}_6)$ versus $P(\text{i-C}_3\text{H}_7\text{SH})$ using a much expanded ordinate scale, Figure 5.5, illustrates the marginal pressure dependence of $\phi(\text{C}_3\text{H}_6)$ on $P(\text{i-C}_3\text{H}_7\text{SH})$. The values for $[\phi(\text{C}_3\text{H}_6) - \phi_3]^{-1}$ at $P_n = 0$ were calculated using $\phi_3 = 0.009$ and were plotted against $\text{i-C}_3\text{H}_7\text{SH}$ pressure in Figure 5.6. The following linear relation was derived by the LMS method, for the condition $P_n = 0$;

$$[\phi(\text{C}_3\text{H}_6) - \phi_3]^{-1} = (23.5 \pm 0.9) + (0.24 \pm 0.03)P_i \quad [8]$$

Combining this equation with Equation [7], ϕ_2 and α were determined to be 0.043 ± 0.002 and $(1.0 \pm 0.1) \times 10^{-2} \text{ Torr}^{-1}$, respectively.

The values of ϕ_2 at higher temperatures may now be determined from the intercepts of Equation [6]. The variations of $[\phi(\text{C}_3\text{H}_6) - \phi_3]^{-1}$ with pressure and temperature are tabulated in Table 5.8 and plotted in Figure 5.7, from which the derived intercepts are listed in Table 5.9. The values of α and ϕ_3 are again assumed to be little affected by temperatures up to 145°C. This assumption for ϕ_3 appears to be valid, from the experimental observation (Table 5.7) that changes in ϕ_3 up to 145°C are within experimental error.

The derived values of ϕ_2 and subsequently ϕ_1 ($\phi_1 + \phi_2 + \phi_3 = 1.0$), are listed in Table 5.10. A slight increase in ϕ_2 (0.043 - 0.074) and consequently a decrease in ϕ_1 (0.95 -

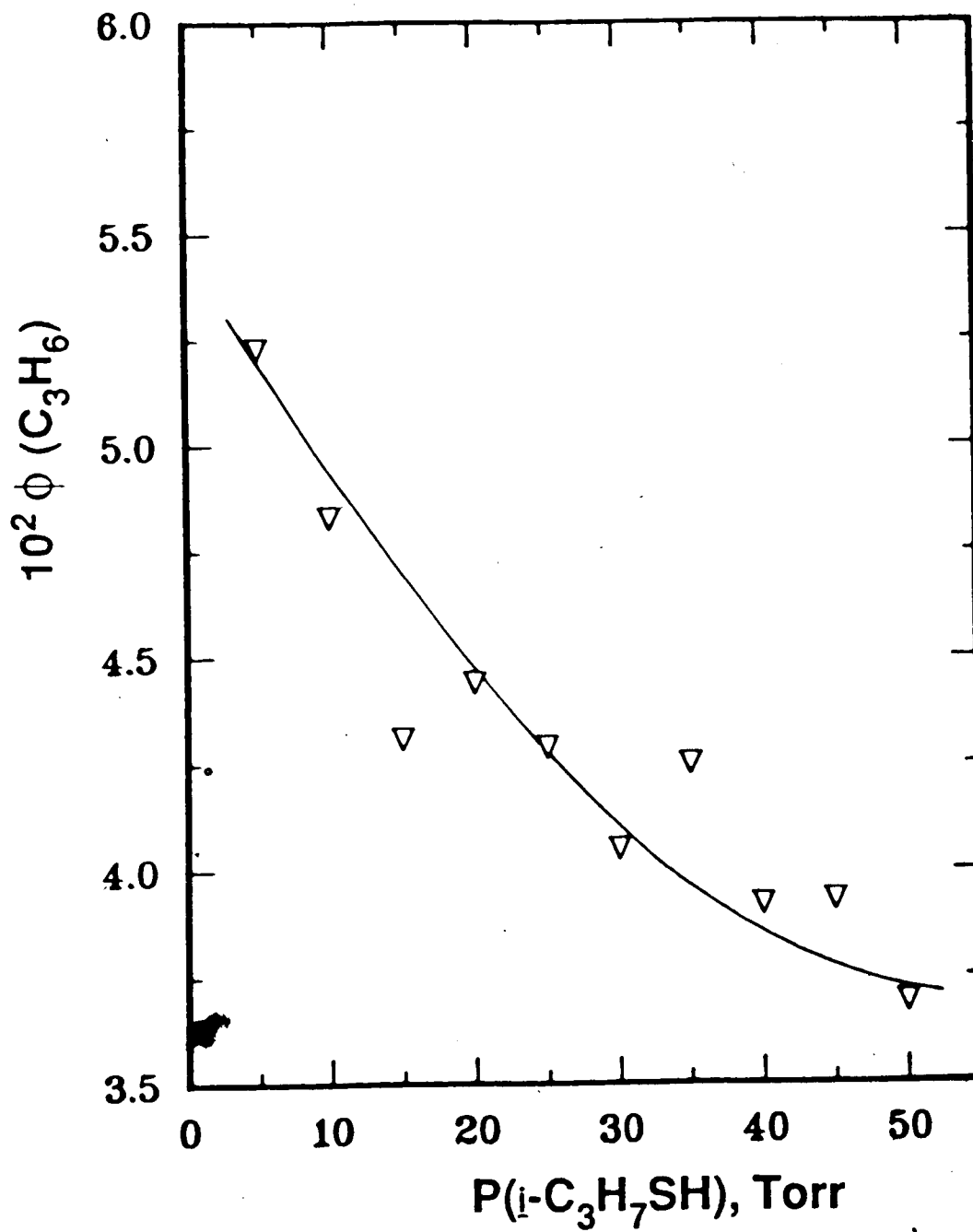


Figure 5.5. Quantum yield of C_3H_6 versus $i-C_3H_7SH$ pressure.

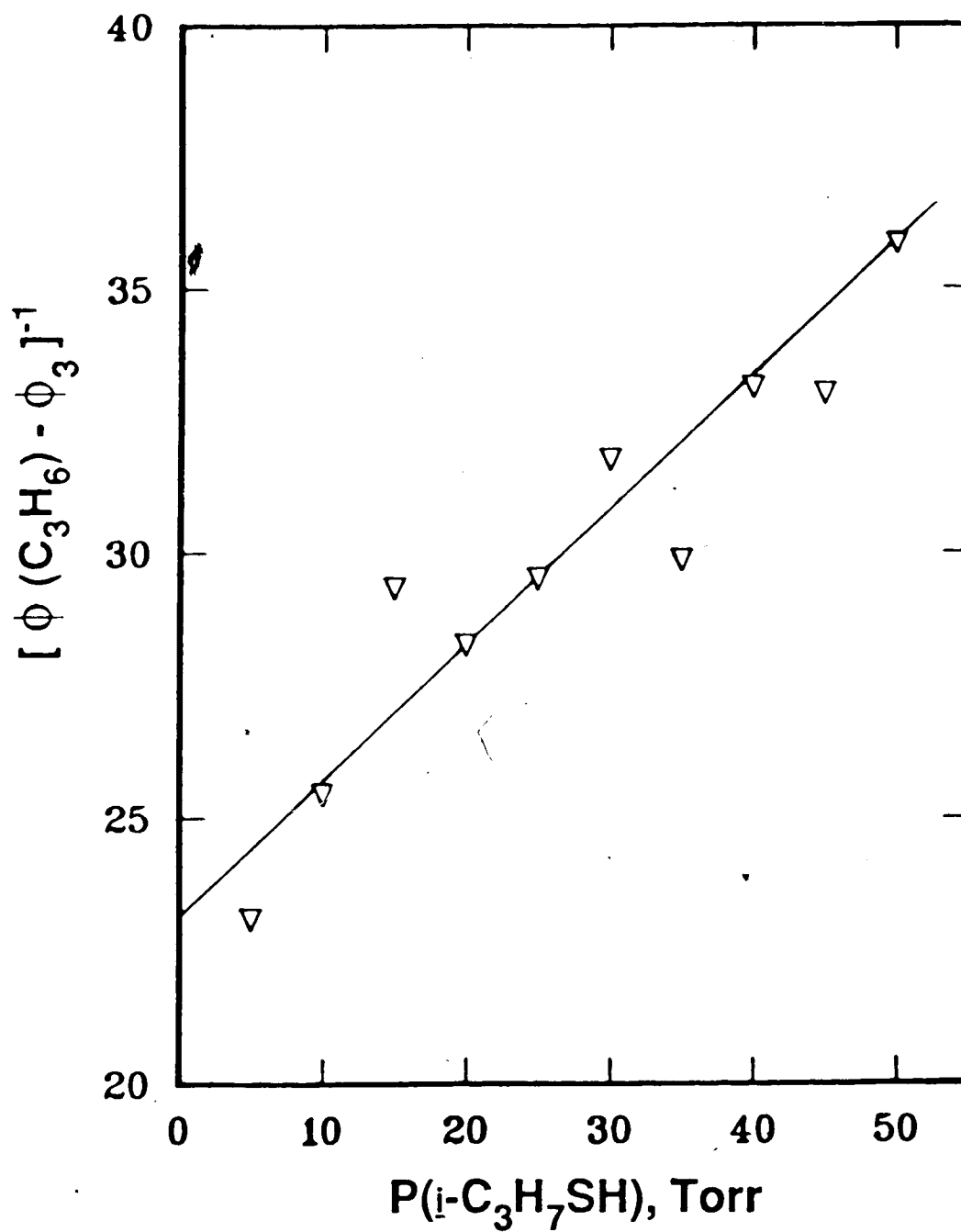


Figure 5.6: $[\phi(\text{C}_3\text{H}_6) - \phi_3]^{-1}$ versus $\text{i-C}_3\text{H}_7\text{SH}$ pressure.
The best fitted value of $\phi_3 = 0.009$ was used.

Table 5.8. Variations of $[\phi(C_3H_6) - \phi_3]^{-1}$ a with Pressure^b and Temperature

[P(n -C ₄ H ₁₀)/P(i -C ₃ H ₇ SH)]	$[\phi(C_3H_6) - \phi_3]^{-1}$		
	25°C	65°C	105°C
0	26.2 ^c	23.3	22.2
1.40	80.8	48.8	45.1
1.75	84.3	71.4	54.4
2.50	106.0	91.7	67.6
3.50	167.4	113.6	106.4
5.00	191.8	166.7	120.5
			145°C
			17.0
			37.7
			45.3
			57.5
			72.5
			101.0

^a $\phi_3 = 0.009$

^bP(n -C₄H₁₀) = 0-140 Torr or [CO₂] $\leq 5.38 \times 10^{-3}$ M

P(i -C₃H₇SH) = 20.0-28.1 Torr or [i -C₃H₇SH] = 1.04×10^{-3} M

5/8.

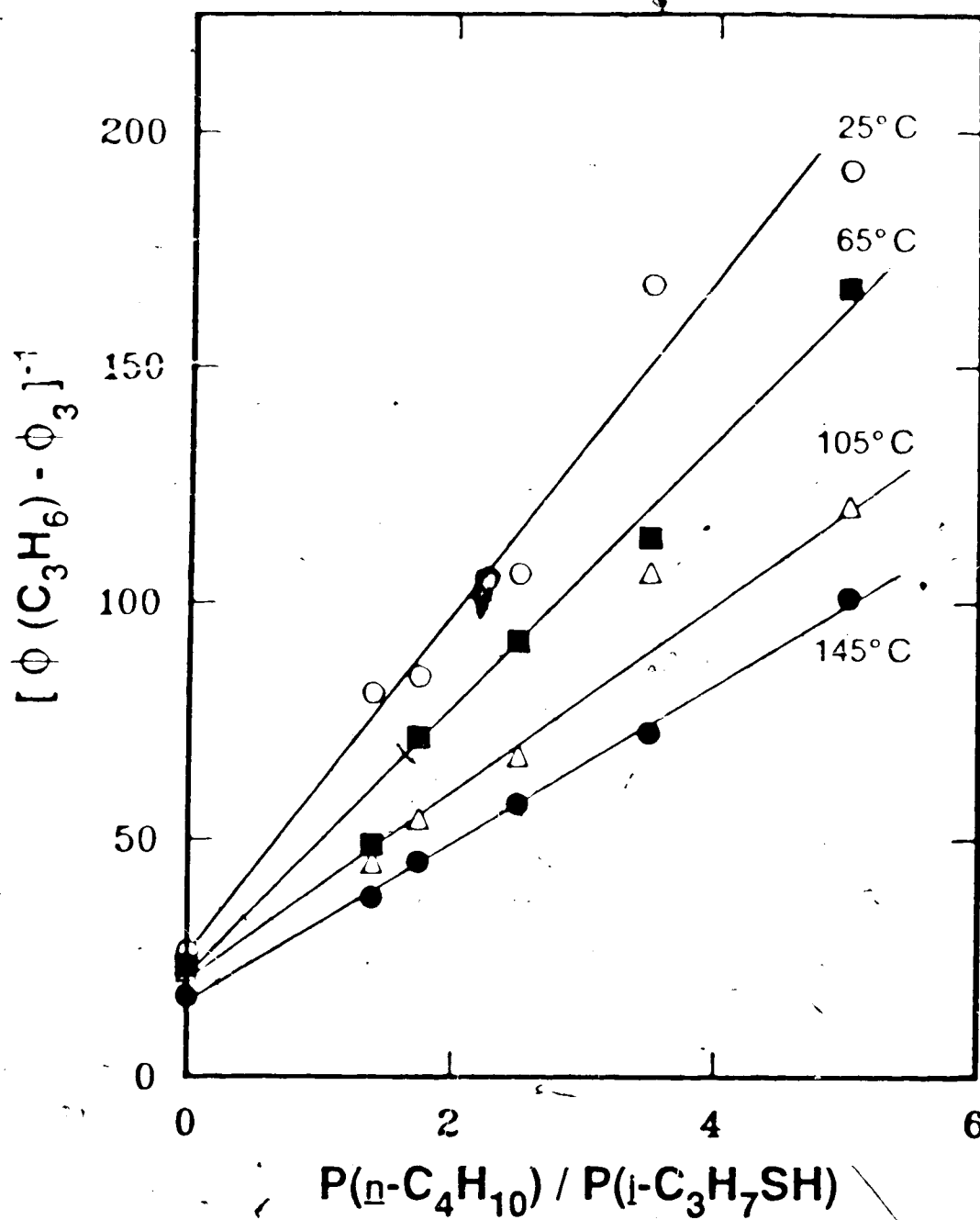


Figure 5.7.: Plots of $[\phi(\text{C}_3\text{H}_6) - \phi_3]^{-1}$ as a function of $P(\text{n-C}_4\text{H}_{10}) / P(\text{i-C}_3\text{H}_7\text{SH})$. The best fitted value of $\phi_3 = 0.009$ was used.

Table 5.9. Intercepts of the Plots in Figure 5.7

Temperature (°C)	P(i-C ₃ H ₇ SH) (Torr)	Intercept ^a	Correlation Coefficient
25	20.0	28 ± 8 ^b	0.993
65	22.7	26 ± 7	0.985
105	25.4	19 ± 6	0.983
145	28.1	17 ± 2	0.998

^aintercept = $(1+\alpha P_i)/\phi_2$; $\alpha = (k_5^*+k_6^*)/k_4^*$, in units of Torr⁻¹
^bstandard error

Table 5.10. Quantum Yields for the Primary Photochemical Processes

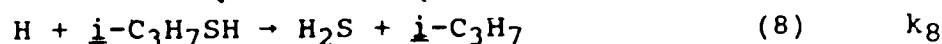
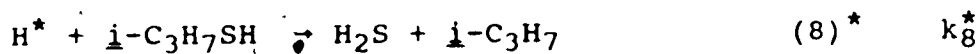
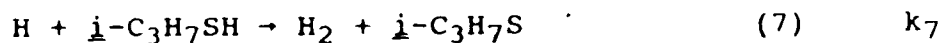
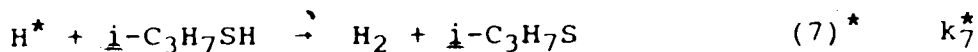
Temperature (°C)	ϕ_1	ϕ_2	ϕ_3
25	0.948 ± 0.012^a	0.043 ± 0.012	$0.009^b \pm 0.001$
65	0.944 ± 0.013	0.047 ± 0.013	0.009 ± 0.001
105	0.926 ± 0.015	0.065 ± 0.015	0.009 ± 0.001
145	0.917 ± 0.009	0.074 ± 0.009	0.009 ± 0.001
Average:	0.93 ± 0.02	0.057 ± 0.024	0.009 ± 0.001

^a standard error
^b assumed to be constant

0.92) are observed with increasing temperature. This variation is slightly larger than for the case of the photolysis of C_2H_5SH but still within the experimental error. As a result, the quantum efficiencies of the primary photochemical reactions can be considered to be independent of temperatures within an experimental error of $\pm 3\%$. The average values for ϕ_1 , ϕ_2 and ϕ_3 from this work are then 0.93 ± 0.02 , 0.057 ± 0.024 and 0.009 ± 0.001 , respectively. When compared with the values obtained for C_2H_5SH , ϕ_1 is slightly lower and ϕ_2 is higher, while ϕ_3 is almost the same, within experimental error. The similar ϕ -values are due to the same (S-H) and (C-S) bond energies for both C_2H_5SH and $i-C_3H_7SH$.

5.2.3 Hydrogen Atom Reactions with Isopropanethiol: Quantum Yields of H_2 and H_2S

As discussed in Chapter 4, the variations of the H_2 and H_2S yields with pressure and temperature shed light on the relative rates of the hot and thermalized H-atom reactions with $i-C_3H_7SH$:



The variations of the ratio $[\phi(H_2) - \delta]/[\phi(H_2S) - \phi_3]$ with $n-C_4H_{10}$ pressure and temperature are tabulated in Table 5.11 and are plotted in Figure 5.11. The resulting trends are observed to be the same as those for the H-atom reactions.

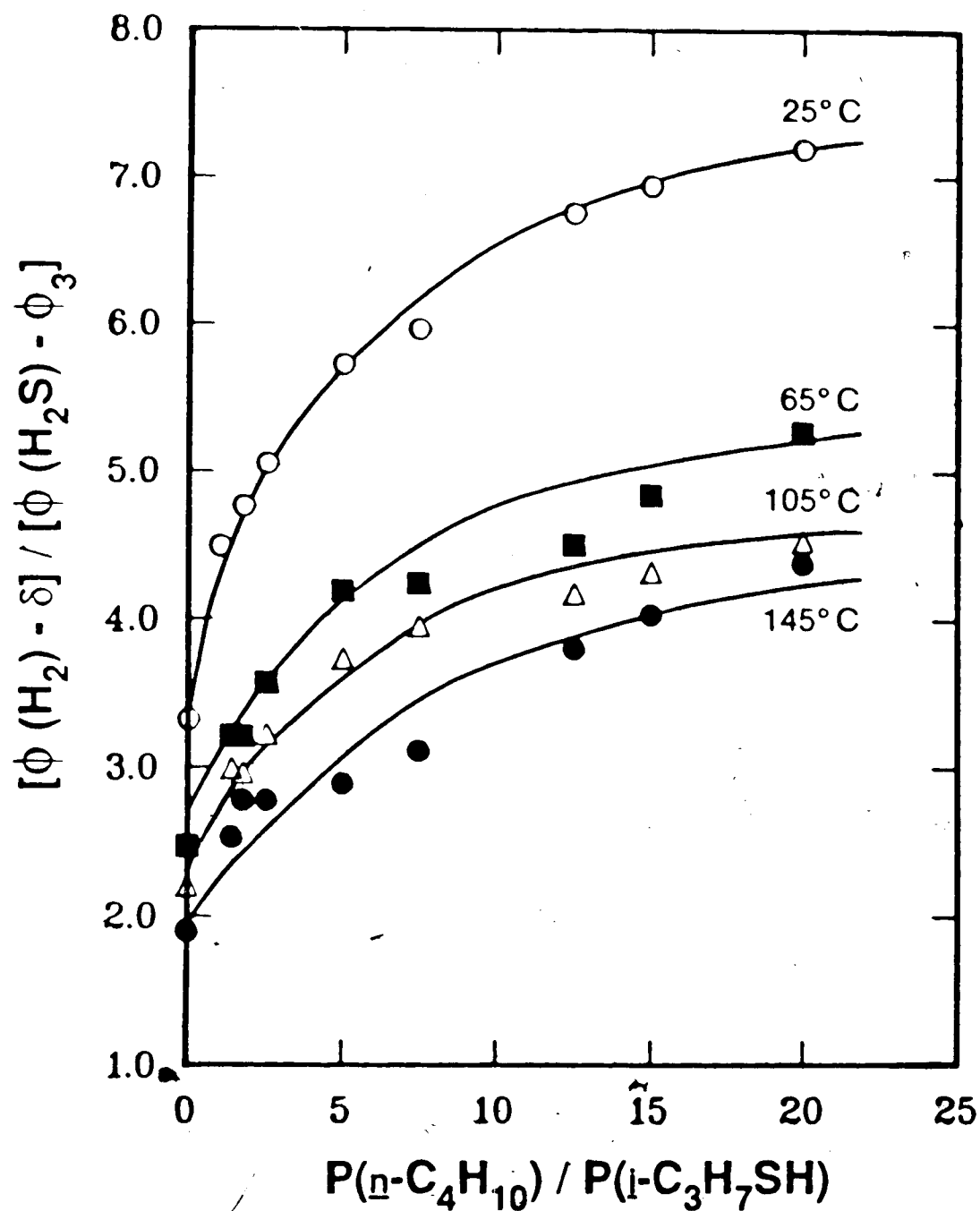
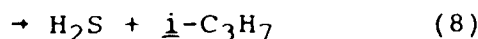


Figure 5.8. Plots of $[\phi(\text{H}_2) - \delta] / [\phi(\text{H}_2\text{S}) - \phi_3]$ as a function of the ratio $P(\text{n-C}_4\text{H}_{10}) / P(\text{i-C}_3\text{H}_7\text{SH})$.

with C_2H_5SH . It is found that at each temperature $[\phi(H_2) - \delta]/[\phi(H_2S) - \phi_3]$ increases with increasing thermalizer pressure, indicating that thermalization of the H atoms favours the H-abstraction reaction, *i.e.* the displacement reaction (8) has a higher activation energy than the H-abstraction reaction (7). Also, $[\phi(H_2) - \delta]/[\phi(H_2S) - \phi_3]$ decreases with increasing temperature, indicating that the rate of the displacement reaction increases faster than the H-abstraction reaction at higher temperatures, as expected.

5.2.4 Relative Rate Parameters for the H-atom Reactions: Quantum Yields of H_2 and C_3H_8

The relative rate parameters for the thermalized H-atom reactions



are determined from the H_2 and C_3H_8 yields. The quantum yield expressions for H_2 and C_3H_8 , given by Equations [2] and [3], respectively, are identical to those formulated for H_2 and C_2H_6 in the photolysis of C_2H_5SH . Thus, the kinetic treatment is carried out in the same manner, as described below.

The plots of $\phi(H_2)$ and $\phi(C_3H_8)$ against inverse $n\text{-}C_4H_{10}$ concentration at each temperature are shown in Figures 5.9 and 5.10. The trends observed in these plots can be correlated with the pressure-dependent terms in Equations [2] and [3],

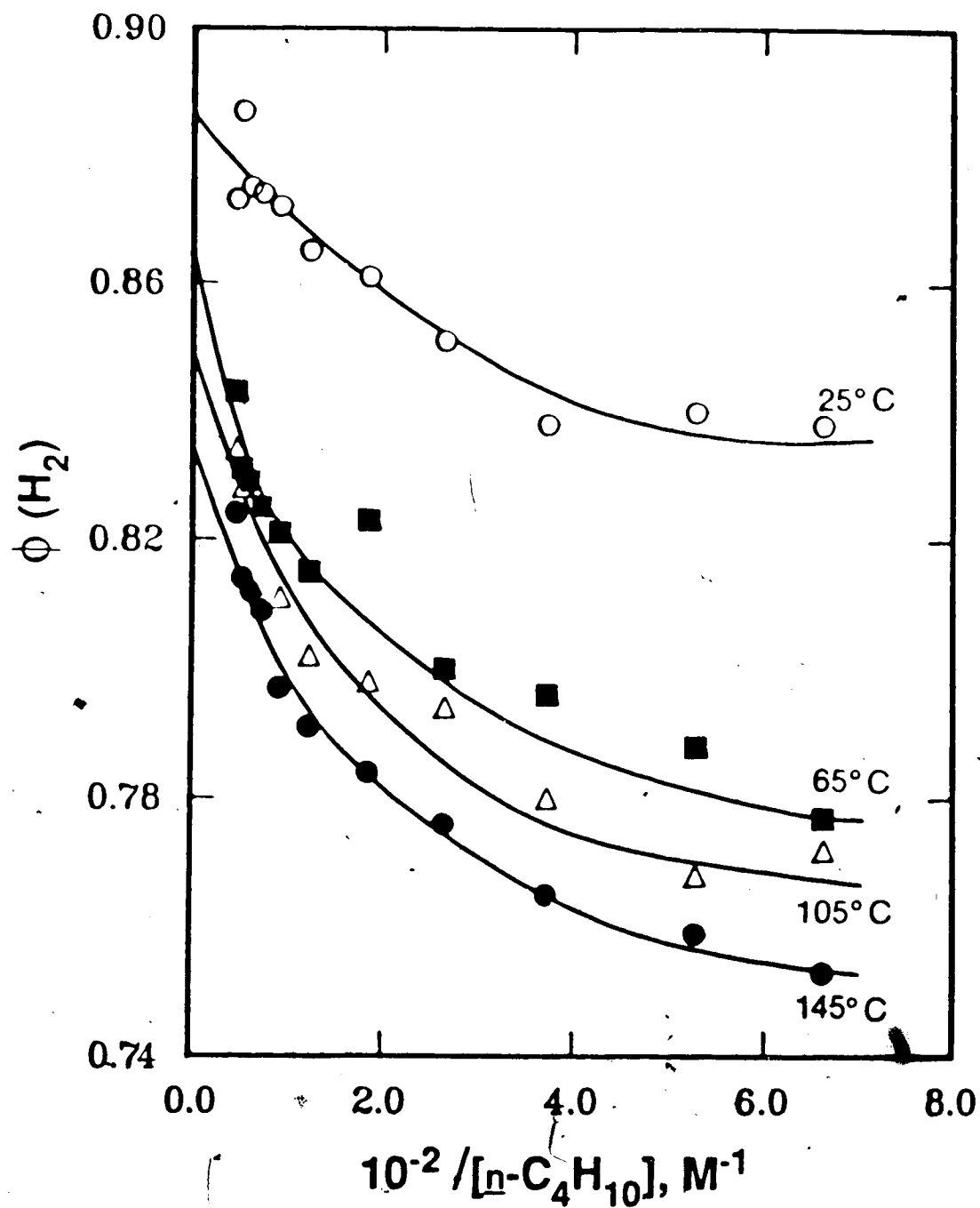


Figure 5.9. Plots of $\phi(\text{H}_2)$ as a function of the reciprocal of $n\text{-C}_4\text{H}_{10}$ concentration at $[i\text{-C}_3\text{H}_7\text{SH}] = 1.04 \times 10^{-3} \text{ M}$.

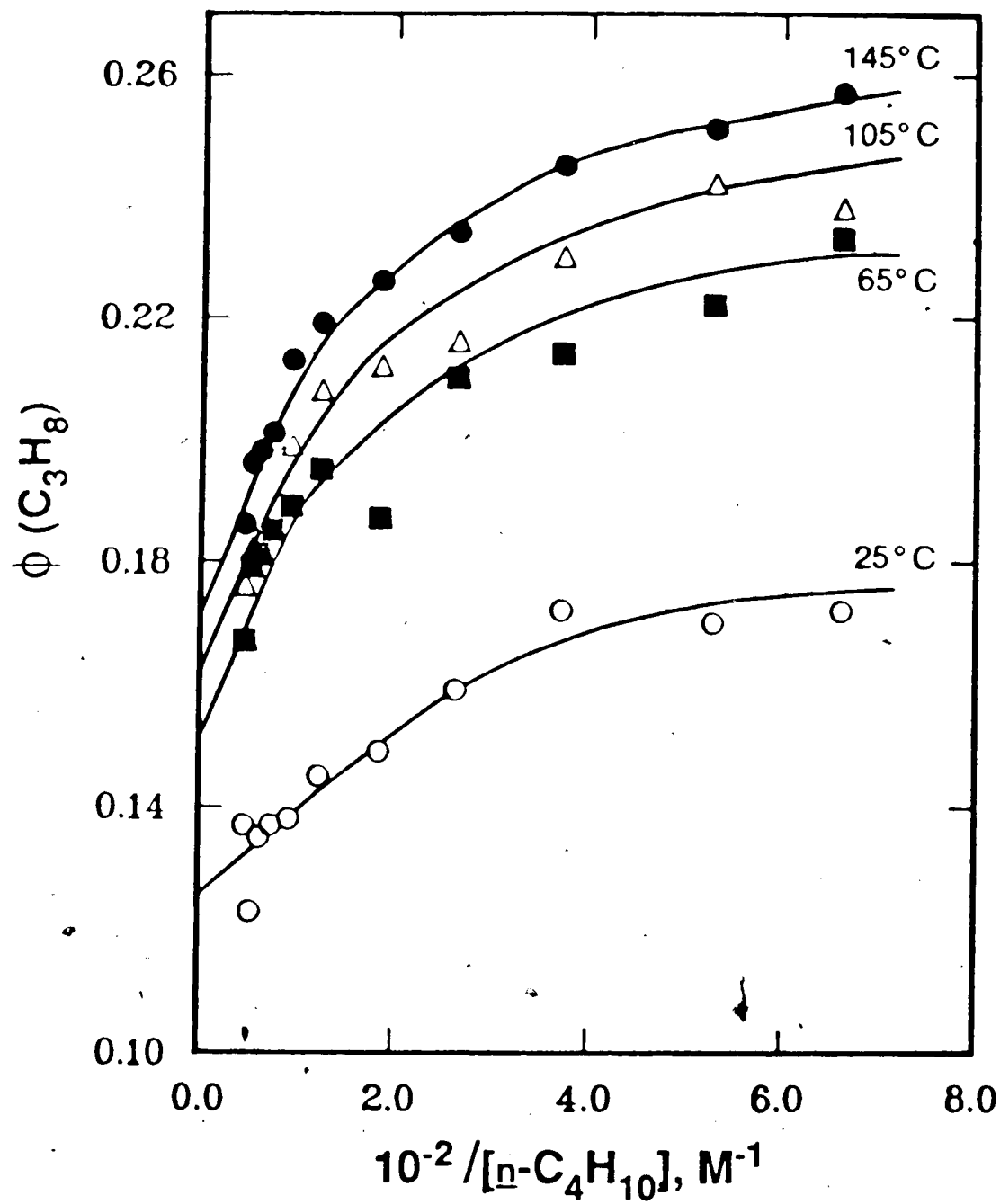


Figure 5.10. Plots of $\phi(C_3H_8)$ as a function of the reciprocal of $n-C_4H_{10}$ concentration at $[i-C_3H_7SH] = 1.04 \times 10^{-3} M$.

$$\frac{(k_7 k_8^* - k_7^* k_8) \phi_1 [i]}{(k_7 + k_8) ((k_7^* + k_8^*) [i] + k_9^* [M])} \quad \text{and}$$

$$\frac{k_4^* k_7 \phi_2}{(k_7 + k_8) (k_4^* + k_5^* [i] + k_6^* [M])}$$

When $[n\text{-C}_4\text{H}_{10}]$ is large, deactivation of hot radicals by $i\text{-C}_3\text{H}_7\text{SH}$ can be neglected and $k_9^* [M]$ and $k_6^* [M]$ become $k_{9n}^* [n]$ and $k_{6n}^* [n]$, respectively. Also, for the condition $P_n \gg P_i$, the terms $((k_7^* + k_8^*) [i])$ and $(k_4^* + k_5^* [i])$ may be neglected from the pressure-dependent terms. After substituting for $k_9^* [M]$ and $k_6^* [M]$ and rearranging, the resulting linear relations are obtained for the high $n\text{-C}_4\text{H}_{10}$ pressure condition;

$$\phi(\text{H}_2) = \frac{k_7 \phi_1}{(k_7 + k_8)} - \frac{(k_7 k_8^* - k_7^* k_8) k_{6n}^* \phi_1 [i] - k_4^* k_7 k_{9n}^* \phi_2}{(k_7 + k_8) k_{6n}^* k_{9n}^* [n]} \quad [9]$$

$$\phi(\text{C}_3\text{H}_8) = \frac{k_8 \phi_1}{(k_7 + k_8)} + \phi_2 + \frac{(k_7 k_8^* - k_7^* k_8) k_{6n}^* \phi_1 [i] - k_4^* k_7 k_{9n}^* \phi_2}{(k_7 + k_8) k_{6n}^* k_{9n}^* [n]} \quad [10]$$

The linear behaviour of $\phi(\text{H}_2)$ and $\phi(\text{C}_3\text{H}_8)$ at high $n\text{-C}_4\text{H}_{10}$ pressures is illustrated in Figures 5.9 and 5.10 for $P_n > 100$ Torr, or $[n\text{-C}_4\text{H}_{10}]^{-1} < 0.02 \text{ M}^{-1}$. The intercepts of the linear portions of these plots are listed in Table 5.12 and are defined by [9] and [10] to be,

$$\phi(\text{H}_2, P_n \rightarrow \infty) = \frac{k_7 \phi_1}{k_7 + k_8} \quad [11]$$

$$\phi(\text{C}_3\text{H}_8, P_n \rightarrow \infty) = \frac{k_8 \phi_1}{k_7 + k_8} + \phi_2 \quad [12]$$

From the intercepts and the derived values of ϕ_1 and ϕ_2

Table 5.12. Intercepts of the Plots in Figures 5.9 and 5.10a

Temperature (°C)	P(\bar{n} -C ₃ H ₇ SH) (Torr)	Intercepts	
		H ₂	C ₃ H ₈
25	20.0	0.884 ±0.003	0.125 ±0.003
65	22.7	0.866 ±0.007	0.144 ±0.007
105	24.7	0.852 ±0.005	0.158 ±0.005
145	28.1	0.838 ±0.005	0.172 ±0.005

a linear region from $[\bar{n}\text{-C}_4\text{H}_{10}]^{-1} < 0.02 \text{ M}^{-1}$ or $P(\bar{n}\text{-C}_4\text{H}_{10}) > 100 \text{ Torr}$

(Table 5.10), the rate constant ratio, k_7/k_8 , may be calculated at each temperature. Their values are listed in Table 5.13, along with another set of values for k_7/k_8 which were derived directly from the experimental H_2 and C_3H_8 yields at high total pressures (Table 5.7). It is observed that the latter set of k_7/k_8 values are lower than the former. This difference may be due to the fact that the experimental H_2 and C_3H_8 values have not yet reached the true limiting yields.

The Arrhenius plot for the thermalized H-atom reactions (7) and (8), shown in Figure 5.11, is constructed using the kinetically derived values of k_7/k_8 . The Arrhenius expression is given by,

$$\ln k_7/k_8 = (0.35 \pm 0.10) + (770 \pm 40)/T \quad [13]$$

From Equation [13], the activation energy difference, $(E_7 - E_8) = -1.53 \pm 0.07 \text{ kcal mol}^{-1}$, is slightly higher than that obtained for the H-atom reactions with C_2H_5SH , where $(E_7 - E_8) = -1.31 \pm 0.03 \text{ kcal mol}^{-1}$. The ratio of the pre-exponential factors, A_7/A_8 , is also derived from [13] to be 1.43 ± 0.06 . Absolute rate parameters for k_7 and k_8 cannot be derived at this time due to the lack of available data in the literature. However, since the (S-H) bond strengths in C_2H_5SH and $i-C_3H_7SH$ are the same, the k_7 expression for $i-C_3H_7SH$ should be the same as, or close to the one derived for C_2H_5SH in Chapter 4:

$$k_7 \text{ (cm}^3 \text{ mol}^{-1} \text{ s}^{-1}\text{)} \\ = (4.0 \pm 0.7) \times 10^{12} \exp [(-1070 \pm 40)/RT] \quad [14]$$

Table 5.13. Temperature Dependence of k_7/k_8

Temperature (°C)	$(k_7/k_8)^a$	$(k_7/k_8)^b$	Average
25	19 ± 4 ^c	17 ± 2	18 ± 5
65	14 ± 3	9.7 ± 0.9	12 ± 3
105	11 ± 3	8.7 ± 0.4	10 ± 3
145	9 ± 3	7.8 ± 0.5	8 ± 3

^a calculated from ϕ intercept values in Table 5.12

^b calculated from experimental $\phi(H_2)$ and $\phi(C_3H_8)$ yields at high

^c $n-C_4H_{10}$ pressures

^d standard error

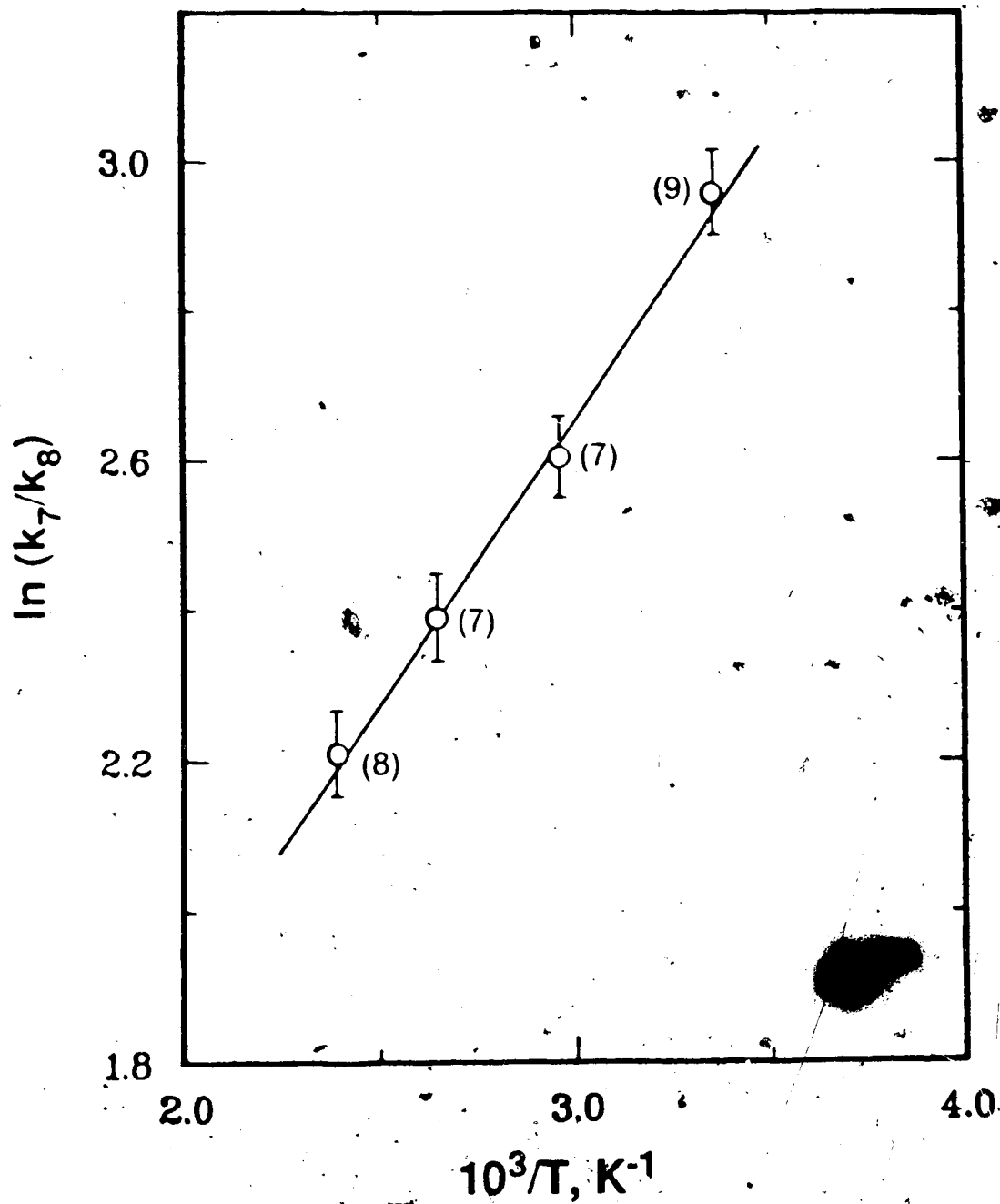
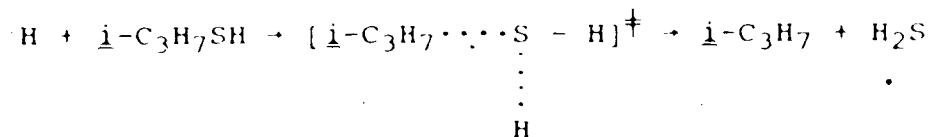


Figure 5.11. Plot of $\ln k_7/k_8$ versus the reciprocal of temperature. Figure in bracket indicates number of experiments.

From this, the k_8 expression for $i\text{-C}_3\text{H}_7\text{SH}$ is then determined to be:

$$k_8 \text{ (cm}^3 \text{ mol}^{-1} \text{ s}^{-1}\text{)} \\ = (2.8 \pm 0.6) \times 10^{12} \exp \{(-2600 \pm 100)/RT\} \quad [15]$$

The experimental entropy of activation, ΔS^\ddagger , calculated from the A factor of (8) is -27.6 eu. for the standard state of 1 atm. Using Benson's method¹⁴¹ for a transition state which involves an initial interaction between the H atom and the non-bonding 3p orbital of the sulfur atom:



we will obtain:

$$\begin{aligned} \Delta S^\ddagger &= S_0^\ddagger - S_0(i\text{-C}_3\text{H}_7\text{SH}) - S_0(\text{H}) \\ &= S_0(i\text{-C}_3\text{H}_7\text{SH}) + R \ln 2 + x - S_0(i\text{-C}_3\text{H}_7\text{SH}) - S_0(\text{H}) \\ &= 1.4 + x - 27.4 = -26.0 \\ x &= -1.6 \text{ eu.} \end{aligned}$$

This low value for the vibrational contribution to ΔS^\ddagger indicates a very tight structure for the activated complex.

In the photolysis of pure $i\text{-C}_3\text{H}_7\text{SH}$, i.e. $P_n = 0$, the resulting expressions for H_2 and C_3H_8 yields a simplified from [2] and [3] as follows;

$$\begin{aligned} \phi(\text{H}_2) &= \frac{k_7 \phi_1}{k_7 + k_8} - \frac{(k_7 k_8^* - k_7^* k_8) \phi_1}{(k_7 + k_8)(k_7^* + k_8^* + k_{9i}^*)} \\ &+ \frac{k_7 \phi_2}{(k_7 + k_8)(1 + \alpha P_i)} \end{aligned} \quad [16]$$

$$\phi(\text{C}_3\text{H}_8) = \frac{k_8 \phi_1}{k_7 + k_8} + \phi_2 + \frac{(k_7 k_8^* - k_7^* k_8) \phi_1}{(k_7 + k_8)(k_7^* + k_8^* + k_{9j}^*)} + \frac{k_7 \phi_2}{(k_7 + k_8)(1 + \alpha P_i)} \quad [17]$$

where α is the rate constant ratio, earlier derived to be $(k_5^* + k_{6j}^*)/k_4^* \approx 1.0 \times 10^{-3} \text{ Torr}^{-1}$. The last term in both of the H_2 and C_3H_8 expressions indicates that $\phi(\text{H}_2, P_n = 0)$ and $\phi(\text{C}_3\text{H}_8, P_n = 0)$ are inverse functions of P_i . However, the predicted pressure dependence is not apparent in Figure 5.1 and $\phi(\text{H}_2)$ and $\phi(\text{C}_3\text{H}_8)$ are approximately constant at 0.80 ± 0.01 and 0.21 ± 0.01 , at 25°C , in the $i\text{-C}_3\text{H}_7\text{SH}$ pressure range 5 - 50 Torr. Thus, the magnitudes of any changes in the pressure term in [16] and [17] is likely to be relatively small and should fall within the range of the experimental error. This prediction is again verified by evaluating the pressure term using the already derived values of ϕ_2 , g and k_7/k_8 . As shown in Table 5.14, this pressure term decreases with increasing $i\text{-C}_3\text{H}_7\text{SH}$ pressure, and the net change is indeed small, being only 0.002 on going from 5 to 50 Torr. Therefore, increasing the $i\text{-C}_3\text{H}_7\text{SH}$ pressure has negligible effects on $\phi(\text{H}_2)$ and $\phi(\text{C}_3\text{H}_8)$, and the pressure terms in [16] and [17] can be considered to be constant.

5.2.5 Disproportionation-Combination of Thiyl Radicals:

Quantum Yield of $(i\text{-C}_3\text{H}_7)_2\text{S}_2$

The quantum yield expression for the formation of $(i\text{-C}_3\text{H}_7)_2\text{S}_2$,

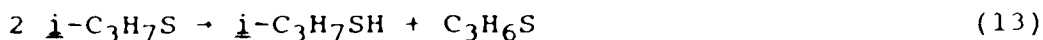
Table 5.14. Derived Values of $\frac{k_7 \phi_2}{(k_7 + k_8)(1 + \alpha P_i)}$ a

P(i -C ₃ H ₇ SH) (Torr)	$\frac{k_7 \phi_2}{(k_7 + k_8)(1 + \alpha P_i)}$
5	0.0540
10	0.0537
20	0.0532
30	0.0527
40	0.0521
50	0.0516

$a_T = 25^\circ\text{C}$, $k_7/k_8 = 18$, $\phi_2 = 0.043$, $\alpha = 1.0 \times 10^{-3} \text{ Torr}^{-1}$

$$\phi[(i-C_3H_7)_2S_2] = \frac{k_{12} \phi_1}{k_{12} + k_{13}} \quad [5]$$

predicts that $\phi[(i-C_3H_7)_2S_2]$ and ϕ_1 are equal to each other if no disproportionation of $i-C_3H_7S$ radicals occurs,



However, the observation that $\phi[(i-C_3H_7)_2S_2]$ is less than ϕ_1 indicates that Reaction (13) occurs in competition with the combination reaction,



The products of disproportionation are the thiol substrate, $i-C_3H_7SH$, and the aliphatic thioketone, thioacetone. The latter is known to be unstable, although it can be isolated in the monomeric thione form as well as in the tautomeric enethiol form.¹⁸⁴ Since, however, $\phi[(i-C_3H_7)_2S_2]$ is only slightly less than $\phi(H_2)$, the disproportionation of $i-C_3H_7S$ radicals should be a relatively minor reaction, in comparison with the combination reaction.

Equation [5] predicts no pressure dependence for $(i-C_3H_7)_2S_2$. This is verified by the $\phi[(i-C_3H_7)_2S_2]$ values obtained both in the absence and presence of $n-C_4H_{10}$ (see Tables 5.3 to 5.6). The disproportionation-combination ratio, k_{13}/k_{12} , is derived from [5] to be:

$$\frac{k_{13}}{k_{12}} = \frac{\phi_1}{\phi[(i-C_3H_7)_2S_2]} - 1 \quad [18]$$

Their values, calculated from Tables 5.3 to 5.7, are listed in Table 5.15 and increase with temperature. However, this increase must be viewed with caution since large errors are

Table 5.15. Temperature Dependence of k_{13}/k_{12}

Temperature (°C)	$(k_{13}/k_{12})^a$	$(k_{13}/k_{12})^b$
25	0.15 ±0.09	0.05 ±0.05
65	0.05 ±0.05	0.06 ±0.05
105	0.11 ±0.09	0.12 ±0.04
145	0.16 ±0.06	0.15 ±0.06

^acalculated from the photolysis of pure i -C₃H₇SH
^bcalculated from the photolysis of i -C₃H₇SH with added
 D-C₄H₁₀ at the high pressure limit

associated with the calculated k_{13}/k_{12} values due to the scatter in the measured yields of $(i-C_3H_7)_2S_2$. The Arrhenius plot, Figure 5.12, is constructed using the high pressure values of the disproportionation-combination steps (13) and (12), respectively. The following rate expression is derived:

$$\ln k_{13}/k_{12} = (1.3 \pm 0.7) - (1300 \pm 300)/T \quad [19]$$

from which $(E_{13} - E_{12}) = 2.7 \pm 0.5 \text{ kcal mol}^{-1}$ and $A_{13}/A_{12} = 3.6 \pm 1.1$. Since the recombination step (12) requires negligible activation energy, E_{13} is therefore estimated to be $-2.7 \text{ kcal mol}^{-1}$ and is smaller than that determined for the disproportionation of C_2H_5S radicals, $3.1 \text{ kcal mol}^{-1}$.

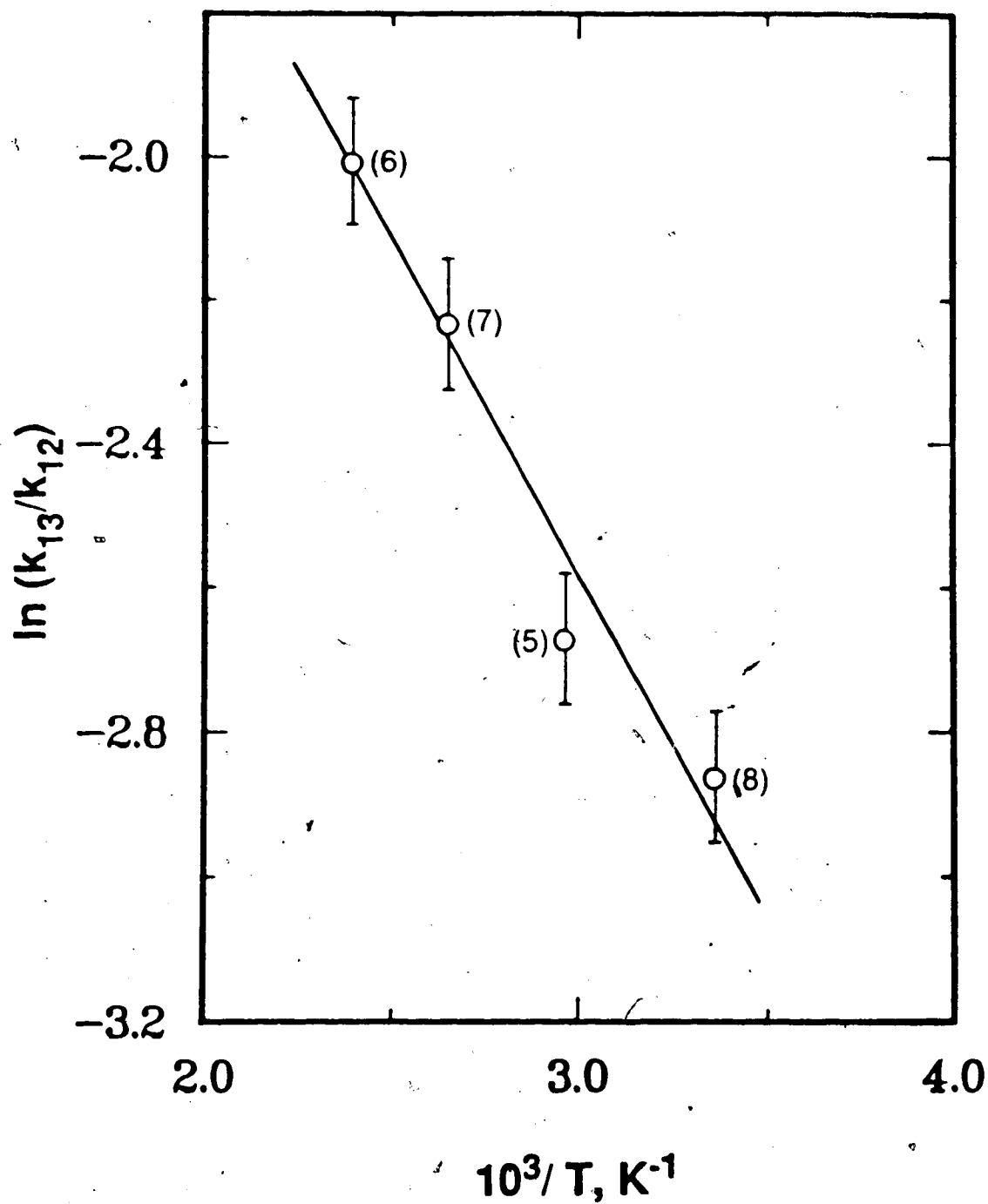


Figure 5.12. Plot of $\ln k_{13}/k_{12}$ versus the reciprocal of temperature. Figure in bracket indicates number of experiments.

CHAPTER SIX

PHOTOLYSIS OF, AND THE REACTIONS OF HYDROGEN ATOMS WITH, t-BUTANETHIOL

6.1 Results

The recorded gas-phase UV absorption spectrum of t-C₄H₉SH is similar to that found in the literature³⁶ and also to that obtained for C₂H₅SH and i-C₃H₇SH. The maximum absorbance is located near 230 nm. At 298K, the extinction coefficient at 254 nm is $4.48 \times 10^{-3} \text{ Torr}^{-1} \text{ cm}^{-1}$, corrected for background reflection by the quartz cell.

The products of the photolysis are H₂, i-C₄H₁₀, H₂S, i-C₄H₈ and (t-C₄H₉)₂S₂. The overall conversion was low, $\leq 5\%$, in order to minimize secondary absorption by H₂S and (t-C₄H₉)₂S₂. Thus, no less than 95% of the incident light was absorbed by t-C₄H₉SH.

6.1.1 H₂S Actinometry

The actinometric set-up as described in Chapters 4 and 5 was used to determine the intensity of light absorbed in the reaction vessel, I_a, from that in the actinometric vessel, I_b. The values of the extinction coefficients for H₂S and t-C₄H₉SH were calculated from the experimental measurements of S₀, S₆ and w_i's. At 254 nm, $\epsilon(\text{H}_2\text{S})$ was found to be $0.99 \times 10^{-4} \text{ Torr}^{-1} \text{ cm}^{-1}$, and $\epsilon(\text{t-C}_4\text{H}_9\text{SH})$, $4.50 \times 10^{-3} \text{ Torr}^{-1} \text{ cm}^{-1}$, in accordance with literature^{63,142} values.

From the results of actinometric runs which are summarized in Table 6.1, the average value for [R(H₂) +

Table 6.1. The Results of Chemical Actinometry in the Photolysis of $t\text{-C}_4\text{H}_9\text{SH}^a$

P($t\text{-C}_4\text{H}_9\text{SH}$) (Torr)	I_a		$R(\text{H}_2) + R(i\text{-C}_4\text{H}_{10})$ (10^{-2} $\mu\text{moles min}^{-1}$)	$R(\text{H}_2) + R(i\text{-C}_4\text{H}_{10})$ I_a
	I_a	$R(\text{H}_2) + R(i\text{-C}_4\text{H}_{10})$		
10	4.99	4.73	0.948	
10	4.49	4.25	0.947	
15	7.00	6.40	0.914	
20	8.34	7.91	0.948	
20	6.68	6.78	1.01	
25	7.68	8.27	1.08	
25	7.33	7.19	0.981	
30	8.61	9.41	1.09	
30	7.50	7.53	1.00	
40	7.86	8.53	1.09	
40	8.89	8.76	0.985	
45	8.33	8.76	1.05	
45	9.28	8.97	0.967	
Average = 1.00 ± 0.06				

 $t=25^\circ\text{C}$; photolysis time=60 min

$R(\underline{i}\text{-C}_4\text{H}_{10})/I_a$ was found to be 1.00 ± 0.06 . From this, the absorbed light intensity in the reaction vessel, I_a , is equal to $[R(\text{H}_2) + R(\underline{i}\text{-C}_4\text{H}_{10})]$. All the quantum yields reported in the photolysis of $\underline{t}\text{-C}_4\text{H}_9\text{SH}$ were calculated by the relation $\phi_i = R_i/I_a$, where R_i [$i = \text{H}_2, \underline{i}\text{-C}_4\text{H}_{10}, \text{H}_2\text{S}, \underline{i}\text{-C}_4\text{H}_8$ and $(\underline{t}\text{-C}_4\text{H}_9)_2\text{S}_2$] is the rate of product formation and $I_a = [R(\text{H}_2) + R(\underline{i}\text{-C}_4\text{H}_{10})]$, as determined from actinometric experiments.

6.1.2 Photolysis of Pure \underline{t} -Butanethiol

Photolysis of pure $\underline{t}\text{-C}_4\text{H}_9\text{SH}$ yields H_2 and $(\underline{t}\text{-C}_4\text{H}_9)_2\text{S}_2$ as major products, with small amounts of $\underline{i}\text{-C}_4\text{H}_{10}$, H_2S and $\underline{i}\text{-C}_4\text{H}_8$. The dark reaction runs at 25°C and 140°C did not produce any measurable products, indicating that $\underline{t}\text{-C}_4\text{H}_9\text{SH}$ is thermally stable within this temperature range. This agrees with the work of Martin and Barroeta⁹¹ who found that $\underline{t}\text{-C}_4\text{H}_9\text{SH}$ is extremely stable at a higher temperature of 323°C . It was observed that reaction times up to 120 minutes did not affect the quantum yields and that these seem to be independent of $\underline{t}\text{-C}_4\text{H}_9\text{SH}$ pressure in the range 10-50 Torr. The product quantum yields are tabulated in Table 6.2 and are plotted against $\underline{t}\text{-C}_4\text{H}_9\text{SH}$ pressure in Figure 6.1. The points for $\phi(\text{H}_2)$, $\phi(\underline{i}\text{-C}_4\text{H}_{10})$, $\phi(\text{H}_2\text{S})$, $\phi(\underline{i}\text{-C}_4\text{H}_8)$ and $\phi[(\underline{t}\text{-C}_4\text{H}_9)_2\text{S}_2]$ were averaged separately over the entire pressure range studied and found to be 0.61 ± 0.03 , 0.39 ± 0.02 , 0.37 ± 0.03 , 0.069 ± 0.006 and 0.68 ± 0.06 , respectively, at 25°C .

Table 6.2. Product Quantum Yields in the Photolysis of Pure $t\text{-C}_4\text{H}_9\text{SH}^a$

$P(t\text{-C}_4\text{H}_9\text{SH})$ (Torr)	$[R(\text{H}_2) + R(i\text{-C}_4\text{H}_{10})]$ (10^{-2} $\mu\text{moles min}^{-1}$)	$\phi(\text{H}_2)$ (± 0.03)	$\phi(i\text{-C}_4\text{H}_{10})$ (± 0.02)	$\phi(\text{H}_2\text{S})$ (± 0.03)	$\phi(i\text{-C}_4\text{H}_8)$ (± 0.006)	$\phi[(t\text{-C}_4\text{H}_9)_2\text{S}_2]$ (± 0.06)
10	4.9 ± 0.5^b (7) ^c	0.613	0.387	0.355	0.0767	0.716
15	6.5 ± 0.2 (2)	0.608	0.392	0.360	0.0737	0.654
20	7.8 ± 0.6 (5)	0.615	0.385	0.347	0.0706	0.683
25	7.7 ± 0.8 (2)	0.604	0.396	0.359	0.0708	0.658
30	9.7 ± 0.7 (3)	0.609	0.391	0.367	0.0677	0.711
35	10.9 ± 0.5 (3)	0.603	0.397	0.383	0.0667	0.697
40	11.3 ± 1.0 (4)	0.610	0.390	0.383	0.0655	0.658
45	11.9 ± 1.4 (3)	0.598	0.402	0.368	0.0647	0.650
50	12.6 (1)	0.600	0.400	0.401	0.0635	0.676
Average		0.61 ± 0.03	0.39 ± 0.02	0.37 ± 0.03	0.069 ± 0.006	0.68 ± 0.06

^a $T = 25^\circ\text{C}$; photolysis time = 60 min; $I_a = [R(\text{H}_2) + R(i\text{-C}_4\text{H}_{10})]$

^bstandard error

^cnumber of experiments

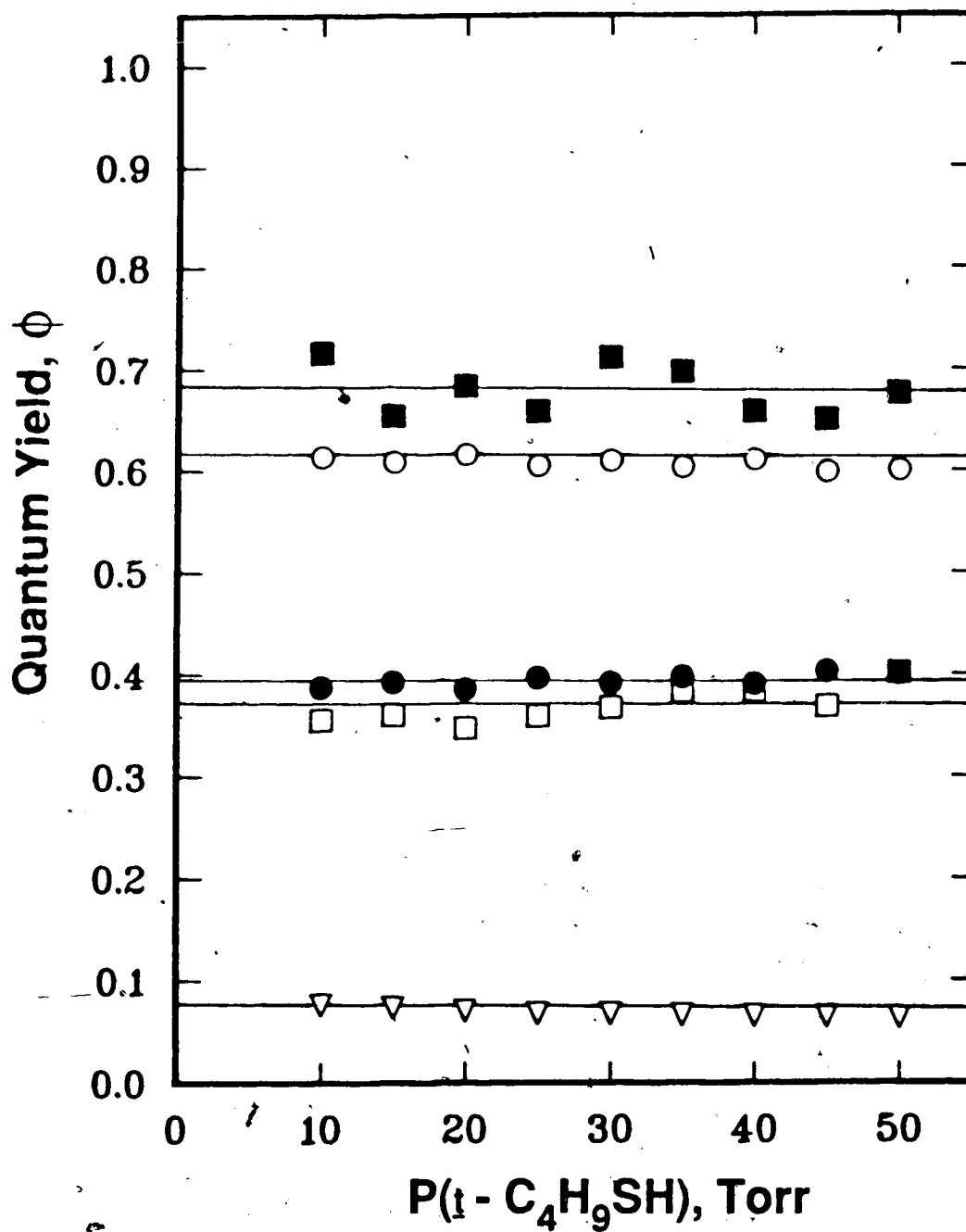


Figure 6.1. Product quantum yields versus $t\text{-C}_4\text{H}_9\text{SH}$ pressure.

■, $[(t\text{-C}_4\text{H}_9)_2\text{S}_2]$; ○, (H_2) ; □, (H_2S) ;

●, $(i\text{-C}_4\text{H}_{10})$; ▽, $(i\text{-C}_4\text{H}_8)$.

6.1.3 Photolysis of t-Butanethiol with Added Thermalized, C_2H_6

Photolysis of 20 Torr t- C_4H_9SH with added thermalizer, 28 - 400 Torr C_2H_6 , was carried out in the next set of experiments. The variation of product yields with increasing thermalizer pressure is tabulated in Table 6.3 and also plotted in Figure 6.2. With increasing C_2H_6 pressure, $\phi(H_2)$ increases while $\phi(i-C_4H_{10})$, $\phi(H_2S)$ and $\phi(i-C_4H_8)$ decrease, all reaching limiting values at about a fifteenfold increase of C_2H_6 pressures over that of the substrate, which is at a C_2H_6 pressure of ≥ 250 Torr. $\phi[(t-C_4H_9)_2S_2]$ appears to be unaffected by thermalizer pressure. It was also observed that the increase in $\phi(H_2)$ compensated for the decrease in $\phi(i-C_4H_{10})$, and that $\phi(H_2S)$ seemed to be lower than $\phi(i-C_4H_{10})$. On the other hand, the absorbed light intensity, $I_a = [R(H_2) + R(i-C_4H_{10})]$, was invariant with thermalizer pressure, as shown in Table 6.3 by the constant value of $(7.8 \pm 0.3) \times 10^{-2} \mu\text{moles min}^{-1}$, obtained for $[R(H_2) + R(i-C_4H_{10})]$.

6.1.4 Effect of Temperature on Product Yields

Photolysis of t- C_4H_9SH with added thermalizer, C_2H_6 , was carried out at higher temperatures, 65°C, 95°C and 140°C. Different product quantum yields were observed with increasing temperature. However, the variation of these yields with increasing C_2H_6 pressure at each temperature was the same as that observed at 25°C. The product quantum yields obtained as a function of C_2H_6 pressure are

Table 6.3. Product Quantum Yields in the Photolysis of $t\text{-C}_4\text{H}_9\text{SH}$

with Added Thermalizer, C_2H_6 , $T = 25^\circ\text{C}$

P(C_2H_6) (Torr)	$[\text{R}(\text{H}_2) + \text{R}(\underline{i}\text{-C}_4\text{H}_{10})]$ ^b (10^{-2} $\mu\text{moles min}^{-1}$) (± 0.2) ^c	$\phi(\text{H}_2)$ (± 0.03)	$\phi(\underline{i}\text{-C}_4\text{H}_{10})$ (± 0.02)	$\phi(\text{H}_2\text{S})$ (± 0.03)	$\phi(\underline{i}\text{-C}_4\text{H}_8)$ (± 0.006)	$\phi(\underline{i}\text{-C}_4\text{H}_9)$ (± 0.06)	$\phi(\underline{i}\text{-C}_4\text{H}_9)_2\text{S}_2$ ^d (± 0.06)
0	7.8 ^d	0.61	0.39	0.37	0.070	0.58	
28	7.6 (2) ^e	0.628	0.372	0.355	0.0502	0.555	
35	7.7 (2)	0.632	0.368	0.317	0.0473	0.522	
50	8.3 (4)	0.634	0.366	0.353	0.0403	0.556	
70	7.7 (2)	0.637	0.363	0.315	0.0352	0.564	
100	8.5 (4)	0.649	0.351	0.323	0.0300	0.580	
150	7.8 (3)	0.651	0.349	0.282	0.0245	0.667	
200	7.5 (4)	0.660	0.340	0.282	0.0215	0.728	
250	7.2 (4)	0.662	0.338	0.262	0.0202	0.666	
300	7.2 (7)	0.666	0.334	0.270	0.0215	0.683	
400	7.3 (5)	0.672	0.328	0.252	0.0210	0.692	

^ap($\underline{i}\text{-C}_4\text{H}_9\text{SH}$) = 20.0 Torr; T = 25°C; photolysis time = 60 min; $I_a = (\text{R}(\text{H}_2) + \text{R}(\underline{i}\text{-C}_4\text{H}_{10}))$

^baverage $[\text{R}(\text{H}_2) + \text{R}(\underline{i}\text{-C}_4\text{H}_{10})] = (7.8 \pm 0.3) \times 10^{-2} \mu\text{moles min}^{-1}$

^cstandard error

^dsee results from Table 6.2

^enumber of experiments

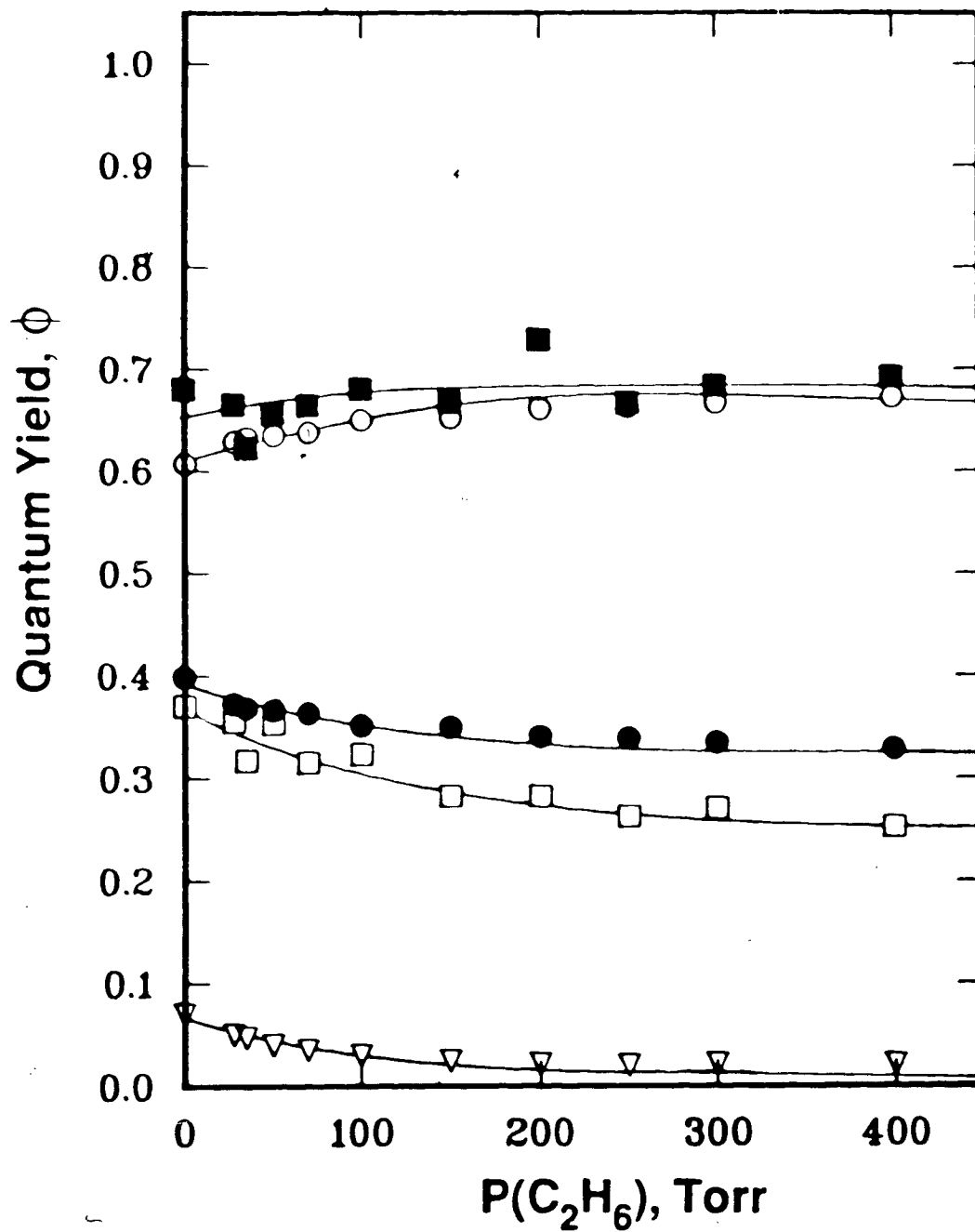


Figure 6.2. Product quantum yields versus C_2H_6 pressure at constant $i\text{-C}_4\text{H}_9\text{SH}$ pressure of 20.0 Torr.

\blacksquare , $[(t\text{-C}_4\text{H}_9)_2\text{S}_2]$; \circ , (H_2) ; \square , (H_2S) ; \bullet , $(i\text{-C}_4\text{H}_{10})$;
 ∇ , $(i\text{-C}_4\text{H}_8)$.

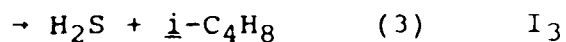
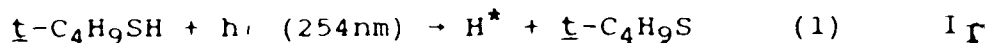
summarized in Tables 6.4 to 6.7, respectively. In all cases, as temperature increases from 25° to 140°C, $\phi(\text{H}_2)$ and $\phi[(\text{t-C}_4\text{H}_9)_2\text{S}_2]$ decrease while $\phi(\text{i-C}_4\text{H}_{10})$, $\phi(\text{H}_2\text{S})$ and $\phi(\text{i-C}_4\text{H}_8)$ increase, and the sum of $R(\text{H}_2)$ and $R(\text{i-C}_4\text{H}_{10})$ remains invariant.

6.2 Discussion

6.2.1 Reaction Mechanism

The nature of products arising from H_2 , alkane, H_2S , alkene and alkyldisulfide observed in the photolysis of $\text{t-C}_4\text{H}_9\text{SH}$ is quite similar to those from the photolyses of $\text{C}_2\text{H}_5\text{SH}$ and $\text{i-C}_3\text{H}_7\text{SH}$ (Chapters 4 and 5). This finding suggests that a reaction mechanism similar to that proposed in the previous Chapters may also be operative here as well. Thus, in order to account for the product formation in quantitative terms an analogous set of elementary reactions can be considered as in the previous cases.

The primary photochemical reactions are as follows:



The enthalpies of reaction for 1, 2 and 3 are 89, 66 - 69 and 17 kcal mol⁻¹, respectively, calculated from thermochemical data in Table 1.2. Although (3) is thermodynamically the most favourable reaction, its activation energy is much higher at 55 kcal mol⁻¹.⁸⁹ From the available photon energy at 254 nm, $E_0 = 113$ kcal Einstein⁻¹, the excess energy residing in the H atoms in step (1) is

Table 6.4. Product Quantum Yields in the Photolysis of $t\text{-C}_4\text{H}_9\text{SH}$

with Added Thermalizer, C_2H_6 ,^a $T = 65^\circ\text{C}$

P(C_2H_6) (Torr)	$[\text{R}(\text{H}_2) + \text{R}(\text{i-C}_4\text{H}_{10})]$ ^b (10^{-2} $\mu\text{moles min}^{-1}$) (± 0.2) ^c	$\phi(\text{H}_2)$ (± 0.03)	$\phi(\text{i-C}_4\text{H}_{10})$ (± 0.02)	$\phi(\text{H}_2\text{S})$ (± 0.03)	$\phi(\text{i-C}_4\text{H}_8)$ (± 0.006)	$\phi(\text{i-C}_4\text{H}_9)_2\text{S}_2$) (± 0.06)
0	8.0	0.609	0.401	0.380	0.0920	0.701
28.4	7.6	0.612	0.388	0.366	0.0655	0.649
58.0	8.1	0.616	0.384	0.353	0.0570	0.682
79.4	7.6	0.620	0.380	0.333	0.0519	0.702
115	8.1	0.626	0.374	0.336	0.0431	0.673
230	7.4	0.632	0.368	0.310	0.0404	0.656
340	7.6	0.634	0.368	0.273	0.0338	0.622
455	7.4	0.641	0.359	0.306	0.0282	0.640

^a $p(\text{i-C}_4\text{H}_9\text{SH}) = 22.7$ Torr or $[\text{i-C}_4\text{H}_9\text{SH}] = 1.04 \times 10^{-3}$ M; photolysis time = 60 min
^baverage $[\text{R}(\text{H}_2) + \text{R}(\text{i-C}_4\text{H}_{10})] = (7.7 \pm 0.5) \times 10^{-2}$ $\mu\text{moles min}^{-1}$; $I_a = [\text{R}(\text{H}_2) + \text{R}(\text{i-C}_4\text{H}_{10})]$
^cstandard error
^dnumber of experiments

Table 6.5. Product Quantum Yields in the Photolysis of t-C₄H₉SH

with Added Thermalizer, C₂H₆,^a T = 95°C

P(C ₂ H ₆) (Torr)	[R(H ₂)+R(<i>i</i> -C ₄ H ₁₀)] ^b (10 ⁻² μmoles min ⁻¹) (±0.2) ^c	φ(H ₂) (±0.03)	φ(<i>i</i> -C ₄ H ₁₀) (±0.02)	φ(H ₂ S) (±0.03)	φ(<i>i</i> -C ₄ H ₈) (±0.006)	φ[(<i>t</i> -C ₄ H ₉) ₂ S ₂] (±0.06)
0	7.9 (2) ^d	0.602	0.408	0.357	0.154	0.598
34.6	7.4 (2)	0.598	0.402	0.342	0.127	0.590
43.2	7.6 (2)	0.600	0.400	0.349	0.137	0.678
62.0	7.9 (2)	0.608	0.392	0.346	0.126	0.615
86.4	7.4 (2)	0.612	0.388	0.328	0.132	0.585
125	7.7 (3)	0.616	0.384	0.358	0.117	0.605
250	7.6 (3)	0.619	0.381	0.302	0.113	0.592
370	7.3 (4)	0.621	0.379	0.300	0.103	0.546
495	7.4 (3)	0.623	0.377	0.293	0.103	0.567

^ap(t-C₄H₉SH)=24.7 Torr or [t-C₄H₉SH]=1.04 × 10⁻³ M; photolysis time=60 min
^baverage [R(H₂)+R(*i*-C₄H₁₀)]=(7.6±0.6) × 10⁻² μmoles min⁻¹; I_a=[R(H₂)+R(*i*-C₄H₁₀)]
^cstandard error
^dnumber of experiments

Table 6.6. Product Quantum Yields in the Photolysis of $t\text{-C}_4\text{H}_9\text{SH}$.with Added Thermalizer, C_2H_6 , $T = 140^\circ\text{C}$

$\text{P}(\text{C}_2\text{H}_6)$ (Torr)	$[\text{R}(\text{H}_2) + \text{R}(\dot{\text{i}}\text{-C}_4\text{H}_{10})]$ ^b (10^{-2} $\mu\text{moles min}^{-1}$) (± 0.2) ^c	$\phi(\text{H}_2)$ (± 0.03)	$\phi(\dot{\text{i}}\text{-C}_4\text{H}_{10})$ (± 0.02)	$\phi(\text{H}_2\text{S})$ (± 0.03)	$\phi(\dot{\text{i}}\text{-C}_4\text{H}_8)$ (± 0.006)	$\phi[(\dot{\text{i}}\text{-C}_4\text{H}_9)_2\text{S}_2]$ (± 0.06)
0	8.1 (2) ^d	0.579	0.431	0.392	0.203	0.478
38.8	7.7 (2)	0.580	0.420	0.394	0.192	0.503
48.5	7.6 (2)	0.584	0.416	0.376	0.180	0.484
69.3	8.1 (2)	0.586	0.414	0.331	0.170	0.485
97.0	7.5 (2)	0.592	0.408	0.340	0.166	0.495
140	8.1 (2)	0.598	0.402	0.320	0.156	0.507
280	7.5 (3)	0.600	0.400	0.306	0.153	0.524
415	7.6 (2)	0.602	0.398	0.297	0.150	0.516
555	7.3 (3)	0.604	0.396	0.304	0.146	0.513

^a $\rho(t\text{-C}_4\text{H}_9\text{SH}) = 27.7$ Torr or $[\dot{\text{i}}\text{-C}_4\text{H}_9\text{SH}] = 1.04 \times 10^{-3}$ M; photolysis time = 60 min
^baverage $[\text{R}(\text{H}_2) + \text{R}(\dot{\text{i}}\text{-C}_4\text{H}_{10})] = (7.7 \pm 0.6) \times 10^{-2}$ $\mu\text{moles min}^{-1}$; $I_a = [\text{R}(\text{H}_2) + \text{R}(\dot{\text{i}}\text{-C}_4\text{H}_{10})]$
^cstandard error
^dnumber of experiments

Table 6.7. Effect of Temperature on Product Quantum Yields^aat High C₂H₆ Pressure Limits^b

Temperature (°C)	$[R(H_2) + R(i-C_4H_{10})]^c$ (10^{-2} μ moles min^{-1})	$\phi(H_2)$	$\phi(i-C_4H_{10})$	$\phi(H_2S)$	$\phi(i-C_4H_8)$	$\phi[(i-C_4H_9)_2S_2]$
25	7.8 $\pm 0.3d$	0.67 ± 0.01	0.33 ± 0.01	0.26 ± 0.03	0.021 ± 0.001	0.69 ± 0.05
65	7.7 ± 0.5	0.64 ± 0.01	0.36 ± 0.01	0.29 ± 0.02	0.030 ± 0.004	0.63 ± 0.06
95	7.6 ± 0.6	0.62 ± 0.01	0.38 ± 0.01	0.30 ± 0.02	0.103 ± 0.010	0.56 ± 0.03
140	7.7 ± 0.6	0.60 ± 0.01	0.40 ± 0.01	0.30 ± 0.02	0.146 ± 0.005	0.51 ± 0.04

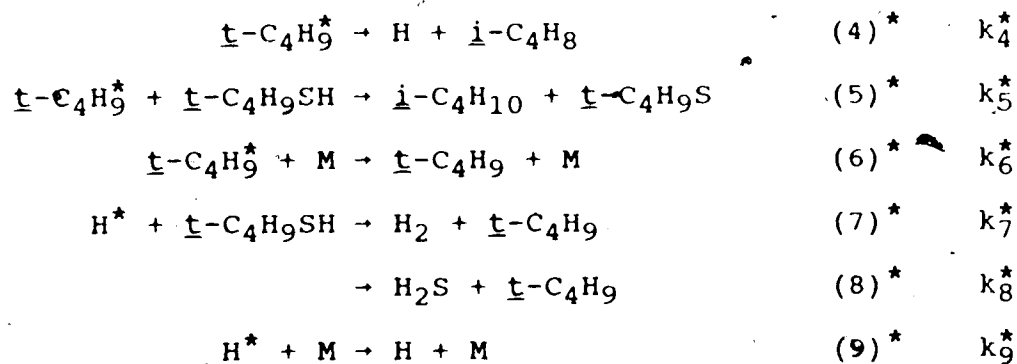
^aeach quantum yield value is the average of 5-10 experimental points^bphotolysis time = 60 min; $I_a = [R(H_2) + R(i-C_4H_{10})]$ $P(i-C_4H_9SH) = 20.0-28.1$ Torr or $[i-C_4H_9SH] = 1.04 \times 10^{-3}$ M $P(C_2H_6) = 300-555$ Torr or $[C_2H_6] = (1.61-2.15) \times 10^{-2}$ M

Coverage of a minimum of 20 experimental values

^dstandard error

24 kcal mol⁻¹, calculated from E₀ - D(S-H). The total excess energy residing in the t-C₄H₉ radicals is 56 - 62 kcal mol⁻¹, the sum of 44 - 46 kcal mol⁻¹, from E₀ - D(C-S) in step (2), and 12 - 16 kcal mol⁻¹, from the thermal energy contribution of 0.5(sRT),¹⁶³ in the temperature range 25 - 140°C.

The sequence of hot reactions for H and t-C₄H₉ radicals is as follows:



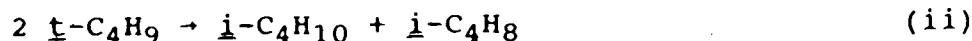
The unimolecular decomposition of t-C₄H₉, Reaction (4)*, has an enthalpy of reaction, 38 - 42 kcal mol⁻¹, estimated from recent enthalpy of formation values in the literature^{51,52} for t-C₄H₉ and i-C₄H₈. The critical energy for (4)* has also been determined by Canosa and Marshall,⁵³ from a study of the azomethane sensitized pyrolysis of isobutane, to be 39.4 kcal mol⁻¹. A higher value of 43.1 kcal mol⁻¹ was reported earlier by Benson and O'Neal.¹⁸⁵ From the difference between the excess energy of 56 - 62 kcal mol⁻¹ carried over to the t-C₄H₉ radicals and the critical energy of 39.4 kcal mol⁻¹, the active energy is -17 - 22 kcal mol⁻¹. Unfortunately, no computations of the experimental rate constants and their active energy

dependence were carried out for the \underline{t} -C₄H₉ radicals. However, the sec-butyl radical decomposition has been thoroughly studied by Rabinovitch and coworkers^{186,187}



and the model for this radical system may be used to adequately represent the similar \underline{t} -butyl radical system.¹⁴² It was found that for an active energy of -17 - 22 kcal. mol⁻¹ $k(\text{i}) \approx 10^8 \text{ s}^{-1}$, thus, it is reasonable to postulate that k_4^* would be of the same order of magnitude.

The possibility of \underline{i} -C₄H₈ and \underline{i} -C₄H₁₀ being formed from the disproportionation of \underline{t} -C₄H₉ radicals,



was considered along with the combination reaction,



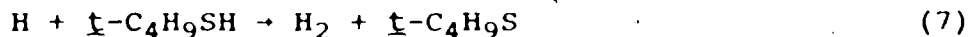
for which the ratio of disproportionation to combination, $k_{\text{ii}}/k_{\text{iii}}$, was determined to be 2.5 - 2.9 at 25°C.^{113,188,189}

However, since the combination product, 2,2,3,3-tetramethylbutane, was not observed in the photolysis products, it is unlikely that \underline{i} -C₄H₁₀ and \underline{i} -C₄H₈ are formed from step (ii).

The collisional deactivating molecules for the quenching of hot \underline{t} -C₄H₉ and H[•] radicals in Reactions (6)* and (9)*, respectively, may be either \underline{t} -C₄H₉SH or C₂H₆. The possibility of extra H₂ being produced from



was rejected on the basis of the relative rate determinations for reactions (iv) and (7),



Cao and Back¹⁹⁰ have reported the rate constant expression for (iv) to be,

$$k_{iv} \text{ (cm}^3 \text{ mol}^{-1} \text{ s}^{-1}\text{)}$$

$$= (5.3 \pm 0.3) \times 10^{14} \exp[-(1410 \pm 100)/T]$$

The rate constant expression for (7) is not known. However, that for a similar H-abstraction reaction with CH_3SH ,

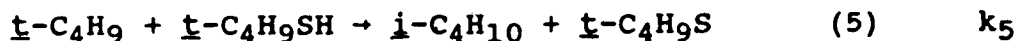


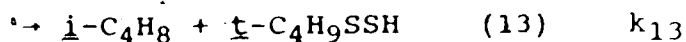
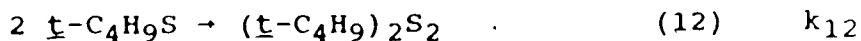
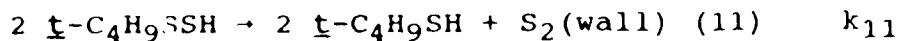
has been determined by Wine *et al.*⁷⁹ to be,

$$k_v \text{ (cm}^3 \text{ mol}^{-1} \text{ s}^{-1}\text{)} = (2.1 \pm 0.1) \times 10^{13} \exp[-(850 \pm 10)/T]$$

and this k_v can be used in the calculation of the relative rates of (iv) and (7). For the highest total concentration used, which is a 20:1 mixture of C_2H_6 : $\text{t-C}_4\text{H}_9\text{SH}$, $\text{Rate(iv)}/\text{Rate(v)} \approx 0.71$. Thus, H_2 is formed from (7) and not from (iv). The purity of C_2H_6 was established on the basis that a blank photolysis run at 254 nm using 50 Torr C_2H_6 gave no products, and that $\phi(\text{H}_2)$ obtained in the photolysis of a 3:1 mixture of C_2H_6 and H_2S was not different from the $\phi(\text{H}_2)$ obtained for the photolysis of pure H_2S . Complete quenching of hot radicals by collisional deactivation occurs at $P(\text{C}_2\text{H}_6) \geq 250$ Torr, as shown by the flat portion of the plot in Figure 6.2.

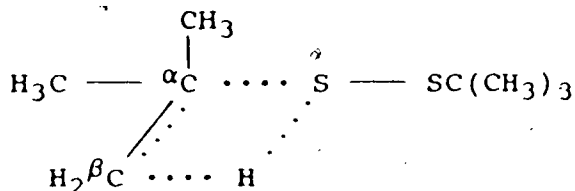
The sequence of thermal reactions is described below:





Overall, the reaction mechanism is analogous to that proposed for $\text{C}_2\text{H}_5\text{SH}$ and $\underline{i}\text{-C}_3\text{H}_7\text{SH}$ in Chapters 4 and 5. The only exception is the disproportionation of $\underline{t}\text{-C}_4\text{H}_9\text{S}$ radicals, Reaction (13), to give the alkene photolysis product, $\underline{i}\text{-C}_4\text{H}_8$, and the unstable hydrodisulfide, $\underline{t}\text{-C}_4\text{H}_9\text{SSH}$.

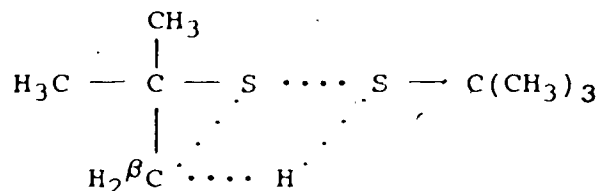
Although the disproportionation of $\underline{t}\text{-C}_4\text{H}_9\text{S}$ radicals has not been reported, it is proposed to account for the significant increase in the $\underline{i}\text{-C}_4\text{H}_8$ yield and the corresponding decrease in the $(\underline{t}\text{-C}_4\text{H}_9)_2\text{S}_2$ yield at elevated temperatures, 95° and 140°C (Tables 6.5 and 6.6). The recombination of thiyl radicals leads to the formation of slightly energized disulfide molecules which, unless stabilized by collisional deactivation, will disproportionate. In the photolyses of $\text{C}_2\text{H}_5\text{SH}$ and $\underline{i}\text{-C}_3\text{H}_7\text{SH}$ (Chapters 4 and 5), the disproportionation of thiyl radicals proceeds via the transfer of a H atom on the carbon α to sulfur and the simultaneous formation of a C-S double bond. However, the situation is different for the case of $\underline{t}\text{-C}_4\text{H}_9\text{S}$ radicals in the photolysis of $\underline{t}\text{-C}_4\text{H}_9\text{SH}$ since there is no H atom on the α carbon. The formation of the disproportionation product, $\underline{i}\text{-C}_4\text{H}_8$, from step (13), is postulated to proceed via the following transition state:



from which the C-S and β (C-H) bonds are broken and the S-H and C=C bonds are simultaneously formed. The idea of the C-S, and not the S-S bond cleavage is surprising, since it is generally known that the photolysis of disulfides leads solely to the cleavage of the S-S bond. However, Callear and Dickson⁹⁹ have reported that in the flash photolysis of CH_3SSCH_3 , both S-S and C-S scissions occur. Also, Byers *et al.*¹⁹¹ have shown by product analysis that the C-S bond cleavage is predominant in the photodecomposition of di-*t*-butyl and dibenzyl disulfide. Recently, Joshi and Yang¹⁹² used a spin-trapping technique to detect radicals formed in the photodecomposition of CH_3SSCH_3 , dibutyldisulfides and dibenzyl disulfide in organic solvents. From product analysis using ESR spectroscopy, they observed that dimethyl, di-*n*-butyl and di-*sec*-butyl disulfides gave spin adducts consisting of only the S-S bond fragments, while di-*t*-butyl and dibenzyl disulfide spin adducts indicated the trapping of both S-S and C-S bond scission products. Thus, the idea of C-S bond cleavage in the disproportionation reaction (13) is a plausible one for the case of *t*- $\text{C}_4\text{H}_9\text{S}$ radicals, in order to account adequately for the increased alkene product, *i*- C_4H_8 .

Alternatively, the disproportionation of *t*- $\text{C}_4\text{H}_9\text{S}$ radicals can also take place with S-S scission. In this

case, the H atom from one of the methyl groups on the α -carbon is transferred over to the sulfur atom and the β C-S bond is formed; the following transition state is then formed:



The ensuing disproportionation products are the substrate, t -C₄H₉SH, and the isobutene episulfide, C₄H₈S. Although the latter is energetically more stable than the other saturated 3-membered rings involving heteroatoms such as O and N atoms,¹⁹³ it was not specifically searched for in the products. However, if the episulfide were formed from reaction (13), it would have been detected, according to the work of O'Callaghan,¹⁹⁴ who used the same g.c. column and similar g.c. conditions to chromatograph the isobutene episulfide product. In the present study, the possibility of C₄H₈S as product is not considered to be important, based on the fact that no new products were formed in the photolysis of t -C₄H₉SH and that reactions (12) and (13) can be substantiated by material balance.

Steady-state treatment of the proposed mechanism results in the following quantum yield expressions:

$$\phi(i\text{-C}_4\text{H}_8) = \phi_3 + \frac{k_4^* \phi_2}{k_4^* + k_5^*[t] + k_6^*[M]} + \frac{k_{13} \phi_1}{k_{12} + k_{13}} \quad [1]$$

$$\phi(\text{H}_2) = \frac{k_7 \phi_1}{k_7 + k_8} - \frac{(k_7 k_8^* - k_7^* k_8) \phi_1 [t]}{(k_7 + k_8) \{ (k_7^* + k_8^*) [t] + k_9^* [M] \}} + \frac{k_4^* k_7 \phi_2}{(k_7 + k_8) (k_4^* + k_5^* [t] + k_6^* [M])} \quad [2]$$

$$\phi(\text{i-C}_4\text{H}_{10}) = \frac{k_8 \phi_1}{k_7 + k_8} + \phi_2 + \frac{(k_7 k_8^* - k_7^* k_8) \phi_1 [t]}{(k_7 + k_8) \{ (k_7^* + k_8^*) [t] + k_9^* [M] \}} - \frac{k_4^* k_7 \phi_2}{(k_7 + k_8) (k_4^* + k_5^* [t] + k_6^* [M])} \quad [3]$$

$$\phi(\text{H}_2\text{S}) = \frac{k_8 \phi_1}{k_7 + k_8} + \phi_3 + \frac{(k_7 k_8^* - k_7^* k_8) \phi_1 [t]}{(k_7 + k_8) \{ (k_7^* + k_8^*) [t] + k_9^* [M] \}} + \frac{k_4^* k_8 \phi_2}{(k_7 + k_8) (k_4^* + k_5^* [t] + k_6^* [M])} \quad [4]$$

$$\phi[(\text{t-C}_4\text{H}_9)_2\text{S}_2] = \frac{k_{12} \phi_1}{k_{12} + k_{13}} \quad [5]$$

ϕ_1 , ϕ_2 and ϕ_3 are the quantum yields associated with the three primary photochemical reactions, (1) - (3). M is the collisional deactivating molecule for hot H^* and $\text{t-C}_4\text{H}_9^*$ radicals and may be either the substrate $\text{t-C}_4\text{H}_9\text{SH}$ or the thermalizer C_2H_6 molecules. The expressions for $k_6^* [M]$ and $k_9^* [M]$ are $k_6^* [t] + k_6^* [e]$ and $k_9^* [t] + k_9^* [e]$, respectively. $[t]$ is the concentration or pressure of $\text{t-C}_4\text{H}_9\text{SH}$ and $[e]$ is that of added C_2H_6 .

6.2.2 Quantum Efficiencies of Primary Photochemical Steps: Quantum Yield of $\text{i-C}_4\text{H}_8$

The variations in $\phi(\text{i-C}_4\text{H}_8)$ as a function of C_2H_6 pressure at 25, 65, 95 and 140°C are plotted in Figure 6.3,

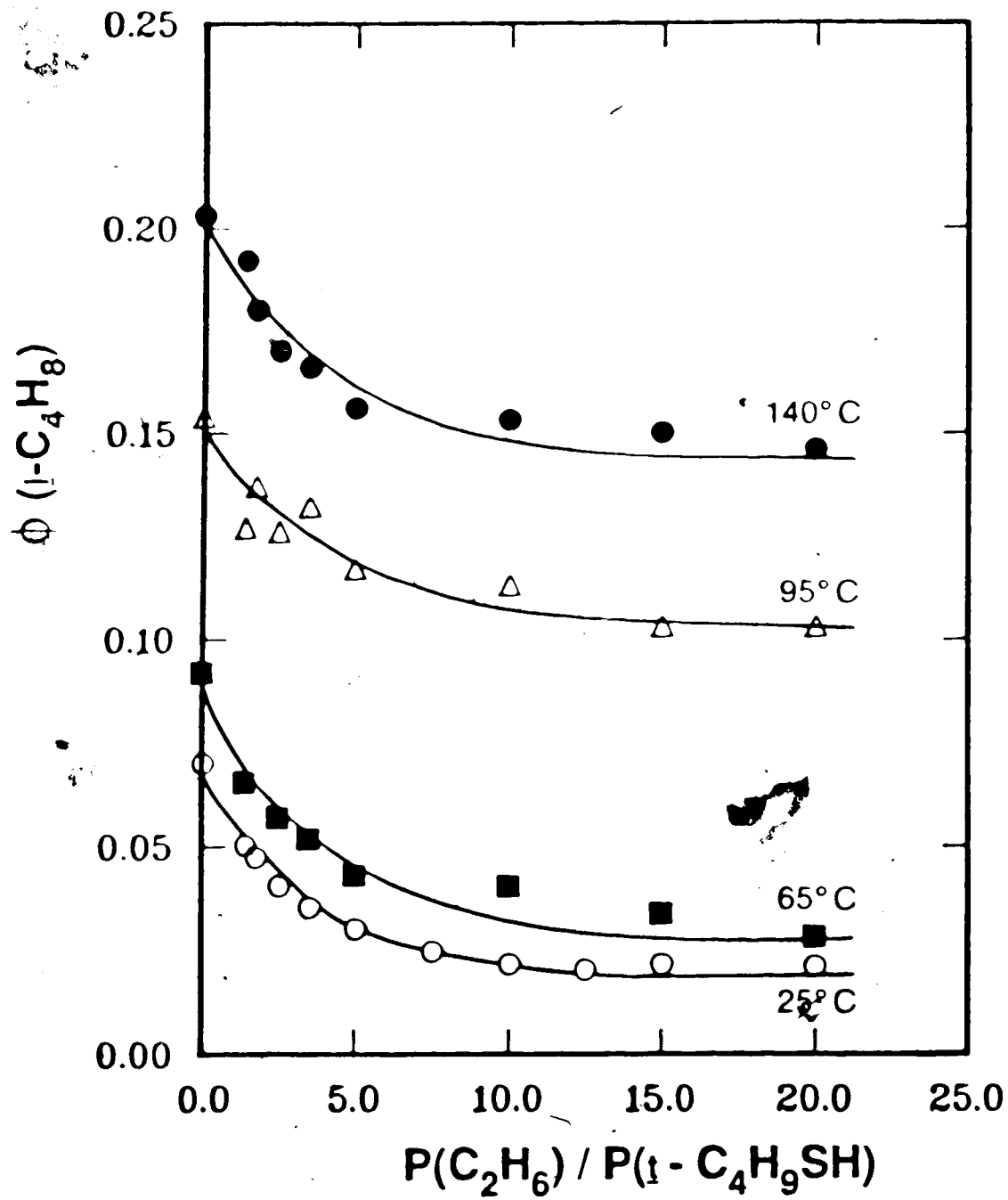


Figure 6.3. Plots of quantum yield of $i-C_4H_8$ as a function of $P(C_2H_6)/P(i-C_4H_9SH)$.

which suggests the different sources of $i\text{-C}_4\text{H}_8$. With increasing C_2H_6 pressure, $\phi(i\text{-C}_4\text{H}_8)$ decreases very rapidly and approaches a constant value at high C_2H_6 pressures. The former corresponds to the unimolecular decomposition step (4)*, while the latter corresponds to both the molecular primary photochemical step (3) and the disproportionation step (13).

The value of ϕ_3 may be determined from the modified form of Equation [1],

$$[\phi(i\text{-C}_4\text{H}_8) - \phi_3]^{-1} = \frac{(1 + \alpha P_i)}{\phi_2} + \frac{\beta P_n}{\phi_2} + \frac{k_{13} \phi_1}{k_{12} + k_{13}} \quad [6]$$

where $\alpha = (k_5^* + k_{6t}^*)/k_4^*$, $\beta = k_{6e}^*/k_4^*$, and $[\phi(i\text{-C}_4\text{H}_8) - \phi_3]^{-1}$ is a linear function of P_e at constant P_t . It has been previously shown for the cases of the C_2H_4 and the C_3H_6 products from the photolyses of $\text{C}_2\text{H}_5\text{SH}$ and $i\text{-C}_3\text{H}_7\text{SH}$ (Chapters 4 and 5) that the optimum value of ϕ_3 fitted from the kinetic treatment matches the value of the alkene yield obtained at the high thermalizer pressure limit. Thus, at 25°C , the value of ϕ_3 is 0.021 (Table 6.7).

Equation [6] becomes a linear function of P_t in the absence of C_2H_6 , *i.e.* $P_e = 0$,

$$[\phi(i\text{-C}_4\text{H}_8) - \phi_3]^{-1} = \frac{1}{\phi_2} + \frac{\alpha P_t}{\phi_2} + \frac{k_{13} \phi_1}{k_{12} + k_{13}} \quad [7]$$

The very marginal effect of $i\text{-C}_4\text{H}_9\text{SH}$ pressure on $\phi(i\text{-C}_4\text{H}_8)$ (Table 6.1) is shown in Figure 6.4 using a much expanded ordinate scale. Using $\phi_3 = 0.021$, the values for $[\phi(i\text{-C}_4\text{H}_8) - \phi_3]^{-1}$ at $P_e = 0$ were calculated and were plotted against

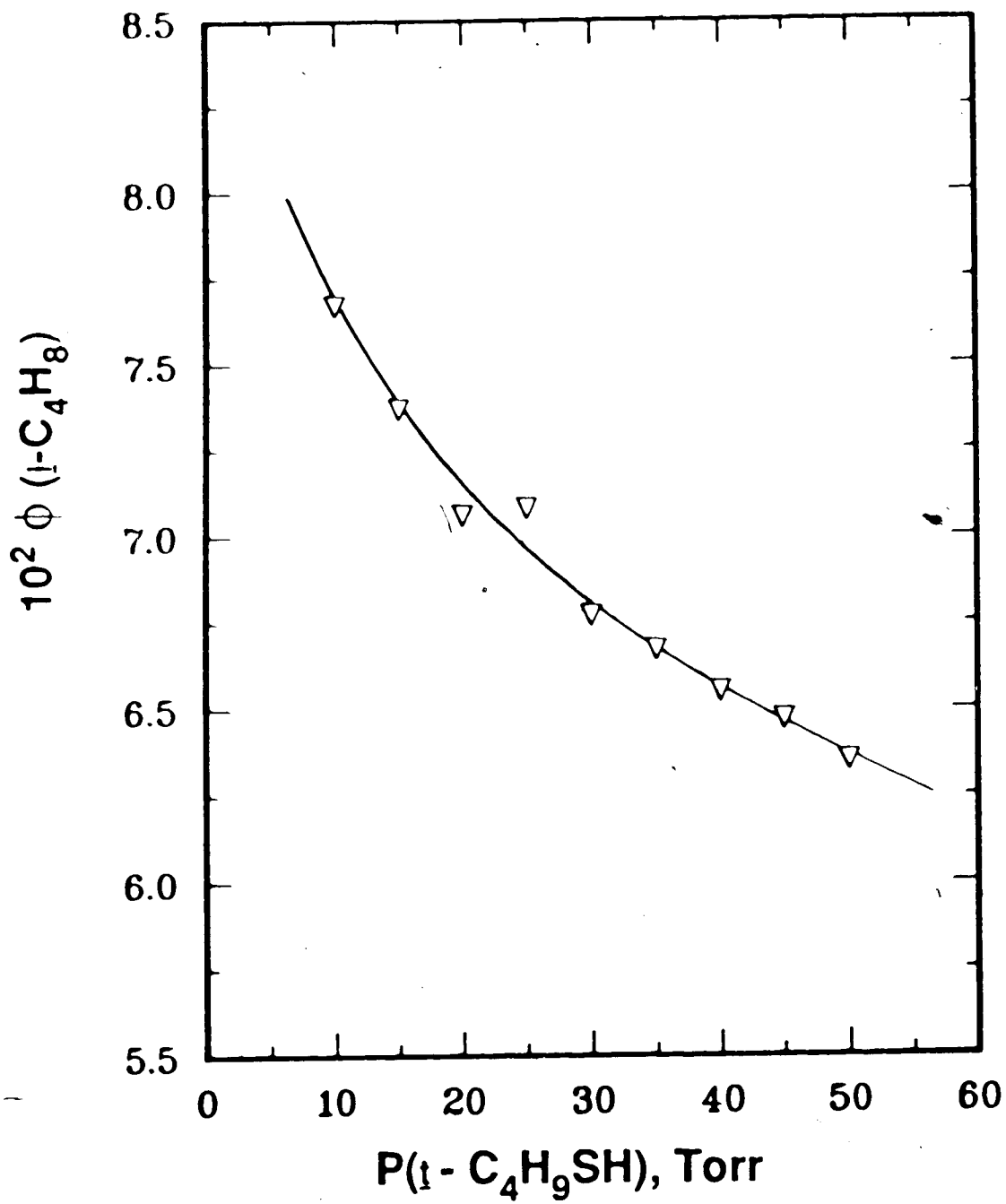


Figure 6.4. Quantum yield of *i*-C₄H₈ versus *t*-C₄H₉SH pressure.

t -C₄H₉SH pressure in Figure 6.5. The linear relation derived by the IMS method for the condition $P_e = 0$ is given by,

$$[\phi(i\text{-C}_4\text{H}_8) - \phi_3]^{-1} = (17.0 \pm 0.3) + (0.135 \pm 0.008)P_t \quad [8]$$

Combining this with Equation [7] and neglecting the small contribution at 25°C from the term $k_{13} \phi_1 / (k_{12} + k_{13})$, the values for ϕ_2 and α were then determined to be 0.059 ± 0.001 and $(8.0 \pm 0.5) \times 10^{-3} \text{ Torr}^{-1}$, respectively.

The values of ϕ_2 and ϕ_3 at higher temperatures cannot be determined precisely from the intercepts of Equation [6] due to the increased contribution from the term $k_{13} \phi_1 / (k_{12} + k_{13})$, for which the rate constant ratio for the disproportionation to combination of t -C₄H₉S radicals, k_{13}/k_{12} , is not known. However, the value of ϕ_3 may be estimated from the values of $\phi(\text{H}_2)$, $\phi(i\text{-C}_4\text{H}_8)$ and $\phi[(t\text{-C}_4\text{H}_9)_2\text{S}_2]$ at the high total pressure limit (Table 6.7).

It will be recalled that for the photolyses of C₂H₅SH and i -C₃H₇SH (Chapters 4 and 5), the disulfide yields are equal to or slightly higher than the hydrogen yields. Although this appears to be the case in the photolysis of t -C₄H₉SH at 25 and 65°C, it is observed that at 95 and 140°C the $(t\text{-C}_4\text{H}_9)_2\text{S}_2$ yield is significantly lower than the H₂ yield, and that the loss in $\phi[(t\text{-C}_4\text{H}_9)_2\text{S}_2]$ appears to correspond to the gain in $\phi(i\text{-C}_4\text{H}_8)$ (see Tables 6.5 and 6.6). Thus, at high total pressures, there are two distinct sources of i -C₄H₈, one from the primary step (3) and the other from the disproportionation step (13). Since the

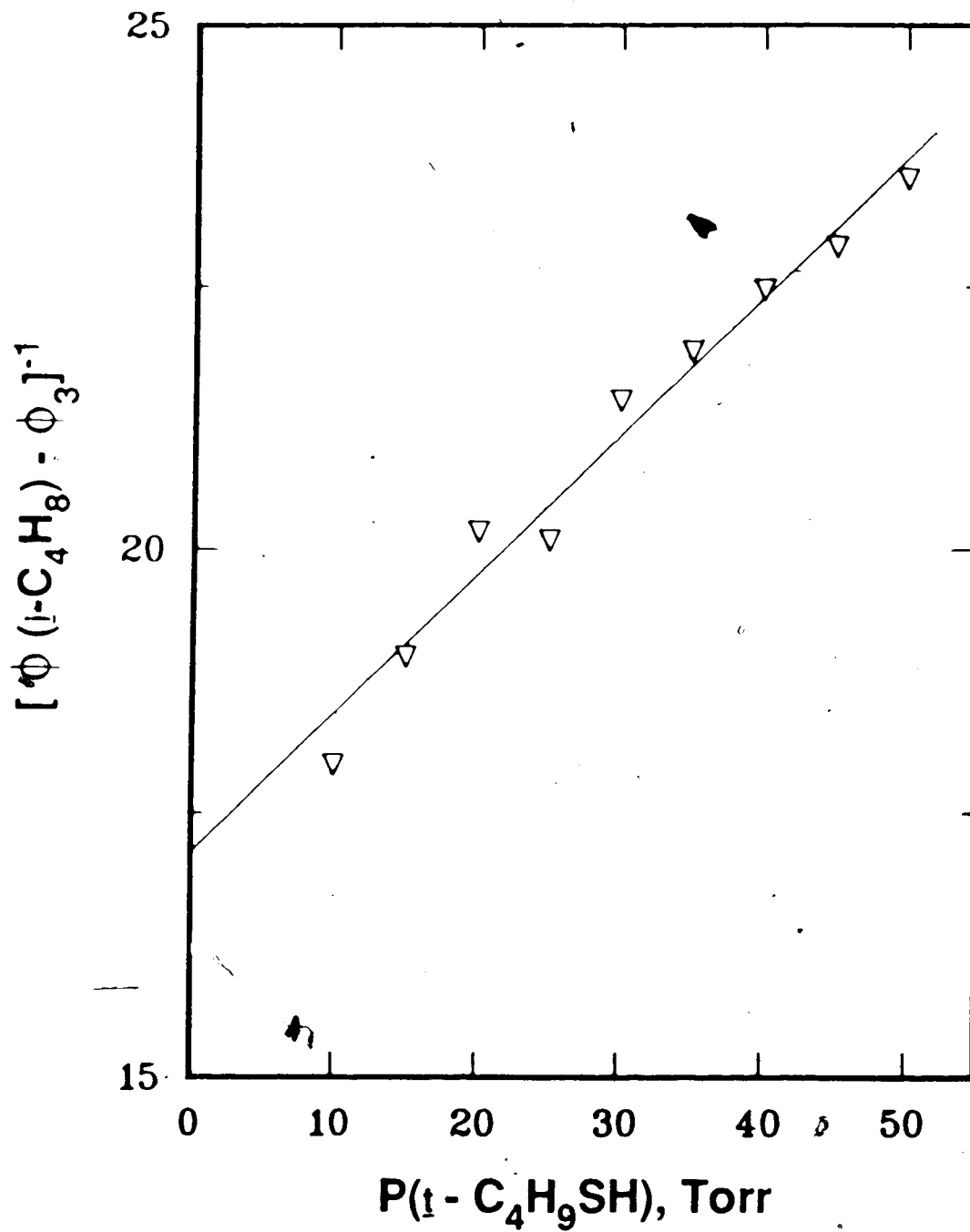


Figure 6.5. $[\phi(i\text{-C}_4\text{H}_8) - \phi_3]^{-1}$ versus $t\text{-C}_4\text{H}_9\text{SH}$ pressure. The value of $\phi_3 = 0.021$ was used.

latter can be determined from the difference between $\phi(\text{H}_2)$ and $\phi[(\text{t-C}_4\text{H}_9)_2\text{S}_2]$, the value of ϕ_3 can be obtained from the expression, $\phi_3 = \phi(\text{i-C}_4\text{H}_8) - (\phi(\text{H}_2) - \phi[(\text{t-C}_4\text{H}_9)_2\text{S}_2])$. After ϕ_3 is obtained, ϕ_1 can then be estimated from the H_2 and H_2S yields at the high pressure limit. Under this condition, quenching of hot H and $\text{t-C}_4\text{H}_9$ is complete and therefore the hot reaction steps (4)* - (9)* do not occur in the reaction mechanism. Steady-state treatment of the simplified mechanism gives the following expressions for $\phi(\text{H}_2)$ and $\phi(\text{H}_2\text{S})$:

$$\phi(\text{H}_2, P_e \rightarrow \infty) = \frac{k_7 \phi_1}{k_7 + k_8} \quad [9]$$

$$\phi(\text{H}_2\text{S}, P_e \rightarrow \infty) = \frac{k_8 \phi_1}{k_7 + k_8} + \phi_3 \quad [10]$$

from which $\phi(\text{H}_2) + \phi(\text{H}_2\text{S}) = \phi_1 + \phi_3$. The derived values of ϕ_3 , ϕ_1 and subsequently ϕ_2 ($\phi_1 + \phi_2 + \phi_3 = 1.0$), are summarized in Table 6.8. The value of ϕ_2 (at 25°C), from Equations [9] and [10] is calculated to be 0.060, in excellent agreement with the value 0.059 derived from Equations [7] and [8]. It is therefore assumed that the values of ϕ_1 and ϕ_3 are in equally good correspondence, within experimental error.

It appears from Table 6.8 that ϕ_1 , ϕ_2 and ϕ_3 are temperature dependent in the photolysis of $\text{t-C}_4\text{H}_9\text{SH}$, in contrast to the $\text{C}_2\text{H}_5\text{SH}$ and $\text{i-C}_3\text{H}_7\text{SH}$ cases, where this was not as obvious (see Table 4.11 and Table 5.10). However, this temperature dependence cannot be ascertained since

Table 6.8. Quantum Yields for the Primary Photochemical Processes

Temperature (°C)	ϕ_1	ϕ_2	ϕ_3
25	0.919±0.03	0.060±0.03	0.021 ^a ±0.004
65	0.906±0.04	0.066±0.04	0.030 ^a ±0.004
95	0.891±0.03	0.073±0.03	0.036 ^b ±0.010
140	0.874±0.04	0.080±0.04	0.046 ^b ±0.010
Average:	0.90±0.04	0.070±0.04	0.033±0.015

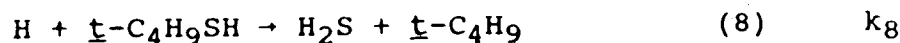
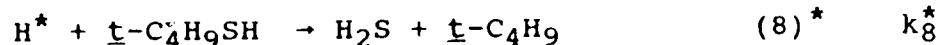
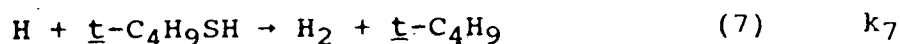
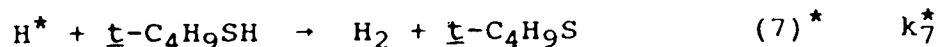
^aobtained from $\phi(\underline{i}\text{-C}_4\text{H}_8)$ at the high pressure limit, Table 6.7
^bcalculated from $\phi(\underline{i}\text{-C}_4\text{H}_8) - (\phi(\text{H}_2) - \phi[(\underline{E}\text{-C}_4\text{H}_9)_2\text{S}_2])$, Table 6.7

the errors associated with the determination of ϕ_1 , ϕ_2 and ϕ_3 are higher for the \underline{t} -C₄H₉SH case. The possible temperature dependence is most likely due to the lower (C-S) bond energy in \underline{t} -C₄H₉SH, which affects step (2), and also to the lower activation energy associated with the H₂S-elimination step (3), both of which are reflected in higher ϕ_2 and ϕ_3 values, respectively, and consequently a lower ϕ_1 value at each temperature.

6.2.3 Hydrogen Atom Reactions with tert-Butanethiol:

Quantum Yields of H₂ and H₂S

The relative rates of the hot and thermalized H-atom reactions with \underline{t} -C₄H₉SH,



are obtained from the variations of the H₂ and H₂S yields with pressure and temperature. In a kinetic treatment analogous to that discussed in Chapter 4, the values of the ratio $[\phi(\text{H}_2) - \delta]/[\phi(\text{H}_2\text{S}) - \phi_3]$ as a function of C₂H₆ pressure and temperature are summarized in Table 6.9 and are plotted in Figure 6.6. The resulting trends are observed to be the same as those for the H-atom reactions with C₂H₅SH and \underline{i} -C₃H₇SH, respectively. Thus at each temperature, $[\phi(\text{H}_2) - \delta]/[\phi(\text{H}_2\text{S}) - \phi_3]$ increases with increasing thermalizer pressure, indicating that the H-abstraction reaction (7) is favoured and thus has a

Table 6.9. Effects of n-C₄H₁₀ Pressure and Temperature on the Values^a
of $[\phi(\text{H}_2) - \delta]/[\phi(\text{H}_2\text{S}) - \phi_3]$ ^b

[P(C ₂ H ₆)/P($\bar{\text{t}}$ -C ₄ H ₉ SH)] ^c	$[\phi(\text{H}_2) - \delta]/[\phi(\text{H}_2\text{S}) - \phi_3]$			
	25°C	65°C	95°C	140°C
0	2.01±0.21 ^d	1.64±0.17	1.63±0.18	1.21±0.15
1.4	1.86±0.19	1.78±0.17	1.68±0.16	1.28±0.14
1.75	2.11±0.20	1.84±0.19	1.59±0.17	1.36±0.15
2.50	2.06±0.22	1.93±0.14	1.66±0.18	1.63±0.19
3.50	2.19±0.21	1.95±0.18	1.61±0.18	1.61±0.17
5.00	2.24±0.25	2.15±0.23	1.82±0.25	1.78±0.19
10.0	2.89±0.31	2.34±0.26	2.01±0.23	1.96±0.21
15.0	3.06±0.32	2.40±0.26	2.24±0.23	2.09±0.23
20.0	3.28±0.35	2.58±0.27	2.33±0.25	2.22±0.26

^aeach value is the average of 2-8 experimental points

^b $\delta = [\phi(\bar{\text{t}}\text{-C}_4\text{H}_8) - \phi_3]$

^cP(C₂H₆) = 0-555 Torr or [C₂H₆] ≤ 2.15 × 10⁻² M

^dP($\bar{\text{t}}$ -C₄H₉SH) = 20.0-28.1 Torr or [$\bar{\text{t}}$ -C₄H₉SH] = 1.04 × 10⁻³ M

^estandard error

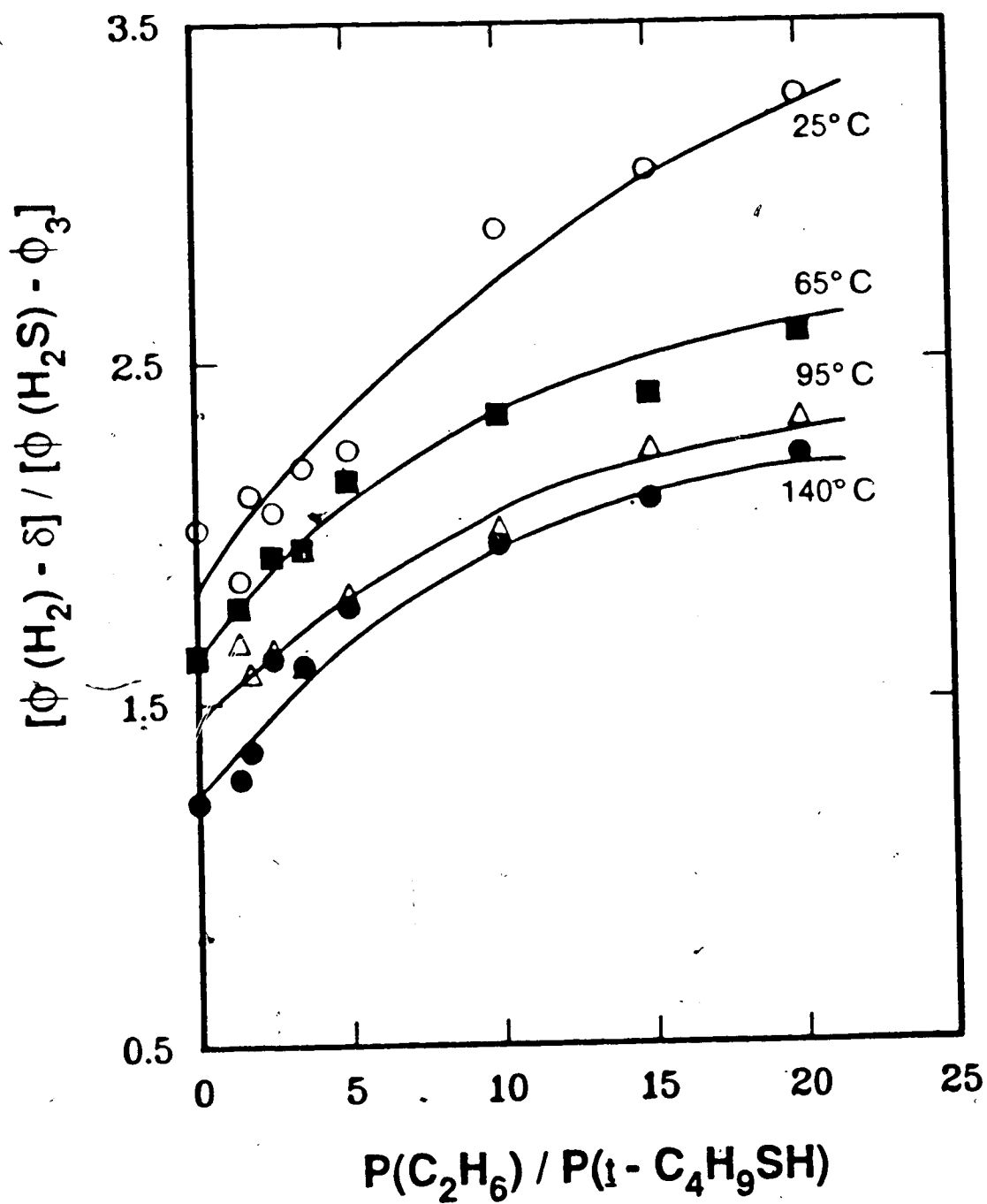
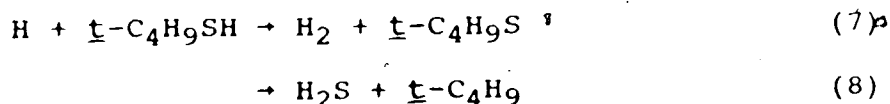


Figure 6.6. Plots of $[\phi(H_2) - \delta] / [\phi(H_2S) - \phi_3]$ as a function of the ratio $P(C_2H_6) / P(t-C_4H_9SH)$.

lower activation energy than the displacement reaction (8), as expected. Also, $[\phi(\text{H}_2) - \delta]/[\phi(\text{H}_2\text{S}) - \phi_3]$ decreases with increasing temperature, but the rate of decrease is smaller than that found in the $\text{C}_2\text{H}_5\text{SH}$ and $i\text{-C}_3\text{H}_7\text{SH}$ cases. These observed trends suggest that although the activation energy for the displacement reaction is higher than the abstraction reaction, the difference is small.

6.2.4 Relative Rate Parameters for the H-atom Reactions: Quantum Yields of H_2 and $i\text{-C}_4\text{H}_{10}$

The relative rate parameters for the thermalized H-atom reactions



are determined from the hydrogen and alkane yields in a manner analogous to that formulated in Chapter 4. The modified forms of Equations [2] and [3], under the condition of high C_2H_6 pressure, are given by:

$$\phi(\text{H}_2) = \frac{k_7 \phi_1}{(k_7 + k_8)} - \frac{(k_7 k_8^* - k_7^* k_8) k_6^* e \phi_1 [t] - k_4^* k_7 k_9^* e \phi_2}{(k_7 + k_8) k_6^* e k_9^* [e]} \quad [11]$$

$$\begin{aligned} \phi(i\text{-C}_4\text{H}_{10}) &= \frac{k_8 \phi_1}{(k_7 + k_8)} + \phi_2 \\ &+ \frac{(k_7 k_8^* - k_7^* k_8) k_6^* e \phi_1 [t] - k_4^* k_7 k_9^* e \phi_2}{(k_7 + k_8) k_6^* e k_9^* [e]} \quad [12] \end{aligned}$$

Equations [11] and [12] predict that $\phi(\text{H}_2)$ and $\phi(i\text{-C}_4\text{H}_{10})$ are linear functions of inverse C_2H_6 concentration. This is evident in the plots of $\phi(\text{H}_2)$ and $\phi(i\text{-C}_4\text{H}_{10})$ versus inverse C_2H_6 concentration, shown in Figures 6.7 and 6.8,

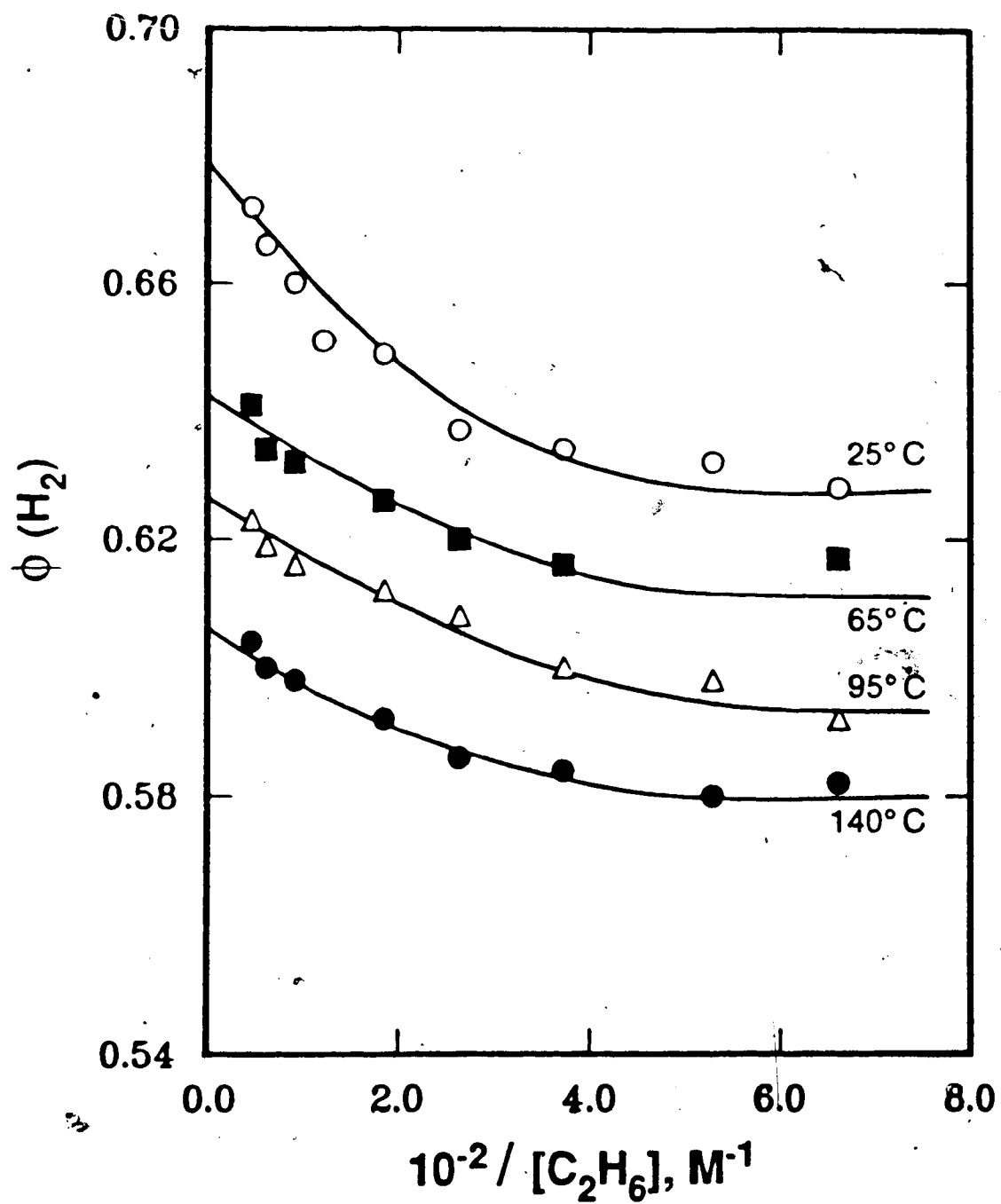


Figure 6.7. Plots of $\phi(\text{H}_2)$ as a function of the reciprocal of C_2H_6 concentration at $[\text{t-C}_4\text{H}_9\text{SH}] = 1.04 \times 10^{-3} \text{ M}$.

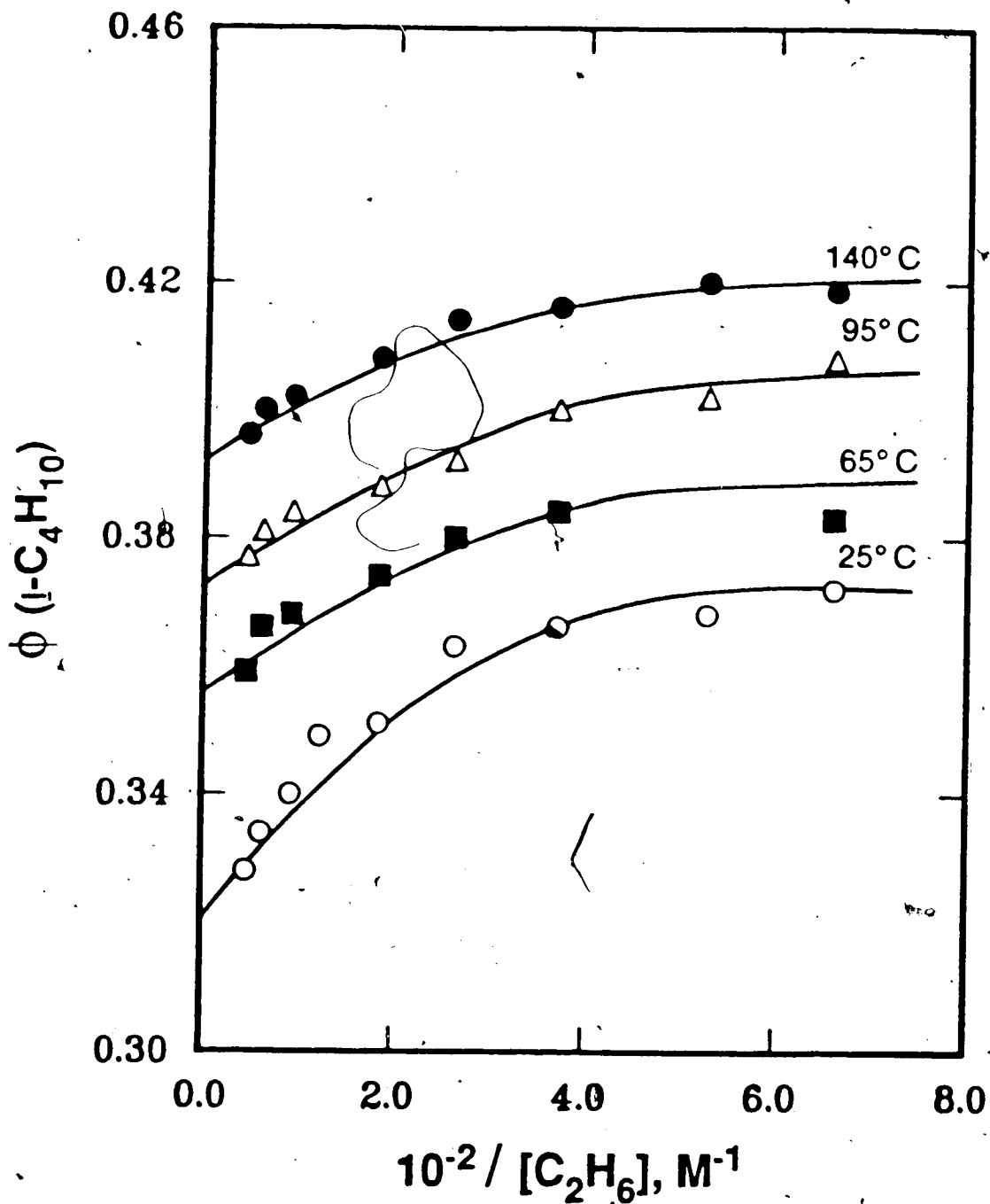


Figure 6.8. Plots of $\phi(i-C_4H_{10})$ as a function of the reciprocal of C_2H_6 concentration at $[t-C_4H_9SH] = 1.04 \times 10^{-3} \text{ M}$.

respectively, at $[C_2H_6]^{-1} < 0.04 M^{-1}$, or $P_e > 50$ Torr. The intercepts of the linear portions of these plots are listed in Table 6.10 and are defined by [11] and [12] to be,

$$\phi(H_2, P_e \rightarrow \infty) = \frac{k_7 \phi_1}{k_7 + k_8} \quad [9]$$

$$\phi(i-C_4H_{10}, P_e \rightarrow \infty) = \frac{k_8 \phi_1}{k_7 + k_8} + \phi_2 \quad [13]$$

The rate constant ratio, k_7/k_8 , may then be calculated at each temperature from the intercepts and the derived values of ϕ_1 and ϕ_2 (Table 6.8). Their values are listed in Table 6.11 and are found to agree with another set of values for k_7/k_8 which were derived directly from the experimental H_2 and $i-C_4H_{10}$ yields at high C_2H_6 pressures (Table 6.7). The average value of k_7/k_8 at 25°C, 2.7, is higher than the value of 0.86, estimated from the radiolysis results of Severs *et al.*⁸¹

The Arrhenius plot (Figure 6.9) is constructed from the average values of k_7/k_8 (Table 6.11). The resulting rate expression for the thermalized H-atom reactions (7) and (8), is given by,

$$\ln k_7/k_8 = (0.3 \pm 0.1) + (210 \pm 40)/T \quad [14]$$

from which $(E_7 - E_8) = -0.42 \pm 0.08$ kcal mol⁻¹ and $A_7/A_8 = 1.32 \pm 0.07$. The difference in activation energy is indeed small, as predicted. Although the absolute rate parameters cannot be determined at this time, they can be estimated from the results obtained for the analogous H-atom reactions with C_2H_5SH (Chapter 4) since the (S-H) bond strengths in

Table 6.10. Intercepts of the Plots in Figures 6.7 and 6.8^a

Temperature (°C)	Intercepts		
	P(<u>l</u> -C ₄ H ₉ SH) (Torr)	H ₂	<u>l</u> -C ₄ H ₁₀
25	20.0	0.675 ±0.003	0.325 ±0.003
65	22.7	0.641 ±0.002	0.359 ±0.002
95	24.7	0.624 ±0.002	0.376 ±0.002
140	28.1	0.606 ±0.001	0.394 ±0.001

^alinear region from $[\text{C}_2\text{H}_6]^{-1} < 0.04 \text{ M}^{-1}$ or $P(\text{C}_2\text{H}_6) > 50 \text{ Torr}$

Table 6.11. Temperature Dependence of k_7/k_8

Temperature (°C)	(k_7/k_8) ^a	(k_7/k_8) ^b	(k_7/k_8) _{av}
25	2.8 ±0.6	2.7 ±0.2	2.7 ±0.6
65	2.4 ±0.5	2.4 ±0.2	2.4 ±0.5
95	2.3 ±0.5	2.3 ±0.4	2.3 ±0.6
140	2.3 ±0.4	2.2 ±0.3	2.2 ±0.5

^acalculated from intercept values in Table 6.10
^bcalculated from experimental $\phi(H_2)$ and $\phi(i-C_4H_{10})$ yields at high C_2H_6 pressures
 c standard error

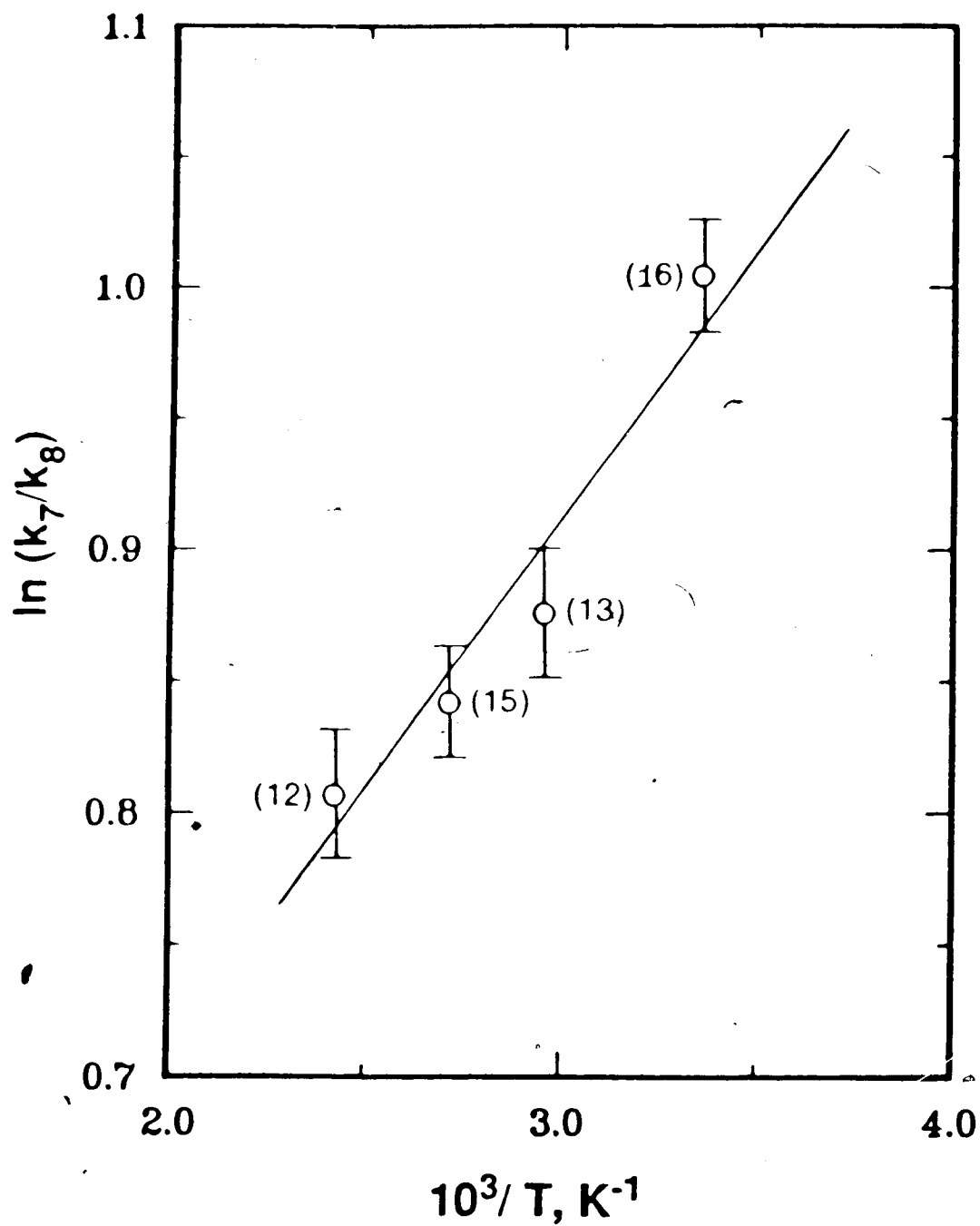


Figure 6.9. Plot of $\ln k_7/k_8$ versus the reciprocal of temperature. Figure in bracket indicates number of experiments.

C_2H_5SH and $t-C_4H_9SH$ are the same. Thus, if k_7 for $t-C_4H_9SH$ is equal to that for C_2H_5SH , i.e.

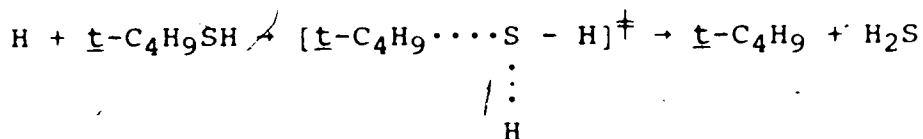
$$k_7 \text{ (cm}^3 \text{ mol}^{-1} \text{ s}^{-1}\text{)} \\ = (4.0 \pm 0.7) \times 10^{12} \exp [(-1070 \pm 40)/RT] \quad [15]$$

then k_8 can be determined from Equations [14] and [15] to be,

$$k_8 \text{ (cm}^3 \text{ mol}^{-1} \text{ s}^{-1}\text{)} \\ = (3.0 \pm 0.7) \times 10^{12} \exp [(-1500 \pm 100)/RT] \quad [16]$$

At 25°C, k_7 and k_8 are calculated from [15] and [16] to be $(7 \pm 1) \times 10^{11}$ and $(2.5 \pm 0.6) \times 10^{11} \text{ cm}^3 \text{ mol}^{-1} \text{ s}^{-1}$, respectively. The value for k_7 is found to be about a twofold higher than that reported by Pryor and Olsen⁷⁰, $3.2 \times 10^{11} \text{ cm}^3 \text{ mol}^{-1} \text{ s}^{-1}$.

The experimental entropy of activation, ΔS^\ddagger , calculated from the A factor of (8), is -27.5 eu. for the standard state of 1 atm. Using Benson's method¹⁴¹ for a transition state which involves an initial interaction between the H atom and the non-bonding 3p orbital of the sulfur atom:



the calculated entropy of activation is -26.0 eu. The small difference of -1.5 eu., which is the vibrational contribution to ΔS^\ddagger , indicates a tight structure for the activated complex.

The expressions for the H_2 and $i-C_4H_{10}$ yields, Equations [2] and [3], are simplified for the condition, $P_e = 0$, as follows:

$$\phi(\text{H}_2) = \frac{k_7 \phi_1}{k_7 + k_8} - \frac{(k_7 k_8^* - k_7^* k_8) \phi_1}{(k_7 + k_8)(k_7^* + k_8^* + k_{9t}^*)} + \frac{k_7 \phi_2}{(k_7 + k_8)(1 + \alpha P_t)} \quad [17]$$

$$\phi(\text{i-C}_4\text{H}_{10}) = \frac{k_8 \phi_1}{k_7 + k_8} + \phi_2 + \frac{(k_7 k_8^* - k_7^* k_8) \phi_1}{(k_7 + k_8)(k_7^* + k_8^* + k_{9t}^*)} - \frac{k_7 \phi_2}{(k_7 + k_8)(1 + \alpha P_t)} \quad [18]$$

The last term in both Equations [17] and [18] predicts that $\phi(\text{H}_2)$ and $\phi(\text{i-C}_4\text{H}_{10})$ are an inverse function of $\text{t-C}_4\text{H}_9\text{SH}$ pressure, P_t . This pressure dependence can be calculated using the already derived values of α , ϕ_2 and k_7/k_8 . The results, shown in Table 6.12, indicate that the magnitude of the change in the pressure-dependent term is small, being only 0.009 on going from 10 to 50 Torr. Thus, the dependence of H_2 and $\text{i-C}_4\text{H}_{10}$ yields on $\text{t-C}_4\text{H}_9\text{SH}$ pressure is marginal and falls within the range of experimental error. This is in agreement with the experimental observation (Table 6.1 and Figure 6.1) that $\phi(\text{H}_2)$ and $\phi(\text{i-C}_4\text{H}_{10})$ are apparently constant at 0.61 ± 0.03 and 0.39 ± 0.02 , respectively.

6.2.5 Disproportionation-Combination of Thiyl Radicals: Quantum Yield of $(\text{t-C}_4\text{H}_9)_2\text{S}_2$

The quantum yield expression for the major condensable product, $(\text{t-C}_4\text{H}_9)_2\text{S}_2$, is given by,

$$\phi[(\text{t-C}_4\text{H}_9)_2\text{S}_2] = \frac{k_{12} \phi_1}{k_{12} + k_{13}} \quad [5]$$

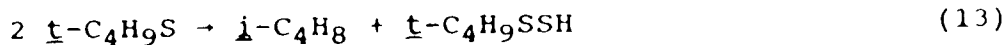
Table 6.12. Derived Values of $\frac{k_7 \phi_2}{(k_7 + k_8)(1 + \alpha P_t)}$ ^a

$P(\underline{C}_4H_9SH)$ (Torr)	$\frac{k_7 \phi_2}{(k_7 + k_8)(1 + \alpha P_t)}$
10	0.0407
20	0.0379
30	0.0354
40	0.0333
50	0.0314

^a $T = 25^\circ C$, $(k_7/k_8)_{av} = 2.7$, $\phi_2 = 0.060$, $\alpha = 8.0 \times 10^{-3} \text{ Torr}^{-1}$

7

From the observation that $\phi[(\underline{t}\text{-C}_4\text{H}_9)_2\text{S}_2]$ is less than ϕ_1 , and that the $\underline{i}\text{-C}_4\text{H}_8$ yield increases with temperature, the disproportionation reaction does in fact occur,



with the hydrodisulfide formed from (13) being lost via Reaction (11). Since $\phi[(\underline{t}\text{-C}_4\text{H}_9)_2\text{S}_2]$ is almost equal to $\phi(\text{H}_2)$ at 25 and 65°C, the disproportionation of $\underline{t}\text{-C}_4\text{H}_9\text{S}$ radicals should be a relatively minor reaction at low temperatures. However, $\phi[(\underline{t}\text{-C}_4\text{H}_9)_2\text{S}_2]$ is significantly less than $\phi(\text{H}_2)$ at 95 and 140°C (see Table 6.7), indicating that the disproportionation reaction (13) is more important at elevated temperatures.

The disproportionation-combination ratio, k_{13}/k_{12} , is derived from [5] to be;

$$\frac{k_{13}}{k_{12}} = \frac{\phi_1}{\phi[(\underline{t}\text{-C}_4\text{H}_9)_2\text{S}_2]} - 1 \quad [19]$$

Their values, tabulated in Table 6.13, are calculated at each temperature from the values of $\phi[(\underline{t}\text{-C}_4\text{H}_9)_2\text{S}_2]$ obtained in the absence of C_2H_6 and also from those obtained in the high C_2H_6 pressure region (Tables 6.3 to 6.6). The values of k_{13}/k_{12} derived for $\underline{t}\text{-C}_4\text{H}_9\text{S}$ radicals are at least threefold higher than those derived for both $\text{C}_2\text{H}_5\text{S}$ and $\underline{i}\text{-C}_3\text{H}_7\text{S}$ radicals in Chapters 4 and 5, respectively. The Arrhenius plot, shown in Figure 6.10, is constructed using the high pressure values of k_{13}/k_{12} . The following rate expression is obtained:

$$\ln k_{13}/k_{12} = (1.7 \pm 0.2) - (850 \pm 70)/T \quad [20]$$

Table 6.13. Temperature Dependence of k_{13}/k_{12}

Temperature (°C)	$(k_{13}/k_{12})^a$	$(k_{13}/k_{12})^b$
25	0.40 ±0.10	0.30 ±0.10
65	0.30 ±0.10	0.40 ±0.10
95	0.50 ±0.10	0.60 ±0.10
140	0.80 ±0.20	0.70 ±0.20

^acalculated from the photolysis of pure *t*-C₄H₉SH
^bcalculated from the photolysis of *t*-C₄H₉SH with added C₂H₆
at the high pressure limit

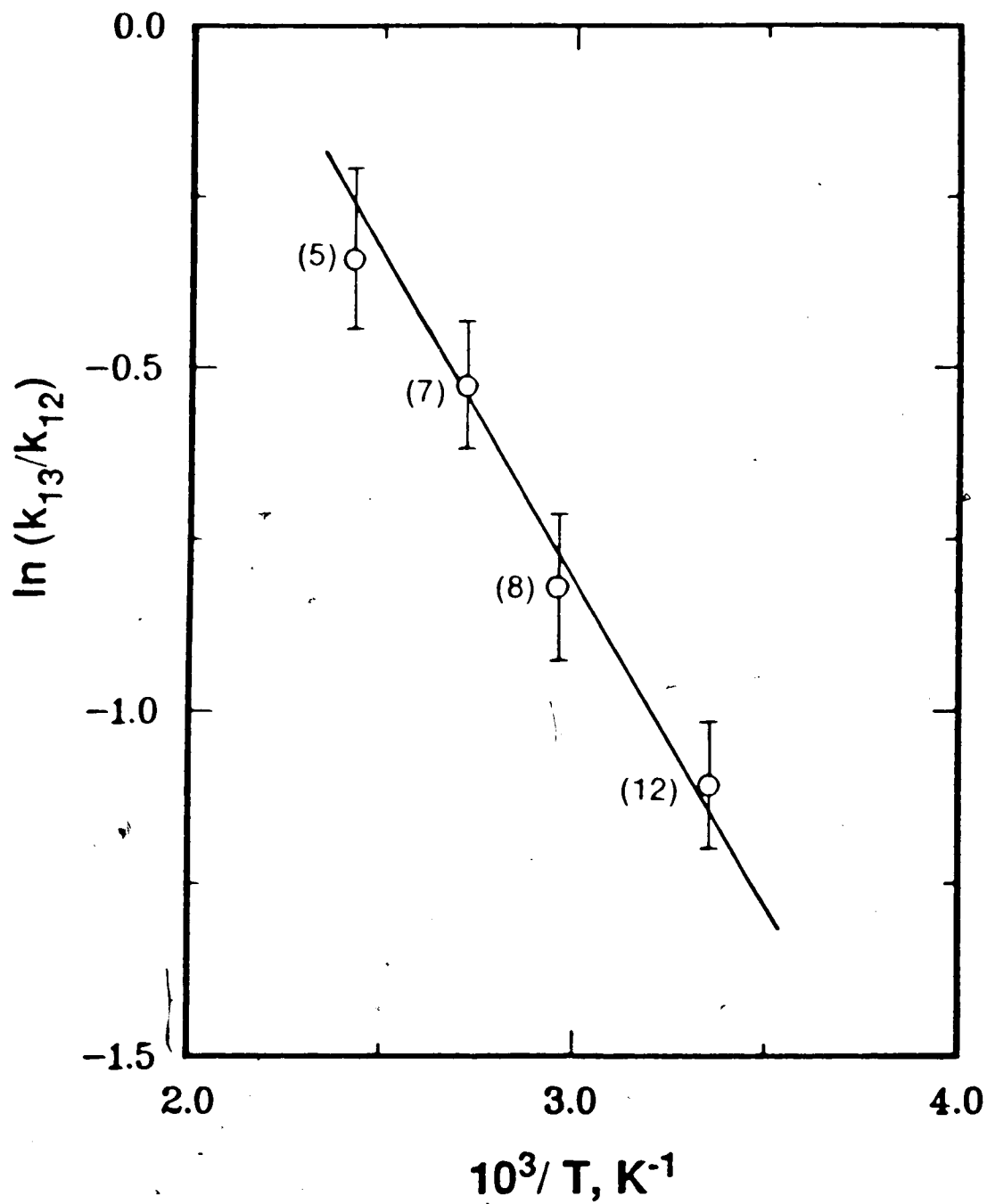


Figure 6.10. Plot of $\ln k_{13}/k_{12}$ versus the reciprocal of temperature. Figure in bracket indicates number of experiments.

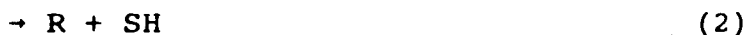
from which $E_{13} - E_{12} = 1.7 \pm 0.1 \text{ kcal mol}^{-1}$ and $A_{13}/A_{12} = 5.6 \pm 0.5$. Since the recombination of radicals requires negligible activation energy, i.e. $E_{12} \approx 0$, E_{13} is therefore $-1.7 \text{ kcal mol}^{-1}$, smaller than the values determined for the disproportionation of $\text{C}_2\text{H}_5\text{S}$ and $\underline{i}\text{-C}_3\text{H}_7\text{S}$ radicals, 3.1 and 2.7 kcal mol^{-1} , respectively.

CHAPTER SEVEN

SUMMARY AND CONCLUSIONS

Direct photolyses of ethanethiol, isopropanethiol and *t*-butanethiol in the gas phase have been investigated at 254 nm in the presence and absence of the thermalizers, carbon dioxide, *n*-butane and ethane, respectively. In all cases, the major products are H₂ and dialkyldisulfides while the minor products include the corresponding alkanes and alkenes, and H₂S. The product distributions depend on the structure of the thiol. The proposed overall mechanism explains satisfactorily not only the formation and distribution of the products but also the observed pressure and temperature effects.

With increasing thermalizer pressure, the quantum yields of H₂ and dialkyldisulfide increase gradually, along with a concomitant decline in the yields of minor products. All the quantum yields attain limiting values at approximately a tenfold excess of the thermalizer pressure over that of the substrate. These results are interpreted in terms of both hot and thermal radicals generated in the following three primary photochemical steps:



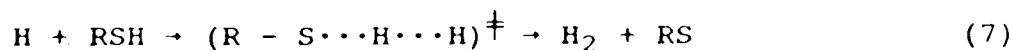
(R = C₂H₅, *i*-C₃H₇, *t*-C₄H₉), the quantum yields of which have been determined and are listed in Table 7.1. The

Table 7.1. Quantum Yields for the Primary Photochemical Processes

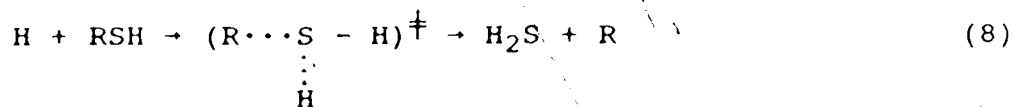
RSH	T (°C)	ϕ_1	ϕ_2	ϕ_3	
C ₂ H ₅ SH	25	0.967	0.023	0.010	
	80	0.963	0.027	0.010	
	120	0.961	0.029	0.010	
	150	0.954	0.036	0.010	
		Average ^a :	0.96±0.01	0.029±0.010	0.010±0.001
i-C ₃ H ₇ SH	25	0.948	0.043	0.009	
	65	0.944	0.047	0.009	
	105	0.926	0.065	0.009	
	145	0.917	0.074	0.009	
		Average ^a :	0.93±0.01	0.057±0.010	0.009±0.001
t-C ₄ H ₉ SH	25	0.919	0.060	0.021	
	65	0.906	0.066	0.028	
	95	0.891	0.073	0.036	
	140	0.874	0.080	0.046	
		Average ^a :	0.90±0.04	0.070±0.04	0.033±0.015

Quantum yields are assumed to be temperature-independent, within experimental errors

results show that the most important primary step in the photolysis of thiols is the cleavage of the S-H bond, ϕ_1 , forming hot H atoms with high quantum yields (Table 7.1). Subsequently, the H atoms react with the substrate either via H-atom abstraction,



or via a SH-displacement reaction



The results from the experiments on the $\text{Hg}(^3\text{P}_1)$ sensitization of H_2 in the presence of $\text{C}_2\text{H}_5\text{SH}$ have shown conclusively that both the H-atom abstraction and the SH-displacement occur with thermalized H atoms. The variation of the rate constant ratio, k_7/k_8 , with temperature for the different thiols is summarized in Table 7.2. The rate constant ratios k_7/k_8 indicate that H atom abstraction increases while SH-displacement decreases as branching at the carbon atom α to sulfur increases from $\text{C}_2\text{H}_5\text{SH}$ to $i\text{-C}_3\text{H}_7\text{SH}$. On the other hand, the low k_7/k_8 value for the case of $t\text{-C}_4\text{H}_9\text{SH}$ would indicate that steric effects are countered by weaker C-S bond which facilitates SH-displacement.

Relative Arrhenius parameters for (7) and (8) have been determined and summarized in Table 7.3, along with the exothermicities of the reactions, using thermochemical data from Table 1.2. If the rate parameters for H-abstraction are equal for simple alkanethiols from the same S-H

Table 7.2. Variation of k_7/k_8 with Temperature

T (°C)	k_7/k_8 ^a		
	C_2H_5SH	$i-C_3H_7SH$	$t-C_4H_9SH$
25	7.1 ± 0.5	18 ± 5	2.7 ± 0.6
65	---	12 ± 3	2.4 ± 0.5
80	5.1 ± 0.3	---	---
95	---	---	2.3 ± 0.6
105	---	10 ± 3	---
120	4.1 ± 0.2	---	---
140	---	---	2.2 ± 0.5
145	---	8 ± 3	---
150	3.7 ± 0.2	---	---

^a average of experimental and calculated values

Table 7.3. Arrhenius Parameters for Abstraction/Displacement Reactions by H Atoms

Reaction	H + RSH → H ₂ + RS (7)		E ₇ - E ₈	H ^o
	A ₇ /A ₈			
H + C ₂ H ₅ SH → H ₂ + C ₂ H ₅ S	0.78 ± 0.01		-1.31 ± 0.03	-15.6
H + C ₂ H ₅ SH → H ₂ S + C ₂ H ₅				-20.0
H + <u>1</u> -C ₃ H ₇ SH → H ₂ + <u>1</u> -C ₃ H ₇ S	1.43 ± 0.06		-1.53 ± 0.07	-15.9
H + <u>1</u> -C ₃ H ₇ SH → H ₂ S + <u>1</u> -C ₃ H ₇				-20.7
H + <u>2</u> -C ₄ H ₉ SH → H ₂ + <u>2</u> -C ₄ H ₉ S	1.32 ± 0.07		-0.42 ± 0.08	-14.9
H + <u>2</u> -C ₄ H ₉ SH → H ₂ S + <u>2</u> -C ₄ H ₉				-21.6

(kcal mol⁻¹)

bond energies, i.e.

$$k_7 \text{ (cm}^3 \text{ mol}^{-1} \text{ s}^{-1}\text{)}$$

$$= (4.0 \pm 0.7) \times 10^{12} \exp [(-1070 \pm 40)/RT]$$

then the absolute parameters for SH-displacement may then be calculated. The rate constants, pre-exponential factors, activation energies, enthalpies of reaction and entropies of activation for some of the displacement reactions by H atoms are listed in Table 7.4.

Over the years, various attempts were made to interrelate the activation energy, E_a , and the enthalpy of reaction, ΔH , in order to determine the E_a of another reaction in a common class of compounds. For example, Evans and Polanyi¹⁹⁵ developed an empirical relationship of the form

$$E_a = c + \alpha \Delta H \quad [1]$$

for the exothermic reactions of Na atoms and CH_3 radicals with a homologous series of molecules. In [1], ΔH is negative and c and α are empirical constants which vary from one series of reactions to another. Equation [1] is sometimes also known as the Polanyi-Semenov relation¹⁹⁶ since Semenov had later shown that the reactions of H, D and OH with selected classes of compounds also follow this trend. Recently, the correlation between E_a and ΔH for the H-atom reactions with COS, CH_3SCH_3 and $\text{C}_2\text{H}_4\text{S}$ was obtained by Yokota and Strausz¹³¹ to be,

$$E_a = 0.489 - 35.1 / \Delta H \text{ kcal mol}^{-1} \quad [2]$$

The plot of E_a versus ΔH for other displacement reactions

Table 7.4. Rate Constants and Arrhenius Parameters for the

Displacement Reactions by H Atoms

Substrate	k_{298} ($\text{cm}^3 \text{ mol}^{-1} \text{ s}^{-1}$)	A	E_a (kcal mol^{-1})	ΔH^\ddagger	ΔS^\ddagger a expt.	x ^b	Reference
CH ₃ SH	4.1×10^{11}	6.9×10^{12}	1.67	-16.3	-25.8	+0.2	77
C ₂ H ₅ SH	9.2×10^{10}	5.1×10^{12}	2.38	-20.0	-26.5	-0.5	This work
i-C ₃ H ₇ SH	3.5×10^{10}	2.8×10^{12}	2.60	-20.7	-27.6	-1.6	This work
n-C ₄ H ₉ SH	3.7×10^{10}	1.6×10^{12}	2.22	-19.8	-28.7	-2.7	80
t-C ₄ H ₉ SH	2.5×10^{11}	3.0×10^{12}	1.49	-17.7	-27.5	-1.5	This work
CH ₃ SCH ₃	2.0×10^{11}	1.7×10^{13}	2.62	-18.0	-24.1	+1.9	164
C ₂ H ₅ SC ₂ H ₅	1.8×10^{10}	4.7×10^{13}	3.80	-17.5	-22.1	+3.9	166
CH ₃ SSCH ₃	4.9×10^{12}	5.7×10^{12}	0.1	-21.0	-26.2	-0.2	110
C ₂ H ₅ SSC ₂ H ₅	2.6×10^{12}	4.7×10^{13}	1.71	-19.5	-22.0	+4.0	115

a calculated from pre-exponential factor

b ΔS^\ddagger expt. - ΔS^\ddagger calc.; ΔS^\ddagger calc. = $R \ln 2 + S_0(H) = -26.0$ eu.

by H atoms, Figure 7.1, clearly indicates two homologous series of compounds. For alkylsulfides and disulfides, Ekwenchi¹⁹⁷ has derived a linear relationship of the form

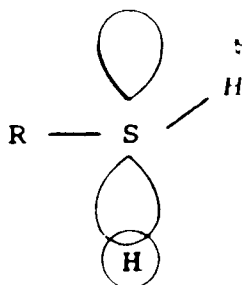
$$E_a = 19.36 + 0.9 \Delta H \text{ kcal mol}^{-1} \quad [3]$$

On the other hand, the alkanethiols follow another linear relationship of the form

$$E_a = 15.08 - 0.37 \Delta H \text{ kcal mol}^{-1} \quad [4]$$

The E_a value for CH_3SH is ignored in the determination of [4] since it appears to be questionable (Figure 7.1). From [4], the E_a for other H-atom reactions with alkanethiols can be predicted, e.g. for $\text{H} + n\text{-C}_3\text{H}_7\text{SH}$ ($\Delta H \approx -18.1 \text{ kcal mol}^{-1}$), $E_a \approx 1.62 \text{ kcal mol}^{-1}$.

The entropies of activation derived for the standard state of 1 atm from the experimental A factors (Table 7.4) are high and negative, suggesting a tight transition state. Good agreement is obtained between the experimental and the calculated entropies of activation if the assumed structure for the activated complex is a rigid complex in which the H atom interacts with the non-bonding 3p orbital of the sulfur atom:



The experimental entropies of activation derived for the

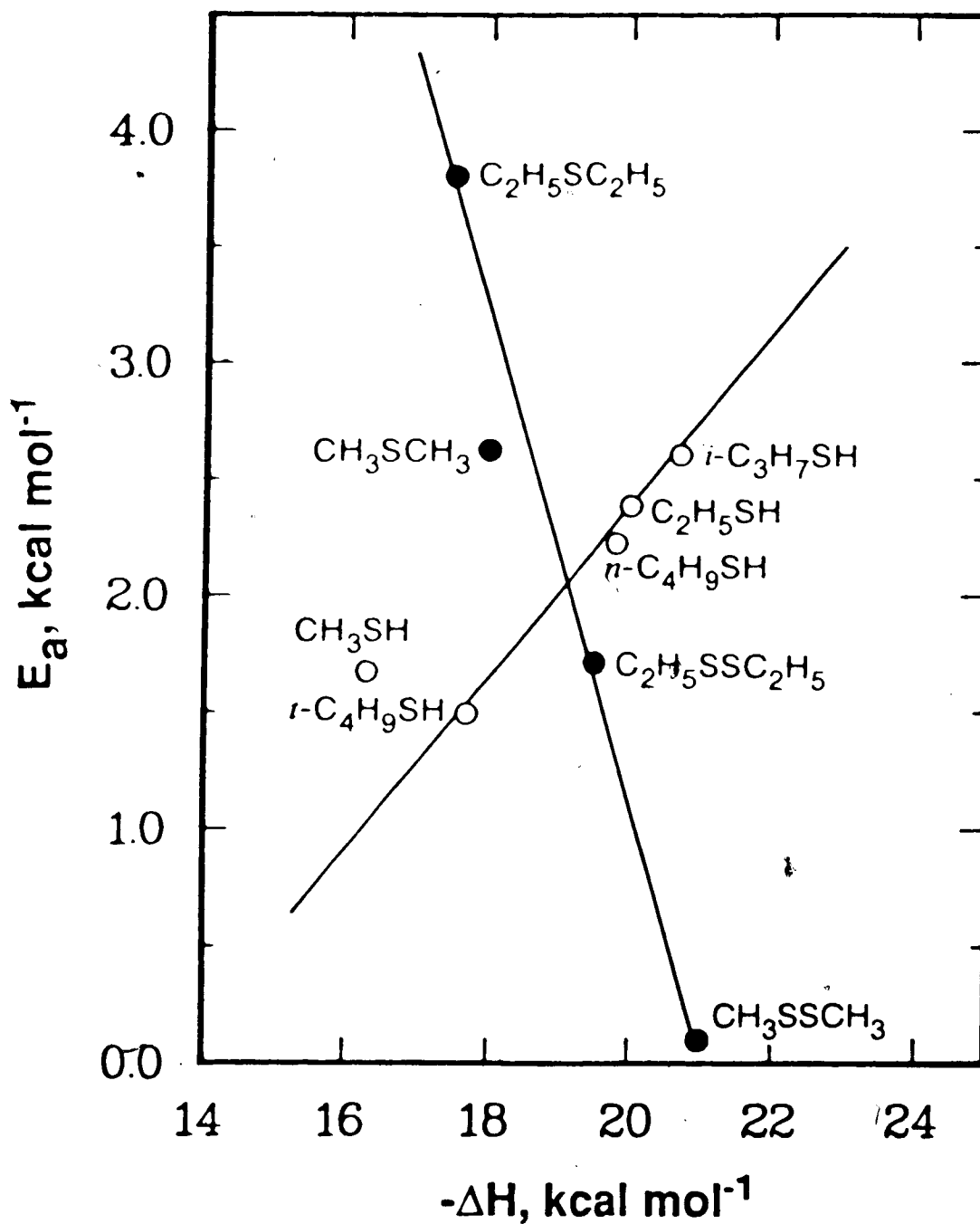


Figure 7.1. Empirical correlation between E_a and ΔH for the displacement reactions by H atoms.

H + thiol reactions are similar to those obtained for H + sulfides, suggesting transition states with similar structures.

The activation energies associated with the H + C₂H₅SH, *i*-C₃H₇SH and *t*-C₄H₉SH reactions are similar to those required for H + CH₃SCH₃ and C₂H₅SC₂H₅ reactions and this can be explained by similar C-S bond strengths. In contrast, the E_a's associated with the above reactions are somewhat higher than those derived for the corresponding H + disulfide reactions and this is undoubtedly due to the energy difference between the C-S and S-S bonds.

Relative Arrhenius parameters for the disproportionation/combination reactions of thiyl radical,



are tabulated in Table 7.5. If the activation energy required for the combination of thiyl radicals is negligible, *i.e.* E₁₂ ≈ 0 kcal mol⁻¹, then the difference in the activation energy, E₁₃ - E₁₂, is simply equal to E₁₃ and also, the rate constant for (12) has the same value as the pre-exponential factor, *i.e.* k₁₂ ≈ A₁₂. The rate constant for the recombination of CH₃S radicals, k₁₂ = 2.4 × 10¹³ cm³ mol⁻¹ s⁻¹,¹⁰⁹ has been found to be close to that for the recombination of CH₃ radicals, 2.5 × 10¹³ cm³ mol⁻¹ s⁻¹.¹¹³ Thus, from the values of the rate constants for the combination of alkyl radicals, the pre-exponential factors for the disproportionation of thiyl radical

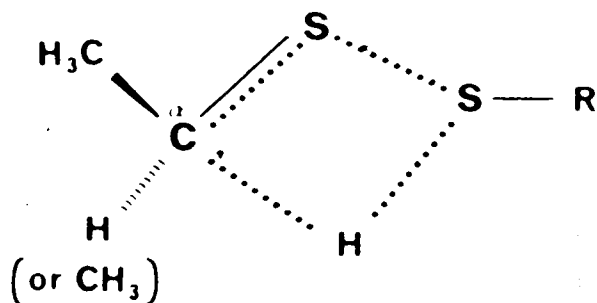
Table 7.5. Arrhenius Parameters for Disproportionation/Combination

Reactions of Thiyl Radicals

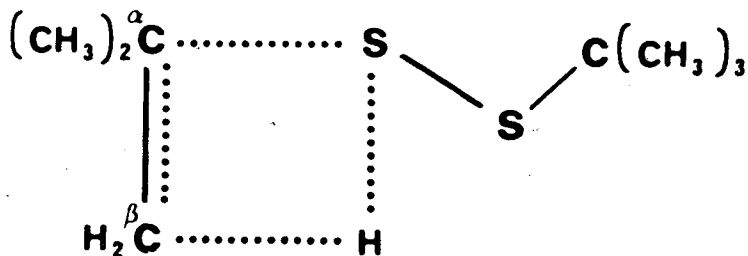
2 RS → RSSR (12)		→ dispr. products (13)		ΔS^\ddagger expt.
Reaction	A_{13}/A_{12}	$(E_{13} - E_{12})^a$ (kcal mol ⁻¹)	A_{12}^b (cm ³ mol ⁻¹ s ⁻¹)	
2 C ₂ H ₅ S → C ₂ H ₅ SSC ₂ H ₅	7 ± 3	3.1 ± 0.7	1.0 × 10 ¹³	-25.1
→ C ₂ H ₅ SH + CH ₃ C(S)H			7.3 × 10 ¹³	-21.2
2 <i>i</i> -C ₃ H ₇ S → (<i>i</i> -C ₃ H ₇) ₂ S ₂	4 ± 1	2.7 ± 0.5	5.0 × 10 ¹²	-26.5
→ <i>i</i> -C ₃ H ₇ SH + (CH ₃) ₂ CS			1.8 × 10 ¹³	-23.9
2 <i>t</i> -C ₄ H ₉ S → (<i>t</i> -C ₄ H ₉) ₂ S ₂	5.6 ± 0.5	1.7 ± 0.1	1.3 × 10 ¹²	-29.2
→ <i>i</i> -C ₄ H ₈ + <i>t</i> -C ₄ H ₉ SSH			7.1 × 10 ¹²	-25.8

^a(E₁₃ - E₁₂) ≈ E₁₃, since E₁₂ ≈ 0 kcal mol⁻¹ bestimated from k₁₂ for the combination of the corresponding alkyl radicals

reactions, A_{13} , can be estimated (Table 7.5). The experimental entropies of activation derived from the A factors of the disproportionation reactions, also listed in Table 7.5, are negative and slightly lower than those predicted for the displacement reactions (Table 7.4). The transition state for the former reaction is therefore a somewhat "looser" complex than that proposed for the latter. For C_2H_5S and $i-C_3H_7S$ radicals, the activated complex has the following assumed structure:



which leads to the cleavage of S-S and $\alpha C-H$ and the formation of C=S and S-H bonds. For $t-C_4H_9S$ radicals, however, product analysis and kinetic treatment of experimental results suggest the following structure for the activated complex:



in which the cleavage of C-S and β C-H and the formation of C=C and S-H bonds occur.

The entropies of activation increase with increasing alkyl substitution on the carbon α to sulfur atom, *i.e.* from C₂H₅S to \underline{t} -C₄H₉S radicals and this is due to hindered internal rotations which give rise to additional contributions to the entropy.

The lower activation energy associated with the disproportionation of \underline{t} -C₄H₉S radical, relative to that of C₂H₅S and \underline{i} -C₃H₇S radicals, is again attributed to the weaker C-S bond.

Results from the present investigation provide further insights into the industrially and biologically important processes involving organosulfur compounds. The mechanism of the photolysis of thiols has been reconciled from a complete kinetic treatment of the experimental results. Furthermore, reactions of H atoms with thiols are now better understood and thus provide a rationale for the observation that in the hydrodesulfurization of petroleums, large quantities of volatile, sulfur-containing material are produced, leaving hydrocarbon products. The rate constants obtained in the elementary reactions in the H + thiol systems serve to reduce the gap towards the basic understanding of the biological systems where the thiols and disulfides co-exist. It is hoped that the elucidation of the reactions of H atoms with relatively simple alkane thiols will provide an impetus for future studies towards

elucidating the effects of increasing the electron density on the sulfur atom, e.g. thiophenic and benzylic substrates. The ultimate aim would be to establish a suitable reference data base for this vital yet little understood process and, for the cases where data are not readily available for other molecules, to generate reasonable rates from computer simulation.

BIBLIOGRAPHY

1. P.C. Jocelyn, "Biochemistry of the SH Group", Academic Press, London, 1972.
2. J.E. Packer, "The Chemistry of the Thiol Group", S. Patai, Ed., Wiley, London, 1974, pp. 481 - 517.
3. Y.M. Torchinsky, "Sulfur in Proteins", translated by W. Wittenberg, Pergamon Press, London, 1981.
4. M.S. Blois, Jr., H.W. Brown, R.M. Lemmon, R.O. Lindblom and M. Weissbluth, Eds., "Free Radicals in Biological Systems", Academic Press, N.Y., 1961.
5. T. Henriksen, T.B. Melø and G. Sarebøl, "Free Radicals in Biology", W.A. Pryor, Ed., Academic Press, N.Y., Vol. II, 1976, pp. 213 - 256.
6. D. Harman, *ibid.*, Vol. V, 1982, pp. 255 - 275.
7. P. Markakis and A.L. Tappel, J. Am. Chem. Soc., 82, 1613 (1960).
8. A. Al-Thannqn, R.M. Peterson and C.N. Trumbore, J. Phys. Chem., 72, 2395 (1968).
9. J. T. Wu and R.R. Kuntz, Radiat. Res., 64, 662 (1975).
10. T.L. Tung and R.R. Kuntz, Radiat. Res., 55, 10 (1973).
11. D.A. Armstrong and V.G. Wilkening, Can. J. Chem., 42, 2631 (1964).
12. V.G. Wilkening, M. Lal, M. Arends and D.A. Armstrong, Can. J. Chem., 45, 1209 (1967).
13. V.G. Wilkening, M. Lal, M. Arends and D.A. Armstrong, J. Phys. Chem., 72, 185 (1968).
14. M.Z. Hoffman and E. Hayon, J. Am. Chem. Soc., 94,

- 7950 (1970).
15. G.C. Goyal and D.A. Armstrong, *Can. J. Chem.*, 54, 1938 (1976).
 16. G.C. Goyal and D.A. Armstrong, *J. Phys. Chem.*, 80, 1848 (1976).
 17. M. Lal and D.A. Armstrong, *Can. J. Chem.*, 63, 30 (1985).
 18. C.W. Gehrs, D.S. Shrimmer, S.E. Herbes, E.J. Salmon and H. Perry, "Chemistry of Coal Utilization", M.A. Elliott, Ed., Wiley, N.Y., Suppl. Vol. 2, 1981, pp. 2159 - 2233.
 19. W.L. Orr, "Oil Sand and Oil Shale Chemistry", O.P. Strausz and E.M. Lown, Eds., Verlag Chemie International, Inc., 1978, pp. 223 - 243.
 20. Y. Kawaguchi, I.G. Dalla Lana and F.D. Otto, *Can. J. Chem. Eng.*, 56, 65 (1978).
 21. H. Kwart, G.C.A. Schuit and B.C. Gates, *J. Catal.*, 61, 128 (1980).
 22. N.K. Nag, *Appl. Catal.*, 10, 53 (1984).
 23. M.L. Selucky, Y. Chu, T. Ruo and O.P. Strausz, *Fuel*, 56, 369 (1977).
 24. *ibid.*, *Fuel*, 57, 9 (1978).
 25. S.E. Stein, "Chemistry of Coal Conversion", R.H. Schlosberg, Ed., Plenum Press, N.Y., 1985, pp. 13 - 42.
 26. E.C. Kooymenn, *Pure Appl. Chem.*, 15, 81 (1967).
 27. K.K. Baldrige, M.S. Gordon and D.E. Johnson,
-

- J. Phys. Chem. 91, 4145 (1987).
28. R. Shaw, "The Chemistry of Thiol Group", S. Patai, Ed., Wiley, London, 1974, p. 160.
29. A. Ohno and S. Oae, "Organic Chemistry of Sulfur", S. Oae, Ed., Plenum Press, New York, N.Y., 1977, pp. 119 - 187.
30. P.W. Allen and L.E. Sutton, Acta Crystallogr., 3, 46 (1950).
31. T. Kojima, J. Phys. Soc. Jpn, 15, 1284 (1960).
32. A. Rauk and S. Collins, J. Mol. Spectrosc., 105, 438 (1984).
33. R.E. Schmidt and C.R. Quade, J. Chem. Phys., 62, 3864 (1975).
34. A.S. Manocha, W.G. Fateley and T. Shimanouchi, J. Phys. Chem., 77, 1977 (1973).
35. M. Ohsaku, T. Ichiishi, A. Imamura and M Hayashi, Bull. Chem. Soc. Jpn, 57, 2791 (1984).
36. W. Haines, R.V. Helm, C.W. Bailey and J.S. Ball. J. Am. Chem. Soc., 58, 270 (1954).
37. DMS UV Atlas of Organic Compounds, Butterworths, Vol. IV, I/6 (1966).
38. S.D. Thompson, D.G. Carroll, F. Watson, M. O'Donnell and S.P. McGlynn, J. Chem. Phys., 45, 1367 (1966).
39. G. Capozzi and G. Modena, "The Chemistry of the Thiol Group", S. Patai, Ed., Wiley, London, 1974, pp. 785 - 839.
40. A.R. Knight, ibid., pp. 455 - 479.

41. C. von Sonntag and H.P. Schuchmann, "The Chemistry of Ethers, Crown Ethers, Hydroxyl Groups and their Sulphur Analogues", S. Patai, Ed., Wiley, London, 1981, pp. 923 - 934.
42. R.A. Alberty, E. Burmenko, T.H. Kang and M.B. Cheung, J. Phys. Chem. Ref. Data., 16, 193 (1987).
43. K. Pihlaja and K. Rossi, J. Chem. Eng. Data, 30, 387 (1985).
44. B.K. Janousek, K.J. Reed and J.I. Brauman, J. Am. Chem. Soc., 102, 3125 (1980).
45. S.W. Benson, Chem. Rev., 78, 23 (1978).
46. H. Mackle and P.A.G. O'Hare, Tetrahedron, 19, 961 (1963).
47. H. Mackle, Tetrahedron, 19, 1159 (1963).
48. L.G.S. Shum and S.W. Benson, Int. J. Chem. Kinet., 17, 749 (1985).
49. M. Brouard, P.D. Lightfoot and M.J. Pilling, J. Phys. Chem., 90, 445 (1986).
50. R. Hiatt and S.W. Benson, Int. J. Chem. Kinet., 4, 151 (1972).
51. W. Tsang, Int. J. Chem. Kinet., 10, 821 (1978).
52. T.S.A. Islam and S.W. Benson, Int. J. Chem. Kinet., 16, 995 (1984).
53. C.E. Canosa and R.M. Marshall, Int. J. Chem. Kinet., 13, 303 (1981).
54. JANAF Thermochemical Tables, 2nd ed., NSRDS-NBS, No. 37, 1971.

55. M. Messner and H.W. Thompson, *Trans. Far. Soc.*, 34, 1238 (1938).
56. N.P. Skerrett and H.W. Thompson, *Trans. Far. Soc.*, 37, 81 (1941).
57. W.E. Haines, G.L. Cook and J.S. Ball, *J. Am. Chem. Soc.*, 78, 5213 (1956).
58. T. Inaba and B. de B. Darwent, *J. Phys. Chem.*, 64, 1431 (1960).
59. R.P. Steer, B.L. Kalra and A.R. Knight, *J. Phys. Chem.*, 71, 783 (1967).
60. B.G. Dzantiev, A.V. Shishkov and M.S. Unukovich, *Khim. Vys. Energii*, 3, 111 (1969).
61. R.P. Steer and A.R. Knight, *J. Phys. Chem.*, 72, 2145 (1968).
62. G. Greigg and J.C.J. Thynne, *Trans. Far. Soc.*, 62, 379 (1966).
63. L. Bridges, G.L. Hemphill and J.M. White, *J. Phys. Chem.*, 76, 2668 (1972).
64. R.P. Steer and A.R. Knight, *Can. J. Chem.*, 46, 2878 (1968).
65. G.P. Sturm, Jr. and J.M. White, *J. Chem. Phys.*, 50, 5035 (1969).
66. L. Bridges and J.M. White, *J. Phys. Chem.*, 77, 295 (1973).
67. R.P. Steer and A.R. Knight, *Can. J. Chem.*, 47, 1335 (1969).
68. W.A. Pryor, "Mechanism of Sulfur Reactions", McGraw-

- Hill, New York, N.Y., 1962.
69. D.D. Carlson and A.R. Knight, *Can. J. Chem.*, 51, 1410 (1973).
 70. W.A. Pryor and E.G. Olsen, *J. Am. Chem. Soc.*, 100, 2852 (1978).
 71. W.E. Jones, S.D. MacKnight and L. Teng, *Chem. Rev.*, 73, 407 (1973) and references therein.
 72. I. Safarik and O.P. Strausz, *Rev. Chem. Intermed.*, 6, 143 (1985).
 73. R. Wolfgang, "Progress in Reaction Kinetics", G. Porter, Ed., 3, 97 (1965).
 74. C. Vermeil, *Israel J. Chem.*, 8, 147 (1970).
 75. R.R. Kuntz, *J. Phys. Chem.*, 71, 3343 (1967).
 76. J.H. Lee, J.V. Michael, W.A. Payne and L.J. Stief, *J. Chem. Phys.*, 68, 1817 (1978).
 77. A. Amano, M. Yamada, K. Hashimoto and K. Sugiura, *Nippon Kagaku Kaishi*, 385 (1983).
 78. R.J. Balla and J. Heicklen, *J. Phys. Chem.* 89, 4596 (1985).
 79. P.H. Wine, J.M. Nicovich, A.J. Hynes and J.R. Wells, *J. Phys. Chem.*, 90, 4033 (1986).
 80. O. Horie, J. Nishimo and A. Amano, *Int. J. Chem. Kinet.*, 10, 1043 (1978).
 81. W.L. Severs, P.A. Hamilton, T.L. Tung and J.A. Stone, *Int. J. Radiat. Phys. Chem.*, 8, 461 (1976).
 82. G.G. Jayson, D.A. Stirling and A.J. Swallow, *Int. J. Radiat. Biol.*, 19, 143 (1971).

83. F.E. Littman, E.M. Carr and A.P. Brody, *Radiat. Res.*, 7, 107 (1957).
84. G. Navon and G. Stein, *Israel J. Chem.*, 2, 151 (1964).
85. P. Neta and R.H. Schuler, *Radiat. Res.*, 47, 612 (1971).
86. C.J. Thompson, R.A. Meyer and J.S. Ball, *J. Am. Chem. Soc.*, 74, 3284 (1952).
87. *ibid.*, 3287 (1952).
88. A.H. Sehon and B. de B. Darwent, *J. Am. Chem. Soc.*, 76, 4806 (1954).
89. W. Tsang, *J. Chem. Phys.*, 40, 1498 (1964).
90. T.O. Bamkole, *J. Chem. Soc., Perkin Trans. II*, 439 (1977).
91. G. Martin and N. Barroeta, *Int. J. Chem. Kinet.*, 12, 699 (1980).
92. M. Yamada, T. Yosuke, K. Tohru, Y. Oshima and A. Amano, *Nippon Kagaku Kaishi, Jpn*, 8, 1560 (1985).
93. M. Yamada, T. Kamo, J. Tang Y. Oshima and A. Amano, *Nippon Kagaku Kaishi, Jpn*, 12, 2283 (1985).
94. M.M. Ekwenchi, Ph.D. Thesis, University of Alberta, 1980, pp. 29 - 33.
95. G. Jayson, D. Stirling and A. Swallow, *Int. J. Radiat. Biol.*, 19, 153 (1970).
96. M.Z. Hoffman and E. Hayon, *J. Am. Chem. Soc.*, 94, 7950 (1972).
97. Yu.V. Razskazovsky and M.Ya. Mel'nikov, *J. Photochem.*, 27, 239 (1984).

98. A.B. Callear, J. Connor and D.R. Dickson, *Nature*, 221, 1238 (1969).
99. A.B. Callear and D.R. Dickson, *Trans. Far. Soc.*, 66, 1987 (1970).
100. D.H. Volman, J. Wolstenholme and S.G. Hadley, *J. Phys. Chem.*, 71, 1798 (1967).
101. P.S.H. Bolman, I. Safarik, D.A. Stiles, W.J.R. Tyerman and O.P. Strausz, *Can. J. Chem.*, 48, 3872 (1970).
102. K.J. Rosengren, *Acta Chem. Scand.*, 16, 1401, 1418 (1962).
103. J.K.S. Klan, *Chem. Commun.*, 429 (1967).
104. D.J. Nelson, R.L. Peterson and M.C.R. Symons, *J. Chem. Soc., Perkins Trans. II*, 225 (1978).
105. Yu.V. Razskazovsky and M.Ya. Mel'nikov, *Radiochem. Radioanal. Lett.*, 46, 129 (1981).
106. Yu.V. Razskazovsky and M.Ya. Mel'nikov, *Radiochem. Radioanal. Lett.*, 54, 339 (1982).
107. J. Heicklen, *Rev. Chem. Intermed.*, 6, 175 (1985).
108. P.M. Rao and A.R. Knight, *Can. J. Chem.*, 50, 844 (1972).
109. D.R. Tycholiz and A.R. Knight, *J. Am. Chem. Soc.*, 95, 1726 (1973).
110. M.M. Ekwenchi, A. Jodhan and O.P. Strausz, *Int. J. Chem. Kinet.*, 12, 431 (1980).
111. C.S. Smith and A.R. Knight, *Can. J. Chem.*, 54, 1290 (1976).

112. J. Heicklen and H.S. Johnson, *J. Am. Chem. Soc.*, 84, 4030, 4394 (1962).
113. S.W. Benson, *Account. Chem. Res.*, 19, 335 (1986).
114. P.M. Rao, J.A. Copeck and A.R. Knight, *Can. J. Chem.*, 45, 1369 (1967).
115. M.M. Ekwenchi, I. Safarik and O.P. Strausz, *Int. J. Chem. Kinet.*, 13, 799 (1981).
116. J.A.R. Coope and W.A. Bryce, *Can. J. Chem.*, 32, 768 (1954).
117. J.K. Kochi and P.J. Krusic, "Essays on Free Radical Chemistry", *Chem. Soc. Specialist Periodical Report* no. 24, London, 1971, p. 147.
118. P.J. Krusic and J.K. Kochi, *J. Am. Chem. Soc.*, 93, 846 (1971).
119. T. Kawamura, M. Ushio, T. Fujimoto and T. Monazawa, *J. Am. Chem. Soc.*, 93, 908 (1971).
120. L. Lunazzi, G. Placucci and L. Grossi, *J. Chem. Soc. Chem. Commun.*, 533 (1979).
121. L. Lunazzi, G. Placucci and L. Grossi, *J. Chem. Soc., Perkin Trans. II*, 703 (1981).
122. R.J. Balla, B.R. Weiner and H.H. Nelson, *J. Am. Chem. Soc.*, 109, 4804 (1987).
123. H. Niki, P.D. Maker, C.M. Savage and L.P. Breitenbach, *J. Phys. Chem.*, 87, 7 (1983).
124. D. Gutman, N. Sanders and J.E. Butler, *J. Phys. Chem.*, 86, 66 (1982).

125. R.J. Balla and J. Heicklen, *Can. J. Chem.*, 62, 162 (1984).
126. S. Hatakeyama and H. Akimoto, *J. Phys. Chem.*, 87, 2387 (1983).
127. R.J. Balla and J. Heicklen, *J. Photochem.*, 29, 297 (1985).
128. D. Grosjean, *Environ. Sci. Tech.*, 18, 460 (1984).
129. R.J. Balla and J. Heicklen, *J. Phys. Chem.*, 88, 6314 (1984).
130. P.M. Rao and A.R. Knight, *Can. J. Chem.*, 46, 2462 (1968).
131. T. Yokota and O.P. Strausz, *J. Phys. Chem.*, 83, 3196 (1979).
132. W.A. Pryor and K. Smith, *J. Am. Chem. Soc.*, 92, 2731 (1970).
133. M. Bonifacic and K.D. Asmus, *J. Phys. Chem.*, 88, 6286 (1984).
134. K. Sayamol and A.R. Knight, *Can. J. Chem.*, 46, 999 (1968).
135. D. Gupta and A.R. Knight, *Can. J. Chem.*, 58, 1350 (1980).
136. H. Pelzer and E. Wigner, *Z. Phys. Chem. (Leipzig)*, B15, 445 (1932).
137. H. Eyring, *J. Chem. Phys.*, 3, 107 (1935).
138. S. Glasstone, K.J. Laidler and H. Eyring, "Theory of Rate Processes", McGraw-Hill, New York, 1940.

139. D.G. Truhler, W.L. Hase and J.T. Hynes, J. Phys. Chem., 87, 2664 (1983).
140. S.W. Benson, "Proceeding of the Symposium on Chemical Kinetics Data for the Upper and Lower Atmosphere", S.W. Benson, D.M. Golden and J.R. Basker, Ed., Wiley, N.Y., 1975, pp. 359 - 377.
141. S.W. Benson, "Thermochemical Kinetics", 2nd ed., Wiley, N.Y., 1976.
142. B.S. Rabinovitch and D.W. Setser, "Advances in Photochemistry", Vol. 3. W.A. Noyes, G.S. Hammond and J.N. Pitts, Jr., Ed., Wiley, New York, N.Y., 1964.
143. T.L. Pollock, Ph.D. Thesis, University of Alberta, 1971.
144. R.J. Cvetanovic, "Progress in Reaction Kinetics", Vol. II. G. Porter, Ed., Pergamon Press, New York, N.Y., 1963.
145. R.A. Back, Can. J. Chem., 37, 1834 (1959).
146. G.S. Forbes, J.E. Cline, and B.C. Bradshaw, J. Am. Chem. Soc., 60, 1005 (1938).
147. B. de B. Darwent, and R. Roberts, Proc. Roy. Soc. (London) A216, 344 (1953).
148. R.G. Gann, and J. Dubrin, J. Chem. Phys. 47, 1867 (1967).
149. L.E. Compton, J.L. Gole and R.M. Martin, J. Phys. Chem., 73, 1158 (1969).
150. G.R. De Maré, O.P. Strausz and H.E. Gunning, Can. J. Chem., 43, 1329 (1965).

151. O.P. Strausz, R.J. Norstrom, D. Salahub, R.K. Gosavi, H.E. Gunning and I.G. Csizmadia, *J. Am. Chem. Soc.*, 92, 6395 (1970).
152. D.R. Stull, *Industrial and Engineering Chemistry*, 39, 517 (1947).
153. G. Gorin and G. Dougherty, *J. Org. Chem.*, 21, 241 (1956).
154. J.G. Calvert and J.N. Pitts, Jr., "Photochemistry", Wiley, New York, N.Y., 1966, p. 490.
155. A.B. Callear and J.C. McGurk, *J. Chem. Soc., Far. Trans. II*, 68, 289 (1972).
156. A.B. Callear and P.M. Wood, *ibid.*, 302 (1972).
157. A.C. Vikis and D.J. LeRoy, *Can. J. Chem.*, 51, 8207 (1973).
158. *ibid.*, 50, 595 (1972).
159. T.L. Pollock, E.J. Jakubowski, H.E. Gunning and O.P. Strausz, *Can. J. Chem.*, 47, 3474 (1969).
160. G.P. Sturm, Jr. and J.M. White, *J. Phys. Chem.*, 72, 3679 (1968).
161. A. Jones, S. Yamashita and F.P. Lossing, *Can. J. Chem.*, 46, 833 (1968).
162. S. Yamashita and F.P. Lossing, *Can. J. Chem.*, 46, 2925 (1968).
163. W.B. DeMore and S.W. Benson, "Advances in Photochemistry", W.A. Noyes, G.S. Hammond and J.N. Pitts, Jr., Eds., Vol. 2, Wiley, New York, N.Y., 1964.

164. W.L. Hase and H.B. Schlegel, *J. Phys. Chem.*, 86, 3901 (1982).
165. M.M. Ekwenchi, I. Safarik and O.P. Strausz, *Can. J. Chem.*, 59, 3226 (1981).
166. J.E. Baldwin and R.C.G. Lopez, *J. Chem. Soc. Chem. Comm.*, 18, 1029 (1982).
167. J.M. White, R.L. Johnson, Jr. and D. Bacon, *J. Chem. Phys.*, 52, 5212 (1970).
168. J.M. White and R.L. Johnson, Jr., *J. Chem. Phys.*, 56, 3787 (1972).
169. R.E. Rebbert and P. Ausloos, *J. Chem. Phys.*, 47, 2849 (1967).
170. P.C. Kobrinsky and R.M. Martin, *J. Chem. Phys.*, 48, 5728 (1968).
171. A.B. Trenwith, *J. Chem. Soc., Far. Trans. 2*, 82, 457 (1986).
172. G.A. Oldershaw and D.A. Porter, *Nature*, 223, 490 (1969).
173. H. Böhme, "Methoden der Organischen Chemie", E. Muller, Ed., Vol. IX, 4th ed., Georg. Thieme Verlag, Stuttgart, 1955, pp. 49 - 54.
174. A. Ohno, "Organic Chemistry of Sulfur", S. Oae, Ed., Plenum Press, New York, N.Y., 1977, p. 196.
175. S.W. Benson and H.E. O'Neal, *Natl. Stand. Ref. Data Ser. (U.S., Natl. Bur. Stand.)*, No. 21 (1971).
176. G.W. Harris and J.N. Pitts, Jr., *J. Chem. Phys.*, 77, 3994 (1982).

177. T. Watanabe, T. Kyogoku, S. Tsunashima, S. Sato and S. Nagase, *Bull. Chem. Soc. Jpn*, 55, 3720 (1982).
178. K.R. Jennings and R.J. Cvetanovic, *J. Chem. Phys.*, 35, 1233 (1961).
179. G.R. Woolley and R.J. Cvetanovic, *J. Chem. Phys.*, 50, 4697 (1969).
180. R.J. Cvetanovic and L.C. Doyle, *J. Chem. Phys.*, 50, 4705 (1969).
181. H.G. Wagner and R. Zellner, *Ber. Bunsenges Ges.*, 76, 518 (1972).
182. P. Arrowsmith, *J. Chem. Soc. Far. Trans. I.*, 74, 3016 (1978).
183. A. Schöberl and A. Wagner, "Methoden der Organischen Chemie", E. Muller, Ed., Vol. IX, 4th ed., Georg. Thieme Verlag, Stuttgart, 1955, p. 43.
184. R. Mayer, "Organic Chemistry of Sulfur", S. Oae, Ed., Plenum Press, New York, N.Y., 1977, p. 55.
185. S.W. Benson and H.E. O'Neal, "Kinetic Data on Gas-phase Unimolecular Reactions", NSRDS-NBS21 (U.S. Dept. of Commerce, NBS, 1970).
186. B.S. Rabinovitch and R.W. Diesen, *J. Chem. Phys.*, 30, 735 (1959).
187. B.S. Rabinovitch, R.F. Kubin and R.E. Harrington, *J. Chem. Phys.*, 38, 405 (1963).
188. D.S. Bethune, J.R. Lankard, P.P. Sorokin, A.J. Schell-Sorokin, R.M. Pleceni and Ph. Avouris, *J. Chem. Phys.*, 75, 2231 (1981).

189. S.W. Benson, *J. Phys. Chem.*, 89, 4366 (1985).
190. J.R. Cao and M.H. Back, *Can. J. Chem.*, 62, 86 (1984).
191. G.W. Byers, H. Gruen, H.G. Giles, H.W. Schott and J.A. Kampmeier, *J. Am. Chem. Soc.*, 94, 1016 (1972).
192. A. Joshi and G.C. Yang, *J. Org. Chem.*, 46, 3736 (1981).
193. U. Zoller, "Small Ring Heterocycles", A. Hassner, Ed., Vol. 42, Part 1, Wiley, N.Y., 1983, pp. 333-449.
194. W.B. O'Callaghan, Ph.D. Thesis, University of Alberta, 1970.
195. M.G. Evans and M. Polanyi, *Trans. Far. Soc.*, 34, 11 (1938).
196. N.N. Semenov, "Some Problems of Chemical Kinetics and Reactivity", Vol. 1, translated by J.E.S. Bradley, Pergamon Press, London, 1958, pp. 27 - 30.
197. Reference 94, p. 158.
198. R.B. Cundall and A. Gilbert, "Photochemistry", Nelson Press, London, 1970.
199. J.O. Hirschfelder, C.F. Curtiss and R.B. Byrd, "Molecular Theory of Gases and Liquids",
200. M.F.R. Mulcahy, "Gas Kinetics", Wiley, N.Y., 1973.

APPENDIX A

COMPETITIVE QUENCHING BETWEEN H_2 AND C_2H_5SH

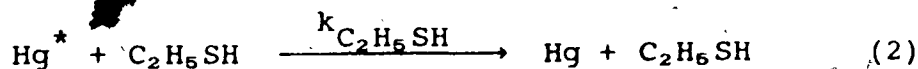
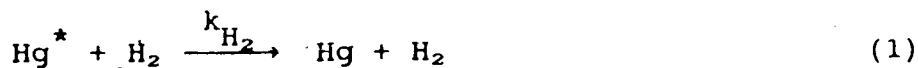
When Hg-photosensitization experiments are carried out in the presence of more than one substrate, the amount of quenching of Hg^* by each substrate can be readily calculated, as shown for the $H_2-C_2H_5SH$ case.

From simple collision theory, the bimolecular quenching rate constant is given by:

$$k_Q = \sigma_Q^2 \left[8\pi RT \left(\frac{M_{Hg} + M_Q}{M_{Hg} M_Q} \right) \right]^{\frac{1}{2}} \quad (i)$$

where σ^2 is the collisional cross-section, M the molecular weight, Q may be either H_2 or C_2H_5SH , and the other terms have their usual significance.

Consider the following reactions:



The rate expressions for reactions (1) and (2) are:

$$\text{Rate (Hg + H}_2) = k_{H_2} [Hg][H_2] \quad (ii)$$

$$\text{Rate (Hg + C}_2H_5SH) = k_{C_2H_5SH} [Hg][C_2H_5SH] \quad (iii)$$

Dividing (ii) by (iii), we have:

$$\frac{\text{Rate (Hg + H}_2)}{\text{Rate (Hg + C}_2H_5SH)} = \frac{k_{H_2} [H_2]}{k_{C_2H_5SH} [C_2H_5SH]} \quad (iv)$$

Substituting for k_{H_2} and $k_{C_2H_5SH}$ in Equation (i), Equation (iv) becomes:

$$\frac{k_{H_2} [H_2]}{k_{C_2H_6SH} [C_2H_6SH]} = \frac{\sigma_{H_2}^2}{\sigma_{C_2H_6SH}^2} \left[\frac{M_{C_2H_6SH} \left(\frac{M_{Hg} + M_{H_2}}{M_{Hg} + M_{C_2H_6SH}} \right)}{M_{H_2}} \right]^{\frac{1}{2}} \quad (v)$$

Since $\sigma_{H_2}^2 = 10 \text{ \AA}^2$,¹⁹⁸ $\sigma_{C_2H_6SH}^2 = 29 \text{ \AA}^2$,¹⁹⁹ $M_{H_2} = 2$, $M_{C_2H_6SH} = 62$, $M_{Hg} = 200$, and in the present study, $[H_2] = 600$ Torr and $[C_2H_6SH] = 60$ Torr, Equation (v) becomes:

$$\frac{k_{H_2} [H_2]}{k_{C_2H_6SH} [C_2H_6SH]} = \frac{10}{29} \left[\frac{62}{2} \left(\frac{202}{229} \right) \right]^{\frac{1}{2}} \cdot \frac{600}{60} = 18.0$$

Therefore, the percentage quenching by H_2 is given by:

$$\frac{k_{H_2} [H_2] [Hg]}{k_{H_2} [H_2] [Hg] + k_{C_2H_6SH} [C_2H_6SH] [Hg]} \times 100$$

$$= \frac{1}{1.056} \times 100 = 94.7\%$$

APPENDIX B

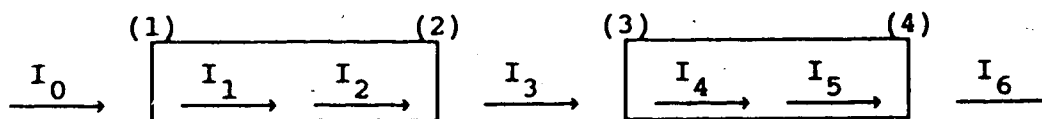
DETERMINATION OF I_a FROM CHEMICAL ACTINOMETRY

When the incident light passes through an absorbing sample placed along its path, its intensity will be altered. For monochromatic light, the Beer-Lambert law defines the intensity of the light transmitted through a sample, I , to be:

$$I = I_0 10^{-\epsilon lc} \quad (i)$$

where I_0 is the intensity of the incident light; ϵ , the extinction coefficient or the absorbance of the sample; l , the path length of light; and c , the concentration of the sample. The transmittance of a sample is given by the ratio, I/I_0 . Also, the intensity of light absorbed by the sample is given by the difference, $(I_0 - I)$.

From the actinometric set-up, two quartz vessels are placed in the optical train. The light intensity is decreased due to absorption by the two vessels and the four vessel windows. This is shown schematically below:



The transmittances of light through the four vessel windows are represented by the following relations: $w_1 = I_1/I_0$, $w_2 = I_3/I_2$, $w_3 = I_4/I_3$, and $w_4 = I_6/I_5$, respectively.

The intensity of light absorbed by the first vessel, I_a , and that by the second vessel, I_b , is given by:-

$$I_a = I_1 - I_2 \quad (ii)$$

$$I_b = I_4 - I_5 \quad (\text{iii})$$

To relate I_a to I_b , Equations (ii) and (iii) are transformed using the light transmittances through the vessel windows, w_1 to w_4 , as follows:

$$I_a = w_1 I_0 - I_3/w_2 \quad (\text{iv})$$

$$I_b = w_3 I_3 - I_6/w_4 \quad (\text{v})$$

Rearranging (v) in terms of I_3 , we have:

$$I_3 = \frac{(I_b + I_6/w_4)}{w_3} \quad (\text{vi})$$

Substituting for I_3 in (iv) gives an expression relating I_a and I_b :

$$I_a = w_1 I_0 - \frac{(I_b + (I_6/w_4))}{w_2 w_3} \quad (\text{vii})$$

I_0 and I_6 are the light intensities when there are no vessels in the optical train, and when both are present, respectively. Their values are determined from the output signals, S_0 and S_6 , on the readout meter by the following expressions:

$$I_0 = \sigma S_0 \quad (\text{viii})$$

$$I_6 = \sigma S_6 \quad (\text{ix})$$

where, σ is the correlation factor between light intensity and output signal of the photocell. Using (viii) and (ix) to substitute for I_0 and I_6 in (vii), we have the final derived expression relating I_a to I_b :

$$I_a = [w_1 S_0 - (S_6 / w_2 w_3 w_4)] \sigma - I_b / w_2 w_3$$

The values of w_1 to w_4 are obtained directly from the ratio S_6/S_0 at the beginning of each experiment using empty vessels. Finally, σ is determined from H_2S photolysis experiments using 760 Torr H_2S in both vessels.

APPENDIX C

COMPETITIVE QUENCHING BETWEEN THIOL AND ADDED THERMALIZER

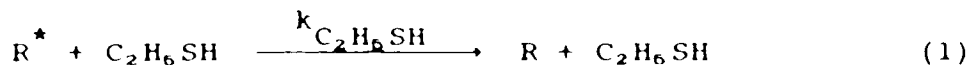
In the photolysis of thiol with added thermalizer, quenching of hot H atoms and hot alkyl radicals may be effected by either the thiol molecule or the thermalizer molecule. In the case of H atoms, the excess energy is kinetic while in the case of alkyl radicals it is probably vibrational. The cooling of hot atoms has been discussed extensively by Wolfgang⁷³ and that of vibrationally excited radicals has been treated by Rabinovitch and Setser¹⁴² in terms of strong and weak collision models. In both cases, these processes have been shown to be multi-collisional rather than a single collision process, however, single collision equations can be applied, and are an acceptable approximation. Thus, the amount of quenching by each can be readily calculated using simple collision theory model, as shown in the following example for the C₂H₅SH - CO₂ case.

From simple collision theory, the bimolecular quenching rate constant is given by:

$$k_Q = \sigma_Q^2 \left[8\pi RT \left(\frac{M_{R^*} + M_Q}{M_{R^*} M_Q} \right) \right]^{\frac{1}{2}} \quad (i)$$

where σ^2 is the collisional cross-section, M the molecular weight, Q may be either C₂H₅SH or CO₂, R* may be either H* or C₂H₅* , and the other terms have their usual significance.

Consider the following reactions:



The rate expressions for reactions (1) and (2) are:

$$\text{Rate } (R + C_2H_6SH) = k_{C_2H_6SH} [R^*] [C_2H_6SH] \quad (ii)$$

$$\text{Rate } (R + CO_2) = k_{CO_2} [R^*] [CO_2] \quad (iii)$$

Dividing (ii) by (iii), we have:

$$\frac{\text{Rate } (R + C_2H_6SH)}{\text{Rate } (R + CO_2)} = \frac{k_{C_2H_6SH} [C_2H_6SH]}{k_{CO_2} [CO_2]} \quad (iv)$$

Substituting for $k_{C_2H_6SH}$ and k_{CO_2} in Equation (i), Equation (iv) becomes:

$$\frac{k_{C_2H_6SH} [C_2H_6SH]}{k_{CO_2} [CO_2]} = \left[\frac{\sigma_{C_2H_6SH} + \sigma_{R^*}}{\sigma_{CO_2} + \sigma_{R^*}} \right]^2 \cdot \left[\frac{M_{CO_2}}{M_{C_2H_6SH}} \left(\frac{M_{R^*} + M_{C_2H_6SH}}{M_{R^*} + M_{CO_2}} \right) \right]^{\frac{1}{2}} \cdot \frac{[C_2H_6SH]}{[CO_2]} \quad (v)$$

Since $\sigma_{C_2H_5OH} = 4.5 \text{ \AA},^{199}$ we can estimate $\sigma_{C_2H_6SH} \approx 4.9 \text{ \AA}$.

Also, $\sigma_{CO_2} = 3.9 \text{ \AA},^{199}$ $M_{C_2H_6SH} = 62$, $M_{CO_2} = 44$, $[C_2H_6SH] = 10 \text{ Torr}$, $[CO_2] = \text{variable at } 20 - 400 \text{ Torr}$, and for $R^* = C_2H_6^*$, $\sigma_{C_2H_6^*} \approx \sigma_{C_2H_6} \approx 4.9 \text{ \AA},^{142}$ $M_{C_2H_6} = 29$, Equation (v) becomes:

$$\frac{k_{C_2H_6SH} [C_2H_6SH]}{k_{CO_2} [CO_2]} = \frac{96}{77} \left[\frac{44 \left(\frac{91}{73} \right) \right]^{\frac{1}{2}} \cdot \frac{10}{[CO_2]} = \frac{11.7}{[CO_2]} \quad (vi)$$

Therefore, the percentage quenching of $C_2H_6^*$ by CO_2 is given

by:

$$\frac{k_{\text{CO}_2} [\text{CO}_2] [\text{C}_2\text{H}_6^*]}{k_{\text{CO}_2} [\text{CO}_2] [\text{C}_2\text{H}_6^*] + k_{\text{C}_2\text{H}_6\text{SH}} [\text{C}_2\text{H}_6\text{SH}] [\text{C}_2\text{H}_6^*]} \times 100$$

$$= \frac{[\text{CO}_2]}{[\text{CO}_2] + 11.7} \times 100 \quad (\text{vii})$$

Similarly, for $R^* = \text{H}^*$, $\sigma_{\text{H}^*} \approx \sigma_{\text{H}_2} \approx 0.75 \text{ \AA}^{200}$ we have, from Equation (v):

$$\frac{k_{\text{C}_2\text{H}_6\text{SH}} [\text{C}_2\text{H}_6\text{SH}]}{k_{\text{CO}_2} [\text{CO}_2]} = \frac{32}{22} \left[\frac{44}{62} \left(\frac{63}{45} \right) \right]^{\frac{1}{2}} \cdot \frac{10}{[\text{CO}_2]}$$

$$= \frac{14.5}{[\text{CO}_2]} \quad (\text{viii})$$

Therefore, the percentage quenching of H^* by CO_2 is given by:

$$\frac{k_{\text{CO}_2} [\text{CO}_2] [\text{H}^*]}{k_{\text{CO}_2} [\text{CO}_2] [\text{H}^*] + k_{\text{C}_2\text{H}_6\text{SH}} [\text{C}_2\text{H}_6\text{SH}] [\text{H}^*]} \times 100$$

$$= \frac{[\text{CO}_2]}{[\text{CO}_2] + 14.7} \times 100 \quad (\text{ix})$$

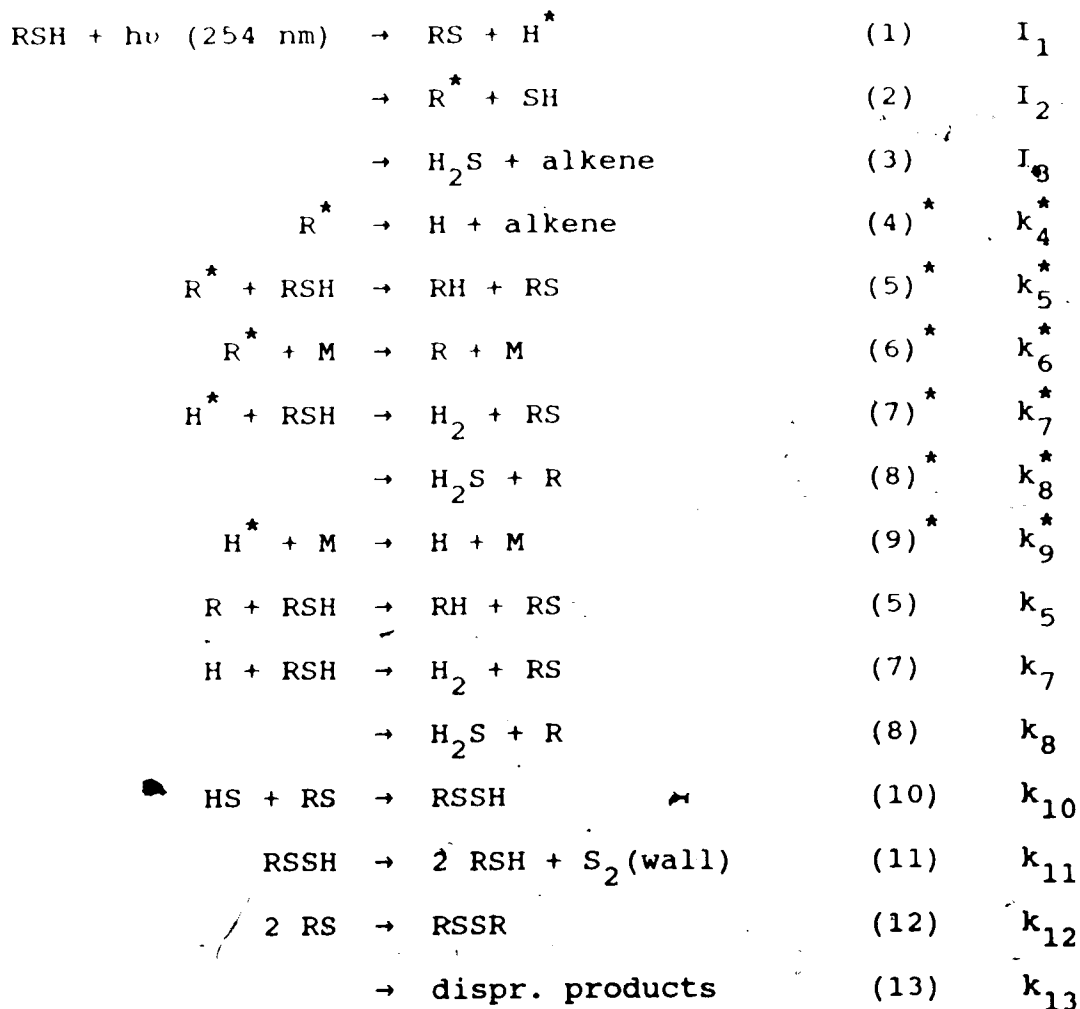
Finally, the percentage quenching of C_2H_6^* and H^* by CO_2 , as given by (vii) and (ix) respectively, is tabulated as a function of $[\text{CO}_2]$ below:

[CO ₂] (Torr)	% quenching by CO ₂	
	C ₂ H ₆ [*]	H [*]
20	63	58
50	81	77
100	90	87
200	94	93
300	96	95
400	97	96

APPENDIX D

PRODUCT QUANTUM YIELD EXPRESSIONS DERIVED IN THE PHOTOLYSIS
OF ALKANE THIOLS

D.1. Reaction Mechanism



where R, RH, alkene and disproportionation products are defined in the following table :

	RSH		
	C_2H_5SH	$i-C_3H_7SH$	$t-C_4H_9SH$
R	C_2H_5	$i-C_3H_7$	$t-C_4H_9$
RH	C_2H_6	C_3H_8	$i-C_4H_{10}$
alkene	C_2H_4	C_3H_6	$i-C_4H_8$
dispr. product	C_2H_5SH + CH_3CHS	$i-C_3H_7SH$ + $(CH_3)_2CS$	$t-C_4H_9SSH$ + $i-C_4H_8$

D.2. Steady-state Expressions for Intermediates

$$\frac{\delta [H^*]}{\delta t} = I_1 - (k_7^* + k_8^*) [H^*] [RSH] - k_9^* [H^*] [M] = 0$$

$$\Rightarrow [H^*] = \frac{I_1}{(k_7^* + k_8^*) [RSH] + k_9^* [M]} \quad (i)$$

$$\frac{\delta [R^*]}{\delta t} = I_2 - (k_4^* + k_5^* [RSH] + k_6^* [M]) [R^*] = 0$$

$$\Rightarrow [R^*] = \frac{I_2}{k_4^* + k_5^* [RSH] + k_6^* [M]} \quad (ii)$$

$$\frac{\delta [H]}{\delta t} = k_4^* [R^*] + k_9^* [H^*] [M] - (k_7 + k_8) [H] [RSH] = 0$$

$$\Rightarrow [H] = \frac{k_4^* [R^*] + k_9^* [H^*] [M]}{(k_7 + k_8) [RSH]} \quad (iii)$$

$$\frac{\delta[R]}{\delta t} = k_6^*[R^*][M] + (k_8^*[H^*] - k_5[R] + k_8[H])[RSH] = 0$$

$$\Rightarrow [R] = \frac{k_6^*[R^*][M] + (k_8^*[H^*] + k_8[H])[RSH]}{k_5[RSH]} \quad (\text{iv})$$

$$\frac{\delta[HS]}{\delta t} = I_2 - k_{10}[RS][HS] = 0$$

$$\Rightarrow [HS] = \frac{I_2}{k_{10}[RS]} \quad (\text{v})$$

$$\begin{aligned} \frac{\delta[RS]}{\delta t} = I_1 + (k_5^*[R^*] + k_7^*[H^*] + k_5[R] + k_7[H])[RSH] \\ - k_{10}[RS][HS] - 2(k_{12} + k_{13})[RS]^2 = 0 \end{aligned}$$

$$\Rightarrow [RS] = \left[\frac{I_1}{k_{12} + k_{13}} \right]^{\frac{1}{2}} \quad (\text{vi})$$

D.3. Rate Expressions for the Photolysis Products

$$\begin{aligned} \text{Rate (alkene)} &= I_3 + k_4^*[R^*] \\ &= I_3 + \frac{k_4^* I_2}{k_4^* + k_5^*[RSH] + k_6^*[M]} \end{aligned} \quad (\text{vii})$$

$$\begin{aligned} \text{Rate (H}_2) &= (k_7^*[H^*] + k_7[H])[RSH] \\ &= \frac{k_7 I_1}{k_7 + k_8} - \frac{(k_7 k_8^* - k_7^* k_8) I_1 [RSH]}{(k_7 + k_8) \left\{ (k_7^* + k_8^*) [RSH] + k_9^* [M] \right\}} \\ &\quad + \frac{k_4^* k_7 I_2}{(k_7 + k_8) (k_4^* + k_5^*[RSH] + k_6^*[M])} \end{aligned} \quad (\text{viii})$$

$$\begin{aligned}
 \text{Rate (alkane)} &= (k_5^*[R^*] + k_5[R])[RSH] \\
 &= \frac{k_8 I_1}{k_7 + k_8} + I_2 + \frac{(k_7 k_8^* - k_7^* k_8) I_1 [RSH]}{(k_7 + k_8) \left\{ (k_7^* + k_8^*) [RSH] + k_9^* [M] \right\}} \\
 &\quad - \frac{k_4^* k_7 I_2}{(k_7 + k_8) (k_4^* + k_5^* [RSH] + k_6^* [M])} \quad (ix)
 \end{aligned}$$

$$\begin{aligned}
 \text{Rate (H}_2\text{S)} &= I_3 + (k_8^*[H^*] + k_8[H])[RSH] \\
 &= \frac{k_8 I_1}{k_7 + k_8} + I_3 + \frac{(k_7 k_8^* - k_7^* k_8) I_1 [RSH]}{(k_7 + k_8) \left\{ (k_7^* + k_8^*) [RSH] + k_9^* [M] \right\}} \\
 &\quad + \frac{k_4^* k_8 I_2}{(k_7 + k_8) (k_4^* + k_5^* [RSH] + k_6^* [M])} \quad (x)
 \end{aligned}$$

$$\begin{aligned}
 \text{Rate (disulfide)} &= k_{12} [RS]^2 \\
 &= \frac{k_{12} I_1}{k_{12} + k_{13}} \quad (xi)
 \end{aligned}$$

D.4. Quantum Yield Expressions for Photolysis Products

The following quantum yield expressions are obtained by dividing the rate expressions (vii) - (xi) by the absorbed light intensity, I_a , i.e.

$$\phi (\text{products}) = \frac{\text{Rate (products)}}{I_a}$$

For the three primary photochemical steps: $\phi_i = I_i // I_a$, where $i = 1, 2, 3$.

$$\phi (\text{alkene}) = \phi_3 + \frac{k_4^* \phi_2}{k_4^* + k_5^* [\text{RSH}] + k_6^* [\text{M}]} \quad (\text{xii})$$

$$\begin{aligned} \phi (\text{H}_2) = & \frac{k_7 \phi_1}{k_7 + k_8} - \frac{(k_7 k_8^* - k_7^* k_8) \phi_1 [\text{RSH}]}{(k_7 + k_8) \left\{ (k_7^* + k_8^*) [\text{RSH}] + k_9^* [\text{M}] \right\}} \\ & + \frac{k_4^* k_7 \phi_2}{(k_7 + k_8) (k_4^* + k_5^* [\text{RSH}] + k_6^* [\text{M}])} \end{aligned} \quad (\text{xiii})$$

$$\begin{aligned} \phi (\text{alkane}) = & \frac{k_8 \phi_1}{k_7 + k_8} + \phi_2 \\ & + \frac{(k_7 k_8^* - k_7^* k_8) \phi_1 [\text{RSH}]}{(k_7 + k_8) \left\{ (k_7^* + k_8^*) [\text{RSH}] + k_9^* [\text{M}] \right\}} \\ & - \frac{k_4^* k_7 \phi_2}{(k_7 + k_8) (k_4^* + k_5^* [\text{RSH}] + k_6^* [\text{M}])} \end{aligned} \quad (\text{xiv})$$

$$\begin{aligned} \phi (\text{H}_2\text{S}) = & \frac{k_8 \phi_1}{k_7 + k_8} + \phi_3 + \frac{(k_7 k_8^* - k_7^* k_8) \phi_1 [\text{RSH}]}{(k_7 + k_8) \left\{ (k_7^* + k_8^*) [\text{RSH}] + k_9^* [\text{M}] \right\}} \\ & + \frac{k_4^* k_8 \phi_2}{(k_7 + k_8) (k_4^* + k_5^* [\text{RSH}] + k_6^* [\text{M}])} \end{aligned} \quad (\text{xv})$$

$$\phi (\text{disulfide}) = \frac{k_{12} \phi_1}{k_{12} + k_{13}} \quad (\text{xvi})$$

D.5 The Effect of Thermalizer Pressure on the Product Quantum Yield Expressions

M = collisional deactivating molecule for hot H^* and R^* radicals and may be either substrate [RSH] or thermalizer [TH] molecule. Thus, the expressions for $k_6^*[M]$ and $k_9^*[M]$ are as follows;

$$k_6^*[M] = k_{6R}^*[RSH] + k_{6T}^*[TH]$$

$$k_9^*[M] = k_{9R}^*[RSH] + k_{9T}^*[TH]$$

All the product quantum yield expressions, except the one for the disulfide product, are affected by thermalizer pressures. For $[TH] = 0$, the product quantum yield expressions, (xii) - (xv), for the photolysis of pure thiols become:

$$\phi(\text{alkene}) = \phi_3 + \frac{k_4^* \phi_2}{k_4^* + (k_5^* + k_{6R}^*) [RSH]} \quad (\text{xvii})$$

$$\phi(H_2) = \frac{k_7 \phi_1}{k_7 + k_8} - \frac{(k_7 k_8^* - k_7^* k_8) \phi_1}{(k_7 + k_8) (k_7^* + k_8^* + k_{9R}^*)} + \frac{k_4^* k_7 \phi_2}{(k_7 + k_8) \{k_4^* + (k_5^* + k_{6R}^*) [RSH]\}} \quad (\text{xviii})$$

$$\phi(\text{alkane}) = \frac{k_8 \phi_1}{k_7 + k_8} + \phi_2 + \frac{(k_7 k_8^* - k_7^* k_8) \phi_1}{(k_7 + k_8) (k_7^* + k_8^* + k_{9R}^*)} + \frac{k_4^* k_7 \phi_2}{(k_7 + k_8) \{k_4^* + (k_5^* + k_{6R}^*) [\text{RSH}]\}} \quad (\text{xix})$$

$$\phi(\text{H}_2\text{S}) = \frac{k_8 \phi_1}{k_7 + k_8} + \phi_3 + \frac{(k_7 k_8^* - k_7^* k_8) \phi_1}{(k_7 + k_8) (k_7^* + k_8^* + k_{9R}^*)} + \frac{k_4^* k_8 \phi_2}{(k_7 + k_8) \{k_4^* + (k_5^* + k_{6R}^*) [\text{RSH}]\}} \quad (\text{xx})$$

At high [TH], $k_{3T}^* [\text{TH}] \gg k_{3R}^* [\text{RSH}]$ and $k_{6T}^* [\text{TH}] \gg k_{6R}^* [\text{RSH}]$.

Thus, deactivation by the thiol substrate can be neglected.

Consequently, the product quantum yield expressions (xii) -

(xv), for the photolysis of thiol with added thermalizer

become:

$$\phi(\text{alkene}) = \phi_3 + \frac{k_4^* \phi_2}{k_4^* + k_5^* [\text{RSH}] + k_{6T}^* [\text{TH}]} \quad (\text{xxi})$$

$$\phi(\text{H}_2) = \frac{k_7 \phi_1}{k_7 + k_8} - \frac{(k_7 k_8^* - k_7^* k_8) \phi_1 [\text{RSH}]}{(k_7 + k_8) \{ (k_7^* + k_8^*) [\text{RSH}] + k_{9T}^* [\text{TH}] \}} + \frac{k_4^* k_7 \phi_2}{(k_7 + k_8) (k_4^* + k_5^* [\text{RSH}] + k_{6T}^* [\text{TH}])} \quad (\text{xxii})$$

$$\begin{aligned}
 \Phi(\text{alkane}) &= \frac{k_8 \phi_1}{k_7 + k_8} + \phi_2 \\
 &+ \frac{(k_7 k_8^* - k_7^* k_8) \phi_1 [\text{RSH}]}{(k_7 + k_8) \left\{ (k_7^* + k_8^*) [\text{RSH}] + k_{9T}^* [\text{TH}] \right\}} \\
 &- \frac{k_4^* k_7 \phi_2}{(k_7 + k_8) (k_4^* + k_5^* [\text{RSH}] + k_{6T}^* [\text{TH}])} \quad (\text{xxiii})
 \end{aligned}$$

$$\begin{aligned}
 \Phi(\text{H}_2\text{S}) &= \frac{k_8 \phi_1}{k_7 + k_8} + \phi_3 + \frac{(k_7 k_8^* - k_7^* k_8) \phi_1 [\text{RSH}]}{(k_7 + k_8) \left\{ (k_7^* + k_8^*) [\text{RSH}] + k_{9T}^* [\text{TH}] \right\}} \\
 &+ \frac{k_4^* k_8 \phi_2}{(k_7 + k_8) (k_4^* + k_5^* [\text{RSH}] + k_{6T}^* [\text{TH}])} \quad (\text{xxiv})
 \end{aligned}$$